Characterising the expression and interactions of the Endoplasmic Reticulum Oxidoreductase Erol β

Gunasekara, Sanjika Dias

Characterising the expression and interactions of the Endoplasmic Reticulum Oxidoreductase Ero1β

Sanjika Dias Gunasekara

A thesis submitted at the University of Durham for the degree of Doctor of Philosophy

School of Biological and Biomedical Sciences,
University of Durham

October 2006

To my wonderful

parents and family

DECLARATION

I declare that the experiments described in this thesis were carried out by myself in the School of Biological and Biomedical Sciences, University of Durham, under the supervision of Dr. Adam M. Benham. This thesis has been composed by myself and is a record of work that has not been submitted previously for a higher degree.

Sanjika Dias Gunasekara

ACKNOWLEDGEMENTS

I would like to take this opportunity to thank a number of people who have helped me in countless ways through these three years. First, I must thank my supervisor Dr. Adam Benham for giving me this opportunity to do this PhD, for all his help, guidance and advice throughout my studies, for all his patience and support throughout the writing up and whom I feel is one of the best supervisors. A very big thank you to Dr. Marcel-Van-Lith, whom I think is the best post-doc and has been my constant saviour when things kept going wrong, but most of all for being a great friend in good and bad times. A special thanks to all the previous and current members of the lab, especially Steve Walker, Mike Kenning and Andrew Lemin for making everyday work a joy. Many thanks also to Dr. John Gatehouse, Prof. Robert Edwards, Dr. Nick Hole, Dr. Gareth Williams, Dr. Ritu Kataky, Dr. Ian Cummins, Dr. David Scoones, Christine Richardson and Adrian Lapthorn for their knowledge and support.

From a personal point, my biggest thanks go to my aunt, uncle and two cousins, Malaka and Mudara, who gave me love, support, advice and a wonderful place to live throughout my seven years in Durham. They have been my family away from home and I would have never made this journey if not for them.

Also my heartfelt gratitude goes to Rasika, Ally, Hadil, Laura, Vittoria, Heather, Lorna and all my dear, wonderful friends I have made over the past few years.

Last but not least, I would like to say a big thank you to my fiancé Mohan, who listened to all my constant complaints but never failed to believe in me and supported me throughout this time.

Durham has been a very special place for me, and undoubtedly I will miss Durham and all the wonderful people I met here.

ABSTRACT

Proteins destined for the secretory pathway and endoplasmic reticulum (ER) resident proteins are targeted to the ER through an N-terminal signal sequence. Proteins then follow a post-translational maturation process to fold into functional proteins. For most of these proteins the formation of disulfide bonds (S-S) at the correct position is essential for structure and function. In eukaryotes, protein oxidation in the ER is catalysed by Endoplasmic reticulum oxidoreductases (EROs) which donate disulfide bonds to (and accept electrons from) Protein Disulfide Isomerase (PDI). In yeast, Ero1p is essential for viability and protein secretion. Two ER resident homologues have been identified in the human genome, Ero1α and Ero1β, which complement the yeast *ero1-1* temperature sensitive mutation. The main focus of this project was Ero1β.

Under steady state conditions in transfected cells, Ero1β was captured in higher molecular weight complexes in the presence and in the absence of an alkylating agent. Ero-PDI covalent interactions are alkylation dependent, but alkylation independent Ero1β complexes were found in transfected cells and endogenous tissue. In Ero1α the C*XX*C*XX*C C-terminal motif is important for protein folding, structural integrity and complex formation with the PDI. In Ero1β, the A*XX*C*XX*C (C390A) mutation disrupts covalent PDI interactions but does not interfere with homodimer formation. The C*XX*C*XX***A** (C396A) mutation caused disruption of Ero1β homodimer formation. Modelling the dimer onto the Ero1p crystal structure suggested that this 396 cysteine is indirectly disrupting dimer formation by most likely displacing the cofactor FAD. Two FAD binding domain mutants, initially discovered in yeast, were constructed in Ero1β and were found to cause instability of Ero1β through misoxidation during temperature and reducing stress conditions. Ero1β expression patterns were studied using immunohistochemistry on human stomach and pancreas tissues. The data indicated that Ero1β is constitutively strongly expressed in enzyme producing chief cells and hormone producing pancreatic islet cells.

An interesting result from immunohistochemistry stainings of healthy, Barrett's and oesophageal tumour tissue showed that the ER chaperone protein ERp57 is up-regulated only in dysplastic and oesophageal tumour tissue. These initial findings suggest ERp57 has potential as a marker in oesophageal tumour diagnosis.

TABLE OF CONTENTS

LIST OF TABLES

LIST OF FIGURES

ABBREVIATIONS

AMS	4-acetamido-4′-maleimidylstilbene-2,2′-disulfonic acid
APP	amyloid precursor protein
APS	ammonium persulfate
ASGRP	asialoglycoprotein receptor
Asn	asparagines
ATF6	activating transcription factor
Aβ	amyloid ß protein
BiP	binding protein
BSA	bovine serum albumin
BSO	buthionine sulphoximine
CDF	cation diffusion facilitator
CHO	Chinese hamster ovarian cells
CLAP	chymostatin, leupeptin, antipain and pepstatin
CNX	calnexin
CRT	calreticulin
DAF	decay-accelarating fator
DMEM	Dulbecco's modified Eagles's medium
DSBP	disulfide-bonded proteins
DTT	dithiothreitol
EDEM	ER degradation enhancing 1,2-mannosidase like protein
Endo H	endoglycosidase H
ER	endoplasmic reticulum
ERAD	ER-associated degradation
Ero1α	endoplasmic reticulum oxidoreductase α
Ero1β	endoplasmic reticulum oxidoreductase β
FBS	fetal bovine serum
FRET	fluorescence Resonance Energy Transfer
GH	growth hormone
GI	gastrointestinal tract

Gls I	glucosidase I
Gls II	glucosidase II
GPI	glycosylphosphatidyl inositol
Grp78	glucose regulating protein
GSH	reduced glutathione
GSSG	oxidised glutathione
GT	UDP-glucose:glycoprotein glycosyltransferase
GTP	guanosine triphosphate
H_2O_2	hydrogen peroxide
HA	influenza virus hemagglutinin
HC	heavy chain
HCMV	human cytomegalovirus
HCV	hepatitis C virus
hERO	human endoplasmic reticulum oxidoreductase
HIF-1	hypoxia-inducible factor 1
HIP	Hrd1p-independent proteolysis
IDDM	insulin-dependent diabetes mellitus
INM	inner nuclear membrane
INM-SM	INM sorting motif
IP	immunoprecipitation
IP_3R	inositol 1,4,5-trisphosphate receptor
IRE1	inositol requiring kinase 1
JcM	murine J chain
KCl	potassium chloride
KOAc	potassium acetate
L4	longest ER facing loop 4
LDL	low density lipoprotein
MDCK	Madin-Darby canine kidney cells
MEM	minimum essential medium
MgOAc	magnesium acetate
MHC	major Histocompatibility Complex
Mns I	mannosidase I

MYTHS	membrane-based yeast two-hybrid system
$NaHCO_3$	sodium hydrogen carbonate
NEM	N-ethylmaleimide
NHK	null Hong Kong
NIDDM	non-insulin-dependent diabetes mellitus
NK	natural killer cells
NMR	nuclear magnetic resonance
ORF	open reading frame
OST	oligosaccharyl transferase
P4H	prolyl-4-hydroxylase
PBS	Phosphate buffered saline
PDI	protein disulfide isomerase
PDI	Protein Disulfide Isomerase
PE	Pseudomonas exotoxin A
PERK	RNA-activated protein kinase (PKR)- like endoplasmic reticulum kinase
PLP	proteolipid protein
PMD	Perlizaeus–Merzbacher disease
PNGase	peptide:N-glycanase
ppαf	phereomone precursor prepro-alpha-factor
PS	Presenilins
RNC	ribosome nascent chain
ROS	reactive oxygen species
rRNAse	reduced ribonuclease
RyR	ryanodine receptor
SCaMPER	sphingolipid Ca^{2+}-release-mediating protein of endoplasmic reticulum
SCP	signal peptidase complex
SERCA	sarco endoplasmic reticulum calcium ATPase
SFV	semliki Forest Virus
SP cells	semi permeabilised cells
SP	semi permeabilised
SPP	signal peptide peptidase
SR	SRP receptor

SR	sarcoplasmic reticulum
sRNase	scrambled ribonuclease
SRP	signal recognition particle
TAP	transporter associated with antigen processing
TBS	tris buffered saline
TCA	trichloro actetic acid
TEMED	N,N,N',N'-Tetramethylethylenediamine
TGN	trans-Golgi network
TMX2	thioredoxin-related transmembrane protein 2
tPA	tissue-type plasminogen activator
TRAM	translocating chain-associated membrane protein
UPR	unfolded protein response
VEGF	vascular endothelial growth factor
VIMP	VCP-interacting membrane protein
VSV	vesicular Stomatitis virus
XBP1	x-box-binding protein-1
α1-PI	α1-proteinase inhibitor
αHA	anti-HA antibody, against human Influenza virus Hemagglutin
αMyc	anti-Myc antibody, against human c-Myc epitope

CHAPTER 1

GENERAL INTRODUCTION

The native state of a protein generally corresponds to the most thermodynamically stable state under physiological conditions. Folding of a protein to this native conformation is currently modelled using energy landscapes. The unfolded polypeptide is at the surface of the landscape with the highest energy, and searches down a funnel-like energy profile making intramolecular contacts towards the native state (reviewed in (Wolynes, 2005)). Partially folded conformations on this landscape are more prone to aggregation, leading to intermolecular contacts ultimately resulting in protein misfolding diseases (reviewed in (Jahn & Radford, 2005)). Protein misfolding and aggregation are the basis of a number of pathological conditions including Alzhemier's and Parkinson's disease (reviewed in (Scheibel & Buchner, 2006)), Huntington's disease (Qin & Gu, 2004), cystic fibrosis (Kopito, 1999; Sharma et al., 2004), α1-antitrypsin deficiency (Lawless et al., 2004), the rheumatic disease ankylosing spondylitis (Ramos & Lopez de Castro, 2002) and Creuzfeld-Jakob disease (Aguzzi et al., 2004). All of these diseases are at least partly caused by amino acid changes that result in protein misfolding and/or degradation through the endoplasmic reticulum (ER) quality control system.

Misfolded proteins trigger a system called the unfolded protein response (UPR) in which the synthesis of ER membranes and chaperones is induced to cope with the demands of high levels of protein production. This is achieved through ER to nucleus signalling pathways mediated by three ER resident transmembrane proteins; activating transcription factor (ATF6), the inositol requiring kinase 1 (IRE1) and double stranded RNA-activated protein kinase (PKR)-like endoplasmic reticulum kinase (PERK) (reviewed in (Kaufman et al., 2002; Schroder & Kaufman, 2005)). Accumulation of unfolded proteins in the ER results in cleavage of ATF6, to release a cytosolic fragment

(bZIP domain) and of IRE1 to induce splicing of a specific mRNA that encodes XBP-1 (X-box-binding protein-1) in mammalian cells. Processed XBP-1 initiates transcriptional activation of ER stress response genes (or unfolded protein response, UPR, genes) (Yoshida et al., 2001). PERK is also activated to phosphorylate and inactivate the translation initiation factor eIF2α (Kaufman et al., 2002). XBP-1 and ER stress were recently implicated in bipolar disorder (Kakiuchi et al., 2003), obesity and type 2 diabetes (Ozcan et al., 2004), suggesting that the UPR may have an important role in complex disease not previously linked to ER protein misfolding.

With protein misfolding playing a crucial role in many diseases, understanding the fundamentals of protein folding is essential. This chapter focuses on protein folding in the endoplasmic reticulum and the associated quality control mechanisms.

1.1 Protein entry into the ER

Proteins expressed at the cell surface, that reside within the secretory pathway or that get secreted, are targeted to the ER by their signal sequence (Halic & Beckmann, 2005), initially recognised by the signal recognition particle (SRP, (Nagai et al., 2003; Egea et al., 2005)) which forms a ribosome nascent chain (RNC)-SRP complex. This complex then docks onto the membrane bound SRP-receptor (SR) in a GTP dependent manner (Wild et al., 2004). The polypeptide chain is translocated from the ribosome into the ER through the translocon, at the core of which lies an aqueous pore (reviewed in (Johnson & van Waes, 1999)). The translocon, called the Sec61 complex in eukaryotes and SecY complex in eubacteria and archaea, is a heterotrimeric integral membrane protein complex (Brundage et al., 1990; Gorlich & Rapoport, 1993) composed of the α-subunit (SecY in eubacteria and archaea; Sec61α in mammals), the

β-subunit (SecG in eubacteria; Secβ in archaea; Sec61β in mammals) and the γ-subunit (SecE in eubacteria and archaea; Sec61γ in mammals). Electrophysiological studies demonstrated that the Sec61 translocon forms an aqueous, ion-conducting channel (Wirth et al., 2003) which is structurally dynamic, with an estimated maximum dimension of ~15 Å (Breyton et al., 2002). Due to the large diameter of the aqueous pore, a gating mechanism is needed to maintain the permeability barrier and maintain critical ion gradients (e.g. Ca^{2+} stores) across the ER membrane during translocation. These pore structures have been elucidated experimentally by incorporating fluorescent dyes into short nascent chains and determining the accessibility of the probes to the ER lumen using externally added quenching agents (Hamman et al., 1998). The ER permeability barrier is maintained from the cytosolic side of the membrane by the ion-tight binding of the ribosome to the translocon during translocation (Crowley et al., 1994). The lumenal side of the translocation pore is sealed either directly or indirectly by BiP (Hamman et al., 1998) and this seal needs to be in place before the cytosolic side of the pore opens, to maintain a permeability barrier. BiP (Grp78) is a Ca^{2+} and ATP dependent Hsp70 family member which was initially identified as an immunoglobulin heavy-chain binding protein (Haas & Wabl, 1983). BiP is an ER lumen chaperone which has a KDEL ER retention signal (Munro & Pelham, 1987).

The local environment a nascent protein encounters as it is synthesised depends on whether it is destined to be a soluble protein, a membrane spanning protein or a glycosylphosphatidyl inositol (GPI) linked protein, for example. Initial studies indicated that the ribosome, not the translocon, first recognised transmembrane sequences which initiated structural changes at the translocon (Liao et al., 1997). More recently, studies using Fluorescence Resonance Energy Transfer (FRET) have shown that both secretory and membrane proteins already differ in their folding within the

ribosome itself, even before entering the translocon (Johnson, 2004). Hydrophobic transmembrane sequences fold into tight helixes that retain their folded conformation as they move into the translocon, whereas secretory protein sequences take up a more extended conformation inside the tunnel (Woolhead et al., 2004; Sadlish et al., 2005).

The Sec61/SecY complex forms a passive pore which allows a polypeptide chain to slide back and forth but needs to associate with partner proteins which can provide the driving force during translocation. Depending on the partner, the channel can operate in three different translocation modes (reviewed in (Osborne et al., 2005)). In co-translational translocation (Figure 1.1*A*) found in all organisms, a ribosome nascent chain (RNC)-SRP complex is targeted to the membrane via its recognition by SRP, which allows binding of the ribosome to the channel. The ribosome then feeds the polypeptide chain directly into the channel. GTP hydrolysis during translation provides the energy for protein translocation (Halic & Beckmann, 2005). Post-translational translocation, found only in eukaryotes (Figure 1.1*B*), has been described in *Saccharomyces cerevisiae* (Matlack et al., 1999) but is thought to be a conserved mechanism among higher eukaryotes as well. Here the partner proteins are the Sec61 complex, Sec62/63 complex and the ER chaperone BiP, which provides the driving force for a ratcheting mechanism (Matlack et al., 1999). Polypeptides with a less hydrophobic signal sequence that escape binding to SRP are thought to undergo this mode of translocation (Ng et al., 1996) and thus require cytosolic chaperone proteins to keep the polypeptide in an unfolded form. The lumenal J domain of Sec63p interacts with ATP-bound BiP which has an open-peptide binding pocket. This interaction stimulates hydrolysis of ATP and the peptide binding pocket closes around the translocating protein. When the polypeptide has moved a sufficient distance into the ER lumen another BiP molecule binds, and this process is repeated until the entire

polypeptide is translocated. The third mode of translocation, seen only in eubacteria, also occurs post-translationally (Figure 1.1*C*), where the channel partner is a cytosolic ATPase called SecA. SecA pushes the polypeptides through the channel in a stepwise manner (Mori & Ito, 2001; Luirink & Sinning, 2004).

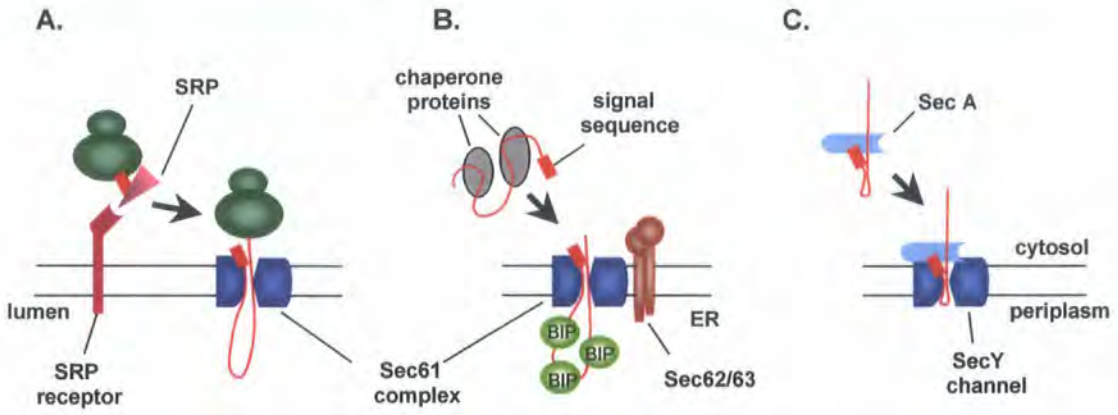

FIGURE 1.1: Components of the three different modes of translocation

A. Cotranslational translocation in all organisms. The signal recognition particle (SRP) binds to the signal sequence of an emerging nascent polypeptide chain and to the ribosome to form a ribosome nascent chain (RNC) – SRP complex. This complex is targeted to the ER membrane by interaction with the SRP receptor, which releases SRP and targets ribosome bound polypeptide to the Sec61 complex. The polypeptide initially inserts into the channel as a loop with the N and C termini in the cytosol, and the remainder of the polypeptide moves through the channel into the ER. **B.** Post translational translocation in yeast and higher eukaryotes. Polypeptides synthesised in the cytosol are kept unfolded by binding cytosolic chaperones. This complex is targeted to the Sec61, Sec62/63 translocon through the signal sequence of the polypeptide after which the chaperone proteins are released. ADP bound BiP binds to the polypeptide chain as it emerges in to the ER lumen and when the polypeptide has moved a sufficient distance into the lumen another BiP molecule binds. This process is repeated until the entire polypeptide is translocated. **C.** SecA mediated posttranslational translocation in eubacteria. Polypeptides with a signal sequence are targeted to the SecY channel after binding to SecA and are inserted as a loop into the channel. The SecA polypeptide-binding groove is involved in pushing the polypeptide chain into the periplasm in a stepwise manner. Adapted and modified from (Osborne et al., 2005).

1.2 ER protein sorting

Proteins that enter the ER need to reach various ultimate destinations to function properly. A protein may reside in the ER, assemble into complexes, remain as a monomer or get directed to the nuclear membrane, for example. How does the ER sort these proteins according to their destination? For ER resident lumenal proteins, the carboxy-terminal tetrapeptide, KDEL, has been shown to be necessary and sufficient to ensure their ER localisation (Munro & Pelham, 1987; Pelham, 1989), whereas the KKXX or di-lysine motif ensures ER localisation of membrane proteins (Nilsson et al., 1989; Townsley & Pelham, 1994). ER localisation of soluble resident proteins largely depends on KDEL receptor-mediated retrieval from the intermediate compartment or Golgi apparatus (Pelham & Munro, 1993), whereas retrieval and retention mechanisms seem to cooperate in determining the ER localisation of certain proteins like calreticulin (Sonnichsen et al., 1994). The existence of a true ER retention mechanism was evident from experiments using chimeric human cathepsin D molecules (Isidoro et al., 1996). These cathepsin D molecules were made by either attaching a KDEL motif or by attaching a C-terminal sequence from IgM μ chain (μtp) with a cysteine residue. These results indicated that μtp does not require recycling between Golgi and the ER and that thiol-mediated ER residency is due to true retention in this organelle. So while the evidence for a retrieving function with the KDEL receptor is overwhelming, it seems clear that additional mechanisms do contribute in determining the localisation of ER resident proteins (Isidoro et al., 1996).

Another less-well characterised sorting motif is the arginine-based ER-localisation signal, first discovered in the context of MHC class II and invariant chain transport (Bakke & Dobberstein, 1990). Arginine-based signals can localise a broad range of

proteins to the ER, and this exposed signal can localise unassembled subunits or incompletely assembled complexes to the ER (e.g. G protein-coupled γ-aminobuyric; $GABA_B$, receptor; (Margeta-Mitrovic et al., 2000)). After functional complex assembly, the signal motif gets masked and this allows the transport of the complex to the cell surface (Zerangue et al., 1999). From information generated so far, a consensus motif Φ/Ψ/R-R-X-R has been put together for the arginine-based signal, where Φ/Ψ denotes an aromatic or bulky hydrophobic residue and X represents any amino acid. These signals do not require exposure at the distal terminus of a membrane protein and only require being approximately 16-46 Å away from the lipid bilayer in order to be functional ((Shikano & Li, 2003) and reviewed in (Michelsen et al., 2005)). A surprising finding has been that an arginine based signal is able to mediate access to viral type I membrane proteins from the ER to the inner nuclear membrane (INM) (Meyer & Radsak, 2000; Meyer et al., 2002), where the virus undergoes a characteristic maturation phase. Using immunofluorescence and cell fractionation studies on glycoprotein B from human cytomegalovirus (HCMV), Meyer and Radsak demonstrated that the DRLRHR sequence at the C-terminus was sufficient to target the membrane protein to the INM (Meyer & Radsak, 2000). This C-terminal sequence did not show any detectable nuclear localisation signal activity for soluble β-Galactosidase and could not be substituted by the nuclear localisation signal of SV40 T antigen (Meyer & Radsak, 2000). These more recent findings suggest potential alternative functions for this arginine-based signal motif.

Sorting and quality control of inner nuclear membrane proteins has had comparatively less attention than the quality control of secreted proteins. This situation is now beginning to change (Mattaj, 2004). The INM is contiguous with the ER membrane and it was generally presumed that, after leaving the translocon, membrane proteins

destined for INM diffuse through the ER membrane to reach the INM where the proteins are retained by binding to nuclear proteins or DNA (Worman & Courvalin, 2000). This 'passive' diffusion-retention model has been challenged by more recent studies. An INM sorting motif (INM-SM) consisting of 18 hydrophobic amino acids was first discovered by Hong and colleagues using the viral envelope protein E66 (Hong et al., 1997). Arthur Johnson's group used a photo cross-linking approach to study both cellular and viral proteins with an INM-SM-like sequence to show that an initial sorting decision is likely to occur early, within the translocon itself. This was based on preferential interaction of INM-SM with the TRAM (translocating chain-associated membrane protein, a component of the translocon) protein and Sec61α (Saksena et al., 2004). The data also revealed that viral and host INM proteins interacted similarly with translocon proteins and that the translocon could discriminate between INM proteins and other membrane proteins (Saksena et al., 2004). More recently, the ER membrane associated importin-alpha-16 protein was found adjacent to Sec61α, and was shown to cross-link to INM-SM suggesting a possible involvement of this protein in the trafficking of integral membrane proteins to the INM (Saksena et al., 2006). These results challenge the previous diffusion-retention model and suggest that sorting of INM proteins is an active signal driven process and also point to TRAM and importin-alpha-16 as important proteins in nuclear membrane sorting.

A protein can also move apically or baso-laterally along the secretory pathway of polarised cells. Cellular polarity is essential for the proper function of many epithelial and endothelial cells (Nelson & Yeaman, 2001). In epithelial cells, baso-lateral sorting is directed by signal motifs found in cytoplasmic domains. Usually these motifs contain a conserved tyrosine residue (Y) and are of the form NPXY or YXXΦ (where X can be any amino acid and Φ is a hydrophobic residue), although some motifs are di-

hydrophobic (e.g. the LDL receptor and Fc receptor) (Matter et al., 1994). Apical sorting signals are less well defined, and are generally present in the ER lumen side rather than the cytoplasm. Targeting may also be achieved by a GPI-anchor, as for decay-accelerating factor (DAF) (Lisanti et al., 1989). N-glycans are also found to act as an apical targeting signal for secretory proteins. Growth hormone (GH), which is normally non-glycosylated is secreted from both apical and basolateral sides from MDCK (Madin-Darby canine kidney) cells. However it is secreted from the apical side when glycosylated (Scheiffele et al., 1995). During biosynthetic transport, endolyn, a type I transmembrane protein, is targeted from the trans-Golgi network (TGN) to the apical cell surface of MDCK cells via a targeting signal found in the lumenal domain of the protein. This targeting signal is thought to override/compete with the basolateral and lysosomal sorting information found in the cytoplasmic tail (Ihrke et al., 2001). Site directed mutagenesis studies have pointed to a subset of the eight N-glycosylation sites as being necessary and sufficient for apical sorting of endolyn (Potter et al., 2004; Potter et al., 2006). In general, the decision between apical and baso-lateral sorting occurs mainly in the trans-Golgi network. However, the relationship between translocation, "early" sorting events and ER protein folding is sure to develop in the coming years.

1.3 Signal peptide cleavage

All proteins that get inserted co-translationally into the ER through the translocon have an N-terminal signal sequence that is recognised by a multi-protein complex termed the signal recognition particle (SRP) (Egea et al., 2005). The signal sequence is almost always cleaved from the mature polypeptide by signal peptidases (Gilmore, 1991). The signal peptidase complex (SPC) of the ER was biochemically and genetically

characterized in the 1990's, in both yeast and in mammalian systems (Shelness et al., 1993). In mammalian cells the SPC is a hetero-oligomeric membrane complex comprised of 12, 18, 21, 22/23 and 25 kDa subunits (Evans et al., 1986). In *Saccharomyces cerevisiae*, the Sec11p is necessary for signal peptide processing and cell viability, and is homologous to the 18 kDa and 21 kDa mammalian subunits (Bohni et al., 1988).

Details are beginning to emerge as to how signal peptides can influence glycoprotein folding and how the timing of signal peptide cleavage can influence glycoprotein maturation. This area is particularly interesting for virologists, because many viral proteins start out as unprocessed polyproteins. Compact viral genomes use their limited complement of nucleotides by encoding proteins that must be processed from immature precursors. Processing by signal peptidase and related proteases can influence whether an immature polyprotein goes on to fold productively. In Semliki Forest Virus (SFV) for example, the p62-E1 coding unit encodes the precursor protein that is cleaved into the spike subunits p62 and E1 by host signal peptidases. This step is required for p62 and E1 to form heterodimers from the same precursor protein (cis-heterodimerisation), and is co-ordinated with the ER chaperones calnexin and calreticulin, prior to transport to the plasma membrane (Andersson & Garoff, 2003). Another example is the Hepatitis C virus (HCV), which encodes two envelope glycoproteins, E1 and E2, which are released from HCV polyprotein by signal peptidase cleavage. This step is required for maturation (Voisset & Dubuisson, 2004). Thus efficient signal peptide cleavage can be seen as a component of the ER quality control for many viral glycoproteins.

In addition to the signal peptidase complex, a signal peptide peptidase (SPP) has been identified and characterized (Weihofen et al., 2002). SPP is an unusual polytopic

aspartic acid type intra-membrane protease with homology to presenilin (Xia & Wolfe, 2003). Presenilins (PS) 1 and PS 2 are required for the intra-membrane cleavage of the type I membrane protein amyloid precursor protein (APP) to form the amyloid β protein (Aβ), which is believed to be the initiator of pathogenesis in Alzheimer disease (Weihofen & Martoglio, 2003). The APP class of proteins is now attracting the interest of biologists interested in protein processing and misfolding. Ironically, viruses themselves exploit SPP. The capsid of Hepatitis C virus is composed of the p21 core protein which is formed by cleavage of the transmembrane domain of the precursor form (p23) by SPP. Although this SPP-catalysed cleavage is now thought to be non-essential for HCV budding, it is still important for the stability of the viral capsid (Vauloup-Fellous et al., 2006).

Signal peptides have uses after being cleaved from the mature polypeptide. One interesting example is in the antigen presentation function of Major Histocompatibility Complex (MHC) class I molecules. MHC class I molecules usually present peptide fragments derived from pathogens to $CD8^+$ T cells of the immune system. Classical MHC class I molecules bind to viral peptides as they are synthesized in the ER. However, the non-classical MHC class I molecule HLA-E, doesn't bind to viral peptides but instead binds to peptides derived from the highly conserved signal sequences of other classical MHC class I molecules. This reassures cells of the immune system, particularly natural killer (NK) cells, that the cell is not virus-infected and inhibits NK-cell mediated cell lysis (Braud et al., 1998). Certain virus-infected cells fail to express classical MHC class I molecules at the cell surface, preventing recognition by T-cells. However, due to the additional level of control provided by HLA-E peptide-complexes, these infected cells will get eliminated by NK cells (Ljunggren & Karre, 1990; Lanier, 1998). The signal peptide was found to be cleaved at the transmembrane

region (Weihofen et al., 2000) by signal peptide peptidase (Lemberg et al., 2001). This releases a peptide fragment into the cytosol which gets transported back into the ER lumen through the TAP transporter in order to bind HLA-E (Lemberg et al., 2001; Lee et al., 1998).

Another recent function assigned to SPP is in dislocation of MHC class I heavy chains (HC) from the ER (Loureiro et al., 2006). In human cytomegalovirus (HCMV) infected cells, several viral proteins are synthesised to prevent surface expression of MHC class I molecules and thus allow HCMV to evade the host immune response. US2 and US11 are two of these immunoevasins that induce the dislocation of HC molecules from the ER and target them for proteosomal degradation in the cytosol (Jones & Sun, 1997; Wiertz et al., 1996). Using short hairpin RNAs (shPNAs) to reduce the expression of SPP in U373-MG cells expressing US2, Ploegh and colleagues have shown that interaction between US2 and SPP is essential for US2 (and not US11) mediated ER dislocation of HCs (Loureiro et al., 2006). Thus it is now emerging that SPP might not only be involved in signal peptide processing but also in other processors such as ER dislocation.

1.4 Chaperone selection during glycoprotein folding in the ER

Newly synthesised polypeptide chains targeted to the ER fold as they move through the translocon complex, and continue to fold co-translationally with the help of a variety of molecular chaperones and folding enzymes present in the ER lumen. Although most proteins that fold in the ER are glycoproteins, not all ER proteins are glycosylated (Apweiler et al., 1999). About 90% of glycoproteins are likely to carry N-linked glycans (Apweiler et al., 1999). N-linked glycosylation begins on the cytoplasmic side

of the ER with the assembly of the dolichol-linked oligosaccharide donor. This oligosaccharide gets 'flipped' to the ER luminal side and is transferred *en bloc* to an asparagine (Asn) residue in the Asn-X-Ser/Thr consensus sequence by the oligosaccharidetransferase (OST) (Figure 1.2; (Helenius & Aebi, 2004)). Although glycosylation is generally thought to be a post-translational modification, the majority of N-linked glycans are initially transferred co-translationally (Nilsson & von Heijne, 1993; Kowarik et al., 2002).

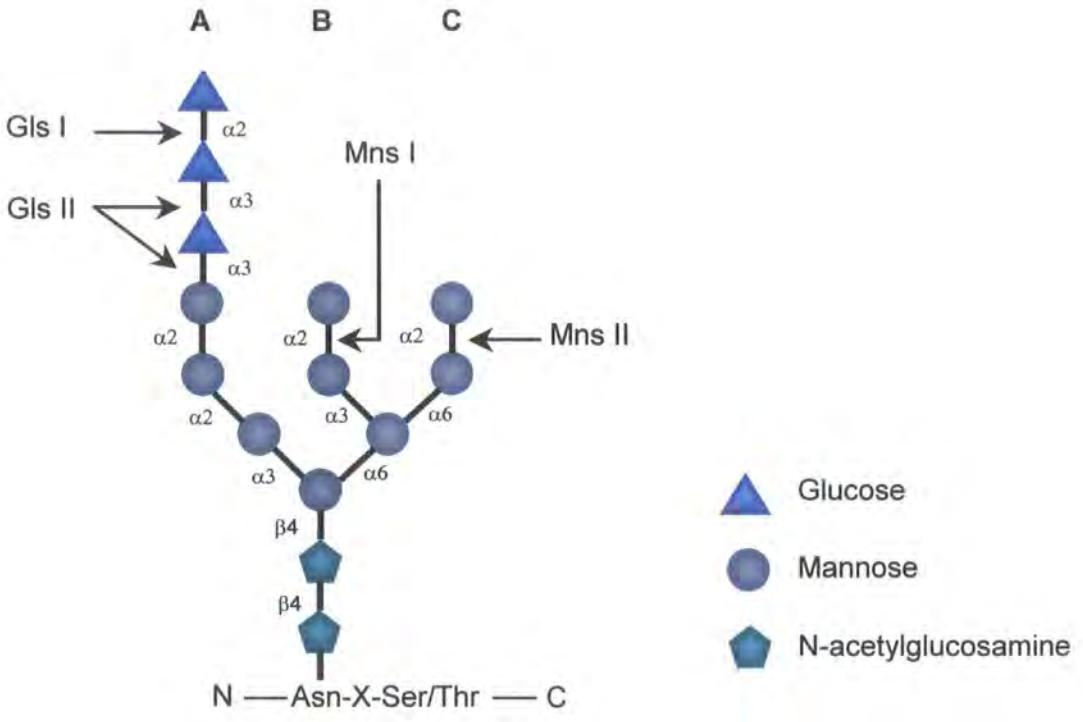

FIGURE 1.2: The N-linked core glycan

The initial composition of the carbohydrate ($Glc_3Man_9GlcNAc_2$) transferred by the oligosaccharyl transferase (OST) onto potential N-glycosylation sites. Glycosidic linkages and site of action of various glycosidases are indicated. Gls and Mns indicates glucosidase and mannosidase cleavage sites respectively. Adapted and modified from (Hebert et al., 2005).

The need for N-linked glycans for efficient secretion was first realised in the 1970's with the availability of an N-linked glycosylation inhibitor, tunicamycin (Olden et al., 1982; Olden et al., 1978). Although glycosylation has been proven to be important for proper folding of many proteins, it should be noted that not all glycoproteins are equally dependent on their glycans for folding and secretion (reviewed in (Helenius, 1994)). Some proteins only show partial misfolding in the absence of sugars. For example, nonglycosylated MHC class I antigens were still recognised by cytotoxic T cells, although their expression at the cell surface was greatly reduced. This defect in cell surface expression was not due to rapid degradation of the antigens but due to a defect in intracellular transport which effected expression at the plasma membrane (Helenius, 1994; Miyazaki et al., 1986). Secretion of different classes of immunoglobulins is inhibited to different extents when incubated with tunicamycin. For example in plasma cells, IgM secretion was inhibited 81% compared to just over background level inhibition of IgG secretion (Hickman & Kornfeld, 1978).

The presence of glycans on nascent polypeptide chains attracts the attention of two Ca^{2+} binding lectin chaperones, calnexin and calreticulin. Calnexin is a type I ER membrane protein (Wada et al., 1991; David et al., 1993) whereas calreticulin is a soluble paralogue localised to the ER lumen by a KDEL retention sequence (Fliegel et al., 1989; Smith & Koch, 1989). The thiol-disulfide oxidoreductase ERp57 associates selectively with nascent glycoproteins in a complex with calnexin and calreticulin (Oliver et al., 1997). A protein that has been extensively studied as a model for glycoprotein folding is the influenza virus hemagglutinin (HA), a membrane fusion protein produced by the 'flu' virus and synthesised in the ER. Structures of the HA fusion protein have been solved (Wilson et al., 1981) and the HA folding pathway is

relatively well understood e.g. (Braakman et al., 1991). Mature influenza HA is a homo-trimer, with each monomer comprising an HA1 and HA2 chain linked by an intermolecular disulfide bond. A recent study using truncated ribosome-bound HA nascent chains combined with ER-derived microsomes, followed the initial stages of HA maturation pathway (Daniels et al., 2003). HA chains were synthesised from truncated mRNA without a stop codon, which gave rise to translation intermediates of known lengths. Using ^{35}S-labelled HA translocation intermediates, Daniels and colleagues suggested that multiple N-linked glycans are strategically positioned to bind the lectin chaperones and the oxidoreductase ERp57 as the nascent chain emerges from the translocon complex (Daniels et al., 2003).

Although some proteins like influenza HA interact preferentially with calnexin and calreticulin but not with BiP (Daniels et al., 2003; Mulvey & Brown, 1995), other proteins like vesicular stomatitis virus (VSV) G protein have been found to first interact with BiP and then with calnexin (Hammond & Helenius, 1994b). However, some proteins like unassembled immunoglobulin chains interact sequentially with BiP and GRP94 (Melnick et al., 1994). Insight into chaperone selection during glycoprotein translocation came from monitoring the maturation of two Semliki forest virus (SFV) glycoproteins, p62 and E1 in infected CHO cells (Molinari & Helenius, 2000). Results from this study indicated that if proteins possess N-linked glycans close to the N-terminus (within the first 50 residues) they are likely to enter the calnexin/calreticulin cycle without prior binding to BiP, as seen for p62. However, if glycoproteins have their glycans closer to the C-terminus (e.g. E1 and Vesicular Stomatitis virus; VSV), the proteins are more likely to interact with BiP and not seen by calnexin or calreticulin (Molinari & Helenius, 2000). The suggestion from these studies is that there is a choice between two chaperone systems for assistance with folding during nascent

glycoproteins maturation. One system comprises BiP and possibly PDI (Gonz lez et al., 2002), and the other consists of calnexin, calreticulin and ERp57 (Molinari & Helenius, 2000). However, it should be noted that this 'simple rule' might not be followed by every viral and normal cellular glycoprotein. It also remains unclear whether PDI and ERp57 will perform the same function (disulfide bond oxidation) within these two systems. Future work will undoubtedly shed more light on how chaperone selection is carried out by both viral and cellular proteins.

1.4.1 Calnexin/Calreticulin cycle

Glycoproteins that interact with calnexin and calreticulin are subjected to a rigorous quality control inspection (Figure 1.3). At first, a core oligosaccharide (Figure 1.2) is transferred from a dolichol-linked oligosaccharide donor to a nascent protein with an Asn-X-Ser/Thr motif by oligosaccharyl transferase (OST). This $Glc_3Man_9GlcNAc_2$ moiety has three terminal glucose residues that are trimmed by glucosidase I and II (Gls I and II) to give a monoglucosylated $GlcMan_9GlcNAc_2$ intermediate (Ellgaard & Helenius, 2003). Gls I is a type II membrane glycoprotein that acts rapidly and efficiently to trim the outermost glucose immediately after the addition of a glycan to the polypeptide chain (Deprez et al., 2005). On the other hand, the trimming of the middle glucose by Gls II (a soluble heterodimer) occurred efficiently only when a second glycan was present in the polypeptide chain (Deprez et al., 2005). It is now well established that monoglucosylated substrate proteins bind to both calnexin and calreticulin and are subsequently released following hydrolysis of the mono-glucose residue by glycosidase II (Gls II) (Hammond et al., 1994a). These substrates , may be re-glucosylated by UDP-glucose:glycoprotein glycosyltransferase (GT) allowing them to re-associate with calnexin (Caramelo et al., 2003).

By having a cycle that allows a nascent polypeptide chain to attach to and release from calnexin, the protein has sufficient time to find and fold into its most stable conformation. This system relies on the detection of localised, disordered conformations and exposed hydrophobic patches by GT (Ritter & Helenius, 2000). In this way GT determines whether a protein is misfolded or not and acts as the folding sensor. Thus a folded protein will not be reglucosylated, whereas a misfolded protein will be reglucosylated and sent back to the calnexin/calreticulin cycle. This 'lectin only' model (Figure 1.3) proposes that interaction between a folding glycoprotein and calnexin/calreticulin is controlled solely by the availability of a single terminal glucose residue. A question that arises from this model is how the lectins are able to suppress aggregation of the folding glycoproteins, as there doesn't seem to be any direct masking of hydrophobic sites by calnexin or calreticulin (Williams, 2006). One hypothesis is that the folding glycoprotein might become sequestered between the arm domain and globular lectin domain to reduce aggregation with other folding glycoproteins (Helenius & Aebi, 2004). There are several lines of evidence to support this lectin only model (Wearsch et al., 2004), including the prevention of calnexin/ calreticulin interaction with glycoproteins after the addition of glucosidase inhibitors (Danilczyk & Williams, 2001).

An alternative model is the 'dual-binding' model, where calnexin and calreticulin interact with folding glycoproteins through their lectin sites as well as their polypeptide binding site (Figure 1.3). This model would ensure the binding of hydrophobic segments on the folding glycoproteins by the lectins and thus suppress aggregation of these proteins (Williams, 2006). Over the past decade considerable evidence has come through to support this dual-binding model (Ihara et al., 1999; Saito et al., 1999) including the use of calnexin point mutants within the lectin site that lacked lectin

function but retained the ability to bind ERp57. These mutants were still able to prevent aggregation of a nonglycosylated substrate but were compromised in their ability to prevent aggregation of a monoglucosylated substrate. Selected mutants, when co-expressed with the heavy-chain subunits of MHC class I molecule in *Drosophila* cells, were still able to associate with heavy chains and prevent their rapid degradation showing that lectin-deficient calnexin still retains many of its chaperone functions *in vitro* and *in vivo* (Leach & Williams, 2004). Amidst all the evidence, this model does need further investigating, especially since an obvious hydrophobic binding site has not been precisely pin-pointed on the calnexin crystal structure (Schrag et al., 2001). If a protein still fails to fold properly, the slow acting ER α1,2-mannosidase I will trim the terminal mannose from branch B (Figure 1.2) which will target the misfolded glycoprotein to EDEM (ER degradation enhancing 1,2-mannosidase like protein), another lectin-like ER resident protein (Ellgaard & Helenius, 2003; Molinari et al., 2003; Oda et al., 2003). Disposal occurs through a process called ERAD (ER-associated degradation), which will be discussed in section 1.6.

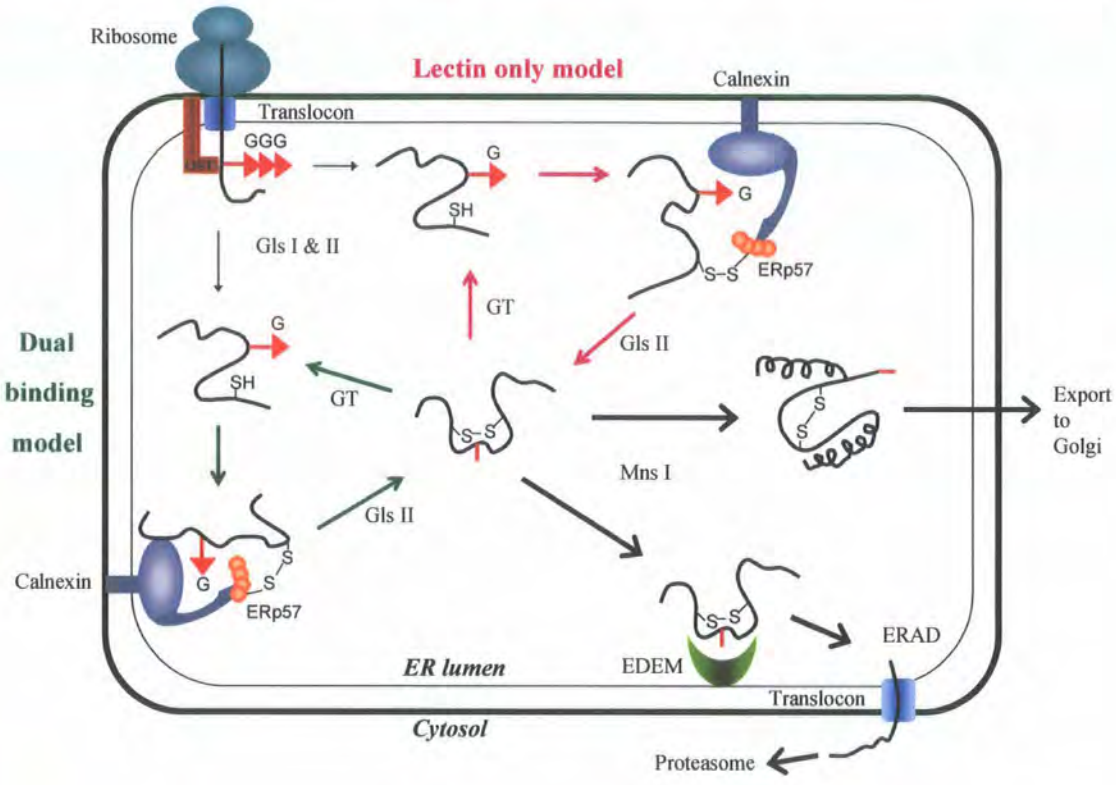

FIGURE 1.3: Two recently proposed models for calnexin/calreticulin mechanism of action

Nascent polypeptides entering the ER lumen through the translocon complex may become N-glycosylated with the transfer of the preassembled $Glc_3Man_9GlcNAc_2$ core oligosaccharide from dolicol phosphate to an Asn-X-Ser(Thr) motif by oligosaccharyl transferase (OST). The two terminal glucose residues are rapidly removed by glucosidase I and II (Gls I & II) to generate the $GlcMan_9GlcNAc_2$ oligosaccharide recognised by calnexin and calreticulin. In the lectin-only model (purple arrows), cycles of glycoprotein release and rebinding are controlled solely by the removal and re-addition of the terminal glucose residue by glucosidase II (Gls II) and UDP-glucose:glycoprotein glycosyltransferase (GT), respectively. Chaperone binding serves to retain non-native glycoproteins within the ER and also recruit ERp57 to promote disulfide bond formation and isomerisation. In the dual-binding model (green arrows) calnexin and calreticulin recognise non-native glycoproteins through their lectin sites as well as through a polypeptide-binding site specific for non-native conformers. In both models, folded proteins are released from the chaperones, followed by further oligosaccharide trimming and export to the Golgi apparatus. Alternatively, for misfolded glycoproteins that remain for prolonged periods in the calnexin/calreticulin cycle, trimming by α-mannosidase I (Mns I) generates a $Man_8GlcNAc_2$ structure that

may be recognised by a putative lectin ER degradation enhancing 1,2-mannosidase like protein (EDEM). EDEM targets proteins for retrotranslocation and proteasomal degradation (ER-associated degradation: ERAD). Three terminal glucose residues are shown as red triangles with letter 'G' alongside. Adapted from (Williams, 2006).

Structural studies are beginning to help form a better understanding of how calnexin/ calreticulin and ERp57 all come together to form a complex that can recognise a wide range of glycans. A combination of NMR and a new membrane-based yeast two-hybrid system (MYTHS) have been used to show that direct interactions occur between the tip of calnexin P-domain (a stable, non-helical fold towards the C-terminus of the protein) and the basic carboxy-terminus of ERp57 (Pollock et al., 2004). The crystal structure of the noncatalytic domains (**b** and **b'**) of ERp57 was published recently which revealed a conserved basic patch of residues in the **b'** domain as the site of calnexin interaction (Kozlov et al., 2006). The NMR structure of the calreticulin P-domain (from rat) has also been studied in detail. This P-domain has a hairpin fold that involves the entire polypeptide chain, with the two chain termini in close spatial proximity, to avoid folding back on itself (Ellgaard et al., 2001). Site-directed mutagenesis has been used to map amino acid residues that are critical for calreticulin function. This recent study has identified four amino acid residues (Glu^{239}, Asp^{241}, Glu^{243}, and Trp^{244}) at the tip of the 'extended arm' of the P domain which are crucial for the formation of a calreticulin-ERp57 complex (Martin et al., 2006). The three dimensional structure of the ER lumenal portion of calnexin has been solved to 2.9 Å which revealed an extended 140 Å β-sandwich arm, including two proline-based motifs, topped with a globular lectin domain. The structure of calnexin is ideally positioned for substrate proteins to interact with ERp57 (Schrag et al., 2001).

Calnexin and calreticulin are sometimes thought of as interchangeable proteins that perform essentially the same function, but calnexin may be able to perform additional tasks by virtue of its transmembrane domain. In particular, calnexin can interact with the tetraspanin glycoprotein CD82 in a transmembrane dependent manner (Cannon & Cresswell, 2001). CD82, a member of the tetraspanin superfamily (Maecker et al.,

1997), is a lymphoid-specific partner of the immune accessory molecules CD4 and CD8. Truncated CD82 molecules lacking one or more transmembrane segments accumulate in the ER and are not transported to the cell surface. This occurs even when CD82 mutants have a properly folded ER lumenal domain, thus ER retention does not necessarily depend on misfolding of lumenal domains. Export of these proteins can be restored by co-expression of the CD82 first transmembrane segment, suggesting that these hydrophobic sequences are important for quality control of CD82. Glycosylated CD82 transiently associates with calnexin (but not with calreticulin), however, the truncated proteins associating with calnexin for an extended period of time imply that calnexin can sense misfolded conformations even within a bilayer (Cannon & Cresswell, 2001).

1.4.2 Calnexin/Calreticulin involvement in non-glycosylated protein folding

In contrast to glycosylated proteins, less is known about the quality control of non-glycosylated proteins. Diseases associated with the ER retention of membrane and secretory proteins (not all of which are glycosylated, e.g. Perlizaeus–Merzbacher disease) highlight the importance of understanding the molecular mechanisms that underlie the quality control of glycosylated as well as non-glycosylated proteins (Brooks, 1997). Calnexin and calreticulin have been shown to bind and promote folding of non-glycosylated proteins, presumably through protein-protein interactions. Most of the evidence for these interactions comes from *in vitro* studies or using drug treatments to inhibit glycosylation artificially (Danilczyk & Williams, 2001; Ihara et al., 1999; Saito et al., 1999). A recent *in vivo* study using proteolipid protein (PLP), a multi-membrane spanning, non-glycosylated ER protein suggests that calnexin contributes directly to ER quality control of PLP (Swanton et al., 2003). PLP is

expressed mainly by oligodendrocytes and Schwann cells, and is a major component of myelin. Naturally occurring mutations in the PLP sequence are associated with diseases including Perlizaeus–Merzbacher disease (PMD) and a milder form of this disorder known as spastic paraglegia type 2 (SPG2) (reviewed in (Inoue, 2005)), which cause the misfolded mutant protein to be retained in the ER, indicating it is recognised by the ER quality control system (Gow & Lazzarini, 1996; Koizume et al., 2006). Results from this *in vivo* study show that calnexin, but not calreticulin, is able to bind to newly synthesised PLP as well as to misfolded mutants of PLP through their transmembrane domain and that this interaction with calnexin inhibits the degradation of misfolded PLP (Swanton et al., 2003). Although the molecular details of how calnexin interacts with PLP (and CD82) need to be investigated further, it would be no surprise if calnexin is found to be important for the quality control of other multi-membrane spanning non-glycosylated proteins.

1.4.3 Other quality control checkpoints

The calnexin cycle is not the only quality control system in the ER. Other decisions must be made and check points passed for a protein to reach its final destination. The assembly of cargo at the correct ER exit point(s) has been intensively worked on in yeast and in mammalian cells (Watanabe & Riezman, 2004). For misfolded, membrane spanning proteins it appears that there are at least two check points that have to be passed. The first checkpoint examines the cytosolic domain, and if it is misfolded the protein is retained in the ER and degraded. Proteins passing this first test face a second checkpoint, which monitors the status of lumenal domains (Vashist & Ng, 2004). Once proteins (soluble and membrane) pass through these and possibly other ER checkpoints,

non-ER proteins are transported to the Golgi where they face another checkpoint and eventually transported to their site of function once deemed fully folded.

1.5 Role of Ca^{2+} and Zn^{2+} in the ER

Another area that should not be overlooked is the role ions and small molecules play in the ER. Optimal calcium concentrations are necessary for protein folding (Ashby & Tepikin, 2001) and is also important for the function of calcium dependent proteins like calnexin and calreticulin. Ca^{2+} is released from the endoplasmic reticulum and the sarcoplasmic reticulum (SR, for a recent review (Rossi & Dirksen, 2006)) via three types of channels; inositol 1,4,5-trisphosphate receptors (IP_3R), ryanodine receptors (RyR) and SCaMPER (sphingolipid Ca^{2+}-release-mediating protein of endoplasmic reticulum) (reviewed in (Berridge et al., 1999)). Intracellular Ca^{2+} waves were initially seen in *medaka* eggs (Ridgway et al., 1977) and later in *Xenopus laevis* oocytes (Lechleiter et al., 1991), hepatocytes (Nathanson et al., 1994) and pig articular chondrocytes (D'Andrea & Vittur, 1995) among others. Ca^{2+} oscillations in *Xenopus* oocytes are triggered by opening of the inositol 1,4,5-trisphosphate receptor (IP_3R) whereas re-uptake in to the ER lumen is mediated by sarco ER calcium ATPases (SERCAs) (Camacho & Lechleiter, 1993; Falcke et al., 2003). Calnexin and calreticulin are found to inhibit Ca^{2+} oscillations in a *Xenopus* oocyte system (Camacho & Lechleiter, 1993; Roderick et al., 2000). Calreticulin interacts with the C-terminal sequence of SERCA 2b and is also involved in recruiting ERp57, which can interact with the two conserved cysteines found in the longest ER facing loop 4 (L4) of SERCA 2b (Li & Camacho, 2004). The authors suggest that the classical calnexin-calreticulin cycle works in parallel with calnexin-calreticulin and SERCA to maintain optimum Ca^{2+} levels to promote proper glycoprotein folding (Li & Camacho, 2004). Another

important cation in the ER is zinc. Certain ER chaperones can depend on Zn^{2+} for their function, including the bacterial Hsp40 homologue, DnaJ and the ER-localised yeast homologue Scj1p (Szabo et al., 1996; Linke et al., 2003; Silberstein et al., 1998). In the bacterial cytoplasm, DnaJ cooperates with the Hsp70 homologue DnaK and the nucleotide exchange factor GrpE in recognising polypeptides in their extended conformation, preventing protein misfolding prior to completion of translation (Houry, 2001). It has also been shown that in yeast Msc2p, a member of the cation diffusion facilitator (CDF) family, is responsible for transporting of Zn^{2+} into the ER lumen (Ellis et al., 2004). Depletion of Zn^{2+} induces an unfolded protein response (UPR) in *S. cerevisiae* and mammalian cells, which indicates the importance of this metal ion in maintaining ER function (Ellis et al., 2004). More recently, Msc2p was found to form a heteromeric zinc transport complex with another CDF family member, Zrg17, in the ER membrane (Ellis et al., 2005). The mammalian homologues of Msc2p and Zrg17 were also found to functionally interact, suggesting heteromeric complex formation to be an evolutionary important concept within this metal ion transporter family (Ellis et al., 2005).

1.6 ERAD

Until recently it was thought that misfolded proteins get degraded within the ER (reviewed in (Fra & Sitia, 1993)), but this view has changed to the currently held concept that misfolded proteins are translocated back into the cytosol and degraded by the 26S proteasome through ER-associated degradation (ERAD) (for a recent review (Kostova & Wolf, 2003)). Interaction with EDEM (ER degradation enhancing 1,2-mannosidase like protein) proteins is thought to release misfolded glycoproteins from the calnexin/calreticulin cycle (Molinari et al., 2003; Oda et al., 2003). In *S. cerevisiae*,

trimming of the terminal mannose residue gives rise to $Man_8GlcNAc_2$ (M8, Figure 1.3) thought to be the glycan signal for binding to EDEM (Jakob et al., 1998). Recently however, Frenkel and colleagues have used the model ERAD substrates ASGRP (asialoglycoprotein receptor) H2a and unassembled CD3δ, to show that mannose trimming can give rise to $Man_6GlcNAc_2$ (M6) and $Man_5GlcNAc_2$ (M5) structures in mammalian cells (Frenkel et al., 2003). These trimmed N-glycans do not have the terminal mannose residue recognised by UDP-glucose:glycoprotein glycosyltransferase (GT). This enables the proteins to escape re-entering the calnexin/calreticulin cycle thus providing a potential mechanism for targeting misfolded proteins for proteasomal degradation (Frenkel et al., 2003). Several other structures have also been shown to act as a glycan signal including $Glc_1Man_7GlcNAc_2$, $Glc_1Man_8GlcNAc$ and $Man_{5-7}GlcNAc$, (Kitzmuller et al., 2003; Hosokawa et al., 2003; Hirao et al., 2006).

Three EDEM proteins have been characterised from mouse (Hirao et al., 2006; Olivari et al., 2005; Hosokawa et al., 2001) and humans (Mast et al., 2005), but so far only EDEM3 is found to stimulate mannose trimming showing α1,2-mannosidase activity *in vivo* (Hirao et al., 2006). However, all three EDEM proteins are able to accelerate ERAD of misfolded glycoproteins, indicating that the mechanisms that underlie their action are likely to be different. Although trimming of N-glycans is the main mechanism for targeting misfolded proteins for degradation, BiP (Plemper et al., 1997), PDI (Tsai et al., 2001) and Eps1p (Wang & Chang, 2003) have also been found to play a key roles in retrograde transport to the cytosol. Retro-translocation of ERAD substrates involves a number of components including a dislocation channel, ubiquitin ligases, AAA ATPase (Cdc48p in yeast and p97 in mammals), and for membrane

extracted substrates accessory factors such as Rad23p and Dsk2p (for a recent review (Meusser et al., 2005)).

The protein conducting channel Sec61p was initially suggested to be involved in the retro-translocation of misfolded proteins by Wiertz and colleagues (Wiertz et al., 1996). They showed that in HCMV (human cytomegalovirus) infected mammalian cells ($US2^+$ cells), the viral ER resident protein US2 targets MHC class I heavy chains (HC) for proteasomal degradation via the Sec61 complex. In a subsequent study, genetic evidence to support the role of Sec61p as a retro-translocation pore came with the isolation of two cold-sensitive mutants of *sec61* (*sec61-32* and *sec61-41*) (Pilon et al., 1997). At 24°C pΔgpαf, the non-glycosylated and misfolded form of the mating phereomone precursor prepro-alpha-factor (ppαf) was found associated with Sec61p in *sec61* mutant membranes (Pilon et al., 1997). Another protein suggested to form the dislocation pore is the yeast protein Der1p (Knop et al., 1996) and its mammalian homologue Derlin-1 (Ye et al., 2004). Derlin-1 was found to interact with the HCMV viral protein US11 and a novel membrane protein VIMP (VCP-interacting membrane protein) during export of MHC class I HC to the cytosol (Ye et al., 2004). Derlin-1 interaction with VIMP is via the ATPase p97, which recognises poly-ubiquitinated proteins (Jarosch et al., 2002) and acts to extract misfolded glycoproteins from the ER membrane (for a recent review (Meusser et al., 2005)). The cytosolic C-terminus of Derlin-1 was recently found to interact with the N-terminus of the deglycosylating enzyme peptide:N-glycanase (PNGase) (Katiyar et al., 2005), showing that for a subset of glycoproteins interacting with Derlin-1, retro-translocation could be coupled to the subsequent steps leading to proteasomal degradation. In a recent study, Derlin-2 and Derlin-3 have been shown to provide the missing link between EDEM and p97 (Oda et al., 2006). Whereas Derlin-1 has not been found to associate with EDEM or the

degradation substrate (the null Hong Kong (NHK) mutant of α1-proteinase inhibitor (α1-PI)), Derlin-2 and -3 do form this complex (Oda et al., 2006). All three Derlin proteins are targets of the IRE1-XBP1 pathway.

1.7 Disulfide bond formation

Disulfide bond formation is a vital part of the protein folding process in the ER (Tu & Weissman, 2004). A disulfide bond is a covalent modification that brings two cysteine residue sulfhydryls together to form a disulfide bridge. This bridge can be either intermolecular (between two cysteine residues in two different polypeptide chains) or intramolecular (between two cysteine residues in the same protein). Disulfide bridges are required for structural stability and enzymatic function, as well as for regulation of protein activity (Ellgaard et al., 1999), and can be formed co-translationally during protein folding in the ER (Bergman & Kuehl, 1979a; Bergman & Kuehl, 1979b; Peters & Davidson, 1982; Bergman & Kuehl, 1979a).

Disulfide bonds are found mostly in secreted and membrane proteins folded in the ER. But there are some important examples of cytosolic proteins like molecular chaperones (HSP33) and transcription factors (OxyR and YAP1) that are subjected to regulated disulfide bond switching (Linke & Jakob, 2003). Thiol-based regulatory switches play central roles in cellular responses to oxidative stress, nitrosative stress, and changes in the overall thiol-disulfide redox balance (Paget & Buttner, 2003). The yeast transcriptional regulator protein Yap1p, which resides in the cytoplasm, requires disulfide bond formation in its N-terminal cysteine rich domain and/or C-terminal cysteine rich domains to accumulate in the nucleus upon oxidative stress (Kuge et al., 1997), in order to induce expression of genes that encode antioxidant proteins (Kuge et

al., 1997; Coleman et al., 1999). A mammalian neuronal cell line HT22 has been used to identify disulfide-bonded proteins (DSBP) after exposure to various oxidative insults. This revealed that disulfide bond formation within families of cytoplasmic proteins is dependent on the nature of the oxidative insult and might provide a common mechanism used to control multiple physiological processes (Cumming et al., 2004).

1.7.1 The role of glutathione in disulfide bond formation

Glutathione is a tripeptide (L-γ-glutamyl-L-cysteinyl-glycine) that is synthesised in the cytosol from the precursor amino acids glutamate, cysteine and glycine and is a ubiquitous molecule produced in all organs, especially the liver (Meister & Anderson, 1983; Ziegler, 1985; Pastore et al., 2003). In the 1960s, Anfinsen and colleagues showed that disulfide bond formation in proteins occurred spontaneously *in vitro* (Anfinsen et al., 1961). These studies led to the long-held assumption that disulfide bond formation was spontaneous *in vivo*. However, *in vivo* disulfide-linked protein folding was a slow process and the discovery of PDI a few years later (from rat liver, (Goldberger et al., 1963)) hinted at this process being enzyme assisted. It was almost thirty years later with the discovery of *dsbA* mutant cells in *Escherichia coli* which secrete proteins (including beta-lactamase and alkaline phosphatase) lacking disulfide bonds, that it was confirmed that disulfide bond formation was in fact a catalysed process *in vivo* (Bardwell et al., 1991).

In eukaryotes, before the discovery that Ero1 oxidises PDI, oxidised glutathione (GSSG) was commonly thought to provide oxidising equivalents for the formation of disulfide bonds. This assumption was based on a study by Hwang and colleagues who measured the ratio between oxidised (GSSG) and reduced (GSH) glutathione within the

secretory pathway using a thiol tetrapeptide (NYTC; N Acetyl-Asn-Try-Thr-Cys-NH_2) (Hwang et al., 1992). The study showed that the ratios changed between 30-100 GSH: 1 GSSG in the cytosol to 3 GSH: 1 GSSG in the secretory pathway (Hwang et al., 1992). This initial work did not, however, measure absolute concentrations or determine glutathione ratios in the ER lumen. More recently, absolute glutathione concentrations have been measured using the thiol-specific probe monobromobimane (mBBr) in rat liver microsomes (Bass et al., 2004), but glutathione can still leak during microsome isolation providing only an approximate ratio between GSH and GSSG (3:1). Taken together the results do show that the ER is more oxidising than the cytosol and has ratios similar to that found in redox buffers optimum for *in vitro* oxidative protein folding.

Ero1 can drive the oxidation of substrates *in vitro* and *in vivo* through PDI in the absence of GSH or GSSG (Frand & Kaiser, 1998; Frand & Kaiser, 1999; Pollard et al., 1998; Tu et al., 2000), or even in the presence of excess GSH (Tu et al., 2000), indicating that the process of disulfide bond formation can occur independently of GSSG. Recent work in mammalian cells, however, shows that glutathione still has an important role to play in the ER. Lowering intracellular GSH levels using specific inhibitors of GSH synthesis caused an acceleration in disulfide bond formation in model proteins such as tPA (tissue-type plasminogen activator) but the majority of these disulfide bonds were non-native and needed to undergo isomerisation to achieve the native state (Chakravarthi & Bulleid, 2004). In microsomes derived from HT1080 cells, the oxidoreductase ERp57 is reduced by GSH in a cytosol-dependent manner and biotinylated glutathione is found in mixed disulfide with ERp57 (Jessop & Bulleid, 2004). The importance of a reducing cytosol for the oxidative function of the ER was also shown by Molteni and colleagues using a semi permeabilised cell system (Molteni

et al., 2004). Correct disulfide bond formation thus requires both Ero1 and GSH, with GSH controlling the reductive pathway of the endoplasmic reticulum, rather than the oxidative pathway (Chakravarthi & Bulleid, 2004). Under steady state conditions more than half of the glutathione in rat liver microsomes exists as mixed disulfides with ER resident proteins (Bass et al., 2004), but whether this pool is a major player in the bigger scheme of *in vivo* disulfide bond formation is yet to be determined.

Another potential role for glutathione is during oxidative stress. Disulfide bond formation in the ER of both yeast and mammalian cells can lead to the formation of reactive oxygen species (ROS) (Harding et al., 2003; Haynes et al., 2004). In *S. cerevisiae*, HIP (Hrd1p-independent proteolysis)-deficient cells (*erv29Δ*) are unable to remove misfolded proteins from the ER (Haynes et al., 2002) and thus show increased sensitivity to ER stress and accumulation of ROS (Haynes et al., 2004). Overexpression of CPY* (a mutant misfolded form of protein carboxypeptidase Y) in *erv29Δ* cells causes accumulation of ROS and inhibition of cell growth, but addition of GSH to the growth medium allows these cells to grow by lowering the levels of ROS (Haynes et al., 2004). Studies from both yeast and mammalian cells have shown that the response to an increase in oxidative stress is a rise in the levels of glutathione, which can be used to eliminate ROS and aid in disulfide bond formation. The emerging picture from all these studies is that glutathione plays a key role in allowing native disulfide bonds to form as well as to protect cells during oxidative stress (for a recent review see (Chakravarthi et al., 2006)).

1.7.2 The role of PDI in disulfide bond formation

PDI has a domain architecture that is based on the prototypical cytoplasmic redox protein thioredoxin (Darby et al., 1996). Limited proteolysis (Darby et al., 1996; Freedman et al., 1998; Freedman et al., 1994) was used to identify the four structural domains of PDI, **abb'a'** (Figure 1.4). The **a** and **a'** domains each contain one catalytically active WCGHC motif, while the **b** and **b'** domains are redox inactive (Farquhar et al., 1991; Kemmink et al., 1997). The high redox potentials for the **a** and **a'** domains of PDI were initially measured in a glutathione redox buffer by measuring the free –SH groups in PDI after alkylation with iodoacetate (~ -175 mV from calf liver PDI) (Lundstrom & Holmgren, 1993). Similar redox potentials were reported recently with yeast PDI (- 188 mV for **a** domain, -152 mV for **a'** domain) (Tian et al., 2006). The PDI redox potentials were in-between the strongest oxidant, DsbA (- 120 mV (Zapun et al., 1993)) and the strongest reductant, thioredoxin (-270 mV (Aslund et al., 1997)), which indicated the ability of PDI to catalyse both oxidation and reduction of disulfide bonds. The **b** and **b'** domains show significant sequence similarity to each other and although their amino acid sequences do not show significant similarity to other members of the thioredoxin family, NMR studies have shown the **b** domain to contain a thioredoxin fold (Kemmink et al., 1997). The **b'** domain provides the primary peptide-binding site, but does require the assistance of the other domains especially during binding of larger substrates like non-native proteins (Klappa et al., 1998; Darby et al., 1998). The refolding activity of the **b** domain was investigated recently using truncated variants of yeast PDI, which showed that deletion of the **b** domain did not greatly influence the refolding of rRNase (reduced ribonuclease) but did decrease the rate of refolding of sRNase (scrambled ribonuclease) (Tian et al., 2006). The data so far suggests that the **b** domain may have a structural role in PDI rather than a catalytic role

(reviewed in (Ellgaard & Ruddock, 2005)), but may also contribute to the refolding rate in selected substrates (Tian et al., 2006). The C-terminal domain (**c**) is acidic and harbours the KDEL ER retention sequence. The existence of an inter-domain linker (x, Figure 1.4) region (19 amino acid residues) between **b'** and **a'** domains was experimentally confirmed by Pirneskoski and colleagues using **b'** and **b'**x constructs from human PDI (Pirneskoski et al., 2004). The physiological importance of having this x region is to be determined.

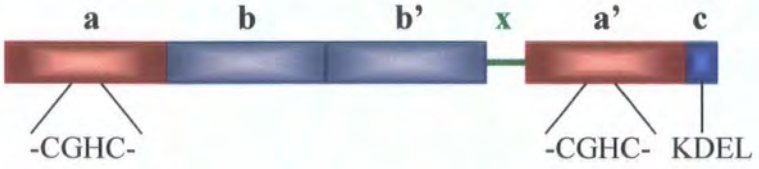

FIGURE 1.4: Domain structure of PDI

PDI is composed of four thioredoxin like domains; **a**, **a'**, **b** and **b'**. Of these **a** and **a'** domains contain the catalytically active thioredoxin motif Cys-Gly-His-Cys, whereas the **b** and **b'** are non-catalytic domains. The **c** region is made up of mainly acidic amino acids and contains the -KDEL ER retention motif whereas the **x** region is a linker between the **b'** and **a'** domains. Adapted and modified from (Freedman et al., 2002).

NMR spectroscopy had been used to determine the individual **a** and **b** domain structures of human PDI but it was only in early 2006 that the first full length PDI crystal structure (to 2.4 Å resolution) was published (Tian et al., 2006). This yeast PDI (Pdi1p) crystal structure revealed that the four thioredoxin domains are arranged in the shape of a twisted 'U' with the active sites facing each other. The crystal structure supplements most of the earlier biochemical data, for example by showing the presence of a highly hydrophobic pocket in the **b'** domain for substrate binding and the detection of a disulfide bridge only between the two cysteines at the **a** and not the **a'** domain (Tian et al., 2006). I272 of human PDI was recognised as an essential residue for substrate binding (using Δ-somatostatin, mastoparan and sRNase) by Pirneskoski and colleagues (Pirneskoski et al., 2004) and has been mapped to the bottom of the hydrophobic pocket in the **b'** domain in the yeast PDI crystal structure, confirming previous mutational data (Tian et al., 2006). A 17 residue connection with a mostly extended conformation corresponding to the x linker region between the **b'** and **a'** domains was confirmed in the crystal structure (Tian et al., 2006). Activity assays carried out with RNase demonstrated that the full length PDI, including the C-terminal tail, is required for full catalytic activity (Tian et al., 2006).

In yeast, Pdi1p is required for oxidation and isomerisation of disulfide bonds. The precise contribution Pdi1p makes to oxidation and isomerisation has been open to debate. Initially using active site mutants of Pdi1p, it was claimed that isomerisation was the essential function of Pdi1p (Laboissière et al., 1995). However, Pdi1p deficient yeast can be reconstituted with an inducible active site **a** domain construct essentially lacking isomerase activity (Solovyov et al., 2004). This module restores both viability and oxidative protein folding to the Pdi1p deficient yeast. These results suggest that

oxidation, rather than isomerisation, is the essential activity of Pdi1p, although both oxidation and isomerisation reactions are likely to be undertaken by Pdi1p *in vivo*.

Work in mammalian cells suggest that PDI is at least partly oxidised, which supports its role as a primary protein oxidant (Mezghrani et al., 2001). A more recent study by Jonathan Weissman and colleagues shows an asymmetry in the rate of oxidation of the two active sites in full length PDI molecules (Kulp et al., 2006). Two active site mutants of PDI were constructed with either the pair of cysteines in the **a** domain active site ($\mathbf{a}_{AXXA}\mathbf{a'}_{CXXC}$) or the **a'** domain active site ($\mathbf{a}_{CXXC}\mathbf{a'}_{AXXA}$) mutated to alanines. The Ero1p oxidative folding pathway was reconstituted using purified Ero1p, FAD, RNAase (Tu et al., 2000) and the oxidase and isomerase activity of the two PDI mutants monitored by using the artificial substrate cCMP (Kulp et al., 2006). Data shows that the C-terminal active site is a disulfide oxidase compared to the disulfide isomerase activity at the N-terminus (Kulp et al., 2006). This asymmetry in active sites is only observed in the context of the full length PDI protein, indicating that the specific order of thioredoxin domains in PDI is important in allowing the **a** and **a'** domains to serve as an isomerase and an oxidase, respectively (Kulp et al., 2006).

PDI is a multifunctional protein that, besides its oxidoreductase activity, can also act as a chaperone to facilitate the folding of proteins devoid of disulfide bonds (Wang & Tsou, 1993). It is able to recognise terminally misfolded proteins, targeting them to proteasomal degradation thus acting as a component of the quality control machinery in the ER (Gillece et al., 1999). PDI is also involved in forming a multi-protein complex in the assembly and retention of procollagen (Bottomley et al., 2001). PDI is required for the export of cholera toxin (Tsai et al., 2001) and Pseudomonas exotoxin A (PE) (McKee & FitzGerald, 1999) from the ER to the cytosol, and for the reduction of ricin

toxin prior to export to the cystoplasm (Spooner et al., 2004). In addition, PDI constitutes the β subunit of prolyl-4-hydroxylase tetramer (P4H, $\alpha_2\beta_2$) (Koivu et al., 1987; Wilson et al., 1998; Myllyharju, 2003) and is a component of the microsomal triglyceride transfer protein complex (Wetterau et al., 1990). Within the P4H tetramer PDI plays a role in retaining the insoluble α subunit in a soluble, active conformation as well as in localising the tetramer within the ER (Vuori et al., 1992a; Vuori et al., 1992b). A recent study has shown that cooperativity between three PDI domains, **a**, **b'** and **a'**, is needed for efficient tetramer assembly, whereas mutations in **b'** domain residues important for peptide binding do not prevent tetramer assembly or reduce P4H enzyme activity (Koivunen et al., 2005). PDI is also found to prevent neurotoxicity associated with ER stress and protein misfolding, a protective role that is inhibited through S-nitrosylation (transferring of NO groups to **a** and **a'** cysteine thiols) in neurodegenerative diseases like Alzheimer's and Parkinson's disease (Uehara et al., 2006).

PDI is not the only protein disulfide isomerase in the ER. In yeast, Pdi1p homologues include Mpd1p, Mpd2p, Eug1p and Eps1p. To some extent the functions of these proteins are overlapping and redundant, although Mpd1p is the only homologue capable of performing all the essential functions of Pdi1p (Norgaard et al., 2001). Eps1 is unusual in that it is membrane associated, and has been implicated in the quality control and trafficking of the yeast H^+-ATPase Pma1p. Eps1p is required for Pma1p cell surface expression (Wang & Chang, 1999). PDI-family members identified so far in humans include ERp57, ERp44 and ERp72; these and other family members are described in a recent review by Ellgaard and Ruddock (Ellgaard & Ruddock, 2005). ERp57 can catalyse oxidation, reduction and isomerisation reactions *in vitro* (Frickel et al., 2004) and is an important component of the calnexin/calreticulin cycle as discussed

in section 1.4.2. Both PDI and ERp57 were found to form transient complexes with two viral glycoproteins, E1 and p62, in Semiliki Forest virus infected CHO cells, but calnexin and calreticulin were only found in ternary complexes with ERp57 (Molinari & Helenius, 1999). ERp57 is also a component of the MHC class I loading complex (Cresswell et al., 1999) but whether it is involved in oxidation, isomerisation or reduction reactions within the complex was unclear (Dick et al., 2002) until a recent study by Zhang and colleagues (Zhang et al., 2006; Solda et al., 2006). They showed that depletion of ERp57 using siRNA in mouse L cells slowed down the formation of the second disulfide bond in MHC class I HC but did not greatly affect peptide loading of class I molecules, indicating the importance of ERp57 in *in vivo* disulfide bond formation (Zhang et al., 2006). In addition, ERp57 was recently shown to play a crucial role in post translational disulfide bond reshuffling during influenza virus hemagglutinin (HA) folding to attain its native conformation (Solda et al., 2006).

ERp44 lacks the C-terminal active site cysteines, but the N-terminal active site cysteines are involved in the ER retention of Ero1 and nascent secretory proteins (Anelli et al., 2002; Anelli et al., 2003). ERp44 was recently shown to be involved in Ca^{2+} signalling (Higo et al., 2005). Inositol 1,4,5-trisphosphate receptors (IP_3R) are Ca^{2+} releasing channels on the ER that play a major role in generating complex Ca^{2+} signalling patterns (reviewed in (Patterson et al., 2004)). ERp44 was shown to interact with the third lumenal loop of IP_3R (IP_3R1) and is thought to act as an ER Ca^{2+} sensor contributing to regulating intralumenal and cytosolic Ca^{2+} concentrations (Higo et al., 2005). The function of the non-thioredoxin-like C-terminal two thirds of ERp44 is still unknown. Less is known about the function of ERp72, other than that it can be selectively found in certain chaperone/substrate complexes, for example in the folding of thyroglobulin (Sargsyan et al., 2002), and in mediating ER retention of misfolded

transmembrane proteins like low density lipoprotein receptor (LDLR) (Sorensen et al., 2006), misfolded secretory proteins like matrilin-3 (MATN3) (Cotterill et al., 2005) and a mutant form of thyroglobulin (cogTg) as well as toxins like cholera toxin (CT) (Forster et al., 2006).

During the past few years several new PDI family members have been reported including, ERp18 (Alanen et al., 2003), ERp46 (Knoblach et al., 2003), ERdj5 (Cunnea et al., 2003), thioredoxin-related transmembrane protein 2 (TMX2 (Meng et al., 2003)), TMX3 (Haugstetter et al., 2005) and PDILT (van Lith et al., 2005), all of which have a wide range of domain architectures and active site motifs (for a recent review (Ellgaard & Ruddock, 2005)). Of these new PDI members, ERp18 possesses the ability to catalyse thiol-disulfide exchange reactions (Alanen et al., 2003). The newest member to join the PDI family is the two domain (**b** and **b'**) ER resident protein ERp27, which lacks a C*XX*C active site making it a non-catalytic family member unable to catalyse thiol-disulfide reactions (Alanen et al., 2006). However, unlike other non-catalytic PDI family members (e.g. ERp29), ERp27 does not seem to follow the general pattern of having one thioredoxin fold domain and one α-helical domain. Instead it has two thioredoxin domains, which the authors suggest could form a novel sub-family within the PDI family (Alanen et al., 2006). ERp27 interacts with ERp57 using the same site on the ERp57 **b'** domain utilized by calnexin and calreticulin, suggesting that ERp57 is unlikely to bind both ERp27 and calnexin/calreticulin together. Identifying the specific substrates of ERp27 and ERp57 could shed more light on the mechanism of action for these proteins (Alanen et al., 2006).

1.7.3 Prokaryotic disulfide bond formation/isomerisation

In prokaryotes, there are two well established pathways, the oxidative pathway which is involved in the formation of disulfides, and the isomerisation pathway, which shuffles incorrectly formed disulfides (Figure 1.5, reviewed in (Collet & Bardwell, 2002; Kadokura et al., 2003)). Disulfide bonds are donated directly to unfolded polypeptides by DsbA; DsbA gets reoxidised by DsbB (Bardwell et al., 1993). Beckwith and colleagues used a DsbA mutant that altered the *cis* proline-151 residue, to capture mixed disulfide complexes between DsbA and its substrates *in vivo* to identify potential substrates of DsbA (Kadokura et al., 2004). DsbB generates disulfides from oxidised quinones, which get reoxidised by the electron transport chain (Kobayashi & Ito, 1999). In the isomerisation pathway, the two isomerases DsbC (Zapun et al., 1995) and DsbG (Andersen et al., 1997; Bessette et al., 1999), are kept reduced and thus in their active form by the membrane protein DsbD. DsbD is kept reduced by cytosolic thioredoxin in an NADPH-dependent reaction (Rietsch et al., 1997). Although questions have been answered as to the importance of these pathways in bacteria, numerous questions still remain unanswered including how DsbB utilises quinones as mobile electron carriers and if DsbA and DsbC show specificity in the types of substrates they use (Kadokura et al., 2003).

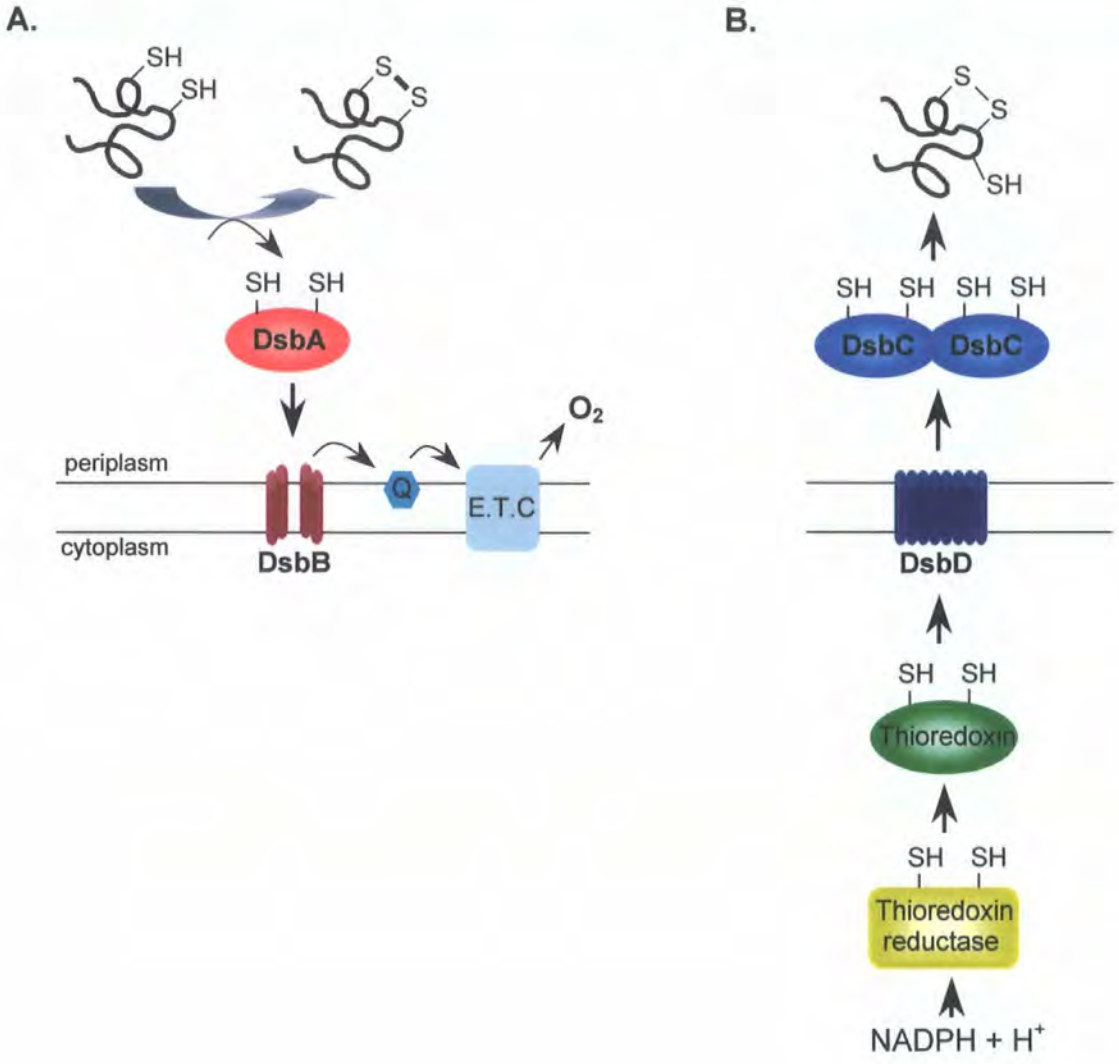

FIGURE 1.5: Disulfide bond formation, isomerisation and reduction pathways in prokaryotes

A. Substrate proteins are oxidised in the bacterial periplasm through a thiol-disulfide exchange reaction with DsbA. DsbA is reoxidised by the cytoplasmic membrane protein DsbB, which in turn transfers electrons to quinones (Q) and via the electron transport chain (E.T.C) to the final acceptor, oxygen. **B.** Disulfide bond isomerisation in the periplasm is catalysed by the soluble oxidoreductase DsbC, which is kept in a reduced form by the cytoplasmic membrane protein DsbD. DsbD is kept in a reduced form by cytoplasmic thioredoxin, which obtains electrons from NADPH via thioredoxin reductase. Black arrows show the flow of electrons. Adapted from (Sevier & Kaiser, 2006a).

1.7.4 Disulfide bond formation by Ero1 in eukaryotes

In yeast, the essential genes required for the catalysis of disulfide bonds in the ER are ERO1 and PDI (Frand & Kaiser, 1998; Pollard et al., 1998). The gene product, Ero1p, is an ER-resident flavoprotein that uses O_2 as its terminal electron acceptor and passes oxidative equivalents on to Pdi1p (Figure 1.6), the yeast protein disulfide isomerase (Frand & Kaiser, 1999; Tu et al., 2000). A second membrane-associated flavoprotein, Erv2p, was identified recently which can operate in parallel with Ero1p in yeast (Gerber et al., 2001; Gross et al., 2002). Ero1p and Erv2p both directly oxidise PDI, but unlike Ero1p, Erv2p is not essential for cell viability (Sevier et al., 2001). Erv2p a small, largely α-helical dimer contain a tightly bound FAD cofactor adjacent to a C*XX*C motif and a second cysteine pair located on a flexible loop (Gross et al., 2002).

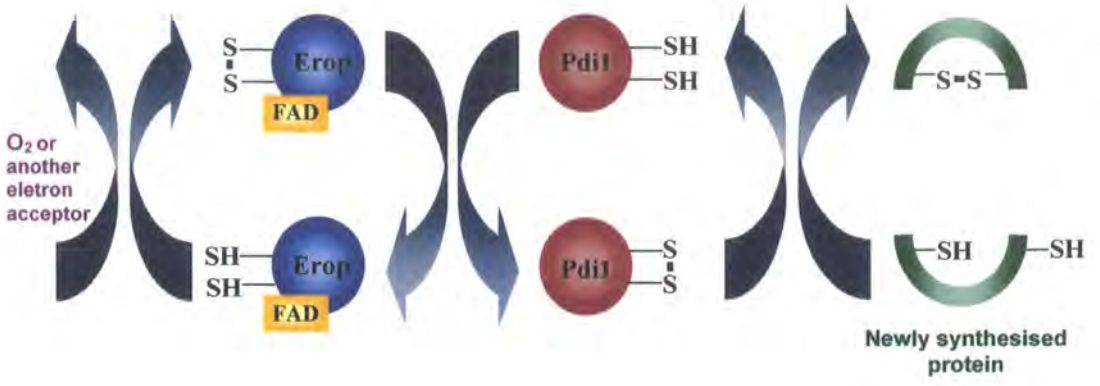

FIGURE 1.6: Oxidising equivalents flow from Ero1p to Pdi1p and target proteins
In *Saccharomyces cerevisiae* (and other eukaryotes) Pdi1p is oxidised through dithiol-disulfide exchange with Ero1p. Proteins folding in the ER requiring disulfide bonds can then be oxidised through thiol-disulfide exchange with Pdi1p. Adapted and modified from (Fassio & Sitia, 2002).

Two clusters of conserved cysteine residues are important for Ero structure and function (Frand & Kaiser, 2000; Benham et al., 2000). Mutational and biochemical studies of the yeast ERO1 gene have shown that the N-terminal active site cysteines are involved in a dithiol-disulfide reaction with PDI. Accepted electrons are then transferred on to the C-terminal active site cysteines that then pass on electrons to molecular oxygen via FAD (Frand & Kaiser, 2000; Tu & Weissman, 2002). The crystal structure of yeast Ero1p was determined recently (Gross et al., 2004) which complimented previous biochemical data and revealed the spatial relationship between the functionally important cysteines and bound cofactor. The *CXXCXXC* motif is in contact with a non-covalently bound FAD molecule and in yeast Ero1p the FAD cofactor is held between helixes α2 and α3 in a bent conformation (Gross et al., 2004). Comparison of the two Ero1p crystal forms revealed a flexible loop containing the C100/C105 disulfide bond which adopts an 'in' and 'out' conformation (Gross et al., 2004). Electrons accepted from PDI by the C100/C105 disulfide bond in the 'out' conformation could shuttle the electrons onto the C352/C355 active site disulfide when in the 'in' conformation.

There are two Ero1p counterparts in mammals, Ero1α and Ero1β (Cabibbo et al., 2000; Pagani et al., 2000). Both hEROs are capable of rescuing the *S. cerevisiae ero1-1* thermosensitive mutant and catalysing the oxidation of model substrates (Mezghrani et al., 2001; Cabibbo et al., 2000; Pagani et al., 2000), indicating that these proteins are involved in disulfide bond formation. Mutational studies at the *CXXCXXC* motif in Ero1α has shown that this active site is important for the folding, structural integrity, as well as the stability of the Ero1α-PDI complex (Benham et al., 2000). Although Ero1α and Ero1β have many similar biochemical properties there are some important

differences between them. At the transcription level, Ero1α and Ero1β mRNAs show some differences in their tissue specific distribution, with Ero1β being noticeably expressed more in secretory tissues such as pancreas, stomach and pituitary gland (Pagani et al., 2000). Ero1β transcript expression can be induced chemically by preventing N-glycosylation and disulfide bond formation, both of which trigger the unfolded protein response (UPR) (Pagani et al., 2000). Ero1α, on the other hand is induced by hypoxia (Gess et al., 2003). Recent evidence examining the disulfide bond rich secreted proangiogenesis factor VEGF (Vascular endothelial growth factor) showed that Ero1α is involved in a HIF-1 (hypoxia-inducible factor-1) mediated pathway used to induce protein secretion under hypoxic conditions (Forsythe et al., 1996; May et al., 2005). May and colleagues found that reducing the level of Ero1α by siRNA significantly inhibited VEGF secretion, compromised proliferation and induced apoptotic death (May et al., 2005). Thus targeting Ero1α expression in tumour cells (where hypoxic conditions prevail) might be a potential therapeutic target for future cancer therapies.

Similar to yeast and animals, higher plants also produce disulfide bonded secretory proteins in the ER. Two Ero1p homologues (AERO1 and AERO2) have been detected in plants (*Arabidopsis thaliana*) (Dixon et al., 2003). The N-terminal C*XXXX*C region of the two AERO proteins were identical (CRLRDC) but were significantly different from yeast and human sequences. At the C-terminus active site, the AERO protein sequences were similar to Ero1β, having a strongly charged C*XX*C*XX*C motif, which was more common among the Ero proteins aligned in this study. Thus the authors suggest the charged β-like C*XX*C*XX*C motif to be the ancestral sequence. Of the two AERO genes, AERO1 has several upstream UPR response elements, indicating that

like mammals plants might also have one inducible oxidoreductase (similar to Ero1β) and a housekeeping oxidoreductase (Dixon et al., 2003). When *in vitro* translated in HT1080 cells, the plant signal sequences were able to target the two AERO proteins to the mammalian ER where they were glycosylated. Plants also encounter different stress conditions (for example anoxic conditions and free radical damage) similar to ER stresses in animals, thus *Arabidopsis* could be used as a potential model in understanding the biochemistry of disulfide bond formation and how a multi-cellular organism has evolved to deal with different oxidative processes under changing conditions (Dixon et al., 2003).

1.7.4.1 Localisation of EROs in the ER

Ero1α and Ero1β both lack a known ER localisation motif, making it unclear how these hEROs are retained in the ER lumen. Yeast Ero1p has a C-terminal tail of 127 amino acids that enable this protein to be localised in the ER (Pagani et al., 2001). Mutant Ero1pΔC (Ero1p lacking the C-terminal tail) and Ero1α, when expressed in yeast cells with the endogenous ERO gene disrupted (ΔERO1), behave like soluble proteins and fail to complement ΔERO1 cells (Pagani et al., 2001). This was somewhat surprising since biochemical analysis has shown that hEROs are closely associated with ER membranes in human cells (Pagani et al., 2000). *In vitro* translated hEROs in presence of semi permeabilised (SP) HT1080 cells, were used in extraction experiments at pH 11 and pH 13. Membrane associated proteins like calreticulin are partially extracted from the membranes at pH 11, but completely extracted at pH 13. Ero1α and Ero1β behaved similar to calreticulin and thus suggested that the hEROs are soluble proteins that form strong associations with some component of ER membranes. Taken together, the literature suggests that the mechanism which mediates retention of

Ero proteins has diverged from yeast and mammalian cells. More recently Ero1α has been found in mixed disulfide complexes with ERp44. ERp44, a member of the thioredoxin family, is a UPR-induced ER resident protein with an RDEL ER localisation motif (Anelli et al., 2002). ERp44 has been shown to form mixed disulfides with folding intermediates as well as with both hEROs (Anelli et al., 2002; Anelli et al., 2003). Thus covalent interactions between ERp44 and hEROS are likely to contribute to their ER localisation. Another protein that could mediate ER retention of Ero proteins is PDI, as shown through over-expression experiments, probably by virtue of its KDEL motif (Otsu et al., 2006). Further analysis of human EROs will be discussed in the relevant subsequent chapters.

1.8 Aims of this thesis

In yeast, the oxidoreductase Ero1p is involved in disulfide bond formation and the ERO1 gene is found to be essential for cell viability. Of the two human Ero1p homologues, Ero1β has been the main focus of this project. The main objectives of this project were:

- ★ To study the folding pattern, biosynthesis and possible dimerisation of Ero1β.

- ★ To investigate the importance of the Ero1β carboxy-teminal C*XX*C*XX*C active site in PDI interactions and dimer formation.

- ★ To investigate the role of two FAD domain mutants of Ero1β, discovered initially in yeast. The importance of these two mutations was studied in context of their ability to dimerise and interact with PDI, as well as to withstand temperature and various stress conditions.

- ★ To establish the expression pattern of Ero1β and a number of ER chaperone proteins in different secretory human tissues and in tumours of the digestive system.

CHAPTER 2

MATERIALS AND METHODS

2.1 Antibodies and tissues

The polyclonal antiserum against Ero1β was raised against the unique internal Ero1β peptide YTGNAEEDADTKTLL (Sigma Genosys). Thirteen of the fifteen residues were conserved between mouse and human Ero1β. Polyclonal rabbit anti-serum, against PDI was raised against purified rat PDI as described (Benham et al., 2000). αEro1α (D5) was raised in rabbit against reduced, non-reduced and denatured forms of an *E. coli* expressed and purified MBP fusion protein (Mezghrani et al., 2001). The polyclonal PDIp antiserum was a gift from Michael Lan (Desilva et al., 1997), polyclonal anti-ERp57 and anti-ERp72 (used only in immunohistochemistry) were a gift from Prof. Neil Bullied, monoclonal ERp44a (36C9/39) and ERp44b (39E5/39) were a gift from Prof. Roberto Sitia. Polyclonal antisera against BiP and insulin (H-86) (both Santa Cruz), polyclonal antisera against ERp72 (Calbiochem, used in immunoblotting), the mouse monoclonal antibody HA-7 (Sigma, antigen YPYDVPDYA), the anti-Myc antibody clone 9B11 and the anti-Myc polyclonal antibody (antigen EQKLISEEDL, both Cell Signalling) were commercially available. In immunoblotting, the secondary antibodies used were swine anti-rabbit HRP and goat anti-mouse HRP conjugates, both from DAKO. For immunoflouresence, swine anti-rabbit TRITC, donkey anti-rabbit FITC and donkey anti-mouse FITC (all DAKO) were used as secondary antibodies. Normal goat serum was obtained from DAKO and normal rabbit serum (NRS) was obtained from a pre-immune rabbit used to generate the PDI antibody. Murine tissue samples were obtained from male Balb/c or CD1 mice. Anonymous healthy human stomach and pancreas tissue samples and healthy human oesophagus (3396-00 B1), Barrett's oesophagus (6199-02 A2), oesophageal tumour (1039-03 B2), gastroesophageal (OG) junction tumour (6199-02 A4) and gastric tumour (6591-01 C4) tissue were obtained embedded in wax from Medical Solutions,

Nottingham, UK and James Cook University Hospital, Middlesbrough, UK respectively, with full ethical consent.

2.2 Immunohistochemistry

2.2.1 Protocol 1

Paraffin embedded tissues were sectioned at 4 μm thickness onto Apes coated slides and placed at 60°C for 1 hr. The slides were cleared through xylene and 100% - 70% alcohol before blocking endogenous peroxidase activity in 0.5% hydrogen peroxide (BDH) in methanol (Fisher Scientific) for 10 min. Slides were washed in ddH_2O prior to performing four different antigen retrieval techniques.

1. Trypsinisation: sections were pre-heated to 37°C in distilled water and transferred to a freshly prepared pre-heated (36-38°C) trypsin solution (0.2 g porcine pancreatic trypsin to 200 ml of 0.1% $CaCl_2$, pH 7.8) for 5 min.
2. Pressure cooker: in 90 mM citrate buffer (BDH, pH 6.0) for 2 min.
3. Microwave: in 10 mM citrate buffer (BDH, pH 6.0) for 20 min.
4. Microwave: in 600 ml of 1x high pH target retrieval solution (DAKO) for 20 min.

Slides were washed 5 min each, in ddH_2O and TBS (130 mM NaCl, 5 mM Tris pH 7.4) and tissue sections blocked in 1% normal goat serum (DAKO) for 10 min prior to incubating with different primary antibodies at 4°C overnight. Sections were washed in TBS for 5 min, incubated with 0.01% biotinylated goat anti-mouse/rabbit antibodies (DAKO) for 30 min and developed using StreptABComplex/ HRP Duet (DAKO) and diaminobenzidine (DAB, Sigma). Primary and secondary antibodies as well as the

blocking solution was made in TBS. Counterstaining was with haematoxylin.

2.2.2 Protocol 2

Paraffin embedded tissues were sectioned at 4 μm thickness onto polylysine coated slides and placed at 50°C overnight. The slides were cleared through histoclear and 100% - 70% alcohol before blocking endogenous peroxidase activity in 3% hydrogen peroxide (BDH) in methanol (Fisher Scientific) for 10 min. Slides were washed in ddH_2O for 5 min and sections digested in a 90°C water bath with 10 mM citrate buffer for 20 min. After the antigen retrieval technique, the slides were allowed to reach room temperature prior to washing in 0.2% BSA (Sigma) in PBS for 5 min. Tissue sections were blocked in 5% normal goat serum (DAKO) for 30 min and incubated with different primary antibodies for 1 hr. Slides were washed in 0.2% BSA in PBS for 5 min, incubated with 0.01% biotinylated goat anti-mouse/rabbit antibodies (DAKO) for 45 min and developed using StreptABComplex/ HRP Duet (DAKO) and diaminobenzidine (DAB, Sigma). Primary and secondary antibodies as well as the blocking solution were made in 0.2% BSA in PBS. All antibody incubations were at room temperature. Counterstaining was with haematoxylin.

2.3 Molecular Biology

2.3.1 Construction of Ero1β mutants

The wild-type pcDNAEro1β-HA and pcDNAEro1β-Myc constructs were a kind gift from Roberto Sitia. Site directed mutagenesis (Quikchange, Stratagene) was used to create Myc and HA tagged Ero1β mutants with the following forward primers:

C390A:
GAATATCTCCCGTATAATGGACGCTGTTGGATGTGACAAATGCAG

C393A:
GTATAATGGACTGTGTTGGAGCTGACAAATGCAGATTATGGGG

C396A:
GACTGTGTTGGATGTGACAAAGCCAGATTATGGGGAAAATTACAG

G252S:
GAGTCTTCTATAAGCTTATATCGTCACTTCATGCTAGCATCAATTTAC

H254Y:
CTATAAGCTTATATCGGGACTTTATGCTAGCATCAATTTACATCTATG

Each construct was verified by DNA sequencing. Ero1βG252S-HA and Ero1βH254Y-HA mutants were constructed by cloning the appropriate mutation region from the Myc tagged counterparts into the wild-type pcDNAEro1β-HA vector. pcDNAEro1β-HA, Ero1βG252S-Myc and Ero1βH254Y-Myc (3 μg each) were digested with 1.5 μl *NheI* (Promega) at 37°C for 2 hr. The 5' phosphate group from the vector was removed by incubating pcDNAEro1β-HA at 37°C with 2 μl of alkaline phosphatase (Promega) for 30 min. This treatment will prevent self-ligation of the vector and enhance ligation with the insert DNA. The appropriate bands were cut out on a UV illuminator after

separating the vector and the two inserts on a 1% agarose gel (section 2.3.4). DNA was extracted from these bands according to manufacturer instructions using the QIAquick Gel Extraction kit (Qiagen). 1.5 µl of vector was ligated with 12 µl of insert (G252S of H254Y) at 37°C for 1 hr. DH5α competent bacterial cells were transformed using the ligation products as described in section 2.3.3. The Ero1α-Myc tagged constructs have been previously described (Benham et al., 2000).

2.3.2 XL1-Blue transformation

Following site directed mutagenesis, the non-mutated parental DNA template was digested with 1 µl of *Dpn1* restriction enzyme for 1 hr at 37 °C and the mutated plasmid DNA used to transform XL1-Blue supercompetent cells (Stratagene). 1 µl plasmid DNA was mixed with 50 µl bacteria cells and incubated on ice for 30 min. Bacteria were heat shocked at 42°C for 45 sec, incubated on ice for a further 2 min prior to mixing with 500 µl of pre-heated (42°C) NZY broth (10 g/l NZ amine, 5 g/l yeast extract, 5 g/l NaCl, pH 7.5 supplemented with 12.5 mM $MgCl_2$, 12.5 mM $MgSO_4$, 20 mM glucose) at 37°C for 1 hr with constant agitation. Bacteria cells were centrifuged at 800 g (Eppendorf) for 2 min at room temperature and the resuspended bacterial pellets were spread on LB-agar plates (10 g/l tryptone, 5 g/l yeast extract, 10 g/l NaCl, 15 g/l agar) supplemented with 0.1 mg/ml ampicillin and grown overnight at 37°C. Next day, a single colony was inoculated in 5 ml of LB supplemented with ampicillin (0.1 mg/ml), and grown overnight at 37°C with constant agitation. The overnight culture was used to extract plasmid DNA (using the Qiagen MiniPrep according to manufacturer protocol) and mutations were verified by DNA sequencing.

2.3.3 *DH5α transformation*

DH5α competent cells were transformed with the mutant plasmid DNA and used in transfections (section 2.5). For each transformation, 50 µl of DH5α competent cells was mixed with purified plasmid DNA (~1-2 ng) and incubated on ice for 10 min. Bacteria were heat shocked at 42°C for 1.5 min, returned to ice for a further 10 min after which 500 µl of LB was added. Cells were incubated at 37°C for 30 min and centrifuged at 800 g (Eppendorf) for 2 min at room temperature. Resuspended bacteria pellets were spread on LB-agar plates supplemented with 0.1 mg/ml ampicillin and grown overnight at 37°C. A single colony was picked the next day and innoculated overnight (at 37°C with constant agitation) into 100 ml of LB supplemented with 0.1 mg/ml ampicillin. The overnight culture was used to extract plasmid DNA (using Qiagen MaxiPrep kit, according to manufacturer instructions).

2.3.4 *Agarose gel electrophoresis*

Agarose gel electrophoresis was used to separate PCR and restriction digest products. The appropriate amount of agarose (Bioline) was melted in a suitable volume of TAE (20 mM Tris, 0.002% glacial acetic acid, 0.5 mM EDTA, pH 8.0) buffer in a microwave. Ethidium bromide was added to a final concentration of 0.6 mg/ml prior to pouring into a tray to set. The percentage of the gel was decided according to the size of the DNA fragments to be separated. The gel was submerged in TAE buffer and samples were loaded into the wells after mixing 6:1 with 6x loading buffer (15% Ficoll; type 400, Pharmacia, 5 mM EDTA, pH 8.0, 0.25% bromophenol blue). Following electrophoresis, gels were visualised by UV illumination and photographed using a BioRad Gel Doc.

2.4 Cell culture

Human cervical carcinoma HeLa cells were maintained in Minimum essential medium (MEM, Invitrogen) and human fibrosarcoma HT1080 cells were maintained in Dulbecco's modified Eagles's medium (DMEM, Invitrogen), both supplemented with 8% fetal bovine serum (FBS, Sigma), 2 mM glutamax (Invitrogen), 100 units/ml penicillin and 100 µg/ml streptomycin (Invitrogen) at 5% CO_2. Both cell lines were serially passaged at 70-80% confluency using 0.05% trypsin (Trysin-EDTA, Invitrogen) to digest the monolayer.

2.5 Transfection

Transfections with Lipofectamine 2000 (Invitrogen) were performed according to manufacturer's instructions. Sub-confluent cells in 6 cm dishes were washed twice with PBS (Invitrogen), and transfected with 1 or 2 µg DNA for 6 hr in the presence of Optimem serum free medium (Invitrogen). The medium was replaced after 6 hr with complete medium and the cells analysed 24 hrs post-transfection.

2.6 SDS-PAGE and immunoprecipitation

Cells were lysed in lysis buffer (20 mM MES, 30 mM Tris, 100 mM NaCl, pH 7.4) with 1% Triton X-100 (Sigma), supplemented with 10 µg/ml each of chymostatin, leupeptin, antipain and pepstatin A, (CLAP) and 20 mM N-ethylmaleimide (NEM) where required. Nuclei were removed by centrifugation at 16,100 g (Eppendorf) for 10 min at 4°C. Post-nuclear cell lysates, immunoprecipitates or comparable amounts of mouse tissue lysates were taken up in 2x sample buffer ((Laemmli, 1970), 1 M Tris, pH

6.8, 20% SDS, 5% glycerol, 0.01% bromophemol blue), heated at 95°C for 5 min and analysed by SDS-PAGE (resolving gel consists of 8% or 10% acrylamide, 0.375 M Tris (pH 8.8) and 0.1% SDS, 0.1% APS, 0.04% TEMED; stacking gel consists of 5% acrylamide, 0.125 M Tris (pH 6.8), 0.1% SDS, 0.075% APS and 0.075% TEMED; Hoefer system). For non-reducing analysis, DTT was left out of the sample buffer, whereas for reducing conditions, 50 mM DTT was added. Immunoprecipitations (IP) were carried out using 1 µl of monoclonal antibodies or 8 µl of polyclonal antibodies immobilised on 50 µl of a 20 % suspension of Protein A sepharose beads (Sigma) for 2 hr at 4°C, followed by two washes with lysis buffer (without NEM or CLAP). The gel running buffer used was 1x Tris-Glycine SDS running buffer (25 mM Tris, 192 mM glycine, 0.1% SDS, pH 8.6, Sigma).

2.7 Western blotting

Following SDS-PAGE proteins were transferred to PVDF membranes (Millipore) in transfer buffer (190 mM glycine, 25 mM Tris in 20% Methanol) at 150 mA for 2 hrs or 30 V overnight using a Bio-rad powerpack 200. The membranes were blocked in 8% milk/PBST (PBST made up of 1x PBS with 0.001% Tween 20) for 1 hr or overnight. A list of primary antibodies, their host species together with the corresponding dilutions used in immunoblotting is shown in table 2.1. After washing six times with PBST, membranes were incubated with corresponding secondary antibodies (DAKO) at 1:3000 for 1 hr, washed extensively, and visualised by ECL (Amersham) and exposure to film (Kodak). Protein markers were from Biorad.

Table 2:1: List of primary antibodies and dilutions used in immunoblotting

Primary antibody	Host	Dilution
αMyc	Mouse	1:5000
αMyc	Rabbit	1:1000
αHA	Mouse	1:2000
αErolα (D5)	Rabbit	1:1000
αPDI	Rabbit	1:1000
αErolβ	Rabbit	1:50
αCNX	Rabbit	1:1000
αBiP	Rabbit	1:200
αERp72	Rabbit	1:1000

2.8 Determination of protein concentration

Protein concentrations were determined using the Bio-Rad DC protein assay, which is a colorimetric assay compatible with a wide range of detergents based on the Lowry protocol (Lowry et al., 1951). The assay is based on the reaction of protein with an alkaline copper tartrate solution and Folin reagent, which gives a characteristic blue color with a maximum absorption at 750 nm. BSA protein standards from 0.5 mg/ml to 1.5 mg/ml were used to plot a standard curve. The components recommended in the manufactures protocol were scaled down 5 times, and thus 20 µl of standards or samples were mixed with the appropriate volume of reagents. Absorbance was read after 15 min at 750 nm. All samples measured in this assay were in lysis buffer (section 2.6) and thus 20 µl of lysis buffer (without NEM or CLAP) was mixed with the protocol reagents and used as the blank.

2.9 Metabolic labelling and pulse-chase analysis

Subconfluent cells in 6 cm dishes were starved with MEM or DMEM lacking cysteine and methionine (both ICN Biomedicals Inc.) for 40 min, pulse-labelled for the times stated with MEM or DMEM lacking cysteine and methionine supplemented with 10 mM HEPES, pH 7.4 (Invitrogen) and 75 µCi of *in vitro* ^{35}S-labeling mix (GE Healthcare/Amersham) per dish and subsequentely chased when necessary with complete medium supplemented with 5 mM methionine (Sigma), 5 mM cysteine (Sigma), 5% FBS and 10 mM HEPES, pH 7.4.

At given time intervals the chase was stopped with ice-cold HBSS (Invitrogen) supplemented with 20 mM NEM to trap folding intermediates. Cells were lysed in 600

µl of lysis buffer (section 2.6) with 1% Triton X-100, supplemented with 10 µg/ml each of chymostatin, leupeptin, antipain and pepstatin A. Proteins from the lysates were subjected to specific immunoprecipitation after removing the nuclei for 10 min at 4°C and 16,100 g. Unbound proteins were washed off using the wash buffer (30 mM NaCl, 10 mM Tris-HCL, 0.05% Triton X-100, 0.05% SDS, pH 8.6) prior to being taken up in 2x sample buffer. Samples were boiled, reduced with 50 mM DTT where required and analysed by 8% SDS-PAGE.

Gels were fixed in 1x fixing solution (12% w/v trichloracetic acid, 3.5% 5-sulfosalicylic acid; Sigma) for 30 min and washed in ddH_20 before staining with a Brilliant Blue G Colloidal (mixed 4:1 in methanol, Sigma) solution for 1-2 hrs. Gels were then destained with 10% acetic acid in 25% methanol for 60 sec, rinsed twice in 25% methanol, washed for 5 min in PBS and incubated with 0.5 M Na Salicylate in PBS for 15 min to enhance the radioactive signal. Gels were dried down on a gel dryer (Jencons) before exposing to Kodak BioMax MR film at -80°C.

2.10 Immunofluorescence

HeLa cells were grown on 16 mm coverslips until 70-80% confluent and transfected with appropriate DNA constructs (section 2.5). Coverslips were washed twice in PBS fixed in ice cold MeOH for 10 min, washed twice in PBS and blocked in 0.2% BSA (Sigma) for 1 hr. Primary antibodies (αPDI, 1:500 and αMyc, 1:1000) were applied in the presence of 0.2% BSA for 1 hr at room temperature, washed three times in PBS and incubated with fluorescein labelled donkey anti-mouse Ig (FITC) and rhodamine labelled swine anti-rabbit Ig (TRITC) at 1:50 in 0.2% BSA for 1 hr in the dark. Three PBS washes were carried out before mounting the coverslips onto microscope slides

using vectashield (VECTOR) and analysis under a Zeiss Bio-Rad CSM confocal microscope system.

2.11 DTT, Diamide, BSO, H_2O_2 and temperature treatments on living cells

Transfected HeLa cells were washed with PBS (Invitrogen) and incubated with complete medium containing; 10 mM DTT (Sigma) for 15 min; 5 mM DTT for 30 min; 5 mM Diamide (Sigma) for 5 min; 25 μM BSO (buthionine sulphoximine) for 18 hr; 1.5 M H_2O_2 for 10 min or buffer only at 37°C. Transfected HT1080 cells were also incubated with complete medium containing 5 mM DTT for 30 min at 37°C after washing the cells with PBS. For temperature treatment, transfected HeLa cells were incubated at 24°C, 37°C and 42°C on water baths for 1 hr in complete medium buffered with 10 mM HEPES, pH 7.4 (Invitrogen). Cells were washed three times in PBS and lysed as in section 2.6. Post-nuclear supernatants were subjected to analysis by 8% SDS-PAGE (section 2.6).

2.12 Trypsin sensitivity assay

Post nuclear supernatants were incubated in 0, 0.25, 1.25, 2.5 μg/ml TPCK-treated Trypsin (Sigma) for 30 min at 4°C. Proteolytic digestion was terminated by the addition of 200 mg/ml SBTI, in addition to 10 μg/ml each of chymostatin, leupeptin, antipain and pepstatin A. Samples were taken up in 2x sample buffer and analysed by 10% SDS-PAGE (section 2.6).

2.13 Gel Filtration

Gel filtration was performed using a Superdex 200 Precision Column 3.2/30 (Amersham/GE Healthcare). Chicken egg albumin (45 kDa) and BSA (66 kDa, 132 kDa) (both Sigma) were used as standards. Proteins and tissue lysates injected in a volume of 200 µl were eluted with 50 mM Tris-HCl, 150 mM NaCl, pH 7.0, at a flow rate of 0.5 ml min^{-1}, with samples collected every two minutes. Samples were trichloroactetic acid (TCA; Sigma) precipitated as described in section 2.14.

2.14 TCA protein precipitation

Gel filtration sample fractions were mixed 1:1 with 20% trichloroacetic acid (TCA) and incubated for 30 min at 4°C. Samples were centrifuged at 16,100 g for 20 min after which the supernatants were removed leaving an intact protein pellet. The protein pellet was dried, neutralised with Tris and taken up in 2x sample buffer, heated at 95°C for 5 min and analysed by 8% SDS-PAGE (section 2.6).

2.15 Analysis of ER protein products with/without semi permeabilised cells

2.15.1 RNA preparation

DNA (5 µg) was linearised with a restriction enzyme that cut once downstream of the ORF of interest. The restriction enzyme *Eag1* (Promega) was used for Ero1α and *Xho1* (Promega) for Ero1β. Digestion was carried out at 37°C for 2 hr, after which linearisation was confirmed by 1% agarose gel electrophoresis (section 2.3.4). The volume of each digest was brought to 300 µl with 1x TE before phenol/chloroform and

EtOH precipitating the linearised DNA (section 2.15.1.2). The pellet was dissolved in 10 µl of ddH_20 and used for subsequent transcription. Sterile, RNAase free tips and eppendorfs were used during *in vitro* transcription reactions (section 2.15.1.1).

2.15.1.1 In vitro transcription

Transcription was carried out according to the manufacturer protocol (Promega Riboprobe *in vitro* Transcription System) in a total volume of 50 µl (table 2.2) at 37°C for 1 hr using linearised DNA. The DNA template was removed by digesting with 1 unit of RNase-free DNAse for each µg of template DNA at 37°C for 15 min. Transcribed RNA was phenol/chloroform and EtOH precipitated (section 2.15.1.2) and the pellet resuspended in 50 µl of RNase-free water. For long term storage 1 µl of 100 mM DTT and 1 µl of RNAsin was added to the RNA. DNA and RNA concentration was measured using the Bio photometer (Eppendorf) with a UVette (220-1600 nm range; Eppendorf). Absorbance was read at 260 nm and concentrations calculated for dsDNA 1 OD = 50 µg/ml and for RNA, 1 OD = 40 µg/ml.

Table 2.2: *In vitro* transcription reaction components

Components	Volume (µl)
Linearised DNA (5 µg)	10
5x transcription buffer	10
100 mM DTT	5
RNAsin Ribonuclease inhibitor (50 units)	1.2
rNTP mix (with 2.5 mM each of rATP, rGTP, rCTP and rUTP)	5
40 mM m^7G(5') pppG Cap Analog (Ambion)	0.62
T7 RNA polymerase (40 units)	2
Nuclease free water	16.18
Total volume	50

2.15.1.2 Phenol/Chloroform extraction

Phenol/Chloroform extraction was carried out to precipitate DNA/RNA from solution. Equal volumes of DNA/RNA were mixed with phenol:chloroform:isoamylalcohol (25:24:1, Fisher Scientific) vortexed and centrifuged for 1 min at 16,100 g. The aqueous phase was transferred to a new tube and mixed with equal volume of chloroform (Fisher Scientific), vortexed and centrifuged for 1 min at 16,100 g. The aqueous phase was transferred to a new tube, mixed with 1/10 volume of 3 M sodium acetate pH 5.2 (Fisher Scientific) and 2 volumes of 100% ethanol. The tube was then placed on ice for 15 min and centrifuged for 15 min at 16,100 g at 4°C. The pellet was washed with 70% ethanol, centrifuged for 15 min at 16,100 g at 4°C and air dried until it became translucent. The pellet was resuspended in an appropriate volume of RNAase free water.

2.15.2 Preparation of semi (SP) cells

HeLa cells approx. 80% confluent (~ 6.2 X 10^5 cells/ml) were rinsed in PBS, trypsinised and resuspended in KHM buffer (110 mM KOAc, 20 mM HEPES, 2 mM MgOAc, pH 7.2) with 0.1 mg/ml of SBTI. Cells centrifuged at 260 g for 3 min at 4°C were then resuspended in ice-cold KHM with 40 μg/ml of digitonin (Sigma), mixed immediately by inversion and incubated at 4°C for exactly 5 min. Digitonin was diluted out with ice-cold KHM and centrifuged at 260 g for 3 min at 4°C. Cells were then resuspended in ice-cold HEPES buffer (50 mM HEPES, 90 mM KOAc, pH 7.2) and incubated at 4°C for 10 min before pelleting cells at 260 g for 3 min at 4°C. Cells were resuspended carefully in 1 ml of ice-cold KHM and left on ice. An aliquot of cells was mixed 1:1 with trypan blue (Sigma) and observed on a haemocytometer to check for permeabilisation. Cells were transferred to a microcentrifuge tube, spun at 9,300 g

(Eppendorf) for 30 sec at 4°C and resuspended in 100 µl of KHM with 1 µl of micrococcal nuclease (Sigma) and 1 mM $CaCl_2$, at room temperature for 12 min. Micrococcal nuclease was used to digest DNA and RNA in SP cells to avoid translation from endogenous mRNA. 4 mM EGTA (Sigma) was then added to chelate the calcium and inactivate the nuclease. Cells were washed, centrifuged for 30 sec and resuspended in an appropriate volume of KHM and approx. 10^5 cells were used per 25 µl translation reaction.

2.15.3 In vitro translation

For each 25 µl reaction, components (table 2.3) were added from a Flexi Rabbit Reticulocyte Lysate system (Promega), gently mixed and incubated at 30°C for 1 hr.

Table 2.3: Components for *in vitro* translation

Components	Volume (µl)
Flexi Reticulocyte lysate	16.5
Amino acids lacking Met	0.5
1 M KCl	0.2
mRNA template	1
SP cells (~10^5 cells)	5.25
^{35}S-labeling mix	1
RNase free water	0.55
Total volume	25

Some of the translation reactions were performed in the absence of SP cells and ^{35}S-labeling mix. The samples were quenched by 20 mM NEM and cells centrifuged at 16,100 g for 2 min. The supernatant was either directly analysed on SDS-PAGE after mixing 1:1 with 2x sample buffer or when SP cells were used, the cell pellet was washed in KHM buffer, resuspended by tapping on the microcentrifuge tube and centrifuged at 16,100 g for 2 min. This cell pellet was resuspended in KHM buffer, mixed 1:1 with 2x sample buffer, boiled at 95°C for 5 min and analysed by 8% SDS-PAGE (section 2.6).

2.15.4 Endo H treatment

In vitro translated proteins in the presence of semi permeabilised HeLa cells were lysed in the presence of 20 mM NEM, kept on ice for 10 min and, centrifuged at 16,100 g for 10 min at 4°C. Samples were denatured with 0.5% SDS, boiled, allowed to reach room temperature and were either mock treated or digested with 0.7 µl of endoglycosidase H (Endo H, NEB) at 37°C for 1.5 hr in a total volume of 15 µl. Samples were taken up into 2x sample buffer prior to analysis by 8% SDS-PAGE.

CHAPTER 3

INITIAL CHARACTERISATION OF ERO1β

3.1 Introduction

Disulfide bonds provide proteins with structural stability (Ortega et al., 1991), and are required for enzymatic function and regulation of protein activity (Ellgaard et al., 1999). Under strongly reducing conditions, like those prevailing in the cytosol, disulfide bond formation is kinetically and thermodynamically disfavoured (Seckler & Jaenicke, 1992). However, using the model glycoprotein influenza hemagglutinin, it was shown that excessively oxidising conditions lead to misfolding of proteins through incorrect inter- and intra-molecular disulfide bond formation (Marquardt et al., 1993). Therefore, in order to allow efficient disulfide bond formation, the ER must closely regulate its redox potential. Understanding how cells establish oxidising conditions has been the focus of attention for many biochemists over the last two decades or more. The thiol-disulfide cycle (Figure 1.3) responsible for introducing disulfide bonds to proteins has two key players, protein disulfide isomerase (PDI) and endoplasmic reticulum oxidoreductases (Ero). The PDI protein family was discussed in detail in Chapter 1 (section 1.7.2). Two human equivalents (hEROs) to the yeast Ero1p, Ero1α (Cabibbo et al., 2000) and Ero1β (Pagani et al., 2000) were identified recently. Sequence alignment of the two hEROs with Ero1p from *S. cerevisiae*, spEro1b p from *S.pombe* and ero-1 from *C.elegans* showed similarities between the Ero proteins as well as significant differences (Figure 3.1). Ero1β shows 50% and 74% similarity with and 40% and 65% identity to yeast Ero1p and Ero1α respectively (Pagani et al., 2000). The N-terminal C*XXX*C motif cysteines are conserved between the Ero proteins (Pagani et al., 2000)) as well as the C-terminal C*XX*C*XX*C motifs and TALK residues. Ero1p has a long C-terminal tail (127 amino acid residues) not seen in either of the hERO proteins. Ero1α has 15 cysteine residues whereas Ero1p and Ero1β have 14 (Figure 3.1, shaded in blue).

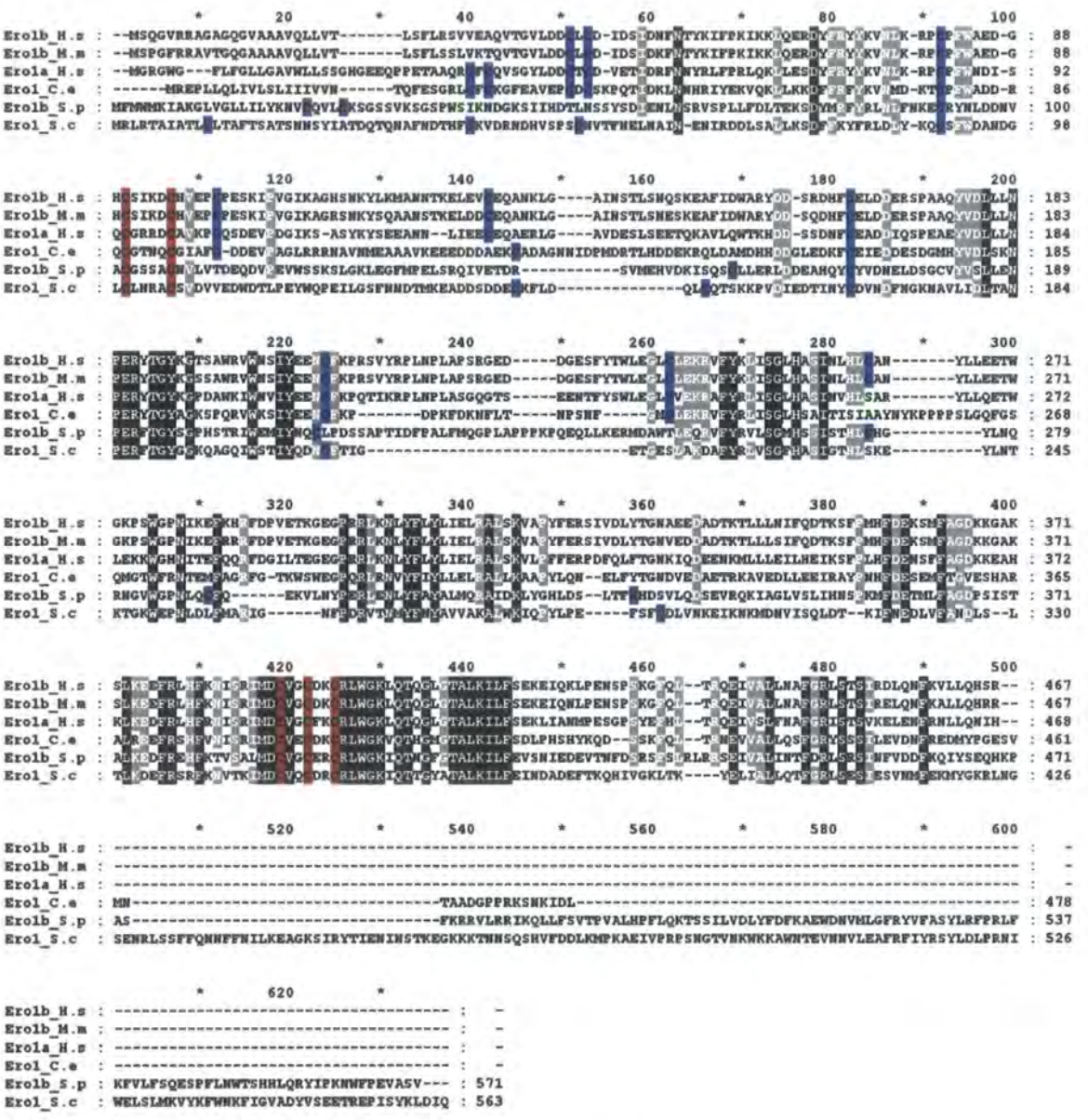

FIGURE 3.1: Sequence alignment of Ero proteins

Sequence alignment of Human Ero1β (Ero1b_H.s, Q86YB8; *H. sapiens*), mouse Ero1b (Ero1b_M.m, Q8R2E9; *M. musculus*), human Ero1α (Ero1a_H.s, Q96HE7; *H. sapiens*), ero-1 (Ero1_C.e, NP_001021704.1; *C. elegans*), spEro1b p (Ero1b_S.p, Q9Y7P1; *S.pombe*), Ero1p (Ero1_S.c, Q03103; *S. cerevisiae*). The N-terminal and C-terminal active site cysteines are shaded red, all other cysteines are shaded blue, identical residues are in black and partially conserved amino acids are shaded in light grey. Alignment made with ClustralX and Genedoc programs.

A schematic diagram of the hEROs is shown in Figure 3.2. Both hEROs have an N-terminal signal sequence that targets these proteins to the ER, where they are resident. Ero1α has a predicted signal sequence (using Signal IP) between positions 23-24 whereas for Ero1β it is at 33-34. Due to the indistinguishable size difference seen between hERO proteins translated in the absence and in the presence of ER membranes (translocated and deglycosylated proteins), the signal sequence was initially thought not to undergo cleavage once in the ER (Cabibbo et al., 2000; Pagani et al., 2000). Work published by Pagani and colleagues did later show through mass spectrometry and N-terminal sequence analysis that the leader sequence does get efficiently cleaved in Ero1α (Pagani et al., 2001). Ero1α and Ero1β both lack a known ER localisation motif and their possible retention mechanisms are discussed in chapter 1 (section 1.7.4.1). Another difference between the hEROs is that Ero1α has a EF calcium binding motif (159-171 amino acids) not found in Ero1β (Cabibbo et al., 2000; Pagani et al., 2000). Both hEROs are capable of rescuing the *S. cerevisiae ero1-1* thermosensitive mutant and catalysing the oxidation of model substrates (Cabibbo et al., 2000; Pagani et al., 2000; Mezghrani et al., 2001), indicating that these proteins are involved in disulfide bond formation.

Ero1α has two N-glycosylation sites (Figure 3.2, at positions 280 and 384), whereas Ero1β has four (Figure 3.2, at positions 122, 140, 145 and 383), but whether glycosylation could affect protein function is largely unexplored. Recent studies using non-glycosylated (NG) Ero1α mutants has shown that glycosylation is not essential for folding into an active conformation which can complement the yeast *ero1-1* mutant (Bertoli et al., 2004). These glycosylation mutants were still able to bind PDI and form OX1 OX2 redox isoforms (Bertoli et al., 2004). But in an over expressed system, wild-

type Ero1α gets secreted whereas the non-glycosylated Ero1α mutants form aggregates and are retained in the ER (Otsu et al., 2006). Studying these mutants in more detail could shed light on the involvement of glycans in hERO function.

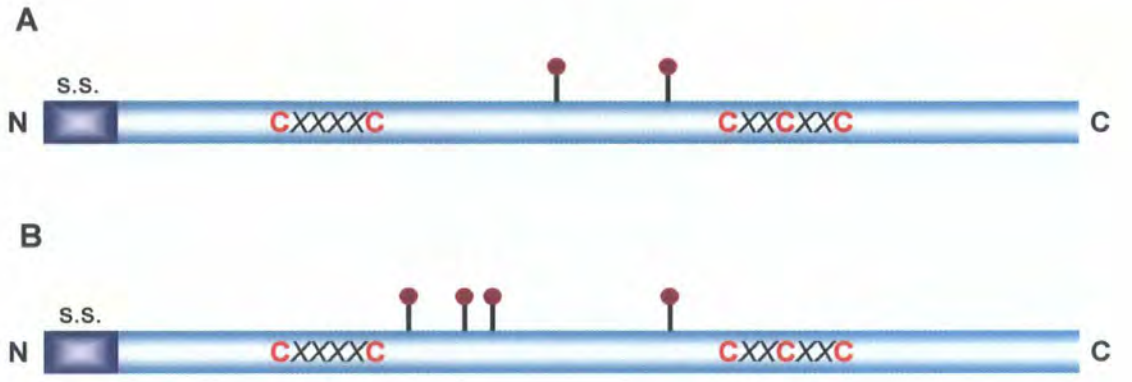

FIGURE 3.2: Schematic representation of hERO proteins

A. Ero1α. **B.** Ero1β. The N-terminal C*XXX*C and C-terminal C*XX*C*XX*C active site motifs are shown. Ball and sticks represents potential N-glycosylation sites. s.s, signal sequence. Adapted from (Dias-Gunasekara & Benham, 2005).

Of the two hERO proteins, much of the attention has been focused on Ero1α, looking at its folding under steady state and pulse-chase conditions (Benham et al., 2000) and its interacting partners (Mezghrani et al., 2001). This chapter has focused on detecting Ero1β from endogenous and transfected cell lines, studying its interacting partners and its possible heterodimerisation with Ero1α.

3.2 Results

3.2.1 Detection of Ero1β protein

Endogenous Ero1β protein levels are very low or almost non-detectable in all mammalian cell lines examined so far, making studying of Ero1β protein behaviour in tissue culture very difficult. To overcome this problem, cells were transfected with Ero1β constructs which provide an alternative model to investigate its interactions *in vivo*. Although transfected cells resemble an over-expressed system it should be noted that this system was used to study interactions of Ero1β, and where possible novel interactions were tested using mouse tissue lysates. Ero1β constructs were either Myc tagged or HA tagged at the C-terminus to aid in detection of the transfected protein. To verify that the constructs could be transfected, HeLa cells were mock transfected (*lane 4*) or transfected with Ero1β-Myc (*lane 1*), Ero1β-HA (*lane 2*), co-transfected with Ero1β-Myc plus Ero1β-HA (*lane 3*) and post-nuclear lysates analysed on reducing SDS-PAGE. Blots probed with αMyc (Figure 3.3*A*) and αHA (Figure 3.3*B*) verified that the tagged proteins (about 60 kDa) were recognised in the relevant lanes.

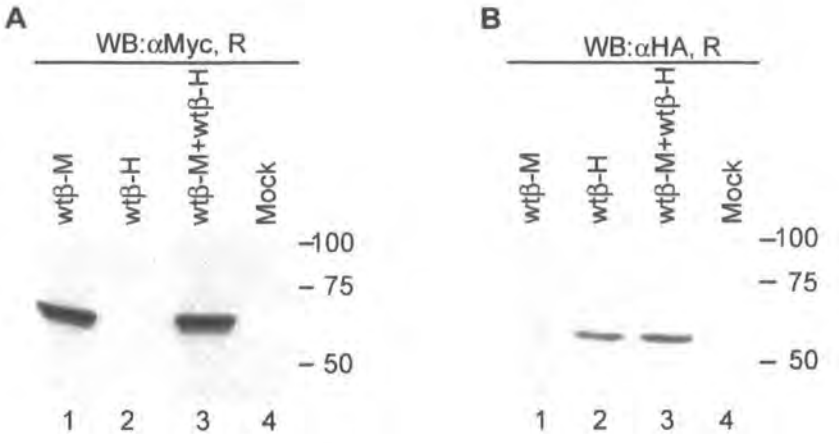

FIGURE 3.3: Expression of transfected Ero1β tagged proteins

HeLa cells mock transfected (*lane 4*) or transfected with wild-type (wt) Ero1β-Myc (*lane 1*), wtEro1β-HA (*lane 2*) or wtEro1β-Myc and wtEro1β-HA (*lane 3*) were lysed in the presence of NEM, analysed under reducing (R) SDS-PAGE, and western blotted (WB) membranes probed with either αMyc (**A**) or αHA (**B**) primary antibody. The tagged Ero1β protein is recognised by both αMyc and αHA antibodies.

Studies at the mRNA level have indicated that Ero1β transcripts are up-regulated in specific tissues like stomach and pancreas (Pagani et al., 2000). In order to detect endogenous Ero1β in tissue samples, a polyclonal antibody was raised against a peptide unique to Ero1β protein (YTGNAEEDADTKTLL). This antibody should not cross react with the second mammalian oxidoreductase Ero1α. An alignment of Ero1β and Ero1α from this region showed that only 7 of the 15 amino acids are conserved between the two hEROs (Figure 3.4*A*). The polyclonal anti-Ero1β serum was then tested to verify that the serum does recognise Ero1β protein. HeLa cells were mock transfected (*lane 3*) or transfected with Ero1α-Myc (*lane 1*) or Ero1β-Myc (*lane 2*), and post-nuclear lysates analysed on reducing SDS-PAGE. Blots were probed with a dilution series of Ero1β serum, starting from 1:500 (no signal observed, data not shown), 1: 100 (Figure 3.4*B*) and 1:50 (Figure 3.4*C*). Ero1β serum used at the highest concentration (Figure 3.4*C*) recognised a protein around 60 kDa not present in Ero1α (*lane 1*) or mock transfectants (*lane 3*). Using the Ero1β serum at this concentration did however give rise to a number of non-specific background bands around 75 kDa.

In order to increase the specificity of the Ero1β serum, 0.1% SDS was added during the antibody incubation and subsequent washing steps. These conditions were then tested on similar reduced lysates as Figure 3.3*A* and *B* with the additional use of Ero1α-Myc transfected lysate (Figure 3.4*D*). Ero1β serum recognised both tagged versions of Ero1β but not Ero1α (Figure 3.4*D*, *lane 1*) indicating its specificity. The use of 0.1% SDS was sufficient to allow the detection of the transfected Ero1β protein without the appearance of background bands. Ero1β-HA migrated faster than Ero1β-Myc due to its size/charge difference at the C-terminal tag (a triple Myc tag apposed to a single HA

tag). As a positive control for Ero1α, the membrane from Figure 3.4*D* was reprobed with D5, a polyclonal serum raised against Ero1α (Benham et al., 2001), which recognised the Ero1α-Myc tagged protein (Figure 3.4*E, lane 1*).

To investigate whether the Ero1β serum could be used to detect disulfide bonded interactions of Ero1β protein, HeLa cells were transfected with Ero1β-Myc (Figure 3.4*F*, *lane 1*) or Ero1β-HA (Figure 3.4*F*, *lane 2*) and post-nuclear lysates analysed by non-reducing SDS-PAGE. Transferred proteins were detected with the Ero1β serum, which was used at the tested concentration (1:50) in the presence of 0.1% SDS. Ero1β serum weakly recognised the differentially tagged monomer states, however, the detection of higher molecular weight complexes was poor (Figure 3.4*F*, *lane 1*) with some non-specific bands (*). Thus the Ero1β serum was not used in subsequent experiments under non-reducing conditions.

One approach for investigating protein-protein interactions is to immunoprecipitate the protein of interest, analyse on SDS-PAGE and western blot with antibodies against potential interacting partner proteins. Lysates from Ero1β-Myc (Figure 3.4*G*, *lane 1*) and mock (Figure 3.4*G*, *lane 2*) were analysed by reducing SDS-PAGE or first subjected to immunoprecipitation with the Ero1β serum. Western blotted membranes probed with the Ero1β serum confirmed the expression of the protein (Figure 3.4*G*, *lane 1*) and also established that this antibody was unable to immunoprecipitate (Figure 3.4*G*, *lane 3*).

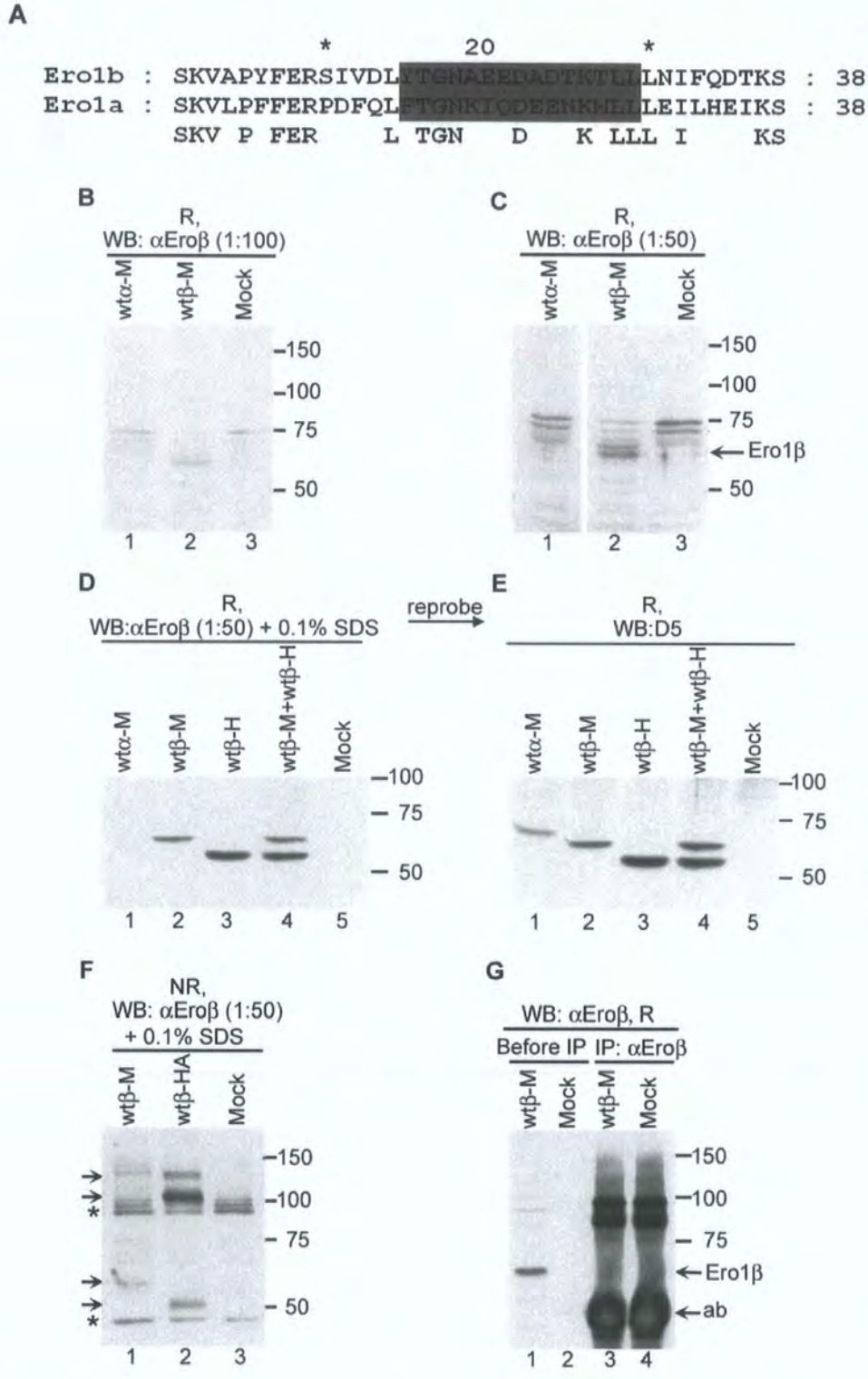

FIGURE 3.4: Optimising conditions for Eroβ serum in immunoblotting

A. Alignment of human Ero1β (accession no: Q86YB8), human Ero1α (accession no: Q96HE7) containing the 15 amino acid residues (shaded in grey) against which the αEroβ serum was raised against. Conserved residues are indicated below the alignment. Different dilutions of αEroβ serum (**B**, 1:100 and **C**, 1:50) were tested in

immunoblotting on wtEro1α-Myc (*lane 1*), wtEro1β-Myc (*lane 2*) or mock transfected (*lane 3*) HeLa cell lysates analysed under reducing (R) SDS-PAGE. A protein corresponding to Ero1β ~60 kDa was weakly identified in **C**, *lane 2*. **D.** HeLa cell lysates from wtEro1α-Myc (*lane 1*), wtEro1β-Myc (*lane 2*), wtEro1β-HA (*lane 3*) and wtEro1β-Myc and wtEro1β-HA (*lane 4*) transfected or mock transfected (*lane 5*) were analysed by reducing SDS-PAGE prior to probing the membrane with αEroβ serum at 1:50 dilution in the presence of 0.1% SDS. αEroβ serum recognises Myc and HA tagged Ero1β (*lanes 2-4*) proteins but not Ero1α (*lane 1*) **E.** the membrane from **D** was reprobed with αEroα serum D5 without stripping the membrane. D5 recognises Ero1α (*lane 1*). **F.** wtEro1β-Myc (*lane 1*), wtEro1β-HA (*lane 2*) or mock (*lane 3*) transfected HeLa cell lysates were analysed under non-reducing (NR) SDS-PAGE, and transferred proteins probed with αEroβ at 1:50 dilution in the presence of 0.1% SDS. Ero1β monomer and higher molecular weight complexes are indicated with arrows; * = non-specific binding. **G.** Immunoprecipitation using αEroβ serum. wtEro1β-Myc (*lane 1* and *3*) and mock transfected (*lane 2* and *4*) HeLa cell lysates were analysed directly (*lanes 1-2*) or immunoprecipitated with αEroβ serum (*lanes 3-4*) prior to reducing SDS-PAGE. The membrane probed with αEroβ recognised the Ero1β protein from cell lysate (*lane 1*) but not after immunoprecipitation (*lane 3*). ab = antibody.

To investigate whether the Ero1β serum recognised endogenous protein, samples of mouse tissue from gut, stomach, liver, kidney and pancreas were lysed in the presence of NEM, clarified by centrifugation, and equal amounts of protein were analysed by reducing SDS-PAGE prior to blotting with αEro1β serum (Figure 3.5*A*). HeLa cells transfected with wild-type Ero1β-Myc were used as a positive control (Figure 3.5*A* and *B*, *lane 1*). Although Ero1β serum recognised a ~60 kDa protein corresponding to the endogenous Ero1β in stomach and pancreas (Figure 3.5*A*, *lanes 3* and *6*), some background bands could be seen in gut, liver and kidney lysates (Figure 3.5*A*, *lanes 2, 4* and *5*). Mouse tissue lysates were subjected to concanavalin A (con A) affinity chromatography prior to reducing SDS-PAGE in an attempt to reduce this non-specific signal (Figure 3.5*B*). Con A is used to isolate glycoproteins with terminal α-D-mannosyl and α-D-glucosyl residues (Figure 3.5*B*). This technique confirmed the detection of N-glycosylated, ER resident Ero1β protein in stomach and pancreas tissues (Figure 3.5*B*, *lanes 3* and *6*). The results indicated that transfected Ero1β protein could be detected using either of the C-terminal tags or the Ero1β serum (Figure 3.3-3.4) and, the endogenous Ero1β protein could be detected by the Eroβ serum (Figure 3.5).

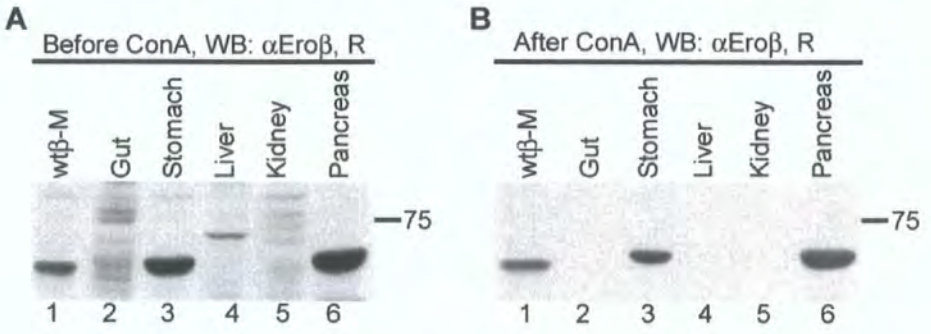

FIGURE 3.5: Detection of endogenous Ero1β protein

A. Equal amounts of murine tissue lysates, lysed in the presence of NEM, were subjected to western blotting after reducing (R) SDS-PAGE. The membrane was probed with αEroβ serum at 1:50 in the presence of 0.1% SDS. **B.** Same lysates as in **A** were first subjected to concanavalin A (ConA) affinity chromatography and immunoblotted with αEroβ serum. Ero1β is specifically detected in stomach (*lane 3*) and pancreas (*lane 6*) tissue. wtEro1β-Myc transfected cell lysates were used as the positive controls (**A** and **B**, *lane 1*).

3.2.2 Ero1β engages in disulfide dependent and alkylation independent interactions in the ER

In vitro translation with semi-permeabilised HT1080 cells and pulse-chase analysis with HeLa cells revealed that Ero1α monomer had three distinct redox states. This included two oxidised forms, OX1, OX2 and a reduced form (Benham et al., 2000). Ero1β monomer oxidation state was investigated by transfecting wild-type Ero1β-Myc into HeLa and HT1080 cells. The transfected cells were lysed in the presence or absence of the alkylating agent NEM. Addition of an alkylating agent blocks the transfer of intermolecular and intramolecular disulfides by binding to free thiols, thus preventing disulfide bond isomerization and rearrangement. In yeast, acid precipitation and alkylation is required to trap Ero1p-PDI mixed disulfide complexes (Frand & Kaiser, 1999) whereas in mammalian cells alkylation alone is sufficient to capture these disulfide interactions (Mezghrani et al., 2001; Benham et al., 2000). Post nuclear supernatants were examined by western blotting after non-reducing and reducing 8% SDS-PAGE. Running the gels under non-reducing conditions preserved disulfide bonds and allowed disulfide dependent interactions to be observed. The transferred proteins were probed with the 9E11 αMyc monoclonal antibody which detected the Myc tagged Ero1β.

In HeLa cells at steady state in the presence of NEM and under non-reducing (NR) conditions, monomeric wild-type Ero1β exists as ~60 kDa partly oxidised partly reduced molecules (OX and R) whereas in the absence of NEM Ero1β monomer was less compact (Figure 3.6*A*, *lanes 1* and *2*), confirming that NEM is required to trap the oxidised monomer. In HT1080 cells, monomeric Ero1β was mainly oxidised and more

compact (OX) in the presence of NEM but remained more reduced in the absence of NEM (Figure 3.6*B*, *lanes 1* and *2*). The exact ratio of oxidised to reduced Ero1β (OX: R) varied to some extent between transfections and was dependent on the cell type. The oxidised molecules migrated faster on SDS-PAGE due to the presence of disulfide bonds which form a more compact molecule. Reduction of the samples with DTT resulted in the appearance of a single reduced band (Figure 3.6*A* and *B*, *lanes 6, 7*) demonstrating that the shifts seen in the non-reducing gels are a result of disulfide bond formations and not degradation. These results are similar but not identical to those found with Ero1α (Benham et al., 2000), the most notable difference is that Ero1β does not form discrete oxidation states like Ero1α when analysed by 8% non-reducing SDS-PAGE (Mezghrani et al., 2001; Benham et al., 2000).

The redox states of Ero1β were also analysed using radio-labelling of transfected cells. HeLa cells were either mock transfected (Figure 3.6*C*, *lanes 5* and *9*) or transfected with Ero1α-Myc (Figure 3.6*C*, *lanes 1* and *2*) and Ero1β-Myc (Figure 3.6*C*, *lanes 3-4* and *7-8*) and starved for 40 min in medium lacking methionine and cysteine. Following starvation, cells were ^{35}S labelled for 15 min, chased for 45 min and lysed in the presence of the alkylating agent NEM. Lysates were immunoprecipitated with αMyc and examined by non–reducing (Figure 3.6*C*, *lanes 1, 3-5*) and reducing (Figure 3.6*C*, *lanes 2, 7-9*) SDS-PAGE. The addition of an alkylating agent upon cell lysis combined with the analysis of lysates on non-reducing SDS-PAGE, allowed the visualisation of any folding intermediates, oxidation states and disulfide-dependent interactions (Braakman et al., 1992).

For Ero1α, the redox states OX1, OX2 and R were consistent with Benham et al., 2000 (Figure 3.6*C*, *lane 1*), resolving into a single band when reduced with DTT (R; Figure 3.6*C*, *lane 2*). Ero1β on the other hand resolved as a smear of bands under non-reducing conditions (OX, Figure 3.6*C*, *lanes 3-4*) which compact into a single band upon reduction (R, Figure 3.6*C*, *lanes 7-8*). During a 10 min pulse and a 15-60 min chase, Ero1β continued to remain as a smear of oxidised forms (Figure 3.6*D*, *lanes 1-4*) which even during a 6 hr chase remained unchanged (data not shown). Disulfide-dependent Ero1β higher molecular weight complexes were seen during the 15-60 min chase which were not present in the reduced lysates (*, Figure 3.6*D*, *lanes 6-9*) and were also absent from the mock transfected (Figure 3.6*D*, *lane 10*). To determine the half life of Ero1β, transfected HeLa cells radio labelled for 10 min were chased for 3-22 hr, immunoprecipitated with αMyc and analysed on reducing SDS-PAGE (Figure 3.6*E*). Quantitation of the immunoprecipitates from Figure 3.6*E* showed that Ero1β is a relatively stable protein with a half life of 24-25 hrs.

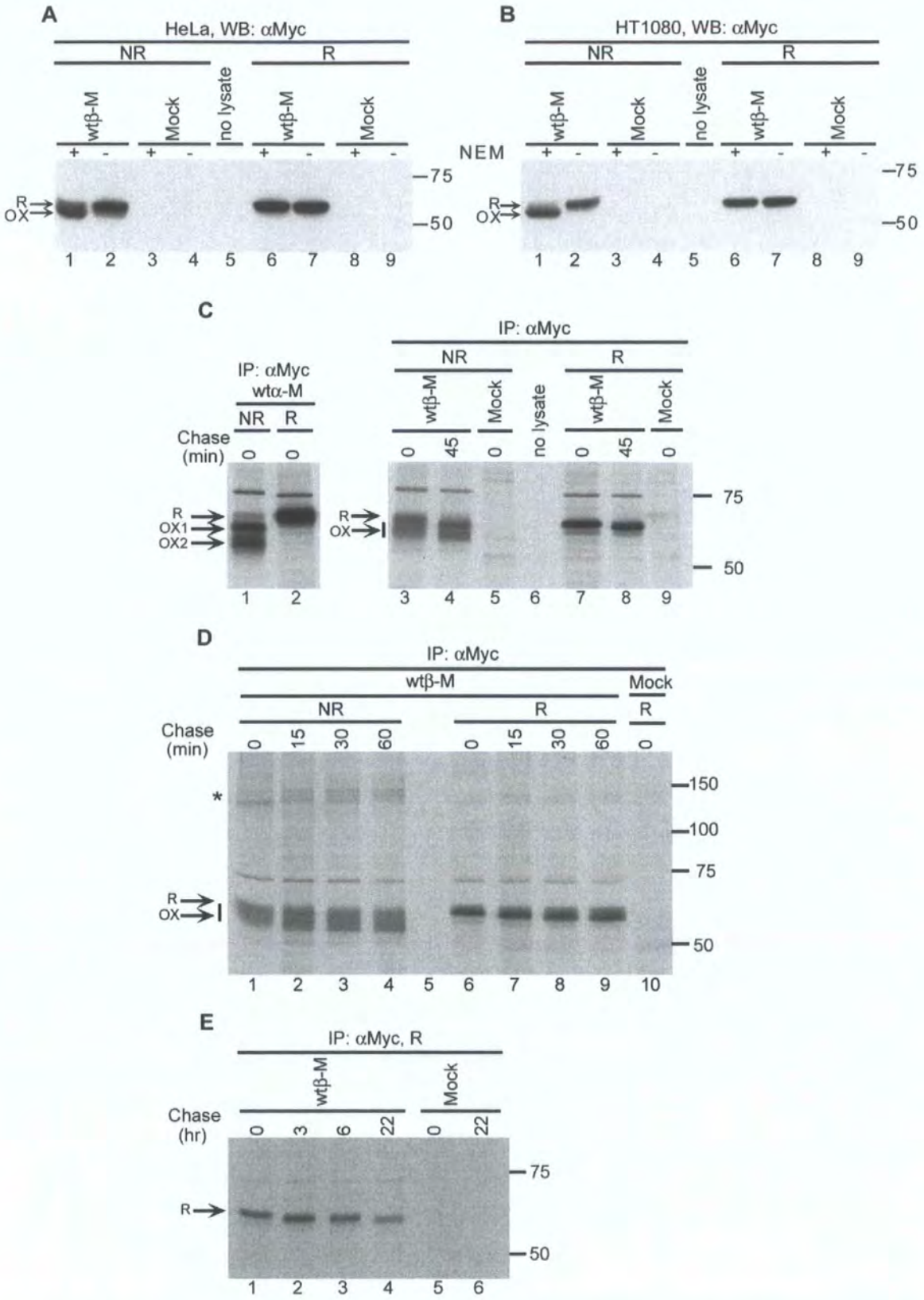

FIGURE 3.6: Ero1β monomer is partly oxidised partly reduced

A. non-reducing (NR, *lanes 1-4*) and reducing (R, *lanes 6-9*) SDS-PAGE of Myc transfected wtEro1β (*lanes 1-2* and *6-7*) and mock transfected (*lanes 3-4* and *8-9*)

HeLa cells lysed in the presence (*lanes 1, 3, 6* and *8*) or absence (*lanes 2, 4, 7* and *9*) of NEM and probed with αMyc. **B.** Same as **A** using HT1080 cell lysates. In both **A** and **B** *lane 5* is loaded with sample buffer only. Ero1β monomer oxidation states are labelled as oxidised (OX) and reduced (R). **C.** wtEro1α-Myc (*lanes 1-2*), wtEro1β-Myc (*lanes 3-4* and *7-8*) and mock (*lanes 5* and *9*) transfected HeLa cells were pulsed-labelled for 15 min, chased for times indicated and immunoprecipitated with αMyc (*lanes 1-9*) prior to non-reducing (*lanes 1, 3-5*) and reducing (*lanes 2, 7-9*) SDS-PAGE. Ero1α oxidation states, OX1 and OX2 are observed under NR conditions, compared to a smear of oxidation states (OX) in Ero1β. *Lane 6* is loaded with only sample buffer. **D.** Same as **C** using wtEro1β-Myc (*lanes 1-9*) and mock (*lane 10*) transfected HeLa cells pulse-labelled for 10 min, analysed by non-reducing (*lanes 1-4*) and reducing (*lanes 6-10*) SDS-PAGE. *Lane 5* is loaded with sample buffer only. * indicates disulfide-linked higher molecular weight complexes. **E.** Same as **D**, with reducing SDS-PAGE of wtEro1β-Myc (*lanes 1-4*) and mock (*lane 5-6*) transfected HeLa cells with chase points from 3-22 hrs (*lanes 2-4* and *6*) to determine the half-life of Ero1β.

To investigate the ability of Ero1β protein to form higher molecular weight complexes, HeLa and HT1080 cells were transfected with Ero1β-Myc (Figure 3.7*A* and *B*, *lanes 1-2, 6-7*) or mock (Figure 3.7*A* and *B*, *lanes 3-4, 8-9*) and analysed under non-reducing (Figure 3.7*A* and *B*, *lanes 1-4*) and reducing (Figure 3.7*A* and *B*, *lanes 6-9*) SDS-PAGE. In both HeLa and HT1080, wild-type Ero1β formed a ladder of higher molecular weight complexes in the presence and in the absence of NEM (Figure 3.7*A* and *B*, *lanes 1, 2*). The smear of bands seen in the absence of NEM was less prominent in HT1080 cells (Figure 3.7*A*, *lane 2* in comparison to *B*, *lane 2*). Addition of the reducing agent DTT to the samples prior to gel electrophoresis disrupted the ladder of higher molecular weight complexes, showing they were disulfide-dependent interactions (Figure 3.7*A* and *B*, compare *lanes 1-2* with *6-7*). The 9E11 αMyc antibody gave a non-specific background band around ~130 kDa seen more prominently in HeLa cell lysates (Figure 3.7*A*). The non-specific nature of the band and the reproducibility of the results were confirmed by using a polyclonal αMyc antiserum which specifically recognised the Myc tagged Ero1β protein complexes (Figure 3.7*C*).

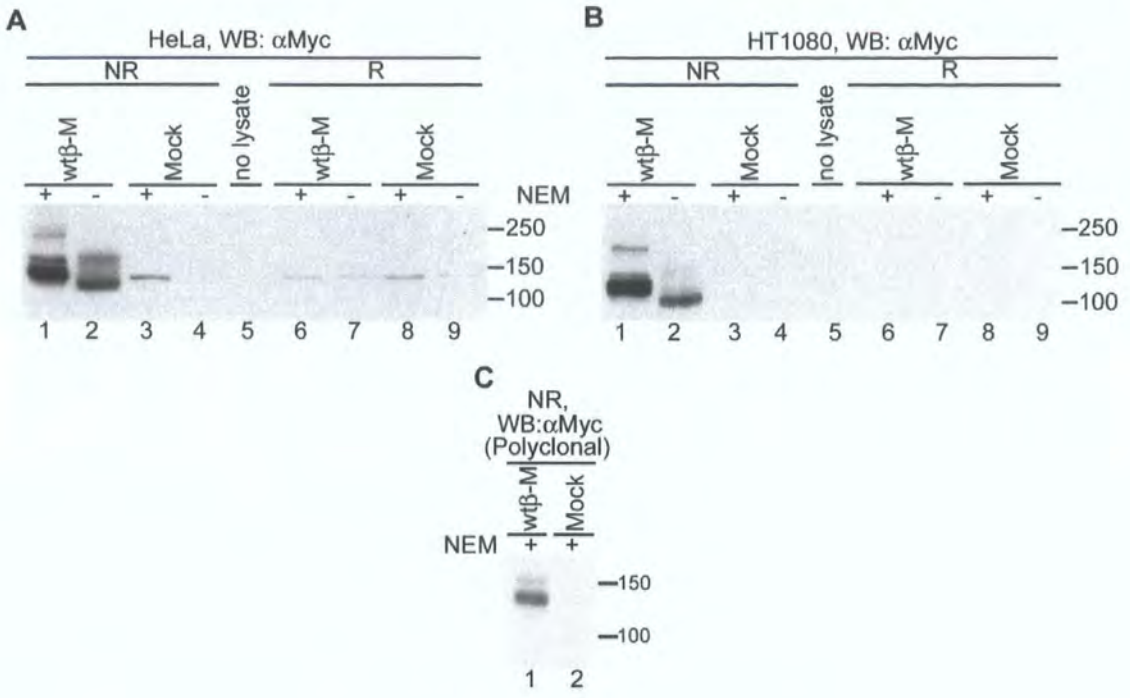

FIGURE 3.7: Ero1β forms alkylation independent complexes

A and **B.** Same lysates as FIGURE 3.6**A** and **B**, but looking at Ero1β complex formation at steady state. In both HeLa and HT1080 Ero1β is able to form disulfide linked complexes in the presence (*lane 1*) and in the absence (*lane 2*) of NEM under non-reducing (NR) SDS-PAGE. *Lane 5* is loaded with sample buffer. Note the presence of a non-specific background band around 130 kDa in **A**. **C.** non-reducing SDS-PAGE analysis of wtEro1β-Myc (*lane 1*) and mock (*lane 2*) transfected HeLa cells lysed in the presence of NEM and probed with a polyclonal αMyc antiserum.

In Figure 3.7*A* and *B*, one of the higher molecular weight bands should correspond to Ero1β-PDI complex (Mezghrani et al., 2001). Mock transfected HT1080 cells lysed in the presence or absence of NEM, analysed by non-reducing and reducing SDS-PAGE and probed with an anti-serum raised against PDI, emphasised the dependency of disulfide-linked PDI complexes on alkylating agents (Figure 3.8*A*, compare *lanes 1* and *2*). Ero1β–Myc and mock transfected HeLa cell lysates were subjected to immunoprecipitation with a αPDI antibody (Figure 3.8*B*). The Ero1β-PDI dimer was NEM dependent as expected (Figure 3.8*B*, *lane 1*).

To further study the nature of Ero1β complexes, endogenous PDI was depleted from Ero1β transfected cell lysates by consecutive rounds of immunoprecipitation. All detectable PDI was removed by this procedure, whereas calnexin levels remained unaffected (Figure 3.8*C*, compare *lane 1* with *lanes 3* and *4*). Analysis of the PDI-depleted lysates by non-reducing SDS-PAGE and immunoblotting with αMyc showed that the Ero1β-PDI complex was selectively removed, whereas the lower complex remained (*) along with the Ero1β monomers (Figure 3.8*D*, *lanes 1, 3* to *4*). The nature of Ero1β disulfide complexes was also investigated during *in vivo* metabolic labelling experiments. HeLa cells transfected with Ero1β (Figure 3.8*E*, lanes *1-2*) and mock (Figure 3.8*E*, lane *3*) were pulse-labelled for 10 min and used in an immunoprecipitation with αMyc and αPDI antibodies prior to analysis by non-reducing SDS PAGE (Figure 3.8*E*). Analysis of the higher molecular weight complexes from these immunoprecipitates revealed that one of the bands (**) is immunoprecipitating with both αMyc and αPDI only from the Ero1β transfected cell lysates (Figure 3.8*E*, *lanes 1* and *2* respectively), indicating the presence of Ero1β-PDI complexes. These data complemented the steady state results from Figure 3.8*D*.

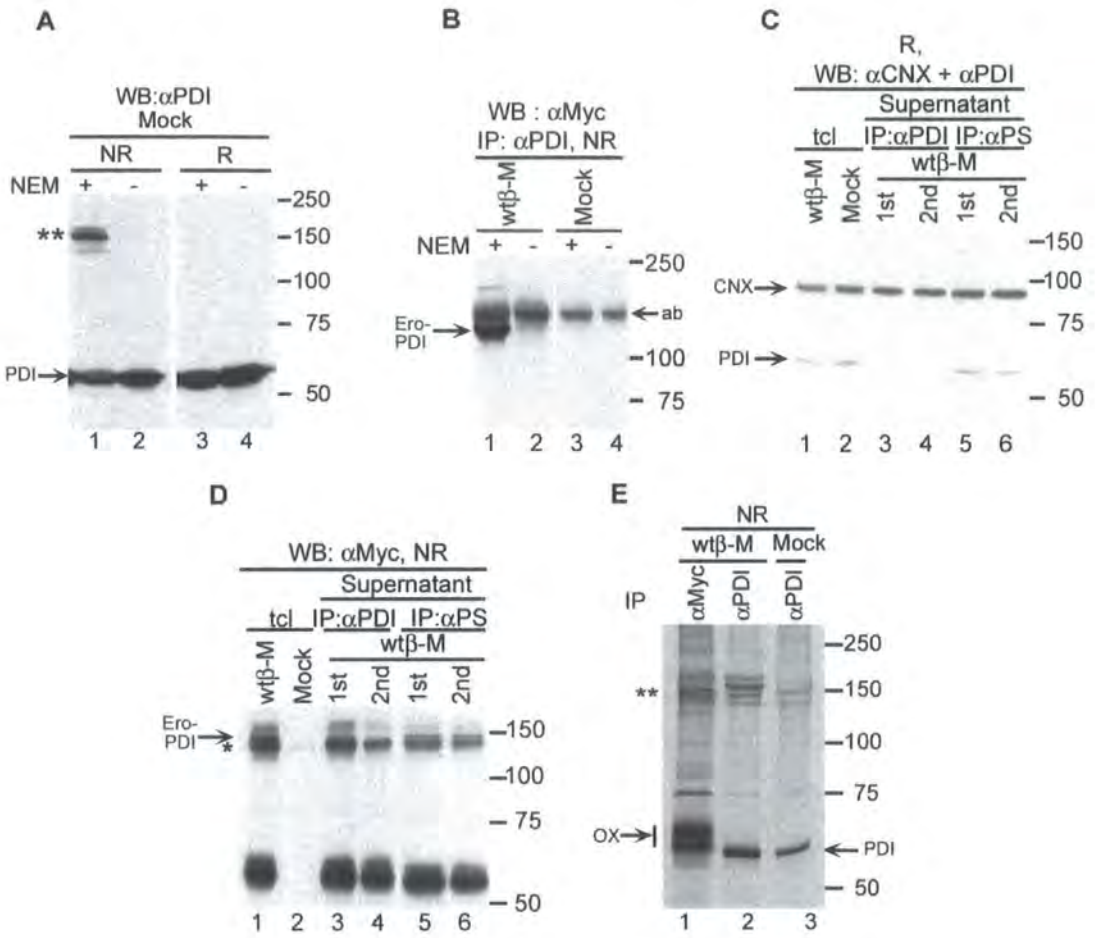

FIGURE 3.8: Ero1β forms non-PDI but disulfide linked complexes

A. non-reducing (NR, *lanes 1-2*) and reducing (R, *lanes 3-4*) SDS-PAGE analysis of mock transfected HeLa cells, lysed in the presence (*lanes 1* and *3*) or in the absence (*lanes 2* and *4*) of NEM, and immunoprecipitated with αPDI. PDI monomer is indicated. Disulfide dependent PDI interactions are preserved only in the presence of an alkylating agent (**). **B.** non-reducing (*lanes 1-4*) SDS-PAGE analysis of Myc tagged wtEro1β (*lanes 1-2*) and mock (*lane 3-4*) transfectants subjected to immunoprecipitation with αPDI and immunoblotted with αMyc. Ero-PDI complex is captured in the presence of NEM. Antibody complexes (ab) migrate just above the Ero-PDI dimer **C.** reducing SDS-PAGE of wtEro1β-Myc transfected HeLa cell lysates subjected to sequential immunodepletion of PDI prior to detection of calnexin (CNX) and PDI. All detectable PDI is specifically removed from the lysates (*lanes 3* and *4*) when compared with the immunodepletion using a rabbit pre-immune serum (*PS, lanes 5-6*). **D.** non-reducing SDS-PAGE analysis of the same lysates used in **C**, but probed with the αMyc antibody. 1^{st} = first immunodepletion, 2^{nd} = second immunodepletion,

tcl = total cell lysate prior to immunodepletion. The Ero-PDI complex is depleted (arrow), whereas the major Ero complex remains (*). **E.** non-reducing SDS-PAGE analysis of wtEro1β-Myc (*lanes 1-2*) and mock (*lanes 3*) transfected HeLa cells pulse-labelled for 10 min, lysed and immunoprecipitated (IP) with αMyc (*lanes 1*) and αPDI (*lanes 2 and 3*). A smear of oxidation states (OX) was observed for Ero1β, and ** indicates the possible Ero-PDI complex. PDI monomer is indicated.

3.2.3 Ero1β forms disulfide-dependent homodimers

A number of thioredoxin family proteins and redox enzymes are known to form dimers (Zhao et al., 2003). Immunodepletion experiments (Figure 3.8*C* and *D*) as well as analysis of Ero1β transfected cell lysates on non-reducing SDS-PAGE (Figure 3.7*A–B*) proved that there were complexes other than Ero1β-PDI present in cells. The ability of Ero1β to form dimers was investigated using two differentially migrating Ero1β-Myc and Ero1β-HA proteins.

HeLa cells were either mock transfected (Figure 3.9*A*, *lane 4*) or transfected with Ero1β-Myc (Figure 3.9*A*, *lane 1*), Ero1β-HA (Figure 3.9*A*, *lane 2*) and Ero1β-Myc plus Ero1β-HA (Figure 3.9*A*, *lane 3*). The cells were lysed in the presence of NEM, analysed by non-reducing SDS-PAGE and after western blotting, the membrane was probed first with αMyc (Figure 3.9*A*, *lanes 1-4*) and the same membrane re-probed with αHA (Figure 3.9*A*, *lanes 5-8*) without stripping the blot. Any mixed disulfide-dependent Ero1β-Myc - Ero1β-HA dimers should appear as an intermediate band present only in the double transfected lysates. An intermediate band of ~125 kDa representing this Ero1β-Myc - Ero1β-HA dimer was present in Figure 3.9*A*, *lanes 3* and *7* (M+H). In the single transfectants the Ero1β-Myc - Ero1β-Myc dimer (Figure 3.9*A*, M+M) and the Ero1β-HA - Ero1β-HA dimer (Figure 3.9*A*, H+H) was also prominent. Note the presence of an extra non-specific band of ~130 kDa in both the Myc and HA blots (Figure 3.9*A*, *lanes 2, 4* and *8*). The same cell lysates as in Figure 3.8A were subjected to immunoprecipitation with αHA-7, and the membrane probed with αMyc after reducing SDS-PAGE (Figure 3.9*B*). The formation of an Ero1β-Myc -

Ero1β-HA dimer was confirmed by the presence of a Myc signal in the immunoprecipitates from the double transfectant (Figure 3.9*B*, *lane 3*).

To investigate whether Ero1β was able to form homodimers in the absence of an alkylating agent, the same experimental setup as in Figure 3.9*A* and *B* was performed where HeLa cell transfectants were lysed in the absence of NEM (Figure 3.9*C* and *D*). Cell lysates were either directly analysed on reducing SDS-PAGE to confirm the expression of the transfected proteins (Figure 3.9*C*) or were subjected to immunoprecipitation with αHA-7 prior to analysis under reducing SDS-PAGE (Figure 3.9*D*). Cell lysates analysed under non-reducing SDS-PAGE before immunoprecipitation (similar to in Figure 3.9*A*), gave a smear of bands around 150 kDa in the Ero1β-Myc - Ero1β-HA double transfected lysates (data not shown), which although not as discrete as in the presence of NEM (Figure 3.9*A*, *lanes 3, 7*), did imply the formation of disulfide-bonded homodimers. Analysis of immunoprecipitates confirmed that the Ero1β-Myc tagged protein could interact with the Ero1β-HA protein (Figure 3.9*D*, *lane 3*). These experiments indicate that Ero1β formed disulfide dependent but alkylation independent homodimers at steady state in the endoplasmic reticulum.

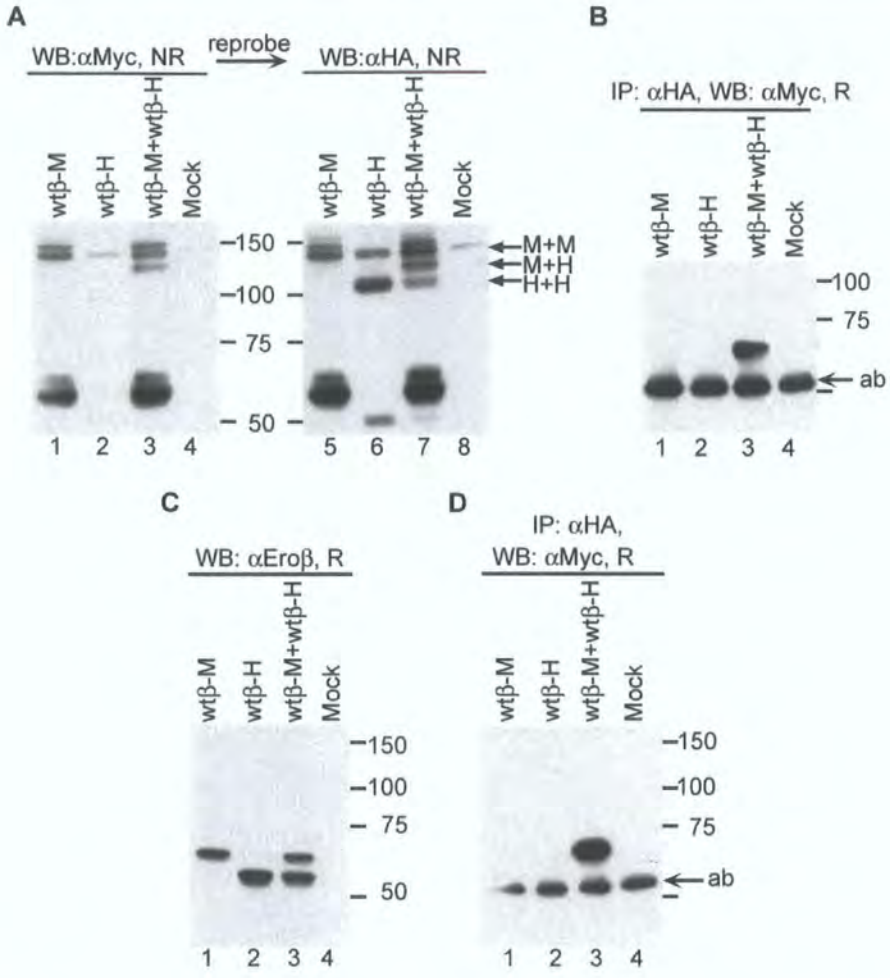

FIGURE 3.9: Dimerisation of Ero1β

A. HeLa cells transfected with wtEro1β-Myc (*lanes 1* and *5*), wtEro1β-HA (*lanes 2* and *6*), wtEro1β-Myc and wtEro1β-HA (*lanes 3* and *7*), and mock transfectants (*lanes 4* and *8*) were lysed in the presence of NEM and subjected to immunoblotting after non-reducing (NR) SDS-PAGE. The membrane was probed with αMyc (*lanes 1-4*) and reprobed without stripping the membrane with αHA (*lanes 5-8*). A mixed wtEro1β-Myc- wtEro1β-HA (M+H) dimer is clearly visible (*lanes 3* and *7*). M+M= wtEro1β-Myc dimer, H+H= wtEro1β-HA dimer. **B.** The same lysates as in **A**, first subjected to immunoprecipitation with αHA prior to reducing (R) SDS-PAGE, and the membrane probed with αMyc. wtEro1β-Myc co-immunoprecipitated with the wtEro1β-HA (*lane 3*) thus forming a specific complex. **C** and **D.** HeLa cells transfected with the same cDNA constructs as in **A**, but lysed in the absence of NEM, and either analysed directly on reducing SDS-PAGE and immunoblotted with αEroβ (**C**) or first subjected to immunoprecipitation with αHA and after western blotting probed with αMyc (**D**). Myc and HA tagged wtEro1β co0immunoprecipitated (**D**, *lane 3*). ab= antibody.

3.2.4 Ero1β complexes differ in abundance in stomach and pancreas

Ero1β is able to homodimerise (section 3.2.3). Mouse stomach and mouse pancreas tissue lysates were used to study the ability of Ero1β to form complexes including dimers *in vivo*. Both tissues were lysed in the absence of NEM, which prevents formation of Ero1β-PDI covalent interactions (Figure 3.8*B*). Ero1β complexes could not be directly detected due to the inability of the αEro1β serum to work under non-reducing conditions (Figure 3.4*F*). As an alternative method, gel filtration was performed where mouse tissue lysates were run on a superdex 200 precision column to separate proteins according to their molecular weight. The elution profile of Ero1β was compared with bovine serum albumin (monomer of 66 kDa and dimer 132 kDa, Figure 3.10*A*) and chicken egg albumin (monomer of 45 kDa, Figure 3.10*B*). Fractions from the gel filtration were trichloroacetic acid-precipitated and analysed by reducing SDS-PAGE prior to immunoblotting with the Ero1β serum. Ero1β from the stomach was recovered in *fractions 10-13*, with a peak in *fraction 12* corresponding to the likely size of the glycosylated monomer (Figure 3.10*C*). *Fractions 10* and *11* probably correspond to Ero1β complexes (Figure 3.10*C*). In contrast, in the pancreas, Ero1β was recovered mainly from *fractions 9* and *10*, which relates to the expected size of the Ero1β dimer, and was also detected in *fractions 13* and *14* (Figure 3.10*D*). These results suggest that Ero1β can be found in complexes (other than Ero-PDI complexes) *in vivo* but their relative abundance in different tissues can vary.

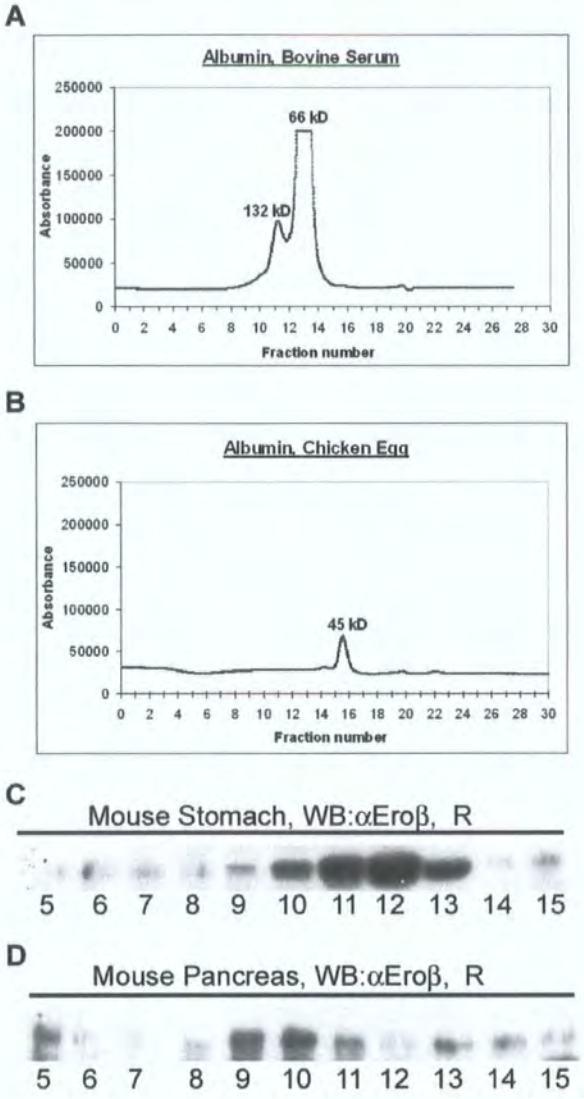

FIGURE 3.10: Gel filtration of Ero1β in stomach and pancreas

A. UV absorption spectra of the bovine serum albumin (66 kDa monomer; 132 kDa dimer) and **B.** albumin standards (45 kDa). **C.** trichloroacetic acid precipitated fractions from mouse stomach and **D.** mouse pancreas were analysed by reducing SDS PAGE and immunoblotted using αEroβ.

3.2.5 Ero1α and Ero1β form mixed disulfide dependent complexes

To investigate whether at steady state the two oxidoreductases, Ero1α and Ero1β, are able to interact, HeLa cells were transfected with Ero1α-Myc, Ero1β-HA or Ero1α-Myc together with Ero1β-HA (Figure 3.11*A* and *B*). Cell lysates were analysed under reducing SDS-PAGE, the western blotted membrane probed with αMyc (Figure 3.11*A*, *lanes 1-4*) and reprobed with αHA (Figure 3.11*A*, *lanes 5-8*) without stripping the membrane. These two figures confirmed the expression of the transfected Ero proteins. The lysates were subjected to immunoprecipitation with αHA-7 followed by probing the western blotted reducing gel with αMyc (Figure 3.11*B*). The co-immunoprecipitated Ero1α-Myc protein was detected as a Myc signal only in the double transfectant (Figure 3.11*B*, *lanes 3*) which showed Ero1α interacting with Ero1β. This experiment demonstrated the ability of the two oxidoreductases to associate in the endoplasmic reticulum.

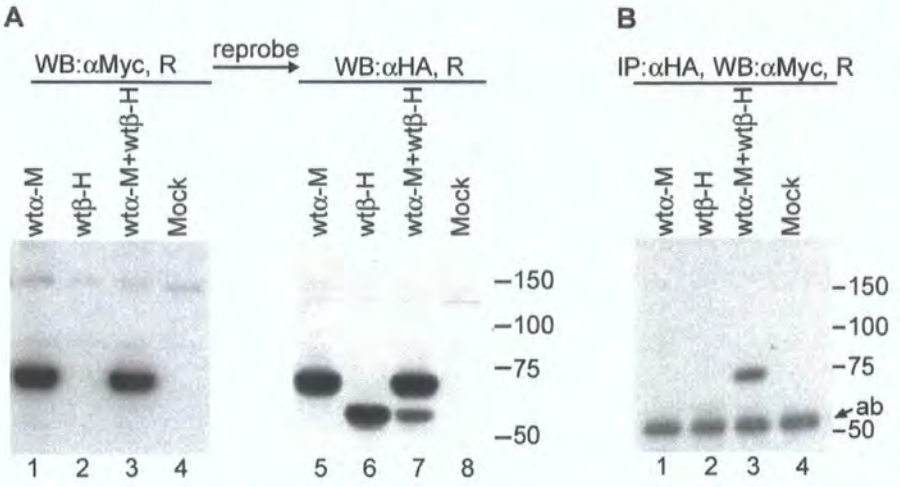

FIGURE 3.11: Complex formation between Ero1α and Ero1β

A and **B.** HeLa cell lysates expressing wtEro1α-Myc (*lanes 1* and *5*), wtEro1β-HA (*lanes 2* and *6*), wtEro1α-Myc and wtEro1β-HA (*lanes 3* and *7*), or mock transfected (*lanes 4* and *8*) were analysed directly by reducing SDS-PAGE (**A**) or first subjected to immunoprecipitation with αHA (**B**). Immunoblotting was with αMyc (**A** and **B**, *lanes 1-4*) and reprobing was with αHA (**B**, *lanes 5-8*). Wild-type Ero1α and Ero1β form a specific complex (**B**, *lane 3*). Ab = antibody.

3.2.6 Under in vivo reducing conditions Ero1β is only partially reduced

Treatment of eukaryotic cells with the membrane permeable reducing agent dithiothreitol (DTT) inhibits disulfide bond formation in the endoplasmic reticulum. To study the effects of the reducing agent DTT on Ero1β proteins, HeLa cells (Figure 3.12*A*) and HT1080 cells (Figure 3.12*B*) were either mock transfected (*lanes 3, 4, 7* and *8*) or transfected with Ero1β-Myc (*lanes 1, 2, 5* and *6*) and were treated *in vivo* with 5 mM DTT for 30 mins prior to analysis on non-reducing (*lanes 1-4*) and reducing (*lanes 5-8*) SDS-PAGE (Figure 3.12*A* and *B*). Treatment of living cells with DTT caused the Ero1β monomer to become partially reduced when compared to the reduction of samples with DTT *in vitro*, where both the OX forms collapsed to form a single reduced band (Figure 3.12*A*, compare *lanes 2* and *6*). The shift seen with DTT treatment also confirms that the monomer banding pattern seen in non-reducing gels (for example Figure 3.6*A* and *B*) is the result of compaction by disulfide bonds and not degradation.

The effect of a reducing environment on Ero1β complex formation was investigated by transfecting HeLa cells with Ero1β-Myc or co-transfecting with Ero1β-Myc and Ero1β-HA. Transfected cells were incubated with DTT before analysing the lysates by non-reducing (Figure 3.12*C*, *lanes 1-6*) and reducing (Figure 3.12*C*, *lanes 7-12*) SDS-PAGE. At steady state, 10 mM DTT in the medium was sufficient to eliminate the majority of disulfide dependent (Ero-PDI and Ero-Ero) complexes (Figure 3.12*C*, *lanes 1* and *3*). The Ero1β monomer form shows the same partial reduction pattern observed in Figure 3.12*A*. The slight variation in shifts seen in the monomer form with DTT treatment between Figure 3.12*A*, *lanes 1-2* and Figure 3.12*C*, *lanes 1-4*, was due to the use of two alkylating agents (NEM and IAA respectively). Samples analysed by

reducing SDS-PAGE recovered a single reduced band for each protein (Figure 3.12*C*, *lanes 7-10*), which also confirmed the expression of the transfected proteins. The small shift in mobility of Ero1β after exposing the cells to DTT was a consequence of increasing availability of –SH groups to the alkylating agent (Figure 3.12*C*, compare *lanes 7* and *8*, and *lanes 9* and *10*).

To confirm that Ero1β complex formation was abolished by *in vivo* DTT treatment, DTT-treated and untreated cell lysates were subjected to immunoprecipitation with αMyc and probed with αEro1β serum after immunoblotting. As expected, the Ero1β-Myc protein from single transfectants was detected regardless of DTT treatment (Figure 3.12*D*, *lanes 1* and *2*). However, Ero1β-HA was co-immunoprecipitated with Ero1β-Myc only in the absence of DTT treatment (Figure 3.12*D*, *lane 4*). The conclusion from these experiments was that a strong reducing environment was able to disrupt the majority of Ero1β-mediated covalent and non-covalent interactions at steady state.

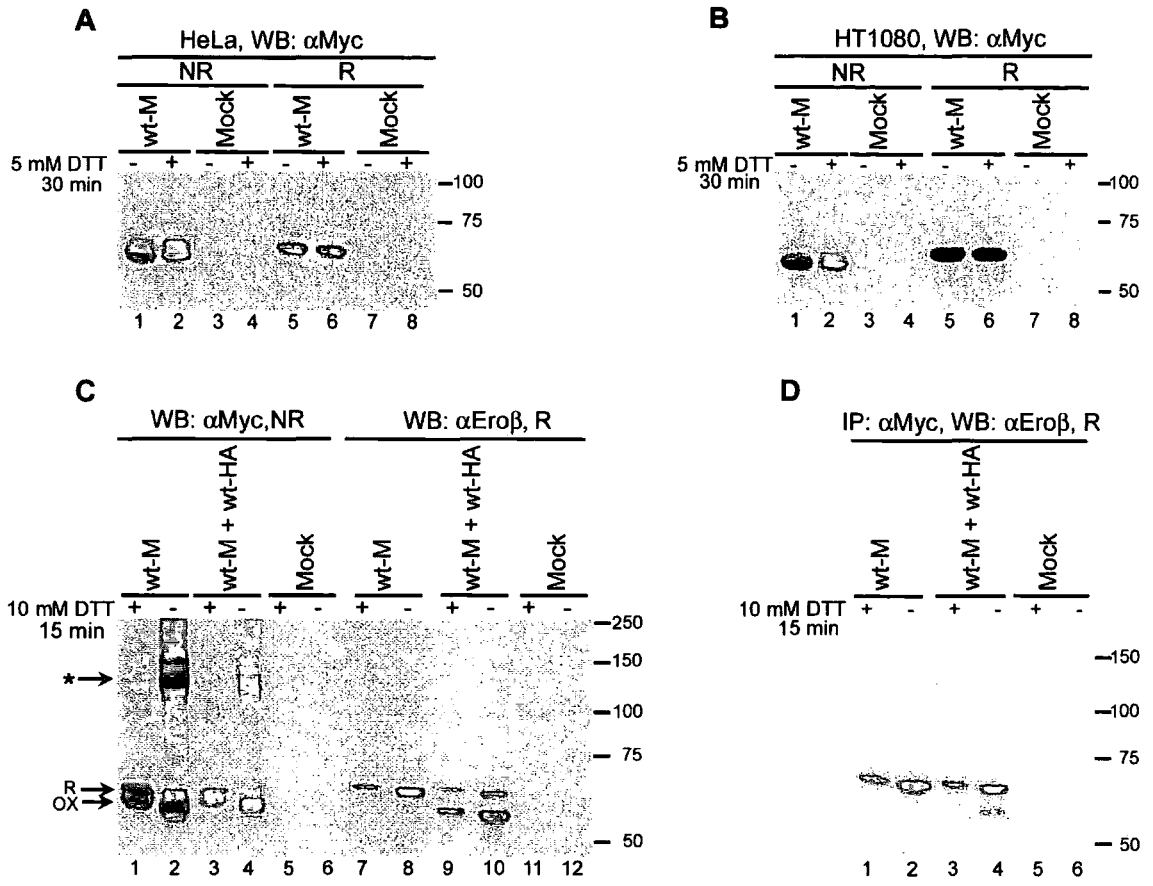

FIGURE 3.12: *In vivo* reduction of Ero1β

HeLa (**A**) and HT1080 (**B**) cells transfected with wtEro1β-Myc (*lanes 1-2* and *5-6*) and mock (*lanes 3-4* and *7-8*) were treated with (*lanes 2, 4, 6* and *8*) or without (*lanes 1, 3, 5* and *7*) 5 mM DTT for 30 min, and lysed in the presence of NEM and analysed by non-reducing (NR, *lanes 1-4*) or reducing (R, *lanes 5-8*) SDS-PAGE. Immunoblotting was with αMyc. **C** and **D.** HeLa cells transfected with wtEro1β-Myc (*lanes 1-2, 7-8*), wtEro1β-Myc and wtEro1β-HA (*lanes 3-4, 9-10*) and mock (*lanes 5-6, 11-12*) were treated with 10 mM DTT for 15 min. Cells were lysed in the presence of NEM and analysed by immunoblotting with αMyc after non-reducing SDS-PAGE (*lanes 1-6*) and with αEroβ after reducing SDS-PAGE (*lanes 7-12*) or after **D** immunoprecipitation with αMyc. * = disulfide-dependent Ero-PDI and Ero-Ero complexes. Oxidation states of Ero1β monomer are indicated as OX (oxidised) and R (reduced).

3.3 Discussion

In this chapter the Ero1β protein, one of the two human ER oxidoreductases discovered to date, was characterised by the use of C-terminally tagged DNA constructs transfected into two different cell lines. Tagged Ero1β proteins can restore viability to yeast Ero1p temperature sensitive mutants (Pagani et al., 2000) and support oxidative protein folding of model substrates (Mezghrani et al., 2001), demonstrating that tagging does not effect Ero1β function. A new polyclonal antibody raised against a unique peptide of Ero1β was optimised for use in western blotting to detect tagged transfected Ero1β protein (Figure 3.4) as well as to detect endogenous Ero1β from murine tissue lysates (Figure 3.5).

At steady state (Figure 3.6*A* and *B*) and during biosynthesis (Figure 3.6*C*), Ero1β was present as a smear of oxidised forms, collapsing into a single reduced form upon *in vitro* reduction. On the other hand Ero1α, formed more distinct OX1/OX2 states of which the more compact OX2 was regarded the most stable state *in vivo* (Figure 3.6*C*; (Benham et al., 2000)). The variation in Ero1β redox states observed between cell lines in this study could be partly due to the influence of other chaperone proteins and/or the redox potential of the protein in the different cell lines. Both Ero1β and Ero1α have long half-lives (from this study and (Benham et al., 2000) respectively) compatible with a role for the proteins in ER homeostasis. Ero1β is expressed at low levels in cultured cell lines and thus the general assumption is that low expression of an oxidoreductase is sufficient to drive the oxidation of many substrate proteins through the use of many PDI molecules. At the same time, electron acceptors like Ero proteins could cause damage through production of free radicals if expressed at high levels *in*

vivo. To overcome this situation, Ero proteins might be expressed in low abundance but will then need to catalyse a large number of thiol-disulfide reactions through PDI. However, Figure 3.5 shows that Ero1β is expressed at surprising high levels in stomach and pancreas, suggesting that it may do more than just act as a catalyst for PDI.

The ability of Ero1β to form mixed disulfides with PDI was first demonstrated by Mezghrani et al using a pulse-chase approach (Mezghrani et al., 2001). Ero1β-PDI complexes are alkylation dependent (Figure 3.8*A* and *B*) as previously observed for Ero1α and Ero1p (Mezghrani et al., 2001; Benham et al., 2000; Frand & Kaiser, 1999). However, Ero1β was able to form disulfide-dependent complexes in the presence and in the absence of an alkylating agent (Figure 3.7*A* and *B*). In PDI immunodepletion experiments (Figure 3.8*C* and *D*), the existence of non-PDI disulfide linked complexes was strongly evident.

Although protein oxidation is inhibited by DTT, it is reversible and protein translation, translocation, N-glycosylation and signal sequence cleavage are not affected (Braakman et al., 1992). For example, addition of DTT to *S. cerevisiae* cells blocked the folding and transport of carboxypeptidase Y (CPY), but it did not however interfere with secretion of invertase, a protein that lacked disulfide bonds (Simons et al., 1995). Data from this chapter shows that subjecting Ero1β transfected cells to a reducing (DTT) environment disrupts the majority of Ero1β-mediated covalent and non-covalent complexes, but that an oxidised monomer pool of Ero1β still remained.

Looking at the electrophoretic pattern of Ero1α and Ero1β in diagonal, non-reducing/reducing gels, Mezghrani and colleagues initially suggested formation of a

covalent homodimer in hEROs (Mezghrani et al., 2001). The ability of Ero1β to form these covalent homodimers was shown in this chapter using Myc and HA tagged Ero1β proteins (Figure 3.9). These homodimers were recovered irrespective of whether an alkylating agent was present at the point of lysis. Dimerisation has been a feature of a number of thioredoxin proteins (Liepinsh et al., 2001; Zapun et al., 1995). DsbC, the prokaryotic counterpart of PDI, exhibits both disulfide isomerase and chaperone activity and it is shown to be a V-shaped homodimer (Chen et al., 1999; McCarthy et al., 2000). *DsbC* mutant proteins present as a monomer were able to complement a DsbA null mutation in the presence of DsbB, which suggested that mutant DsbC was converted from an isomerase into an oxidase. These results suggest that keeping DsbC protein in a dimer prevents its oxidation by DsbB, preventing cross-talk between the oxidative and reductive pathways and allowing them to co-exist *in vivo* in the bacterial periplasm (Bader et al., 2001). Hybridising DsbA domains with no isomerase or chaperone activity to DsbC monomers created dimers with increased chaperone and isomerase activity (Zhao et al., 2003). These results suggest that dimerisation could be a possible means of bestowing novel activity to monomeric proteins, which would be an interesting feature for hERO proteins. The recovery of Ero1α-Ero1β heterodimers adds to the complexity of interactions found between oxidoreductases in the ER. Although complexes other than Ero1β-PDI were recovered at different abundance from murine tissue lysates, some of which correspond to possible dimers, the *in vivo* picture still remains incomplete. The molecular requirements for Ero1β dimer formation will be studied and discussed in more detail in Chapter 4.

CHAPTER 4

CXXCXXC MUTANTS OF ERO1β

4.1 Introduction

The interactions and behaviour of wild-type Ero1β were discussed in Chapter 3. Ero1α and Ero1β both have two conserved redox active motifs, a C*XXXX*C motif towards the N-terminus and a C*XX*C*XX*C motif near the C-terminus (Figure 3.2, *A* and *B*, (Cabibbo et al., 2000; Pagani et al., 2000)). The importance of these two motifs in dithiol-disulfide exchange was initially identified in yeast Ero1p (Frand & Kaiser, 2000). The authors showed that mutants with cysteine to alanine substitutions at C100, C105, C352 and C355 were not able to restore growth to *ero1-1* temperature sensitive cells at the restrictive temperature, or rescue the inviability associated with a chromosomal deletion of ERO1. These mutants when expressed in *ero1-1* cells retained the vacuolar protease CPY in a reduced form within the ER, indicating that these four cysteines are required for efficient disulfide-bond formation. A CGHS-CGHS active site mutant of Pdi1p and a CQHA mutant of Mpd2p were used to identify C100 as the cysteine preferentially attacked in Ero1p. TCA precipitation and AMS modification was used to examine the oxidation states of these mutants *in vivo* which showed that the majority of C352 and C355 mutants were in the reduced form. Taken together, data from this paper suggested that the C100/C105 pair was important for thiol-disulfide exchange with Pdi1p and Mpd2p, whereas the C352/C355 pair was required to maintain the fully oxidized state of Ero1p (Frand & Kaiser, 2000).

These mutational and biochemical studies of the yeast ERO1 gene have shown that the N-terminal active site cysteines are involved in a dithiol-disulfide reaction with PDI. Accepted electrons are then transferred on to the C-terminal active site cysteines that then pass on electrons to molecular oxygen via FAD (Figure 4.1; (Frand & Kaiser, 2000; Tu & Weissman, 2002)).

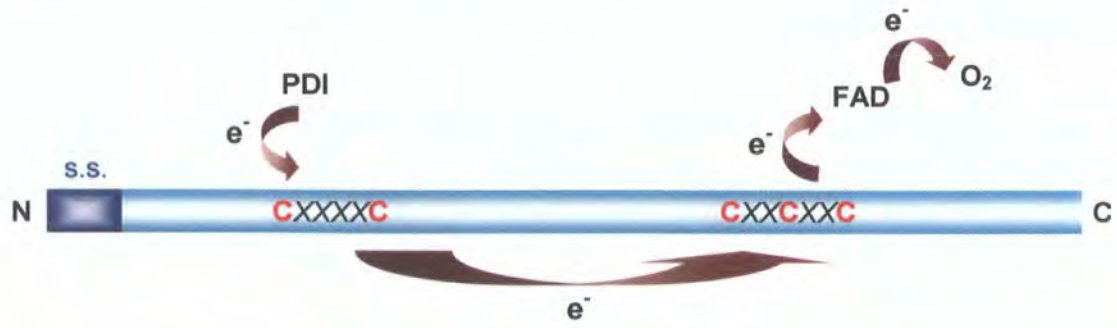

FIGURE 4.1: Schematic representation of dithiol-disulfide exchange of Ero1
Model of the flow of electrons donated from PDI to molecular oxygen via Ero and FAD. The N terminal C*XXX*C and C-terminal C*XXCXX*C active site motifs are shown. s.s = signal sequence. (Reproduced from (Dias-Gunasekara & Benham, 2005)).

The yeast C353/C355 pair is part of a conserved C*XXCXX*C motif found in both Ero1α and Ero1β (Figure 3.1 and 4.2).

FIGURE 4.2: Alignment of the C*XXCXX*C motifs
Human Ero1α (Ero1a_H.s, Q96HE7; *H. sapiens*), human Ero1β (Ero1b_H.s, Q86YB8; *H. sapiens*) and yeast Ero1p (Ero1_S.c, Q03103; S.cerevisiae) are aligned. The C-terminal active site cysteines C*XXCXX*C are shaded red, and identical residues are shaded in black.

Mutational studies at the C*XXCXX*C motif in Ero1α has shown that this active site is important for the folding, structural integrity, as well as the stability of the Ero1α-PDI complex (Benham et al., 2000). Mutations at C394 (C394A) and C397 (C397A) inhibited oxidation of two soluble immunoglobulin subunits; glycosylated JcM (Murine

J chain) with three intra-chain disulfide bonds and the non-glycosylated κ chains (Mezghrani et al., 2001). This work showed that the C394/C397 pair was essential in Ero1α mediated oxidative folding of substrate proteins and complemented Ero1p work by Frand and Kaiser (Frand & Kaiser, 2000). A more recent study by Bertoli and colleagues using a panel of cysteine replacement mutants showed that Ero1α contains two essential cysteine triads, C85/C94/C99 and C391/C394/C397 which cooperate in electron transfer (Bertoli et al., 2004). In Ero1β, the role of the C*XX*C*XX*C motif had not been previously studied and this chapter investigates these Ero1β mutants and the requirement for the C*XX*C*XX*C motif in Ero1β interactions.

4.2 Results

4.2.1 Construction of Ero1β CXXCXXC mutants

To investigate the nature of Ero1β C-terminal active site (C*XX*C*XX*C) mutants, wild-type pcDNAEro1β-Myc and pcDNAEro1β-HA constructs were used in site-directed mutagenesis to create cysteine to alanine mutants, namely Ero1βC390A-Myc, Ero1βC393A-Myc, Ero1βC396A-Myc and Ero1βC390A-HA, Ero1βC393A-HA, Ero1βC396A-HA. The primers used have been detailed in Chapter 2, section 2.3.1.

4.2.2 ER localisation of Ero1β CXXCXXC mutants

ER localisation of wild-type Ero1α and Ero1β gene products in mammalian cells were determined in COS-7 and HeLa cells using immuno-localisation studies (Cabibbo et al., 2000; Pagani et al., 2000). To determine the intracellular localisation of the three C-terminal mutants of Ero1β, HeLa cells were transfected with wild-type Ero1β-Myc (Figure 4.3*A*), Ero1βC390A-Myc (Figure 4.3*B*), Ero1βC393A-Myc (Figure 4.3*C*), and Ero1βC396A-Myc (Figure 4.3*D*). Transfected cells were fixed in MeOH prior to co-staining with an anti-serum against the ER resident protein PDI (Figure 4.3*A-D*, *panel 2*) and a Myc monoclonal antibody (Figure 4.3*A-D*, *panel 1*). Immunofluorescence analysis using confocal microscopy showed that wild-type Ero1β and the three C*XX*C*XX*C mutant distribution largely overlapped with that of PDI (Figure 4.3*A-D*, *panel 3*) demonstrating their localisation in the ER and consistent with the isolation of Ero1β by Con A (Figure 3.5*B*).

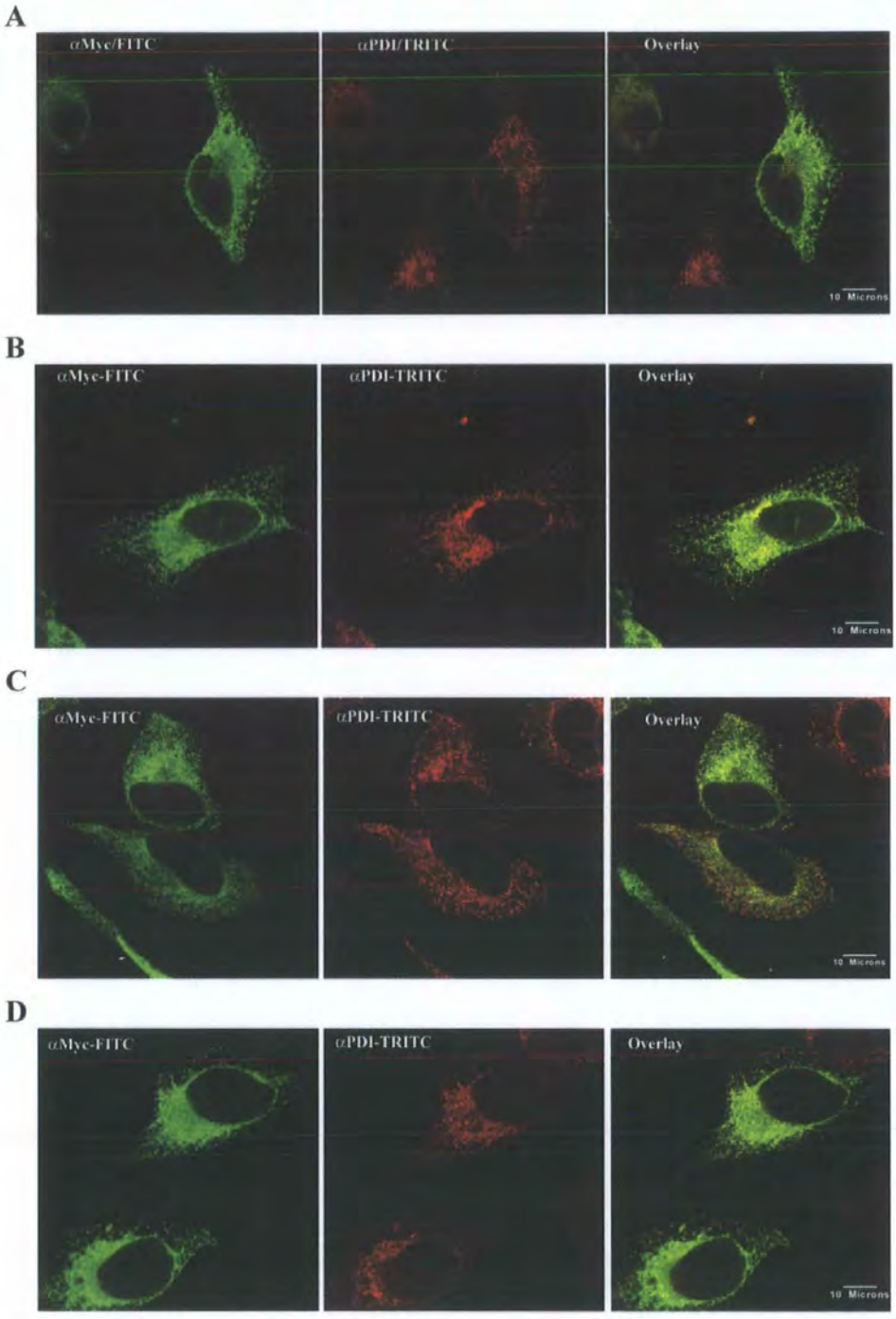

FIGURE 4.3: Wild-type Ero1β and the three active site mutants localise to the ER

A-D. HeLa cells transfected with pcDNA3.1 wild-type Ero1β and three Ero1β C*XX*C*XX*C mutants were fixed 24 hrs after transfection in ice cold MeOH and co-stained with αMyc and αPDI primary antibodies, followed by fluorescein donkey anti-mouse Ig (FITC) and TRITC swine anti-rabbit Ig before analysis under confocal microscopy. Each panel of three images has the αMyc-FITC, αPDI-TRITC and the αMyc/αPDI overlap image from left to right. **A.** wild-type Ero1β, **B.** Ero1βC390A, **C.** Ero1βC393A and **D.** Ero1βC396A.

4.2.3 Ero1β CXXCXXC mutants form alkylation independent complexes

Analysis of Ero1α C*XX*C*XX*C mutants has demonstrated that this C-terminal active site motif is important for protein folding, function, structural integrity, protein half life and the stability of the Ero1α-PDI complex (Benham et al., 2000; Mezghrani et al., 2001). Pulse-chase experiments were carried out to examine the oxidative folding of Ero1β C-terminal mutants in living cells. Ero1βC390A-Myc, Ero1βC393A-Myc and Ero1βC396A-Myc constructs were transfected into HeLa cells, starved for 40 min in medium lacking cysteine and methionine, radio-actively pulse-labelled for 10 min, chased for the indicated times and lysed in the presence of NEM. Post-nuclear supernatants were subjected to immunoprecipitation with αMyc antibody and analysed on non-reducing (Figure 4.4*A*, *lanes 5-10*; 4.4*B*, *lanes 5-10*) and reducing SDS-PAGE (Figure 4.4*A*, *lanes 1-3* and *12-14*; 4.4*B lanes 1-3* and *12-14*). Wild-type Ero1β formed the same smear of oxidised bands (OX) as Figure 3.6*D* under non-reducing SDS-PAGE (Figure 4.4*A*, *lanes 5-7*). Ero1βC390A was less compact and mostly reduced (R) after the 10 min pulse and remained predominantly the same after the 60 min chase (Figure 4.4*A*, *lanes 8-10*). Ero1βC393A was the most similar to wild-type but even this mutant was more reduced (R) after the longest chase time point (Figure 4.4*B*, *lanes 5-7*). Ero1βC396A on the other hand, was more compact and remained reduced (R, Figure 4.4*B*, *lanes 8-10*). These results indicated that mutations at the C*XX*C*XX*C motif affected the redox state of Ero1β. Note the presence of a band around 75 kDa present in wild-type and all three C*XX*C*XX*C mutants, (not present in mock transfectants) but showing far less intensity with Ero1βC396A (Figure 3.6, *C* and *D* and 4.4, *A* and *B*). Attempts to identify this Ero1β interacting protein will be discussed in Chapter 5.

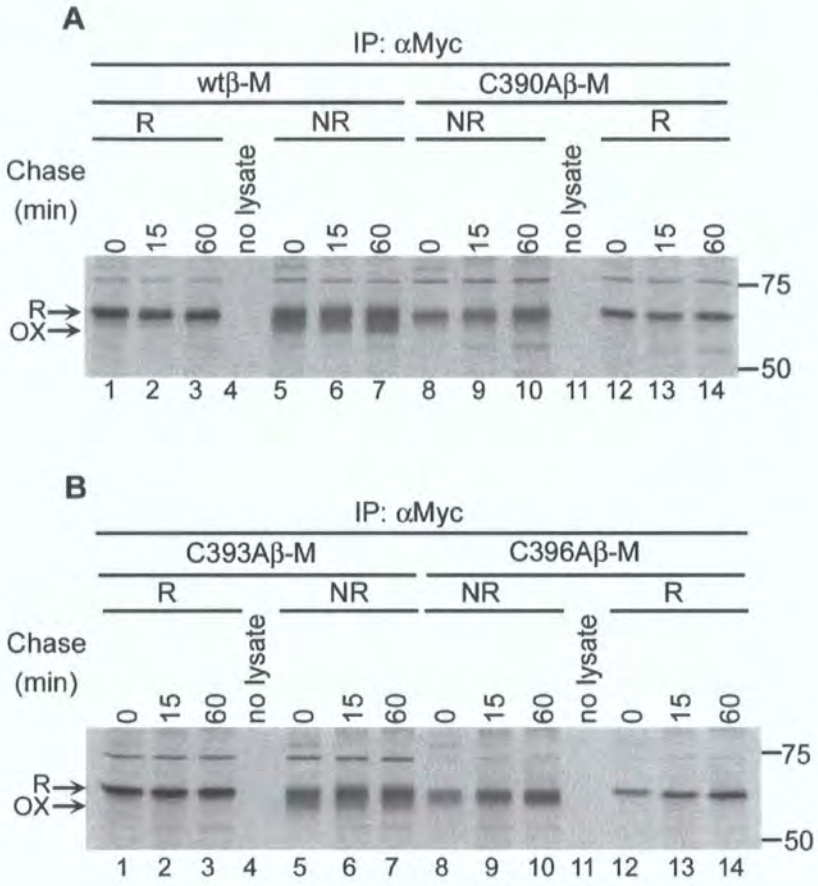

FIGURE 4.4: Oxidative folding of Ero1β *CXXCXXC* mutants

A. HeLa cells transfected with wtEro1β-Myc (*lanes 1-7*) and Ero1βC390A-Myc (*lanes 8-14*) were starved for 40 min, pulse labelled for 10 min, chased for the times indicated and immunoprecipitated (IP) with αMyc (*lanes 1-14*) prior to non-reducing (NR, *lanes 5-10*) and reducing (R, *lanes 1-3* and *12-14*) SDS-PAGE. **B.** Same as for **A**, but transfected with Ero1βC393A-Myc (*lanes 1-7*) and Ero1βC396A-Myc (*lanes 8-14*). Under non-reducing conditions wtEro1β (**A**, *lanes 1-3*) and Ero1βC393A (**B**, *lanes 1-3*) monomers form a smear of oxidation states (OX) compared to Ero1βC390A (**A**, *lanes 8-10*) and Ero1βC396A (**A**, *lanes 8-10*) which are more reduced (R). Note the band around 75 kDa seen at varying intensities in wild-type and mutant Ero1β.

To investigate the behaviour of the Ero1β C*XX*C*XX*C mutants at steady state, HeLa cells were transfected with the three Myc-tagged mutants, Ero1βC390A-Myc, Ero1βC393A-Myc, Ero1βC396A-Myc together with wild-type Ero1β-Myc. The transfected cells were lysed either in the presence or in the absence of the alkylating agent NEM, and the post nuclear supernatants were examined by western blotting using a Myc antibody after non-reducing and reducing 8% SDS-PAGE.

At steady state, wild-type Ero1β monomer is party oxidised partly reduced (Figure 4.5*A*, *lane 1*) as seen in Chapter 3. Ero1βC390A was in a less compact state (Figure 4.5*A*, *lane 3*) which was comparable to the Ero1αC391A mutant (Benham et al., 2000). Ero1βC393A was found as a mixture of oxidised (OX) and reduced (R) forms (Figure 4.5*A*, *lane 5*), similar to wild-type Ero1β, whereas Ero1βC396A was found predominantly in a reduced state (Figure 4.5*A*, *lane 7*). Alkylation was required to trap the oxidation states (Figure 4.5*A*, compare *lanes 1* and *2)*. The mock transfectants were negative (Figure 4.5*A*, *lane 9* and *10*). Reduction of the samples with DTT prior to SDS-PAGE analysis gave a single band (Figure 4.5*B*). These results are similar to the Ero1α C*XX*C*XX*C mutant behaviour, although in Ero1α the monomer oxidation states are more discrete ((Benham et al., 2000) and Figure 3.6*C*, *lane*). The behaviour of Ero1β monomer states was comparable between steady state and pulse chase analysis.

The same lysates when analysed under non-reducing SDS-PAGE, were used to study the ability of the mutants to form higher molecular weight complexes (Figure 4.5*C*). The transferred proteins were probed with αMyc to detect Ero1β protein. In the presence and in the absence of NEM, wild-type Ero1β formed a ladder of complexes similar to that seen in Figure 3.7*A* and *B* (Figure 4.5*C*, *lane 1-2*). All three C-terminal

mutants were able to form a number of higher molecular weight complexes, although they all gave a slightly different pattern from wild-type (Figure 4.5*C*, compare *lanes 1-2* with *lanes 3-8)*. The non-specific nature of the band around 130 kDa (Figure 4.5*C*, *lane 9* and *11*) was discussed in Chapter 3, section 3.2.2.

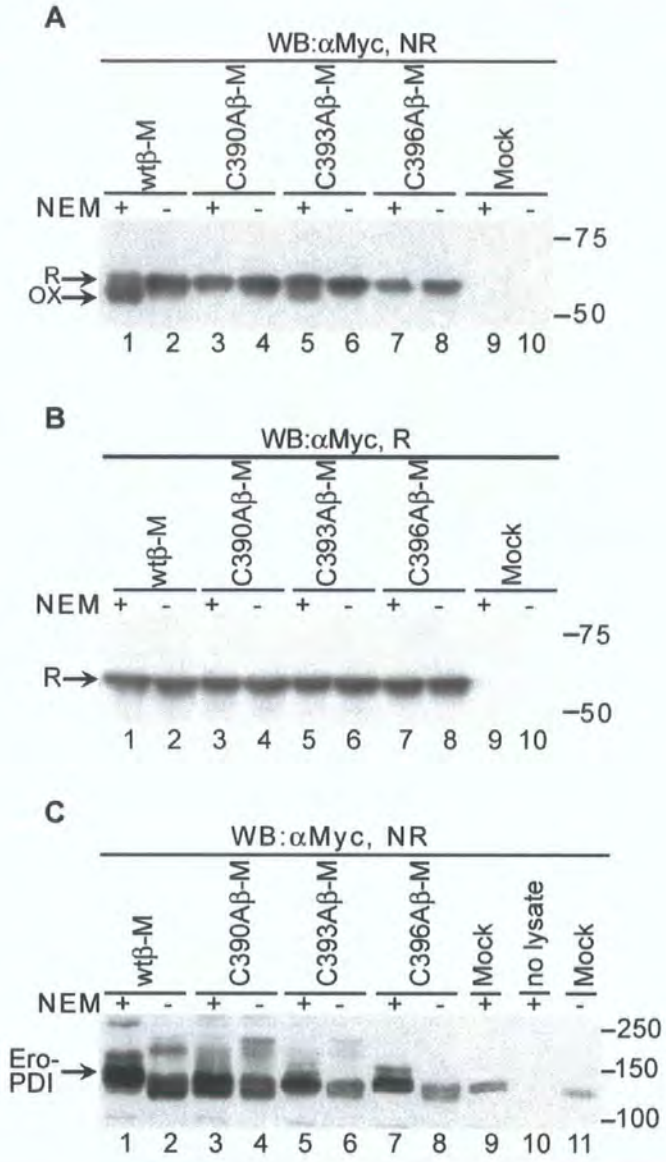

FIGURE 4.5: Ero1β *CXXCXXC* mutants form redox dependent, NEM independent complexes

A. non-reducing (NR) and **B.** reducing (R) SDS-PAGE of Myc tagged wtEro1β (*lanes 1-2*), Ero1βC390A (*lanes 3-4*), Ero1βC393A (*lanes5-6*), Ero1βC396A (*lanes 7-8*), and mock transfectants (*lanes 9-10*) lysed in the presence (*lanes 1*, *3*, *5*, *7* and *9*) or absence (*lanes 2*, *4*, *6*, *8* and *10*) of NEM after western blotting (WB) probed with αMyc. Ero1β oxidised (OX) and reduced (R) monomer forms are indicated. **C.** same as for **A**, except that *lane 10* is loaded with sample buffer only and *lane 11* is loaded with mock transfected cell lysate in the absence of NEM. The Ero-PDI complex is indicated.

4.2.4 Ero1β C390A interacts weakly with PDI

Having established that Ero1β C*XXCXXC* mutants are able to form higher molecular weight complexes, the same lysates as in Figure 4.5 were used to compare their ability to interact with PDI. Wild-type and C*XXCXXC* mutant HeLa cell transfectants, lysed in the presence or in the absence of NEM, were either directly analysed by reducing SDS-PAGE and transferred proteins probed with an anti-serum raised against PDI (Figure 4.6A) to detect the presence of PDI or first subjected to immunoprecipitation with a PDI anti-serum, separated by non-reducing (Figure 4.6*B*) and reducing (Figure 4.6*C*) SDS-PAGE. Transferred proteins were probed with a Myc antibody which should detect any Ero1β-PDI interactions. Wild-type Ero1β forms disulfide-dependent Ero-PDI dimers in the presence of NEM (Figure 4.6*B*, *lane 1*), also seen in Figure 3.8*B*. Ero1βC393A (Figure 4.6*B*, *lanes 5* and *6*) and Ero1βC396A (Figure 4.6*B*, *lanes 7* and *8*) both interacted with PDI in a NEM dependent manner, although less strongly than with wild-type. The Ero1βC390A mutant hardly interacted with PDI (Figure 4.6*B*, *lane 3*) although it did form disulfide dependent complexes (Figure 4.5*C*, *lane 3*). Again, Ero1βC390A complexes were preserved in the absence of an alkylating agent, showing that Ero1βC390A could interact with partner protein(s) other than PDI (Figure 4.5*C*, *lane 4*). All three Ero1β mutants behaved similar to Ero1α C*XXCXXC* mutants with respect to their disulfide dependent interactions with PDI (Benham et al., 2000).

Reduction of the immunoprecipitates prior to SDS-PAGE analysis revealed that wild-type (Figure 4.6*C*, *lane 1*) and the C396A mutant (Figure 4.6*C*, *lane 7*) were able to co-immunoprecipitate with the PDI antibody in the presence of NEM. Both C390A and C393A mutants co-immunoprecipitated weakly, if at all, with PDI in the presence of

NEM (Figure 4.6*C*, *lanes 3* and *5*). Both wild-type Ero1β and Ero1βC396A mutant interacted weakly with PDI in the absence of an alkylating agent (Figure 4.6*C*, compare *lanes 1* and *7* with *lanes 2-6* and *8*). Taken together these results revealed a covalent and a relatively small non-covalent pool of Ero-PDI interactions. These very weak non-covalent interactions are preserved even in the absence of NEM (Figure 4.6*C*, *lanes 2, 4, 6* and *8*).

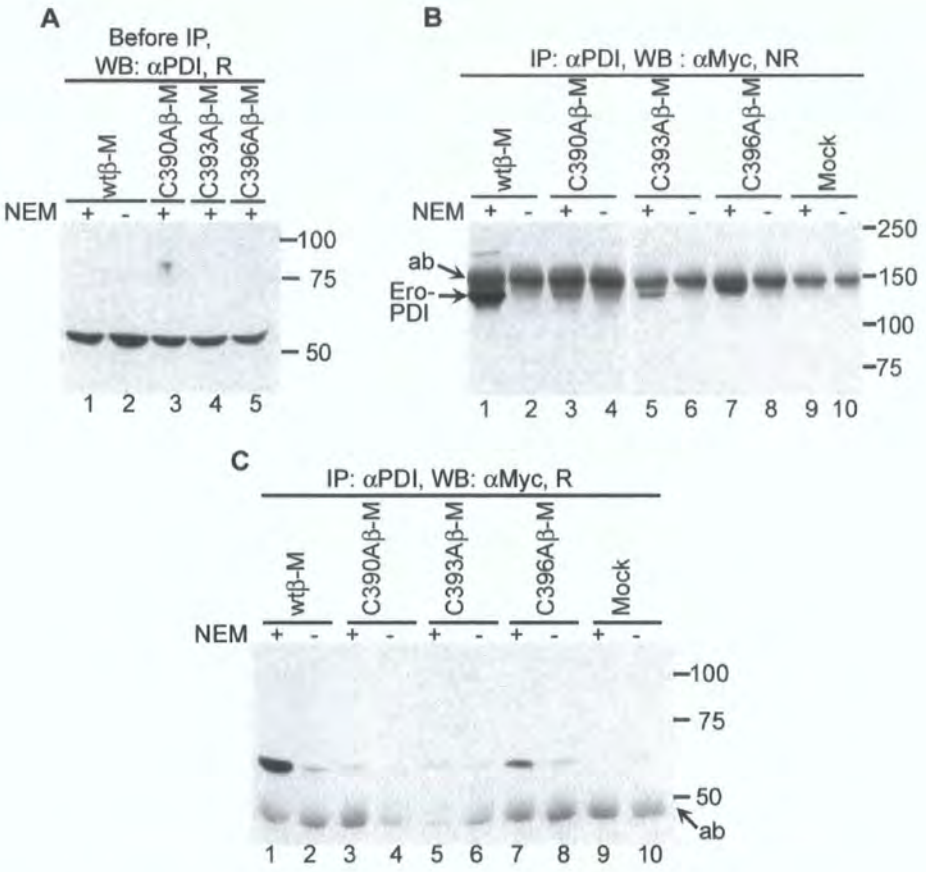

FIGURE 4.6: Ero1βC390A interacts weakly with PDI

A. HeLa cells transfected with Myc tagged wtEro1β (*lane 1-2*), Ero1βC390A (*lane 3*), Ero1βC393A (*lane 4*) and Ero1βC396A (*lane 5*) were lysed in the presence (*lanes 1, 3-5*) and absence (*lane 2*) of NEM and analysed under reducing (R) SDS-PAGE and probed with αPDI. **B.** non-reduced (NR) and **C.** reduced (R) SDS-PAGE of Myc-tagged wtEro1β (*lane 1-2*), Ero1βC390A (*lane 3-4*), Ero1βC393A (*lane 5-6*), Ero1βC396A (*lane 7-8*) and mock transfectants (*lanes 9-10*) lysed in the presence (*lanes 1, 3, 5, 7* and *9*) or absence (*lanes 2, 4, 6, 8* and *10*) of NEM, subjected to immunoprecipitation with αPDI and probed after western blotting (WB) with αMyc. **B.** PDI formed covalent complexes with wtEro1β, Ero1βC393A and Ero1βC396A in the presence of NEM. Antibody complexes (ab) migrated just above the Ero-PDI dimer. **C.** Prominent Ero-PDI interactions (non-covalent plus the covalent pool) were seen with wtEro1β and Ero1βC396A in the presence of NEM. ab= antibody.

4.2.5 Ero1β CXXCXXC mutants can dimerise with wild-type Ero1β

In both Ero1α and Ero1β the C*XX*A*XX*C and C*XX*C*XX*A mutants were able to form disulfide-dependent dimers with PDI ((Benham et al., 2000) and Figure 4.6*B*, *lanes 5* and *7*). However, in Ero1α the C394A and C397A mutants were not able to rescue the temperature sensitivity of the yeast *ero1-1* mutant (Cabibbo et al., 2000). On the other hand, the A*XX*C*XX*C mutant in both Ero1α and Ero1β interacted poorly with PDI ((Benham et al., 2000) and Figure 4.6*B*, *lane 3*), but the C391A mutant of Ero1α was able to rescue the *ero1-1* yeast phenotype (Cabibbo et al., 2000). Taken together these results implied that interactions other than covalent Ero-PDI interactions could be required for Ero function. Given that wild-type Ero1β dimerisation could occur (as discussed in Chapter 3, section 3.2.3) the effects of the active site on dimerisation were investigated.

To investigate whether mutant Ero1β proteins could associate with wild-type Ero1β, Ero1βC390A-Myc (Figure 4.7, *A* and *B*), Ero1βC393A-Myc (Figure 4.7, *C* and *D*) and Ero1βC396A-Myc (Figure 4.7, *C* and *D*) were co-transfected with wild-type Ero1β-HA. Reduced blots showed that single and double transfectants expressed the expected proteins (Figure 4.7, *A* and *C*). Cell lysates were then subjected to immunoprecipitation with the HA antibody, followed by blotting with the Myc antibody (Figure 4.7, *B* and *D*). No co-immunoprecipitaion, thus no signal, was detected in the single or the mock transfectants (Figure 4.7*B*, *lanes 1- 3, 5, 8*; 4.7*D*, *lanes 1-3* and *6*). Wild-type Ero1β-Myc could be co-immunoprecipitated with wild-type Ero1β-HA, verifying this interaction (Figure 4.7*B*, *lane 4*). Ero1βC390A-Myc (Figure 4.7*B*, *lane 6*), Ero1βC393A-Myc (Figure 4.7*D*, lane 4) and Ero1βC396A-Myc (Figure 4.7*D*, lane 5)

specifically co-immunoprecipitated with wild-type Ero1β-HA. Cell lysates used in Figure 4.7*A* and *C*, when analysed under non-reducing SDS-PAGE followed by immunoblotting with αMyc and αHA (Figure 4.7*E*), showed that an intermediate band ~120 kDa (arrow) was present only in the double transfectants (Figure 4.7*E*, *lanes 4*, *5*, *7* and *8*). This intermediate band was more prominent in Ero1βC393A plus wild-type Ero1β (*lane 4*) and Ero1βC396A plus wild-type Ero1β (*lane 5*) compared with the Ero1βC390A (*lane 8*) mutant. Thus mutations of the C*XX*C*XX*C motif do not interfere with disulfide-linked complex formation with wild-type Ero1β.

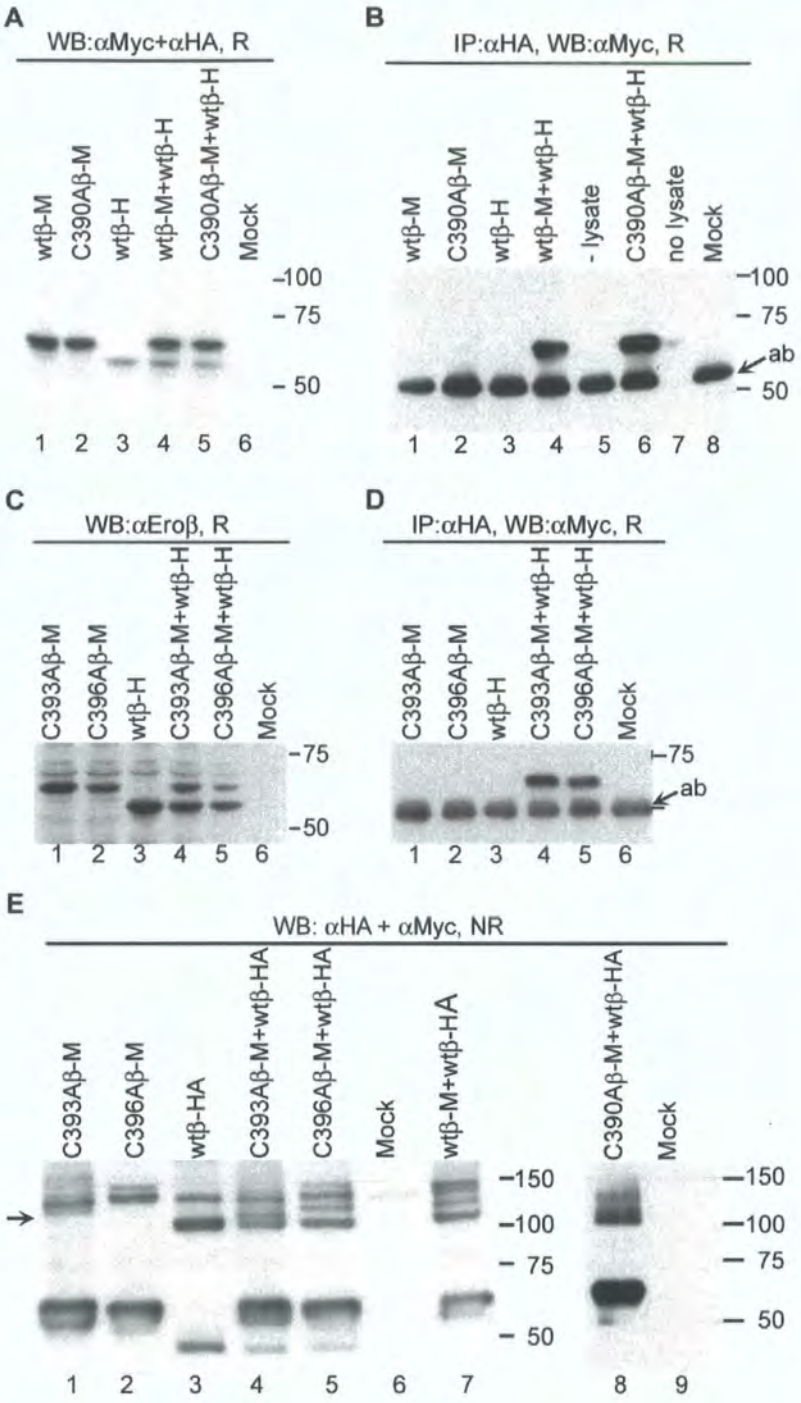

FIGURE 4.7: Ero1β *CXXCXXC* mutants dimerise with wild-type Ero proteins

A. HeLa cell lysates expressing wtEro1β-Myc (*lane 1*), Ero1βC390A-Myc (*lane 2*), wtEro1β-HA (*lane 3*), wtEro1β-Myc and wtEro1β-HA (*lane 4*), Ero1βC390A-Myc and wtEro1β-HA (*lane 5*) and mock transfected (*lane 6*) were analysed by reducing SDS-PAGE and immunoblotted for Ero1β with both αHA and αMyc. **B.** same as for **A**, except that lysates were first immunoprecipitated with αHA prior to immunoblotting with αMyc. *Lanes 1-4* are the same as in **A**, *lane 5* αHA antibody only, *lane 6* is

Ero1βC390A-Myc and wtEro1β-HA, *lane 7* is sham-loaded, and *lane 8* contains the mock sample. Ab = antibody from the immunoprecipitates. **C** and **D.** HeLa cell lysates expressing Ero1βC393A-Myc (*lane 1*), Ero1βC396A-Myc (*lane 2*), wtEro1β-HA (*lane 3*), Ero1βC393A-Myc plus wtEro1β-HA (*lane 4*), Ero1βC396A-Myc plus wtEro1β-HA (*lane 5*), and mock (*lane 6*) were analysed by reducing SDS-PAGE and immunoblotted for Ero1β directly (**C**) or first subjected to immunoprecipitation with αHA and immunoblotted with αMyc (**D**). All C*XXCXX*C mutants interact with wild-type Ero1β. ab = antibody from the immunoprecipitate. **E.** Cell lysates from **A** and **C** analysed under non-reducing SDS-PAGE and probed with both αHA and αMyc. Ero1βC393A and Ero1βC396A showed a more prominent intermediate band ~120 kDa similar to wtEro1β, whereas Ero1βC390A was more smeary.

4.2.6 C396 is required for Ero1β homodimer formation

Since mixed complexes could be formed between wild-type Ero1β and C*XXCXXC* Ero1β mutants, the ability of the C-terminal mutants to form mutant-mutant dimers was investigated. HA-tagged versions of Ero1βC390A, Ero1βC393A and Ero1βC396A were constructed and co-transfected into HeLa cells with the equivalent Myc-tagged Ero1β mutants. Cell lysates were analysed by reducing SDS-PAGE and transferred proteins probed with Ero1β serum to confirm the expression of the proteins (Figure 4.8*A*), or the cell lysates were first subjected to immunoprecipitation with the Myc antibody and immunoblotted with αEro1β (Figure 4.8*B*).

The α-Myc monoclonal antibody did not pull down any HA-tagged Ero1β protein in the mock and single transfectants (Figure 4.8*B*, *lanes 2-5*), but did bring down Myc-tagged protein, as expected (Figure 4.8*B*, *lane 1*). Wild-type Ero1β-HA as well as Ero1βC390A-HA and Ero1βC393A-HA proteins co-immunoprecipitated with their Myc tagged counterparts (Figure 4.8*B*, *lanes 6-8*). However, the Ero1βC396A mutant did not co-immunoprecipitate (Figure 4.8*A*, *lane 9*). These data demonstrated that Ero1β A*XXCXXC* and C*XXAXXC* mutants were able to interact with themselves and with wild-type Ero1β protein. On the other hand, an Ero1β C*XXCXXA* mutant was able to interact with wild-type Ero1β but could not dimerise with the mutant counterpart.

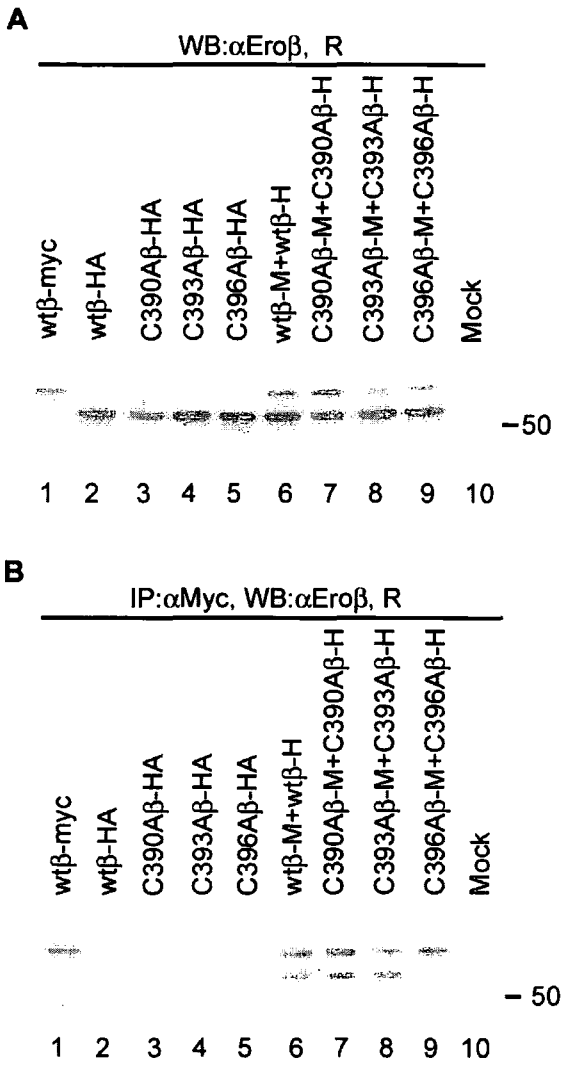

FIGURE 4.8: Ero1βC396A proteins do not form mutant-mutant dimers

A. HeLa cell lysates expressing wtEro1β-Myc (*lane 1*), wtEro1β-HA (*lane 2*), Ero1βC390A-HA (*lane 3*), Ero1βC393A-HA (*lane 4*), Ero1βC396A-HA (*lane 5*), wtEro1β-Myc and wtEro1β-HA (*lane 6*), Ero1βC390A-Myc and Ero1βC390A-HA (*lane 7*), Ero1βC393A-Myc and Ero1βC393A-HA (*lane 8*), Ero1βC396A-Myc and Ero1βC396A-HA (*lane 9*) or mock (*lane 10*) were analysed by reducing SDS-PAGE and immunoblotted with αEroβ. **B.** same as for **A**, except that the lysates were first subjected to immunoprecipitation with αMyc antibody prior to immunoblotting with αEroβ.

The ability of Ero1β C*XX*C*XX*C mutants to interact with their C*XX*C*XX*C counterparts in Ero1α was investigated by double transfecting Ero1β Myc tagged mutants together with non-tagged Ero1α mutants (Figure 4.9). HeLa cells were either mock transfected (Figure 4.9*A* and *B*, *lane 13*), single transfected (Figure 4.9*A* and *B*, *lane 1-8*) or double transfected with wild-type Ero1α and wild-type Ero1β-Myc (Figure 4.9*A* and *B*, *lane 9*), Ero1αC391A plus Ero1βC390A-Myc (Figure 4.9*A* and *B*, *lane 10*), Ero1αC394A plus Ero1βC393A-Myc (Figure 4.9*A* and *B*, *lane 11*) and Ero1αC397A plus Ero1βC396A-Myc (Figure 4.9*A* and *B*, *lane 12*). Cell lysates subjected to immunoprecipitation with αMyc prior to reducing SDS-PAGE and probing the transferred proteins with D5 antibody, showed that the A*XX*C*XX*C (Figure 4.9*A*, *lane 10*), and C*XX*A*XX*C (Figure 4.9*A*, *lane 11*) mutants of Ero1α and Ero1β were able to interact with each other similar to wild-type Ero1α and Ero1β (Figure 4.9*A*, *lane 9*). However, Ero1β C*XX*C*XX*A mutant was unable to interact with the C*XX*C*XX*A Ero1α mutant (Figure 4.9*A*, *lane 12*). The cell lysates were directly analysed by reducing SDS-PAGE, probed with D5 antibody (Figure 4.9*B*) and αMyc (Figure 4.9*C*) to confirm the expression of the transfected proteins. Taken together the results were consistent with a symmetrical, redox-dependent Ero dimer in which the C396/C397 residue was required for dimerisation.

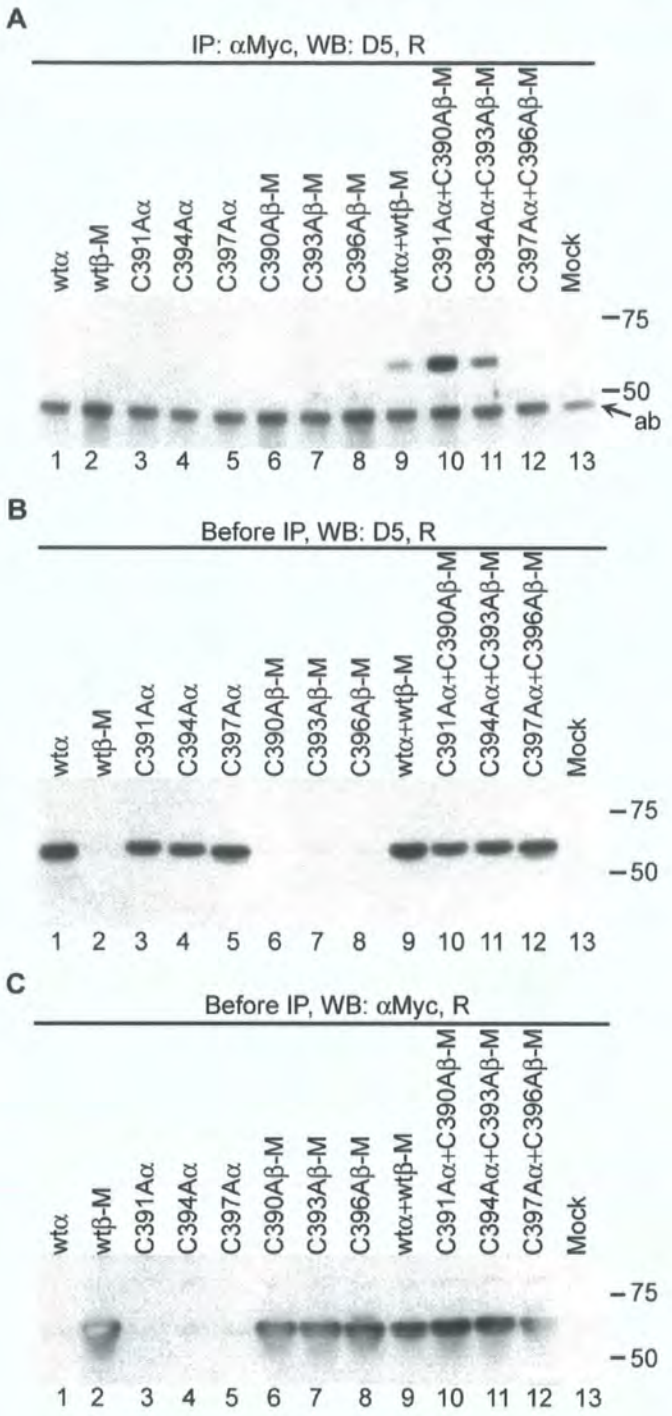

FIGURE 4.9: Ero1α and Ero1β *CXXCXXA* mutants do not interact

A. HeLa cell lysates expressing wtEro1α (*lane 1*), wtEro1β-Myc (*lane 2*), Ero1αC391A (*lane 3*), Ero1αC394A (*lane 4*), Ero1αC397A (*lane 5*), Ero1βC390A-Myc (*lane 6*), Ero1βC393A-Myc (*lane 7*), Ero1βC396A-Myc (*lane 8*), wtEro1α and wtEro1β-Myc (*lane 9*), Ero1αC391A and Ero1βC390A-Myc (*lane 10*), Ero1αC394A and Ero1βC393A-Myc (*lane 11*), Ero1αC397A and Ero1βC396A-Myc (*lane 12*) or mock (*lane 13*) were first subjected to immunoprecipitation (IP) with αMyc antibody

prior to reducing SDS-PAGE analysis and immunoblotting with αEro1α (D5). Ero1αC397A mutant does not co-immunoprecipitate with Ero1βC396A (*lane 12*). ab = antibody from the immunoprecipitate. **B** and **C.** same as for **A**, except that the lysates were directly analysed by reducing SDS-PAGE (Before IP) and immunoblotted with (**B**) αEroα (D5) or with (**C**) αMyc.

4.2.7 Model for the Ero1 dimer

To identify a molecular basis for the dimer of Ero1β, and to understand the role of C396A mutant in disrupting it, the recently determined crystal structure of yeast Ero1p (Gross et al., 2004) was analysed. Although there is only a single monomer in the asymmetric unit of the two different crystal forms of the enzyme reported (PDB codes 1RP4 and 1RQ1), examination of the crystal contacts revealed a single dimer interaction between the monomers (Figure 4.10*A*). This is consistent with the symmetrical dimer suggested by the immunoprecipitation experiments in Figure 4.7 to 4.9. In the model of this dimer, the N termini are bought into close proximity and could thus interact to form part of the dimer interface. This part of the N terminus is absent in the construct used to crystallise the two forms of Ero1p. The crystal structure was of a truncated *S. cerevisiae* Ero1p protein, which shares ~25% sequence identity with full length human Ero1β. The human enzyme has several amino acid inserts, ranging in size from 5 to 25 residues. Analysis of the crystal structure confirmed that these inserts are all found at the surface in positions where additional structure can be accommodated. In addition, none of these inserts would disrupt the presumed dimer interface.

In the proposed Ero1p dimer the monomers are arranged so that the active sites are on the same side of the dimer facing each other. The dimer brings together the adenosine groups of the two FAD moieties to close proximity; in fact the two hydroxyls of the ribose sugars of the adenosine moiety of FAD form hydrogen bonds to each other (Figure 4.10*A*). The FADs contribute to 20% of the dimer interface and therefore might be essential for dimer formation. Mutagenesis at the C*XXCXXC* motif revealed that the Ero1βC396A mutation disrupted dimer formation (section 4.2.6) but this 396 cysteine is buried within the active site (Figure 4.10*B*) and so is highly unlikely to be involved

in an inter-molecular disulfide bond to form the dimer. Rather, due to its contact with the FAD cofactor (Figure 4.10*B*), mutation at C396 is more likely to disrupt FAD binding leading to the FAD-FAD dimer interface being lost.

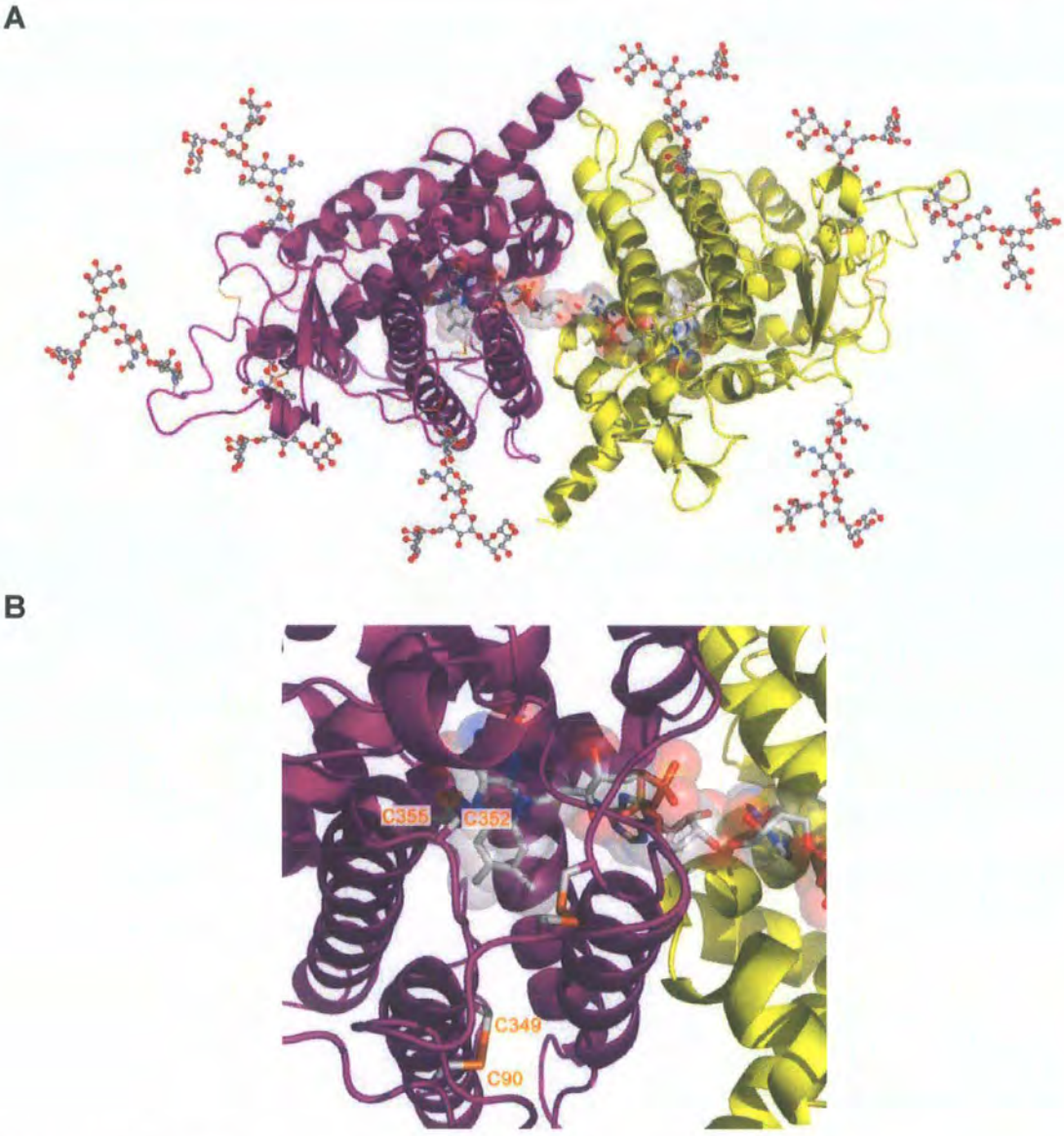

FIGURE 4.10: Structural model of an Ero dimer

A. two Ero1p monomers form significant interactions (non-bonded and four hydrogen bonds) between the two symmetrically related FAD molecules (space filling). The four glycans per monomer are located away from the dimer interface (stick and ball representations). **B.** detail of the dimer interface showing the C90-C349 disulfide bond (C81-C391 in Ero1β), the C353-C355 active site disulfide (C393-C396 in Ero1β), and C100-C105, which is not labelled for clarity. C355 (C396) is buried within the monomer, and is in Van der Waals contact with the FAD (stick and ball representation), but is unlikely to form a dimeric, intermolecular disulfide. Graphics were generated using the PyMOL program (DeLano, W. L., The PyMOL Molecular Graphics System (2002) DeLano Scientific, Can Carlos, CA) by Adrian Lapthorn, University of Glasgow, UK.

4.3 Discussion

This chapter focuses on characterising three Ero1β C-terminal active site mutants. All three mutants showed ER localisation similar to wild-type protein and under steady state conditions formed higher molecular weight complexes independent of an alkylating agent (Figure 4.5). Prior to this study it was known that Ero proteins and PDI are required for disulfide bond formation in the ER (Cabibbo et al., 2000; Pagani et al., 2000; Frand & Kaiser, 2000; Frand & Kaiser, 1999). However, an Ero1α C391A mutant can rescue the temperature sensitivity in yeast *ero1-1*, but had little affinity for PDI (Cabibbo et al., 2000; Benham et al., 2000; Bertoli et al., 2004). Results from this chapter show that in Ero1β, this C390A mutant can still only interact weakly with PDI (Figure 4.6) but is able to homodimerise (Figure 4.8). On the other hand, the inactive Ero1β C396A mutant (Pagani et al., 2000) is able to interact with PDI (Figure 4.6) but cannot homodimerise (Figure 4.8). Although both Ero1α and Ero1β allow the growth of mutant *ero1-1* yeast cells at the restrictive temperature (Cabibbo et al., 2000; Pagani et al., 2000), Ero1α (and probably Ero1β) cannot complement ΔERO1 cells in which the endogenous ERO gene has been disrupted (Pagani et al., 2001). A similar result was seen when an Ero1pΔC mutant (Ero1p mutant lacking the C-terminal tail) was expressed in *ero1-1* and ΔERO1 cells (Pagani et al., 2001). The authors suggest that in the *ero1-1* transformants, functional hetero-dimers are being formed between endogenous Ero1p and the expressed proteins. Taken together, the literature and the data from this chapter suggest that Ero-Ero dimers are important for the functional activity of this family of Ero proteins.

Experimental data from this chapter shows that dimerisation is partly controlled by the C*XX*C*XX*C motif, although other covalent and non-covalent interactions are likely to

play a role in establishment of the dimers. Both the Ero-PDI and Ero-Ero interactions are stable under non-reducing conditions (in the presence of SDS), but the strength of these interactions vary, given that the Ero-PDI interaction requires trapping by an alkylating agent while Ero-Ero interactions do not.

Reconstruction of an Ero-Ero dimer from the Ero1p crystal structure suggests that the glycosylation sites of Ero1p, Ero1α and Ero1β are all located away from the dimer interface, and thus would not prevent Ero-PDI interactions (Figure 4.10*A*). Comparison of the two Ero1p crystal forms revealed a flexible loop containing the C100/C105 disulfide bond which adopts an 'in' and 'out' conformation (Figure 4.11). Electrons accepted from PDI by the C100/C105 disulfide bond in the 'out' conformation could shuttle the electrons onto the C352/C355 active site disulfide when in the 'in' conformation. This likely site for PDI docking is also positioned away from the dimer interface, which suggests that Ero-PDI heterodimers and Ero-Ero dimers might not be separate entities. The immunodepletion experiments from chapter 3 (Figure 3.8*C* and *D*) suggest that Ero-PDI complexes are separate from Ero-Ero dimers in a Triton-X-100 lysate. However it remains possible that tetrameric complexes between Ero-PDI and Ero-Ero could still operate under different situations *in vivo*.

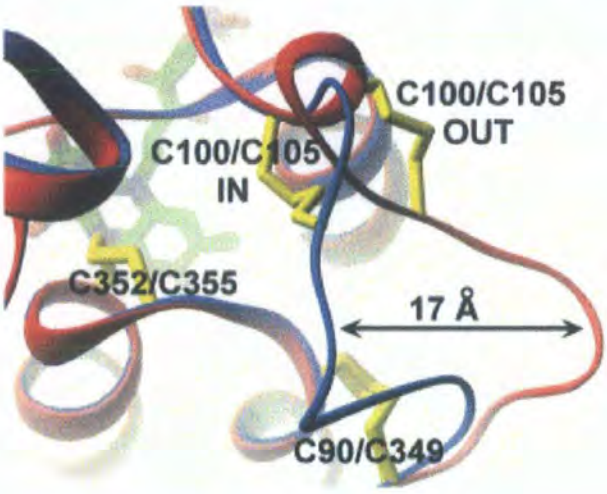

FIGURE 4.11: Flexibility of the Ero1p C100/C105 loop

The two Ero1p crystal forms are superimposed to give the 'in' and 'out' conformations to the C100/C105 loop which can move by about 17 Å. Disulfide bonds are shown in yellow. Reproduced from (Gross et al., 2004).

The Ero1p dimer model is held together by a hydrogen bonding network at the dimer interface (Figure 4.10). Two hydrogen bonds link the two FAD molecules and are likely to be important for stability of the dimer, given that the Ero1βC396A mutation disrupts dimer formation. C396 together with C393 probably passes on electrons to FAD for donation to oxygen (Tu & Weissman, 2002). Thus the loss of C396 is likely to lead to the loss of dimerisation indirectly by disrupting FAD binding. The proximity of the N-termini in the model of the truncated Ero1p dimer, suggests that the N-terminal cysteines upstream of the C*XXX*C redox motif (C42 and C44, Figure 3.1) could be close enough to form an intermolecular disulfide bond. This could explain the appearance of dimers under non-reducing conditions. The Ero1α/Ero1β heterodimers (Figure 4.9) add another level of complexity to the disulfide bond formation pathway, indicating that these heterodimers might play a role in the response to combined UPR and hypoxia.

In Ero1p, the formation of an intra-molecular disulfide bond between C90 and C349 was first suggested through mutagenesis studies (Frand & Kaiser, 2000). Bertoli and colleagues used a panel of Ero1α deletion and cysteine replacement mutants which showed that C85 and C391 (equivalent to C90 and C349 in Ero1p respectively) are important for Ero1α function, probably by allowing efficient PDI oxidation (Bertoli et al., 2004). The prediction for a C90/C349 inter-molecular disulfide bond was confirmed with the published Ero1p crystal structure (Gross et al., 2004). The weak covalent association of Ero1βC390A (equivalent to C349 in Ero1p) mutant with PDI (Figure 4.6*B*), can also be explained using this long-distance intra-molecular disulfide bond, which when disrupted, probably causes structural changes which are needed for interactions with PDI.

Having seen the Ero protein cofactor, FAD, playing an important role in stabilising a model of the homo/heterodimer, two mutations in Ero1β FAD binding domain were investigated and will be discussed in Chapter 5.

CHAPTER 5

BEHAVIOUR OF ERO1β FAD MUTANTS

5.1 Introduction

The C*XX*C*XX*C motif in Ero proteins is in contact with a non-covalently bound FAD molecule and in yeast Ero1p the FAD cofactor is held between helixes α2 and α3 in a bent conformation (Gross et al., 2004). Two mutants of Ero1p, *ero1-1* and *ero1-2* were identified through genetic screens as having a temperature-sensitive and DTT-hypersensitive phenotype, respectively (Frand & Kaiser, 1998; Pollard et al., 1998). In the yeast *ero1-1* strain under restrictive temperatures a subset of secretory proteins showed defects in maturation and were retained in the ER (Frand & Kaiser, 1998), whereas the *ero1-2* strain showed extreme DTT sensitivity and had a modestly up regulated UPR even under non stress conditions (Pollard et al., 1998), thus implying a defect in oxidative protein folding due to both mutations. Each of the mutant strains had a single amino acid substitution; G229S (equivalent to G252S in Ero1β) was responsible for the *ero1-1* phenotype and H231Y (equivalent to H254Y in Ero1β) resulted in the *ero1-2* phenotype. Sequence alignment of FAD binding regions from Ero1β, Ero1α and Ero1p shows the conserved nature of glycine and histidine residues (Figure 5.1).

FIGURE 5.1: Alignment of the FAD binding regions

FAD binding regions from Human Ero1β (Ero1b_H.s; Q86YB8), human Ero1α (Ero1a_H.s; Q96HE7) and yeast Ero1p (Ero1_S.c; Q03103) are aligned. Conserved residues are shaded in black. The conserved Glycine and Histidine residues mutated in the *ero1-1* and *ero1-2* yeast strain are shaded in green.

The flavin fold found in Ero proteins is novel among other known FAD-binding protein and thiol-oxidoreductases (Fraaije & Mattevi, 2000), but is related to that of Erv2p, an alternative oxidoreductase in the yeast ER (Gross et al., 2002). Comparing the crystal structures of Erv2p (Gross et al., 2002) and the recently published Ero1p (Gross et al., 2004), shows that the catalytic cores of both these enzymes are formed by four anti-parallel α-helixes which occur in a different order in the primary sequence, but do create the flavin-binding pocket. The G229 and H231 residues of Ero1p are both within the flavin fold, with H231 in contact with ribose 5'phosphate group of the FAD moiety (Gross et al., 2004). In Ero1p, residues R187, T189, W200, S228, H231 and R260 form hydrogen bonds or salt bridges with the FAD cofactor and are conserved in Ero1α and Ero1β.

Molecular oxygen was found to be the preferred terminal electron acceptor for Ero1p by monitoring the consumption of O_2 during reoxidation of RNase A catalysed by purified Ero1p (Tu & Weissman, 2002). At the structural level however, Ero1p does not have a channel or a clear path for oxygen to gain access to the isoalloxazine ring of the FAD (Gross et al., 2004). This is in contrast to Erv2p which has a channel suitable in diameter for the passage of an oxygen molecule (Gross et al., 2002). The lack of a oxygen channel in Ero1p suggests the presence of a possible gating mechanism to allow access to the active site (Lario et al., 2003).

The ero1 mutants are thus likely to have alterations in their flavin fold due to changes in their structure and charge, which could lead to loss of function by preventing the normal transfer of electrons to occur. However, the biochemistry of the FAD binding site mutants has not been fully examined so far. Since yeast Ero1p and human Ero1β

both share conserved binding site residues (Figure 5.1), this chapter uses the knowledge from the characterised Ero1β protein from Chapters 3 and 4 to study the effects of the *ero1-1* and *ero1-2* mutations on ERO gene products.

5.2 Results

5.2.1 Construction of Ero1β FAD mutants

To investigate the behaviour of Ero1β FAD domain mutants, the wild-type pcDNAEro1β-Myc construct was used in site-directed mutagenesis to create a glycine to serine mutation at 252 (Ero1βG252S) and a histidine to tyrosine mutation at 254 (Ero1βH254Y). The primers used have been detailed in Chapter 2, section 2.3.1. Two FAD domain mutants with an HA tag were constructed by cloning the appropriate mutation region from the Myc tagged counterpart into pcDNAEro1β-HA vector. Vector and both Ero1βG252S-Myc and Ero1βH254Y-Myc constructs were digested with *Nhe1* and ligated as described in Chapter 2 section 2.3.1, to form Ero1βG252S-HA and Ero1βH254Y-HA. Each construct was verified by DNA sequencing.

5.2.2 Biosynthesis of Ero1βG252S and Ero1βH254Y mutants

To investigate whether these FAD mutant proteins were glycosylated, wild-typeEro1β-Myc (Figure 5.2*A*, *lanes 2-3*), Ero1βH254Y-Myc (Figure 5.2*A*, *lanes 4-5*) and Ero1βG252S-Myc constructs were ^{35}S labelled during *in vitro* translation in the presence of semi-permeabilised (SP) cells (Figure 5.2*A*, *lanes 2-7*). Cell pellets were lysed in the presence of NEM, digested with endoglycosidase H (Endo H; Figure 5.2*A*, *lanes 3*, *5* and *7*) and analysed under reducing SDS-PAGE. Endo H cleaves between

the two N-acetylglucosamine residues in high mannose N-glycan structures, thus a protein will be Endo H resistant if its' N-glycans are modified by the Golgi apparatus. The presence of only a non-glycosylated form of Ero1β (nG) after Endo H treatment, indicated that wild-type (Figure 5.2*A*, *lanes 3*) and mutant proteins (Figure 5.2*A*, *lanes 5* and *7*) were Endo H sensitive and confirmed the proteins were glycosylated and resident in the ER.

In Ero1α, mutations at the C-terminal C*XXCXX*C motif altered the half-life of the protein as well as causing folding defects and alteration to Ero-PDI complex formation (Benham et al., 2000). Thus it was formally possible that the reason for the temperature sensitivity and DTT hypersensitivity phenotypes was the rapid turnover of the protein causing disruption of Ero function. To investigate whether protein biosynthesis was affected, HeLa cells were transfected with Ero1βH254Y-Myc (Figure 5.2*B*), Ero1βG252S-Myc (Figure 5.2*C*), wild-type Ero1β-Myc (Figure 5.2*D*), or mock transfected (Figure 5.2*E*) and used in a metabolic labelling experiment. Following a 40 min starvation in cysteine and methionine-free medium, cells were pulse-labelled for 10 min and chased up to one hour, prior to lysis in the presence of NEM. Lysates were subjected to immunoprecipitation with the Myc antibody and analysed by non-reducing (Figure 5.2*B*, *C* and *D*, *lanes 1-4; E, lane 1*) and reducing (Figure 5.2*B*, *C* and *D*, *lanes 6-9; E, lane 2*) SDS-PAGE. Ero1βH254Y-Myc and Ero1βG252S-Myc monomer both resolved as a smear of bands under non-reducing conditions (OX, Figure 5.2*B* and *C*, *lanes 1-4*) which compact to a single band upon reduction with DTT (R, Figure 5.2*B* and *C*, *lanes 6-9*). No folding defect could be detected in the two FAD binding site mutants when compared to wild-type Ero1β (Figure 5.2*D*) during the one-hour chase period. To determine the half-life of wild-type Ero1β and the two FAD mutants, an

extended pulse-chase experiment was carried out with chase points up to 22 hrs (Figure 5.2*F*). Quantitation revealed that wild-type Ero1β is a relatively stable protein with a half life of 24-25 hrs (Figure 5.2 *F*, *lanes 1-4*). Ero1βH254Y (Figure 5.2 *F*, *lanes 5-8*) and Ero1βG252S (Figure 5.2 *F*, *lanes 9-12*) had somewhat shorter half-lives when compared to wild-type Ero1β, these being 16-19 hrs and 15-17 hrs respectively. These results indicate that although the FAD binding domain mutants have slightly reduced half-lives when compared to wild-type Ero1β, the mutant proteins do not rapidly degrade and the mutations do not affect Ero1β behaviour as judged by reducing SDS-PAGE.

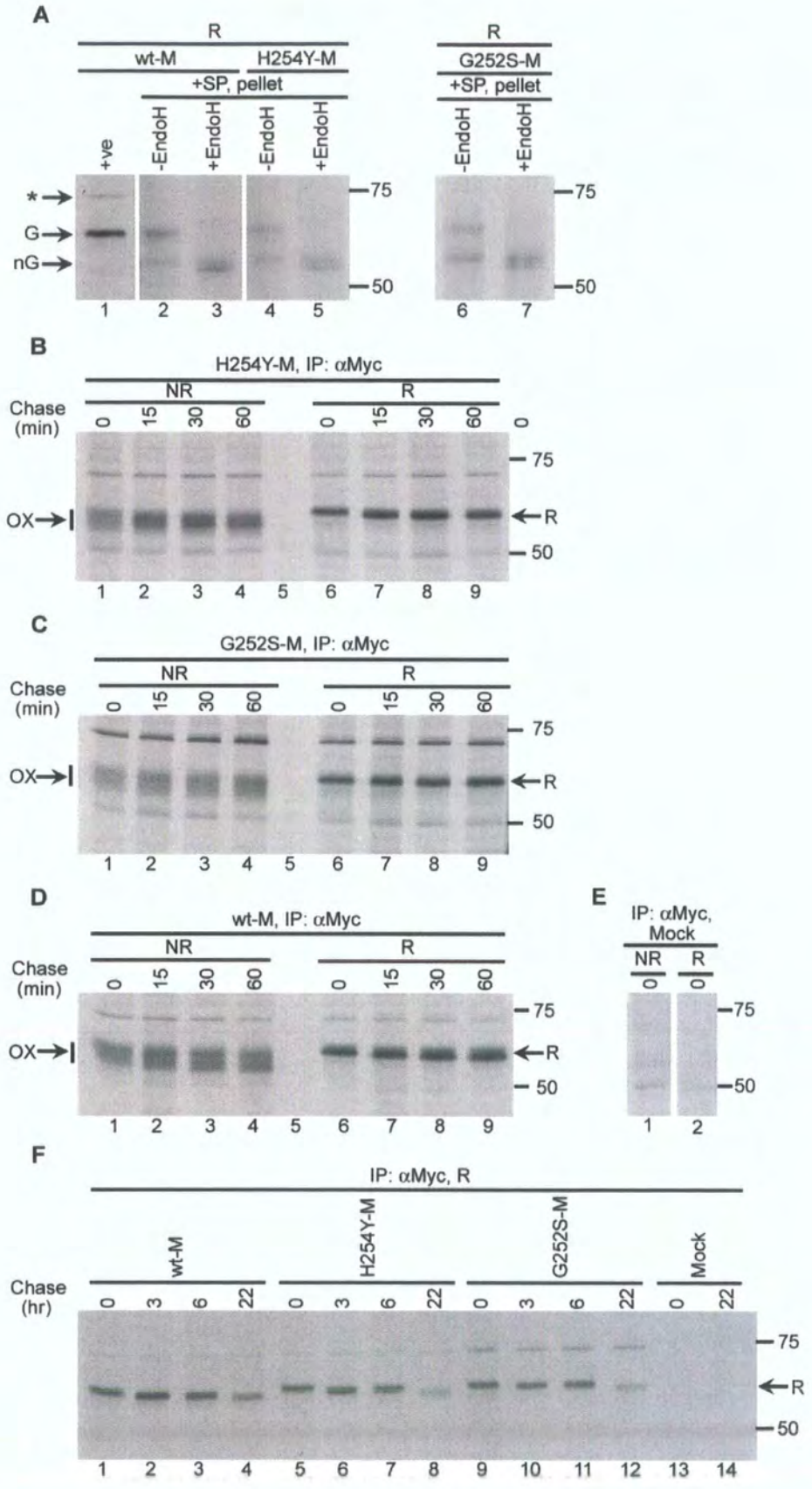

FIGURE 5.2: Biosynthesis of Ero1βH254Y and Ero1βG252S proteins

FIGURE 5.2: Biosynthesis of Ero1βH254Y and Ero1βG252S proteins

A. Wild-type (wt) Ero1β-Myc (*lanes 2-3*), Ero1βH254Y-Myc (*lanes 4-5*) and Ero1βG252S-Myc (*lanes 6-7*) mRNA was translated at 30°C for 1 hr in the presence of ~1 X 10^5 semi-permeabilised (SP) HeLa cells with ^{35}S-cys/meth. The cell pellet was lysed in the presence of NEM and mock treated (-EndoH, *lanes 2, 4* and *6*) or digested with Endo H (+EndoH, *lanes 3, 5* and *7*) for 1.5 hr at 37°C prior to reducing (R) SDS-PAGE. HeLa cells transfected with wtEro1β-Myc, pulse-labelled with ^{35}S-cys/meth for 10 min, lysed in the presence of NEM and immunoprecipitated (IP) with αMyc were used as a positive control (+ve, *lane 1*). G = glycosylated protein, nG = non-glycosylated protein. As expected Ero1β wt and both mutant proteins are glycosylated. HeLa cells were transfected with **B.** Ero1βH254Y-Myc, **C.** Ero1βG252S-Myc, **D.** wtEro1β-Myc or **E.** mock were pulse-labelled with ^{35}S-cys/met for 10 min and chased for 15, 30 and 60 min (**B-D**) prior to lysis in the presence of NEM. Lysates were subjected to immunoprecipitation with αMyc and analysed by non-reducing (NR, *B, C* and *D, lanes 1-4; E, lane 1*) and reducing (R, *B, C* and *D, lanes 6-9; E, lane 2*) SDS-PAGE. Ero1β oxidised (OX) and reduced (R) monomer forms are indicated. **F.** Cells pulse-labelled with ^{35}S-cys/met as in **B-E** and chased for 1, 3, 6 and 22 hr prior to immunoprecipitation with αMyc and analysed by reducing SDS-PAGE.

5.2.3 Ero1β and the FAD mutants interacts with ERp72

Wild-type Ero1β (Figure 5.2*D*, 3.6, *C* and *D*) as well as all mutants investigated during this study (Figure 4.4, *A* and *B*; Figure 5.2, *B* and *C*) co-immunoprecipitated with an unknown protein around 70 kDa, that was not present in the mock transfectants (Figure 5.2*E*). However, the Ero1βC396A mutant interacted weakly with the putative 70 kDa protein (Figure 4.4*B*, *lanes 8-14*), Ero1α transfectants also co-immunoprecipitated with a similar protein around 70 kDa (Figure 3.6*C*; (Benham et al., 2000)). Given that this interacting protein does not shift upon *in vitro* reduction and SDS-PAGE analysis (Figure 5.2*B*, compare *lanes 1-4* with *6-9*), it was unlikely to be a disulfide-rich substrate. Of the possible candidates, BiP and the PDI homologue ERp72 were investigated due to the band being around 70 kDa.

HeLa cells were mock transfected (Figure 5.3*A*, *lanes 4, 8, 12*) or transfected with wild- type Ero1β (Figure 5.3*A*, *lanes 1, 5, 9*), Ero1βH254Y-Myc (Figure 5.3*A*, *lanes 2, 6, 10*) and Ero1βG252S-Myc (Figure 5.3*A*, *lanes 3, 7, 11*), lysed in the presence of NEM and either directly analysed by reducing SDS-PAGE (Figure 5.3*A*, *lanes 1-4*) or subjected to immunoprecipitation with an αERp72 antibody (Figure 5.3*A*, *lanes 5-12*). Expression of ERp72 in the cell lysates was confirmed by probing the transferred proteins with αERp72 antibody (Figure 5.3*A*, *lanes 1-4*). Immunoprecipitation with αERp72 retrieved ERp72 itself, as expected (Figure 5.3*A*, *lanes 5-8*) and co-immunoprecipitated Ero1β (Figure 5.3*A*, *lanes 9-12*).

To investigate whether a similar interaction could be identified between ERp72 and Ero1α, HeLa cells were mock transfected (Figure 5.3*B*, *lane 3*) or transfected with

wild-type Ero1α (Figure 5.3*B*, *lane 1*) or wild-type-Ero1β (Figure 5.3*B*, *lane 2*) and lysed in the presence of NEM. Lysates were analysed directly by reducing SDS-PAGE and transferred proteins probed with αERp72 (Figure 5.3*B*) which detected endogenous ERp72. The lysates were subjected to immunoprecipitation with αERp72 prior to reducing SDS-PAGE analysis, and after western blotting, the membranes were probed with αERp72 (Figure 5.3*C*) and αMyc (Figure 5.3*D*). Immunoprecipitation with αERp72 retrieved ERp72 itself as expected (Figure 5.3*C*) and co-immunoprecipitated Ero1α (Figure 5.3*D*, *lane 1*) and Ero1β (Figure 5.3*D*, *lane 2*). Thus under steady state conditions ERp72 interacts with both human EROs.

The same cell lysates as Figure 5.3*A* were analysed by reducing SDS-PAGE and blotted with αBiP to confirm expression of BiP (Figure 5.3*E*, *lanes 1-4*), prior to subjecting the lysates to immunoprecipitation with αMyc and analysis by reducing SDS-PAGE. Probing the transferred proteins with αBiP showed no co-immunoprecipitation of BiP with wild-type or mutant Ero1β proteins (Figure 5.3*E*, *lanes 5-8*). The αBiP antibody failed to immunoprecipitate (Figure 5.3*E*, *lanes 9*) and so was only used in western blotting. Expression of the transfected proteins was confirmed by analysis of the lysates by reducing SDS-PAGE and blotting with αMyc (Figure 5.3*F*, *lanes 1-4*). Thus under steady-state conditions no interaction could be detected between Ero1β and BiP.

Although ERp72 was recognised as a novel interacting protein of Ero1β at steady state, it is formally possible that this protein might not be identical to the 70 kDa band observed during pulse-chase analysis (Figure 5.2).

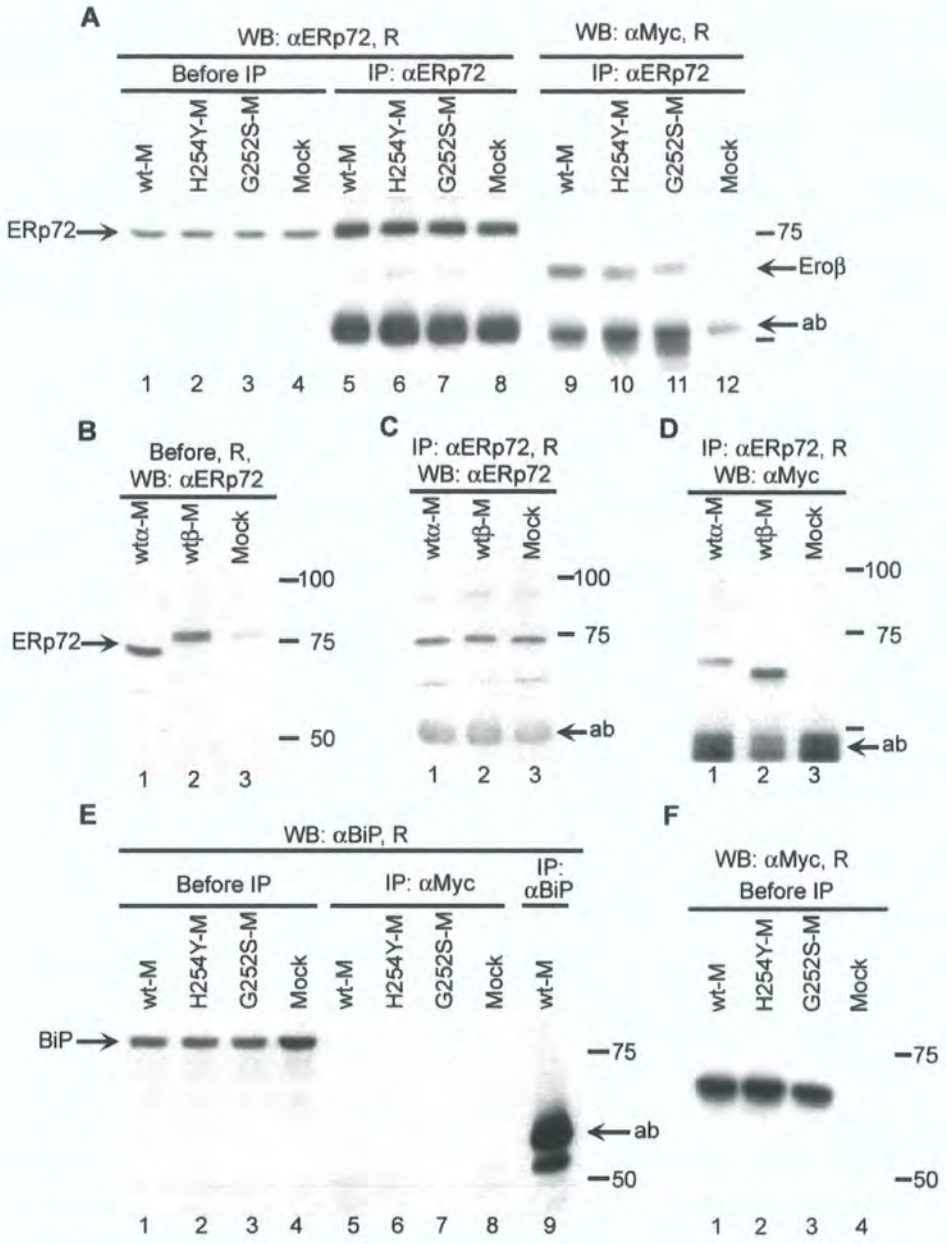

FIGURE 5.3: Ero1β interacts with ERp72 but not with BiP

A. Post nuclear lysates from HeLa cells transfected with wtEro1β-Myc (*lane 1*, *5*, *9*), Ero1βH254Y-Myc (*lane 2*, *6*, *10*), Ero1βG252S-Myc (*lane 3*, *7*, *11*) and mock (*lane 4*, *8*, *12*) were directly analysed (Before IP) by reducing SDS-PAGE and immunoblotted with αERp72 (R, *lanes 1-4*) or first subjected to immunoprecipitation (IP) with αERp72 prior to reducing SDS-PAGE and immunoblotted with αERp72 (*lanes 5-8*) or with αMyc (*lanes 9-12*). ERp72 and Ero1β are indicated, ab = antibody. wtEro1β and the two FAD domain mutants co-immunoprecipitate with αERp72. HeLa cells transfected with wild-type Ero1α-Myc (*lane 1*), wtEro1β-Myc (*lane 2*) or mock (*lane*

3) were **B.** directly analysed by reducing SDS-PAGE and probed with αERp72, or **C** and **D.** subjected to immunoprecipitation with αERp72, and immunoblotted with αERp72 (**C**) and αMyc (**D**). ERp72 is indicated, ab = antibody. wtEro1α co-immunoprecipitates with αERp72. **E.** Same lysates as in **A**, directly analysed (Before IP, *lanes 1-4*) or lysates subjected to immunoprecipitation with αMyc (IP, *lanes 5-8*) or with αBiP (*lane 9*) prior to reducing SDS-PAGE and immunoblotting with αBiP (*lanes 1-9*). BiP is indicated with an arrow, ab = antibody. BiP is not co-immunoprecipitating with wild-type Ero1β or with the two FAD domain mutants. **F.** Same lysates as **A**, directly analysed (Before IP) by reducing SDS-PAGE and immunoblotted with αMyc.

5.2.4 Limited proteolysis of Ero1βG252S and Ero1βH254Y

The FAD binding domain is partly buried within the Ero1β protein (Gross et al., 2004). The two FAD binding domain mutations could cause a conformational change that might lead to protein misfolding, giving the two phenotypes in yeast *ero1-1* and *ero1-2*. To compare the overall conformation of the two Ero1β mutant proteins with wild-type Ero1β, limited proteolysis was carried out on cell transfectants. Partial trypsin digestion can occur at exposed lysine residues in native proteins and has been used effectively to map conformational changes in a number of ER proteins which include PDI (Freedman et al., 1998), CFTR (Zhang et al., 1998; Kleizen et al., 2005) and polyomavirus (Magnuson et al., 2005). Post-nuclear supernatants from HeLa cells transfected with wild-type Ero1β, Ero1βH254Y-Myc and Ero1βG252S-Myc or mock, lysed in the absence of protease inhibitor, were treated with a concentration range of TPCK-trypsin for 30 min on ice. Proteolytic reaction was quenched with soybean trypsin inhibitor and the lysates analysed by reducing SDS-PAGE prior to probing the western blotted membranes with either αMyc or αEro1β antibody. The Myc tag is positioned at the C-terminus whereas the epitope recognised by the αEro1β serum (residues Y329-L343) is located upstream of the C*XX*C*XX*C motif. Use of both these antibodies provided a tool for obtaining positional information about the fragments generated by trypsin digestion.

In wild-type Ero1β, detection with both antibodies gave rise to a fragment around 55 kDa with 1.25 μg/ml concentration of trypsin (fragment A, Figure 5.4*A* and *B*, *lane 3*), which must at least contain the C-terminus Myc tagged region and the C*XX*C*XX*C motif, and is therefore likely to have lost the N-terminus of the protein. However when Ero1β was digested with 2.5 μg/ml of trypsin, a fragment around 45 kDa was detected only

when probed with αEro1β but not with αMyc (fragment B, Figure 5.4*A*, *lane 4* compare with Figure 5.4*B*, *lane 4*). This fragment B lacked the C-terminal Myc tag, but retained the C*XX*C*XX*C motif based on size and the presence of the Y329-L343 epitope. Given the sizes of the fragments generated, the results suggested that Ero1β was selectively cleaved between the two redox active domains where a clustering of lysine residues can be found on an exposed loop.

The digestion pattern of the Ero1βH254Y mutant (Figure 5.4*A* and 5.4*B*, *lanes 5-8*) and the Ero1βG252S mutant (Figure 5.4*A* and 5.4*B*, *lanes 9-12*) and their overall sensitivity to trypsin were comparable to wild-type Ero1β, suggesting that the gross conformation of the two mutants is similar to wild-type protein. However, there were some differences between the substrates, such as the appearance of a shadow band under the full length protein in the mutant digestions when probed with αMyc (Figure 5.4*B*, *lanes 7, 8 11 and 12*) and the lower abundance of fragment B in Ero1βG252S digestion when probed with αEro1β (Figure 5.4*A*, *lanes 12*). The H254Y mutation and in particular the G252S mutation may have subtle or localised effects on the Ero structure and folding. However, given the overall similarity of the digestion product sizes, the data suggest that gross conformational changes are unlikely to result from the point mutations at the FAD binding domain under normal steady state conditions.

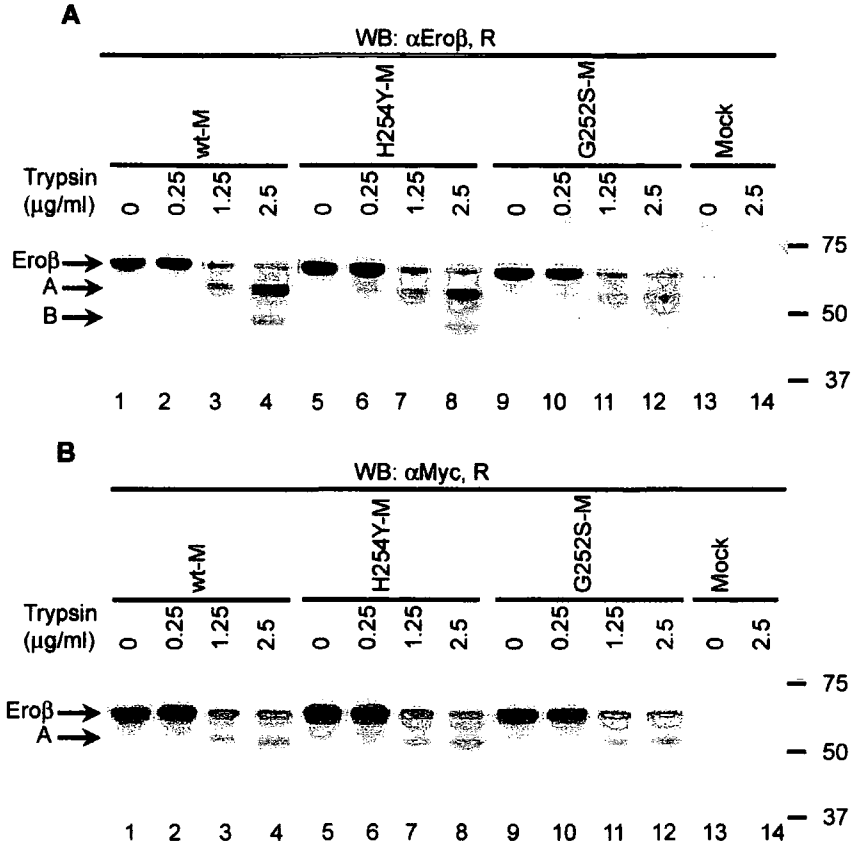

FIGURE 5.4: Limited proteolysis of Ero1βH254Y and Ero1βG252S mutants

Post nuclear supernatants from HeLa cells transfected with wtEro1β-Myc (*lane 1-4*), Ero1βH254Y-Myc (*lane 5-8*), Ero1βG252S-Myc (*lane 9-12)* and mock (*lanes 13-14*) were incubated with 0, 0.25, 1.25 and 2.5 µg/ml TPCK treated trypsin for 30 min at 4 °C, analysed by reducing SDS-PAGE and immunoblotted with αEro1β (**A**) and αMyc (**B**). Generated fragments are labelled A and B.

5.2.5 Differences in the covalent and non-covalent interactions of Ero1βG252S and Ero1βH254Y with PDI

Having seen no major defect in protein biosynthesis, turn-over rate or gross conformational change in Ero1βH254Y-Myc and Ero1βG252S-Myc proteins compared to wild-type Ero1β, the next step was to investigate whether these two mutations disrupted interactions with partner proteins. The ability to form Ero-PDI complexes was studied by analysing HeLa cells transfected with mock, Ero1βG252S-Myc or Ero1βH254Y-Myc and lysed in the presence of an alkylating agent. Post-nuclear supernatants were directly analysed by non-reducing (Figure 5.5*A* and *B, lanes 1-2*) and reducing (Figure 5.5*A lanes 3-4,* Figure 5.5*B lanes 4-5*) SDS-PAGE and transferred proteins probed with αMyc. Under non-reducing conditions, the monomer form of Ero1βG252S mutant ran as a collection of oxidised forms (OX, Figure 5.5*A*, *lane 1*), which disappear upon reduction with DTT giving a single reduced state (R, Figure 5.5*A*, *lane 3*). Ero1βG252S also formed a smear of disulfide dependent complexes (*, Figure 5.5*A*, *lane 1*).

Immunoprecipitation with αPDI serum specifically co-immunoprecipitated Ero1βG252S under reducing conditions (Figure 5.5*A*, *lane 8*) but could not detect any disulfide-dependent Ero-PDI complexes (other than the antibody bands also seen in mock transfectant, Figure 5.5*A*, *lanes 4* and *7*). Similar to Ero1βG252S, the Ero1βH254Y mutant also ran as an oxidised population of monomers (OX, Figure 5.5*B*, *lane 1*) but the trapped, higher molecular weight complexes were more abundant and less diffuse (compare Figure 5.5*B*, *lane 1* with Figure 5.5*A*, *lane 1*). The Ero1βH254Y mutant specifically co-immunoprecipitated PDI (Figure 5.5*B*, *lanes 9* and *10*), but

unlike Ero1βG252S, Ero1βH254Y became trapped in a disulfide-dependent complex with PDI under non-reducing conditions (compare Figure 5.5*B*, *lanes 6* and *7* with Figure 5.5*A*, *lanes 6* and *7*). Note the background band also present in mock transfectant (Figure 5.5*A*, *lanes 2* and *4;* Figure 5.5*B*, *lanes 2* and *5*) which was discussed in section 3.2.2.

The ability of Ero1βG252S-Myc and Ero1βH254Y-Myc mutants to interact with PDI was then directly compared alongside Ero1βC390A-Myc (the C-terminal active site mutant which has altered PDI binding properties) and with wild-type Ero1β. HeLa cells transfected with these constructs were lysed in the presence of NEM and cell lysates either directly analysed by non-reducing SDS-PAGE (Figure 5.5*C*, *lanes 1-4*) or first subjected to immunoprecipitation with αPDI prior to reducing (Figure 5.5*C*, *lanes 5-8*) and non-reducing (Figure 5.5*C*, *lanes 10-13*) SDS-PAGE. Detection of transferred proteins with αMyc showed that prior to immunoprecipitation all Ero1β proteins resolved as a collection of monomeric and disulfide-dependent forms (Figure 5.5*C*, *lanes 1-4*). Ero1βG252S, Ero1βH254Y, Ero1βC390A and wild-type Ero1β all co-immunoprecipitated with αPDI (Figure 5.5*C*, *lanes 5-8*), however, only Ero1βH254Y (Figure 5.5*C*, *lane 11)* and wild-type Ero1β (Figure 5.5*C*, *lane* 13) formed prominent, discrete disulfide-dependent complexes with PDI. These results indicate that both Ero1βG252S and Ero1βH254Y mutants can interact non-covalently with PDI, but that in the Ero1βG252S mutant, inter-molecular disulfide-bonded (covalent) interactions with PDI are compromised.

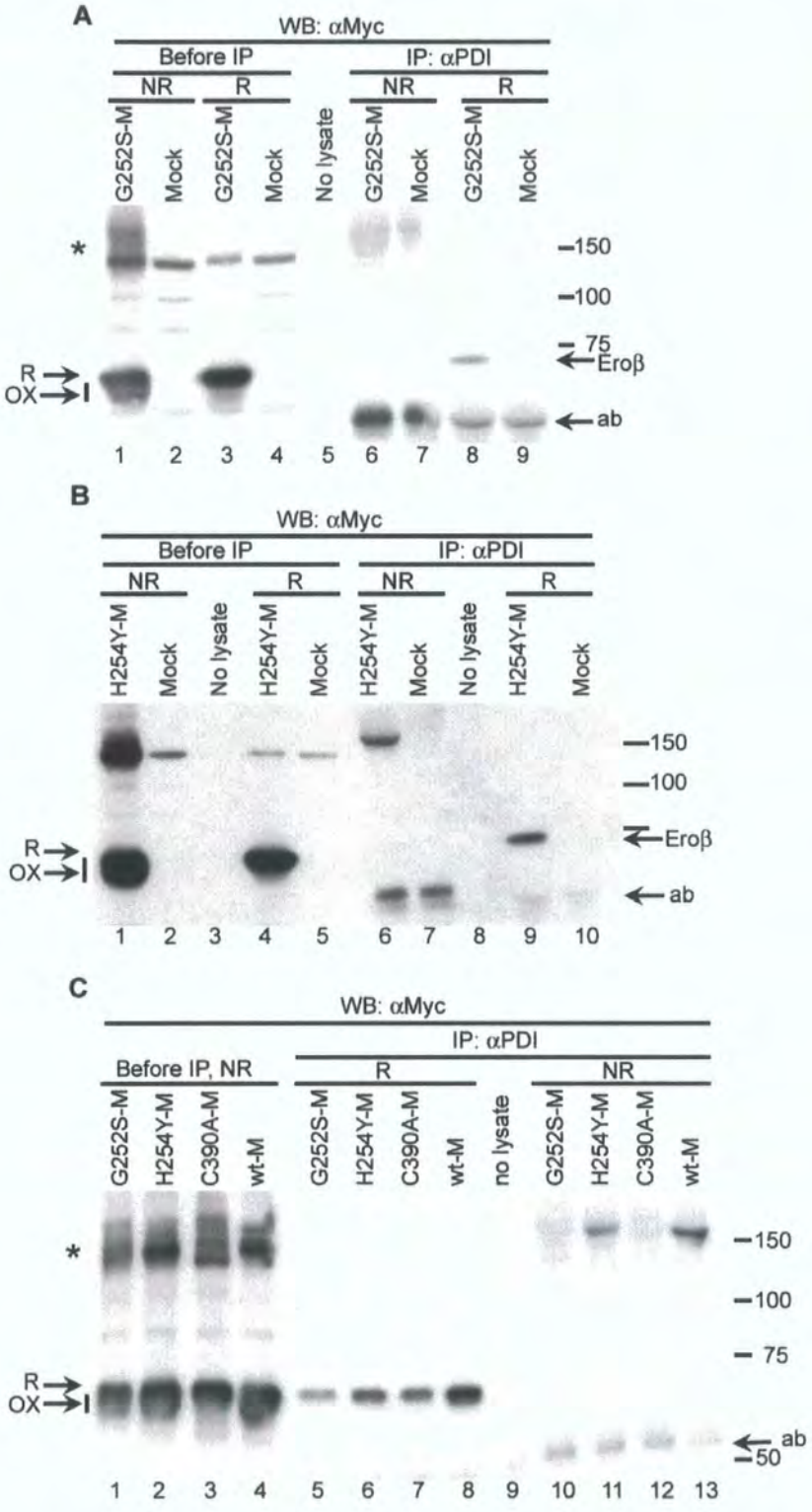

FIGURE 5.5: Ero1βH254Y and Ero1βG252S interaction with PDI

Lysates from HeLa cells transfected with Ero1βG252S-Myc (**A**) and Ero1βH254Y-Myc (**B**) analysed directly by immunoblotting with αMyc after non-reducing or reducing SDS-PAGE (*lanes 1-4*) or after immunoprecipitation with αPDI (*lanes 6-9/10*). **C.** Lysates from HeLa cells transfected with wtEro1β-Myc (*lanes 4, 8, 13*),

Ero1βG252S-Myc (*lanes 1, 5, 10*), Ero1βH254Y-Myc (*lanes 2, 6, 11*), and Ero1βC390A-Myc (*lanes 3, 7, 12*) were immunoblotted with αMyc before (*lanes 1-4*) or after (*lanes 5-13*) immunoprecipitation with αPDI. *Lane 5* from (**A**), *lanes 3* and *8* from (**B**) and *lane 9* from (**C**) are loaded with sample buffer only. ab = cross-reactive antibody. Disulfide dependent complexes are shown as *. Oxidised (OX) and reduced (R) Ero1β monomer forms as well as co-immunoprecipitated Ero1β (Ero1β) are indicated.

5.2.6 Both Ero1βG252S and Ero1βH254Y can dimerise

Wild-type Ero1β is able to homodimerise (section 3.2.3). The Ero1β C-terminal mutant Ero1βC396A is unable to self-complex and is also non-functional (section 4.2.6, (Cabibbo et al., 2000). Having seen the potential importance of the FAD co-factor in a model of dimer formation (Figure 4.10), it was possible that FAD was required for Ero-Ero associations. The two FAD domain mutants ability to complex with wild-type Ero1β was investigated by transfecting HeLa cells with Ero1βG252S-Myc, wild-type Ero1β-HA,. Ero1βG252S-Myc plus wild-type Ero1β-HA. Post nuclear lysates were analysed by reducing and non-reducing SDS-PAGE and transferred proteins probed with αMyc and αHA antibodies. Lysates analysed under reducing conditions allowed the detection of the transfected proteins (Figure 5.6*A*). Under non-reducing conditions any mixed disulfide-dependent dimers should appear as an intermediate band in the double transfected lysates (similar to wild-type Ero1β-Myc - Ero1β-HA dimer, Figure 3.9*A*). An intermediate band (*) was present only in the double transfected lysate (Figure 5.6*B*, *lane 3*) representing a wild-type Ero1β– Ero1βG252S dimer.

Lysates from these transfectants were subjected to immunoprecipitation with αHA prior to analysis by reducing SDS-PAGE (Figure 5.6*C*). Blots probed with αMyc did not detect an Ero1β signal from the single transfectants or mock lysates (Figure 5.6*C*, *lanes 1, 2, 4*). Ero1βG252S-Myc clearly co-immunoprecipitated with wild-type Ero1β-HA (Figure 5.6*C*, *lane 3*). Similar results were obtained with the Ero1βH254Y-Myc mutant: single and double transfected lysates all expressed the differently tagged Ero1β proteins as expected (Figure 5.6*D*, *lanes 1-4*) and the Ero1βH254Y-Myc mutant gave an intermediate band in the double transfectant under non-reducing SDS-PAGE (*,

Figure 5.6*E, lane 3*) and co-immunoprecipitated with wild-type Ero1β (Figure 5.6*F*, *lane 3*). Thus both FAD domain mutants were able to form disulfide-dependent dimers with wild-type Ero1β.

Since both FAD domain mutants were able to interact with wild-type Ero1β, the ability of the mutants to homodimerise was investigated. This was of interest because Ero1βC396A is able to interact with wild-type Ero1β but was not able homodimise, as discussed in section 4.2.6. HeLa cells were mock transfected or transfected with Ero1βH254Y-HA, Ero1βG252S-HA or double transfected with Ero1βH254Y-HA plus Ero1βH254Y-Myc and Ero1βG252S-HA plus Ero1βG252S-Myc. The lysates were analysed by reducing SDS-PAGE to verify transfection and subjected to immunoprecipitation with αMyc prior to immunoblotting with αEro1β antibody. The single and double transfectants expressed the expected proteins (Figure 5.6*G*, *lanes 1-4*) while no signal was observed from the mock transfectants (Figure 5.6*G*, *lane 5*). In both single transfectants as well as mock, no Ero1β signal was detected after immunoprecipitation with αMyc (Figure 5.6*G*, *lane 7, 8, 11*). However, Ero1βH254Y-HA tagged mutant co-immunoprecipitated with the Ero1βH254Y-Myc (Figure 5.6*G*, *lane 9*) and likewise Ero1βG252S-HA co-immunoprecipitated with Ero1βG252S-Myc (Figure 5.6*G*, *lane 10*). These data clearly indicate that both mutations at the FAD binding domain do not prevent interactions (heterodimerisation) with wild-type Ero1β or with themselves (homodimerisation) in the ER.

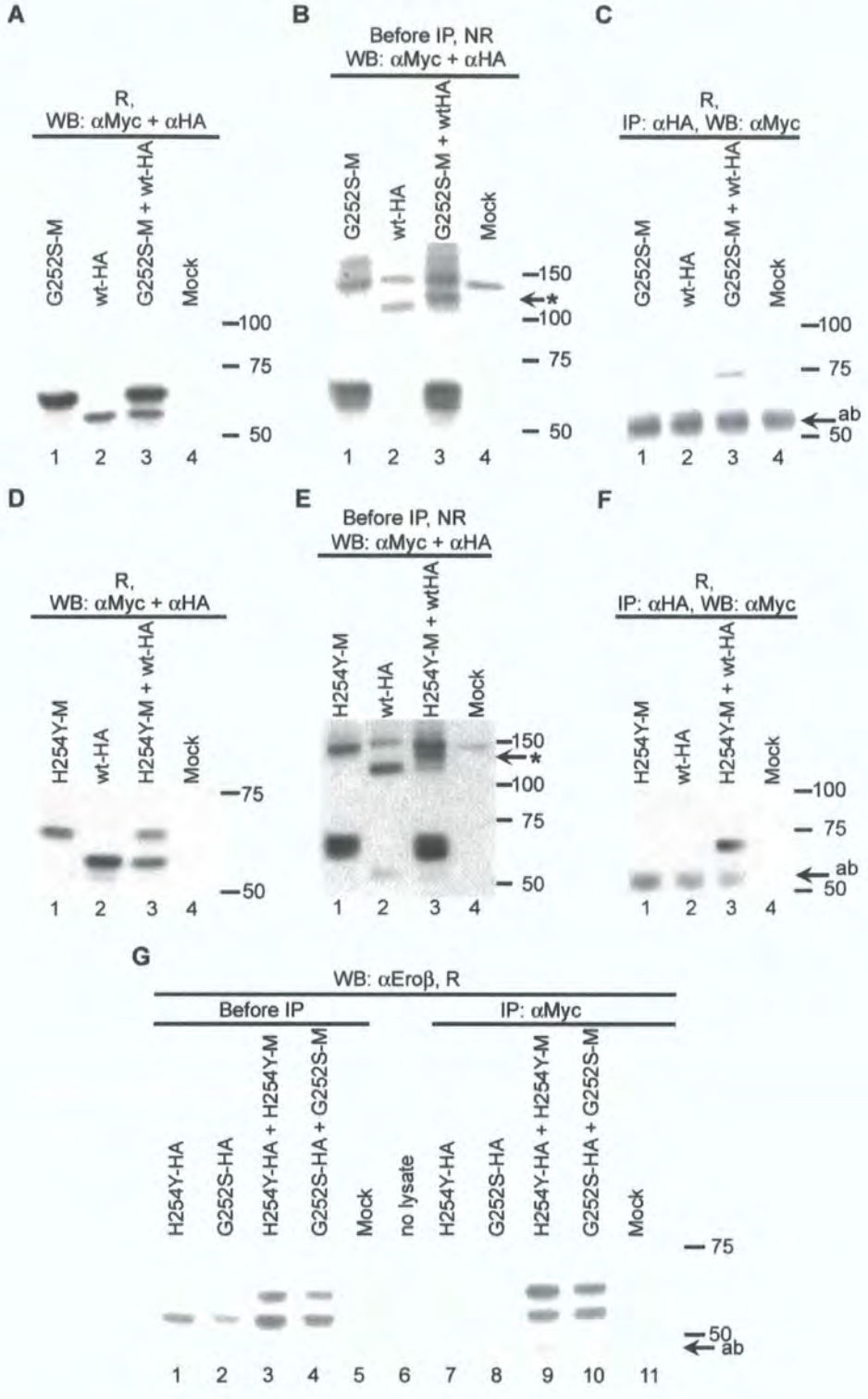

FIGURE 5.6: Dimerisation of Ero1β H254Y and Ero1βG252S

A - C. HeLa cells transfected with Ero1βG252S-Myc (*lane 1*), wtEro1β-HA (*lanes 2*), Ero1βG252S-Myc plus wtEro1β-HA (*lanes 3*) and mock (*lanes 4*) were analysed following reducing (**A**) and non-reducing (**B**) SDS-PAGE by immunoblotting with αMyc and αHA or first subjecting the lysates to immunoprecipitation with αHA (**C**)

prior to immunoblotting with αMyc. **D – F.** HeLa cells transfected with Ero1βH254Y-Myc (*lanes 1*), wtEro1β-HA (*lanes 2*), Ero1βH254Y-Myc plus wtEro1β-HA (*lanes 3*) and mock (*lane 4*) were analysed as for **A-C**. * indicates the mutant-Myc + wt-HA dimer. **G.** HeLa cells transfected with Ero1βH254Y-HA (*lanes 1, 7*) Ero1βG252S-HA (*lanes 2, 8*) Ero1βH254Y-HA plus Ero1βH254Y-Myc (*lanes 3, 9*) Ero1βG252S-HA plus Ero1βG252S-Myc (*lanes 4, 10*) and mock (*lanes 5, 11*) were analysed directly by reducing SDS-PAGE (Before IP) or first subjected to immunoprecipitation with αMyc and immunoblotted with αEroβ. ab = cross-reactive antibody.

5.2.7 Aberrant oxidation of Ero1βG252S and Ero1βH254Y during a reducing stress

The yeast counterparts of Ero1βG252S and Ero1βH254Y are hypersensitive to temperature and reductants (Frand & Kaiser, 1998; Pollard et al., 1998). The effects of the reductant DTT on mammalian cells transfected with wild-type Ero1β was studied in Chapter 3, section 3.2.6, which showed that a reducing environment is capable of abolishing most of wild-type Ero1β disulfide-linked interactions including homodimers under steady state conditions.

The two FAD binding domain mutants, Ero1βH254Y and Ero1βG252S, were subjected to similar *in vivo* DTT treatments. Treated and untreated HeLa cell lysates from Ero1βH254Y-Myc, Ero1βG252S-Myc and wild-type Ero1β-Myc were analysed by non-reducing (Figure 5.7*A*) and reducing (Figure 5.7*B*) SDS-PAGE, prior to immunoblotting with αMyc. Wild-type Ero1β lost the majority of its disulfide-dependent complexes due to DTT treatment similar to Figure 3.12*C* (Figure 5.7*A*, *lanes 1* and *2*; * and **). The two Ero1β mutants behaved differently from wild-type Ero1β. Ero1βH254Y retained most of its complexes in the face of a DTT challenge (Figure 5.7*A*, *lanes 3* and *4*; *), whereas Ero1βG252S not only retained its complexes (Figure 5.7*A*, *lanes 5* and *6*; *) but also formed higher molecular weight complexes and aggregates (**). As an internal control, the Ero1β monomer states were mostly reduced after DTT treatment (R, Figure 5.7*A*, *lanes 1, 3, 5*). *In vitro* reduction with DTT caused all Ero1β proteins to collapse to a single reduced monomer form (R, Figure 5.7*B*, *lanes 1-6*). Data from these experiments suggest mutations at G252 and H254 cause the

Ero1β protein to undergo abnormal oxidation in the face of fairly harsh reducing environments.

To investigate whether misoxidation caused by the two FAD binding domain mutants was reversible, HeLa cells transfected with the most severe mutant, Ero1βG252S-Myc, were treated with 10 mM DTT for 15 min and allowed to recover for 30 min after washing off DTT in the medium and replacing with normal medium. Post-nuclear supernatants were analysed under non-reducing conditions and transferred proteins probed with a αMyc (polyclonal) antibody (Figure 5.7*C*). Misoxidation observed after DTT treatment (Figure 5.7*C*, *lane 2*, **), could be recovered upon removal of DTT (Figure 5.7*C*, *lane 3*).

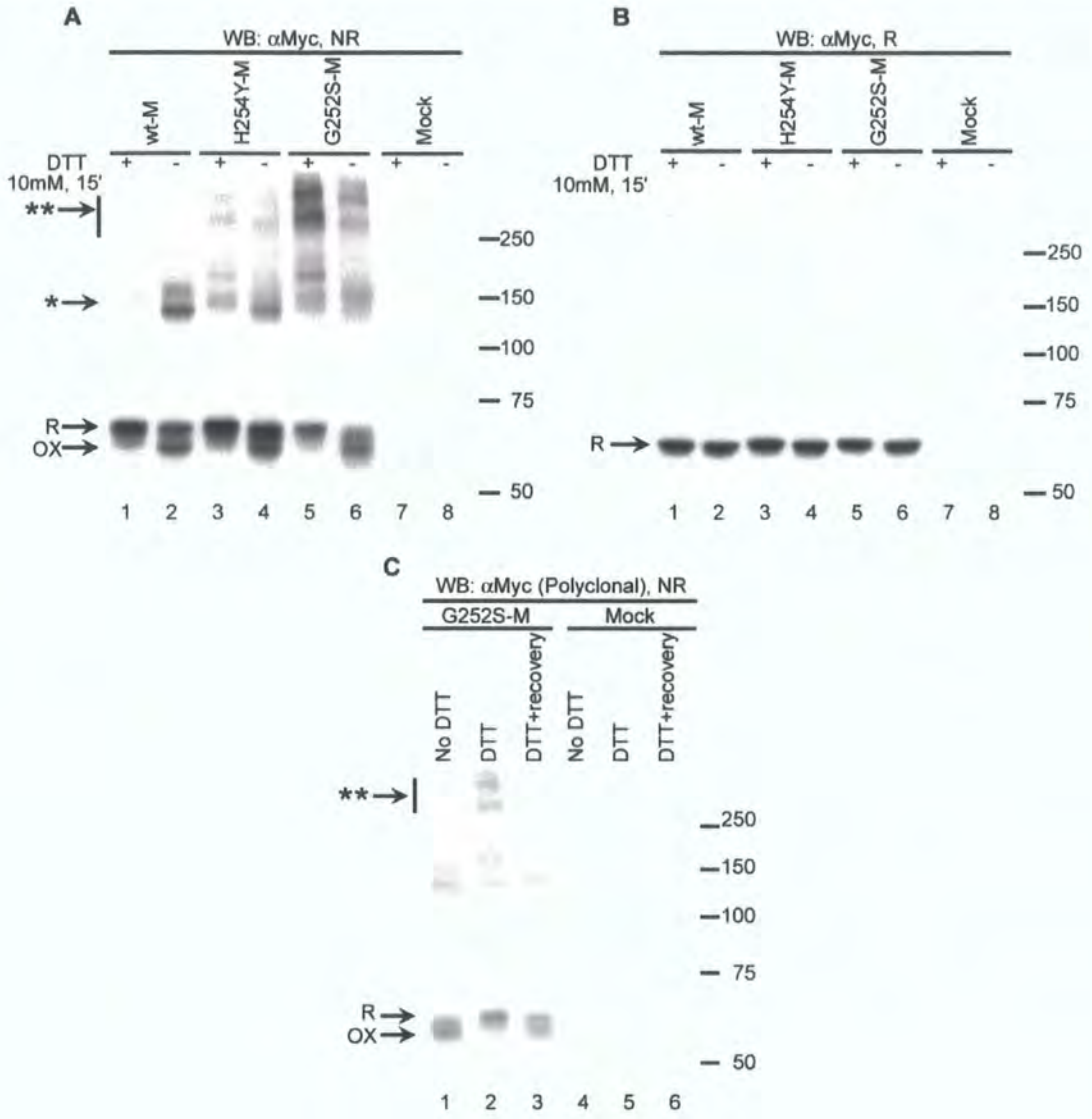

FIGURE 5.7: Oxidative misfolding of Ero1β H254Y and Ero1βG252S

A and **B.** HeLa cells transfected with wtEro1β-Myc (*lanes 1-2*), Ero1βH254Y-Myc (*lanes 3-4*), Ero1βG252S-Myc (*lanes 5-6*), and mock (*lanes 7-8*) were treated with 10 mM DTT for 15 min and post nuclear lysates were analysed under non-reducing (**A**) and reducing (**B**) SDS-PAGE prior to immunoblotting with αMyc. Disulfide dependent Ero-PDI and Ero-Ero complexes are denoted as *, with higher molecular weight complexes and aggregates as **. Oxidation states of Ero1β monomer are shown as OX (oxidized) and R (reduced). **C.** HeLa cells transfected with Ero1βG252S-Myc (*lanes 1–3*) and mock (*lanes 4–6*) were treated with DTT as for **A** (*lanes 2-3* and *5-6*) and allowed to recover by washing out DTT for 30 min (*lanes 3* and *6*). Post-nuclear lysates were analyzed by immunoblotting with a polyclonal Myc antibody after non-reducing SDS-PAGE. Misoxidation of Ero1βG252S protein can be reversed by the removal of DTT.

Ero1βH254Y and Ero1βG252S mutant proteins were also introduced to a number of different cellular stress conditions to study their behaviour. HeLa cells transfected with the above two Myc tagged mutants and wild-type Ero1β-Myc, were subjected to overnight buthionine sulphoximine (BSO) treatment or 10 min of hydrogen peroxide (H_2O_2) treatment. BSO depletes the intracellular pool of glutathione (GSH) by inhibiting the initial enzyme in GSH synthesis (γ-glutamylcysteine synthase, (Griffith & Meister, 1979)), thus altering the redox state within the ER. H_2O_2 is an oxidative stress inducer which producers free oxygen radicals. Under non-reducing conditions both 25 μM BSO and 1.5 M H_2O_2 treatments did not cause oxidative misfolding of either mutant or of wild-type Ero1β at steady state (Figure 5.8*A*, compare *lanes 9-11* with *lanes 1-3* and *lanes 5-7*). *In vitro* reduction of the proteins and analysis by SDS-PAGE showed no alteration to the level of Ero1β protein present after each treatment when compared to mock treatment (Figure 5.8*B*). The membrane-permeable oxidant, diamide, which can drive the formation of disulfide bonds in living cells (Kosower & Kosower, 1995), was also tested on HeLa transfectants with wild-type Ero1β-Myc, Ero1βH254Y-Myc and Ero1βG252S-Myc (Figure 5.8*C*). Diamide treatment increased the proportion of oxidised monomers in each case and caused some oxidative misfolding of wild-type Ero1β as well as both mutant proteins (Figure 5.8*C*, *lanes 1*, *3* and *5*, **). Both mutants showed more aggregates in the stacking gel when compared to wild-type Ero1β (***).

Taken together these results demonstrate that both mutations in the FAD binding site cause Ero1β protein to misoxidise when reducing conditions are encountered but does not alter Ero1β protein behaviour in the presence of the other stress conditions that were tested so far.

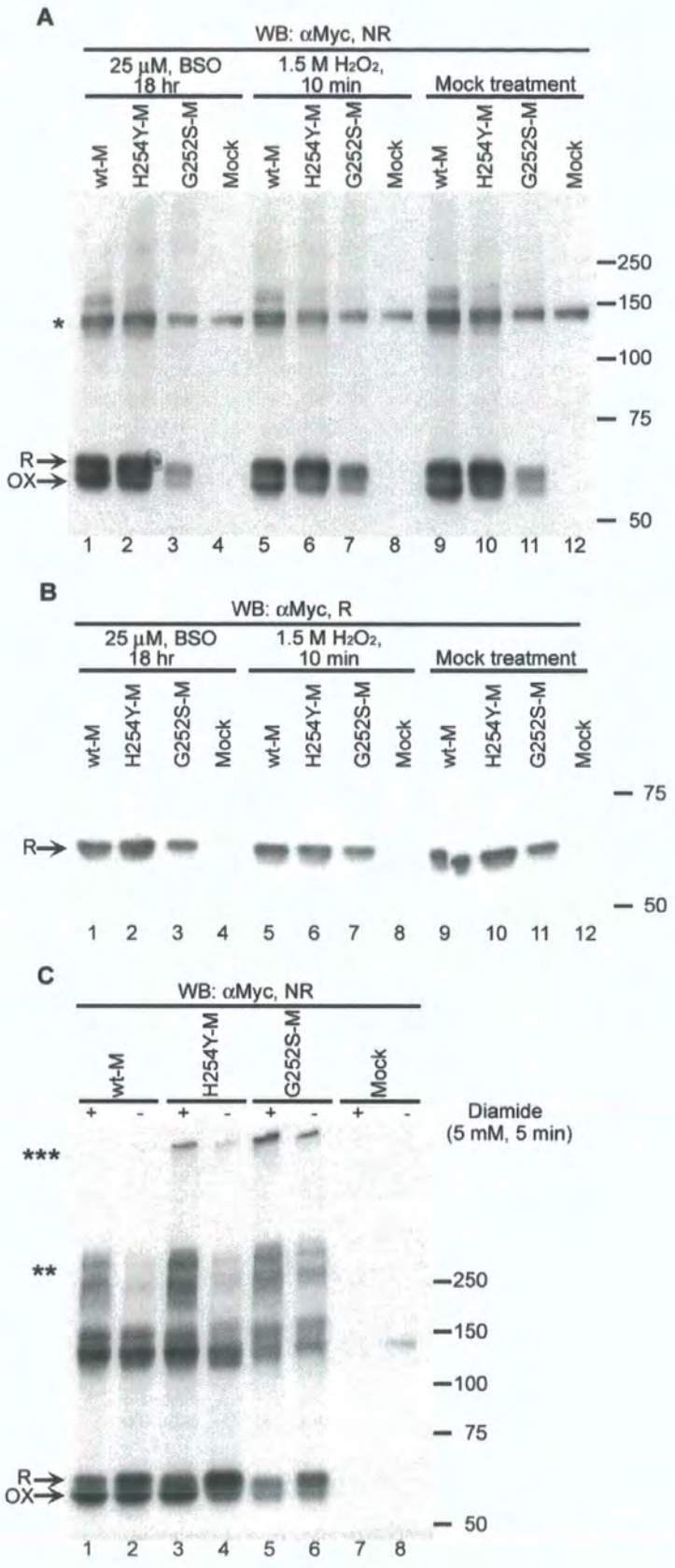

FIGURE 5.8: Glutathione depletion and hydrogen peroxide treatment does not cause oxidative misfolding of Ero1βG252S and Ero1βH254Y mutants

FIGURE 5.8: Glutathione depletion and hydrogen peroxide treatment does not cause oxidative misfolding of Ero1βG252S and Ero1βH254Y mutants

A and **B**. HeLa cells transfected with wtEro1β-Myc (*lanes 1, 5, 9*), Ero1βH254Y-Myc (*lanes 2, 6, 10*), Ero1βG252S-Myc (*lanes 3, 7, 11*) and mock (*lanes 4, 8, 12*) were either mock treated (lanes 9-12), treated with 25 μM butathione sulfoxamine (BSO) for 18 hrs (*lanes 1-4*) or 1.5 M hydrogen peroxide (H_2O_2) for 10 min (*lanes 5-8*). Post-nuclear lysates were analysed on non-reducing (**A**) and reducing (**B**) SDS-PAGE prior to immunoblotting with αMyc. Disulfide dependent Ero-PDI and Ero-Ero complexes are denoted as *. **C.** HeLa cells expressing wtEro1β-Myc (*lanes 1-2*), Ero1βH254Y-Myc (*lanes 3-4*), Ero1βG252S-Myc (*lanes 5-6*), and mock (*lanes 7-8*) were treated with 5 mM diamide for 5 min prior to analysis of post nuclear lysate on non-reducing SDS-PAGE and immunoblotting with αMyc. Oxidative misfolding is indicated as **, and aggregates in the stacking gel indicated as ***. Oxidation states of Ero1β monomer are shown as OX (oxidized) and R (reduced).

5.2.8 Temperature dependent misfolding of Ero1βH254Y and Ero1βG252S

Having seen that DTT is able to cause misoxidation of Ero1β protein with G252S and H254Y mutations, these two mutant proteins were tested against a range of temperatures to study any behavioural changes. Thus transfected HeLa cells were incubated at 24°C, 37°C and 42°C for 1 hr prior to lysis and post-nuclear supernatants analysed by non-reducing and reducing SDS-PAGE. Wild-type Ero1β was stable across the temperature range and maintained their disulfide-bonded complexes, including Ero-PDI and Ero-Ero interactions (Figure 5.9*A*, *lanes 1-3*, *). However, both Ero1βH254Y and Ero1βG252S lost most of its disulfide-linked interactions at 24°C (Figure 5.9*A*, *lanes 4 and 7*, *) and misoxidised at 42°C, with mutant complexes being retained in the stacking gel (Figure 5.9*A*, *lanes 6* and *9*, **). The temperature treatments did not influence the monomer states of either the wild-type or mutant Ero1β. All Ero1β molecules could be reduced to a single band upon *in vitro* DTT treatment prior to SDS-PAGE analysis, showing that all complexes detected on the non-reducing gel were disulfide-dependent (Figure 5.9*B*, *lanes 1-9*).

To investigate whether Ero1β mutant interactions were temperature-dependent, the same lysates as in Figure 5.9*A* were analysed by non-reducing (Figure 5.9*C*) and reducing (Figure 5.9*D*) SDS-PAGE and tested for PDI interactions by western blotting with αPDI. Regardless of temperature and transfected Ero1β protein, under non-reducing conditions PDI expression remained unchanged and was mostly present in the monomer form with a faint smear of bands in the upper part of the gel (Figure 5.9*C*) representing various disulfide-bonded partner proteins (compare Figure 5.9*C* with Figure 5.9*D*). To assess whether Ero-PDI interactions were affected in mutant proteins and wild-type Ero1β after temperature treatment, the same lysates were subjected to

immunoprecipitation with αPDI serum prior to reducing SDS-PAGE analysis. Probing the transferred proteins with αMyc showed no major differences between the Ero1β mutant proteins (Figure 5.9*E*, *lanes 4-6* and *7-9*) or wild-type (Figure 5.9*E*, *lanes 1-3*) after the different temperature incubations, although wild-type Ero1β interacted more strongly with PDI than did the mutant proteins (Figure 5.9*E*, compare *lanes 1-3* with *lanes 4-9*). However, in some experiments, prolonged exposure to high temperatures resulted in an increase of co-immunoprecipitated Ero1β with PDI for both mutants and for wild-type (data not shown).

Data from the above experiments demonstrate that Ero1β and PDI are stable at steady-state between 24°C and 42°C. Both mutations at the FAD binding domain cause Ero1β protein to misoxidise and disrupt disulfide-dependent interactions when subjected to a temperature stress.

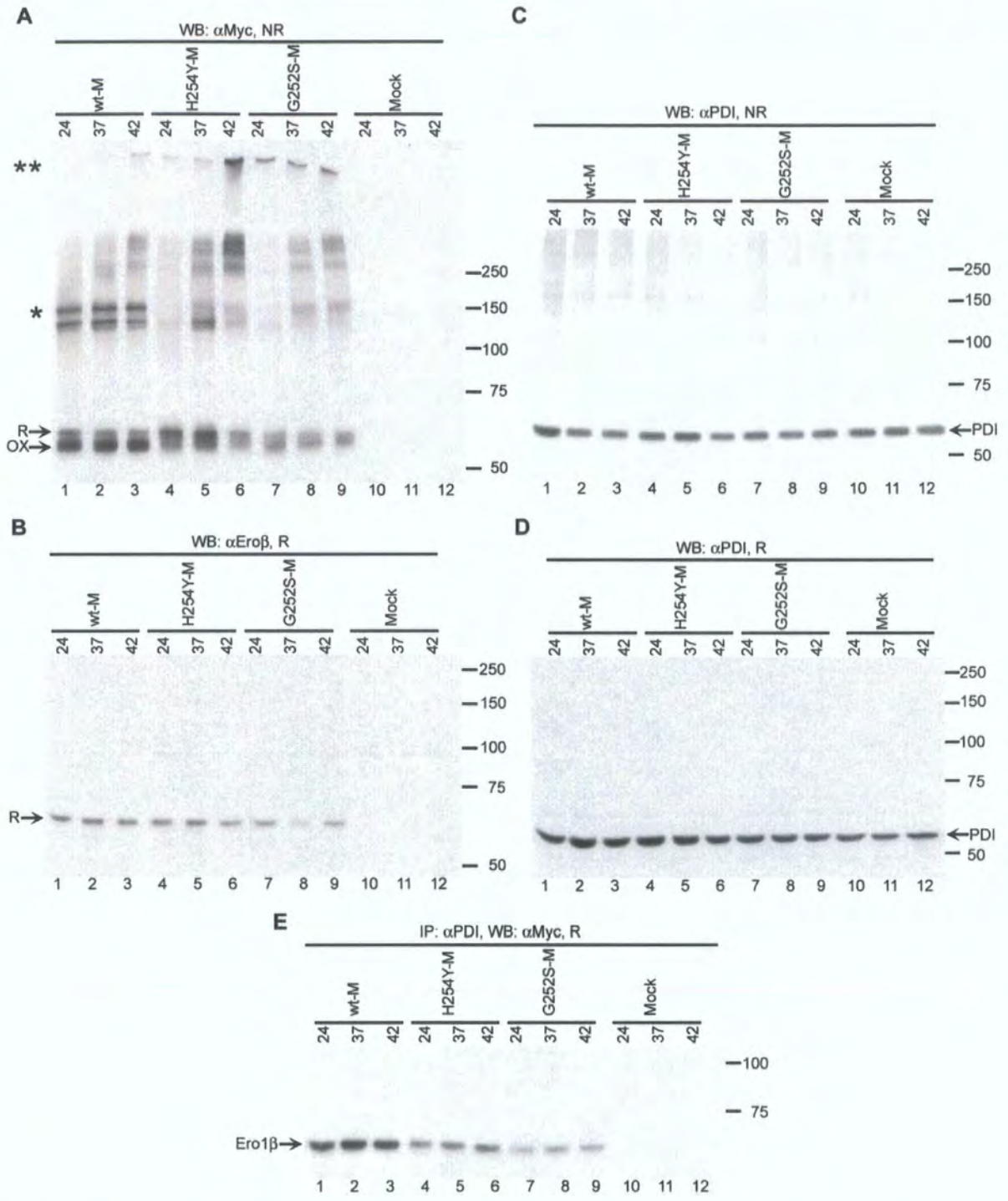

FIGURE 5.9: Misfolding of Ero1β H254Y and Ero1βG252S after temperature stress

A - D. HeLa cells transfected with wtEro1β-Myc (*lanes 1-3*), Ero1βH254Y-Myc (*lanes 4-6*), Ero1βG252S-Myc (*lanes 7-9*), and mock (*lanes 10-12*) were incubated at 24°C, 37°C and 42°C for 1 hr. Post nuclear lysates were analysed on non-reducing (**A** and **C**) and reducing (**B** and **D**) SDS-PAGE prior to immunoblotting with (**A**) αMyc, (**B**)

αEroβ and (**C** and **D**) αPDI. **E.** As for (**A-D**), except lysates were first subjected to immunoprecipitation with αPDI prior to reducing SDS-PAGE and immunoblotting with αMyc. Disulfide dependent Ero-PDI and Ero-Ero complexes are denoted as * with higher molecular weight and aggregates as **. Oxidation states of Ero1β monomer are shown as OX (oxidized) and R (reduced).

5.3 Discussion

This chapter focuses on the behaviour of two FAD binding domain mutants of Ero1β which were first discovered in *Saccaromyces cerevisiae*. It was recently suggested that the glycine to serine substitution at 229 in the yeast *ero1-1* strain might cause a folding or co-factor binding defect which could account for its phenotype (Gross et al., 2006). However, both G252S and H254Y mutant proteins showed no folding defects, any major difference in half-life (Figure 5.2) or substantial difference in trypsin sensitivity (Figure 5.4) when compared with wild-type Ero1β, demonstrating that the human versions of the FAD fold mutants do not have a protein biosynthesis problem or undergo gross conformational changes. The two FAD domain mutant proteins do however have an inducible misoxidation defect when subjected to reducing conditions or temperature changes. Both G252S and H254Y show misoxidation when introduced to a DTT environment, with G252S mutant being more severe. This defect was reversible with the removal of the reductant (Figure 5.7), presumably allowing normal oxidation conditions to prevail. Indeed, when both mutants encountered a more oxidising environment (treatment with diamide) their monomer forms showed the ability to increase the ratio of oxidised monomers (Figure 5.8). These findings may explain why oxidising agents such as diamide can restore viability to the *ero1-1* yeast strain (Frand & Kaiser, 1998). Upon DTT treatment, the mutant Ero proteins seemed incapable of becoming properly oxidised thus revealing free –SH groups which form incorrect intermolecular disulfide bridges. Introducing cells to H_2O_2 and the glutathione synthesis inhibitor BSO, did not markedly affect wild-type or mutant Ero1β redox state or complex formation (Figure 5.8). Recent studies using BSO on tPA (tissue-type plasminogen activator)-expressing CHO cells showed that lowering the level of glutathione increased the rate of non-native disulfide bond formation of tPA molecules

but did not affect the redox state of PDI (Chakravarthi & Bulleid, 2004). In light of these studies BSO not having an effect on Ero1β redox state is not surprising.

Misoxidation of the two Ero1β FAD mutants mainly affected the ability of Ero proteins to engage in disulfide dependent interactions (Figure 5.7 and 5.9). PDI was still able to form non-covalent interactions with Ero1β mutant proteins even after temperature stress, but whether this association is due to PDI docking onto Ero protein prior to misoxidation, or whether PDI was operating as a chaperone trying to refold Ero1β is a question that needs further investigation. Recently it was shown that a PDI mutant lacking its four active site cysteines (PDI-ASAS) was still able to interact with Ero1α non-covalently, which suggests PDI is able to chaperone Ero proteins (Otsu et al., 2006).

ERp72 was identified as a novel interacting partner of Ero1β and Ero1α (Figure 5.3) and could also act as an alternative electron donor for hEROs. Previous studies using pulse-labelled cell lysates and αMyc immunoprecipitations had failed to detect an interaction between ERp72 and hERO proteins (Mezghrani et al., 2001). However, experimental conditions used in this study (at steady state using αErp72 immunoprecipitaion) were different from the published literature, thus it is possible that these interactions are preserved/detected under specific conditions. Further work is required to identify functional differences between Ero-PDI and Ero-ERp72 interactions. immunodepletion (as in Figure 3.8) could be used to monitor the effects of ERp72 and Ero-ERp72 interactions. *In vivo*, it will be interesting to find out if reducing the levels of PDI through RNAi would effect levels of ERp72 and would compromise or compensate Ero1 mediated oxidative folding. Although ERp72 could be the 70 kDa

interacting protein detected under pulse-chase conditions, mass spectrometric analysis of this band is needed to verify the identity of this protein. An interaction between Ero1β and BiP could not be readily detected under the steady-state conditions used in this study.

Chapters 3-4 and recent studies by Seiver and Kaiser (Sevier & Kaiser, 2006b) have shown that Ero-Ero dimers contribute to Ero function. It was possible that mutations at the FAD binding domain could also prevent dimerisation leading to loss of function in the *ero1-1*, *ero1-2* mutants. However, data from this chapter shows that Ero-Ero associations do not depend entirely on the FAD binding domain (Figure 5.6) and so inability to self-complex is not likely to explain the yeast mutant phenotypes. It still remains possible that intermolecular disulfide bond formation is altered in these two mutants, but this would require structural and mass spectrometry studies to be carried out on the G252S and H254Y mutants.

CHAPTER 6

EXPRESSION PATTERN OF OXIDOREDUCTASES IN THE HUMAN DIGESTIVE SYSTEM

6.1 Introduction

Expression of Ero1α and Ero1β differ at the transcriptional level in human tissues, with an up regulation of Ero1α in the oesophagus and Ero1β in the stomach, pancreas, testis, liver, appendix, thyroid and pituitary glands (Pagani et al., 2000). Chapter 3 section 3.2.1 discussed the specific detection of Ero1β in mammalian stomach and pancreas tissues.

6.1.1 Histology of the pancreas

The human pancreas is made up of two types of tissues; exocrine and endocrine tissue. Exocrine tissue consists of acini which synthesise and secrete several digestive enzymes transported via a duct system to the duodenum. The endocrine tissue consists of the islets of Langerhans which secrete hormones into the bloodstream. The islets house four major cell types, glucagon producing alpha-cells, insulin producing beta-cells, somatostatin producing delta-cells and pancreatic polypeptide producing F cells (Kierszenbaum, 2002; Stevens & Lowe, 1993). Insulin-secreting beta cells occupy the central area of the islets and are the most common cell type. Insulin is a 6 kDa polypeptide derived from proinsulin which consists of a disulfide linked A and B chain connected with a C peptide (Brange & Langkjoer, 1993). Mature insulin is produced in secretory vesicles by the cleavage of peptide C. Hyperglycemia is a result of increased blood glucose levels for prolonged periods of time leading to diabetes (Kierszenbaum, 2002). Type I diabetes or insulin-dependent diabetes mellitus (IDDM), is a lack of insulin caused by autoimmune, toxic or viral damage to beta cells. Although 90% of the cases begin in childhood (juvenile diabetes), it can occur at any time of life. Type II diabetes or non-insulin-dependent diabetes mellitus (NIDDM) is caused by insufficient

insulin secretion relative to glucose levels and by resistance of peripheral target tissue to insulin. This type of diabetes is more common and observed in adults, and within first-degree relatives the risk of developing type II diabetes is ~20-40% compared with ~5-7% in the population at large (Kierszenbaum, 2002; Kumar et al., 1997).

6.1.2 Histology of the upper GI tract

The oesophagus is a muscular tube which transports undigested but fragmented food to the stomach for digestion. The oesophageal mucosa is composed of non-keratinised stratified squamous epithelium and an underlying lamina propria and muscularis mucosa. Cells at the basal membrane have rounded nuclei and are pyramidal or polygonal in shape. The more mature epithelial cells not in direct contact with the basement membrane take a more flattened squamous morphology with elliptical nuclei. Mucosal and submucosal glands are found in the oesophagus which continuously produce a thin layer of mucus to lubricate the surface of the epithelium (Kierszenbaum, 2002).

The squamous epithelium of the oesophagus is protected from the exposure of gastric acid especially at the gastroesophageal junction (OG junction) by the anatomical arrangement of the OG junction as well as by the small oesophagogastric muscular sphincter, which in most cases prevents the reflux of gastric contents in to the lower oesophagus (Stevens & Lowe, 1993). However this system can fail, allowing the reflux of gastric acid and digestive enzymes from the stomach into the oesophagus which gives rise to Barrett's oesophagus. Barrett's oesophagus is considered a premalignant condition and is identified by the replacement of the normal distal stratified squamous mucosa by columnar type epithelium, which is gastric, intestinal or mixed in

composition (Kumar et al., 1997). Prolonged and recurrent gastroesophageal reflux can lead to inflammation leading from specialised metaplasia to dysplasia and onto adenocarcinoma. Dysplastic cells show considerable variation in size and shape, and often posses abnormally large nuclei for the size of the cell. Cancerous cells also have extremely hyperchromatic large nuclei with the nuclear-cytoplasm ratio reaching 1:1 instead of 1:4 or 1:6 in normal cells. Barrett's oesophagus is one of the recognised precursors of oesophageal adenocarcinoma (Kumar et al., 1997).

In healthy tissue, at the gastroesophageal junction the stratified squamous epithelium changes to a simple columnar type which marks the beginning of the stomach tissue. The surface area of the stomach is increased by the formation of glands which secrete acid and digestive enzymes. The two major cell types found in these gastric glands are parietal or oxyntic cells and chief or peptic cells. Parietal cells are large pyramidal cells with a central nuclei and pale eosinophilic cytoplasm which secrete hydrochloric acid and intrinsic factor. Chief cells on the other hand have large basal nuclei and secrete the inactive enzyme precursor, pepsinogen into the gastric lumen where it is converted to the proteolytic enzyme pepsin by gastric acid. Other cell types found within these glands are mucous cells (surface and neck mucous cells), stem cells and enteroendocrine cells (Kierszenbaum, 2002; Stevens & Lowe, 1993).

Studies have not been published on Ero1β or Ero1α protein expression in the digestive system. This chapter uses healthy human stomach and pancreas tissue as well as healthy oesophagus, Barrett's oesophagus, oesophageal tumour, OG junction tumour and gastric tumour tissue to investigate, using immunohistochemistry, the protein expression patterns of hEROs and several chaperone proteins found in the ER.

6.2 Results

6.2.1 Expression of hEROs and chaperone proteins in healthy human pancreas

6.2.1.1 Optimisation of antigen retrieval techniques

Human pancreatic tissue sections were treated as described in section 2.2.1 prior to carrying out a series of digestion techniques. Digestion techniques and antibody dilutions for some of the primary antibodies (αPDI, αBiP, D5) used in this study had been previously optimised by an undergraduate project student, but for the rest of the primary antibodies (H-86, αERp72, αERp57, αEroβ, αERp44) different digestion techniques and dilutions were performed (all of the antibody dilution data are not shown).

When primary antibody was omitted during pancreas section staining (TBS, Figure 6.1 left panels), microwave digestion in high pH citrate buffer gave a very faint non-specific staining (Figure 6.1*A*) but gave negative staining after microwave digestion in citrate buffer (Figure 6.1*C*), trypsin digestion (Figure 6.1*E*) and pressure cooker digestion in citrate buffer (Figure 6.1*G*). Sections exposed to pre-immune rabbit sera (PS, Figure 6.1 right panels) instead of primary antibody gave a faint non-specific staining after microwave high pH citrate digestion (Figure 6.1*B*), negative staining after microwave digestion in citrate buffer (Figure 6.1*D*), and trypsinisation (Figure 6.1*F*) and a very faint staining after pressure cooker digestion (Figure 6.1*H*). Overall the pre-immune serum gave a faint non-specific staining after all four digestion techniques.

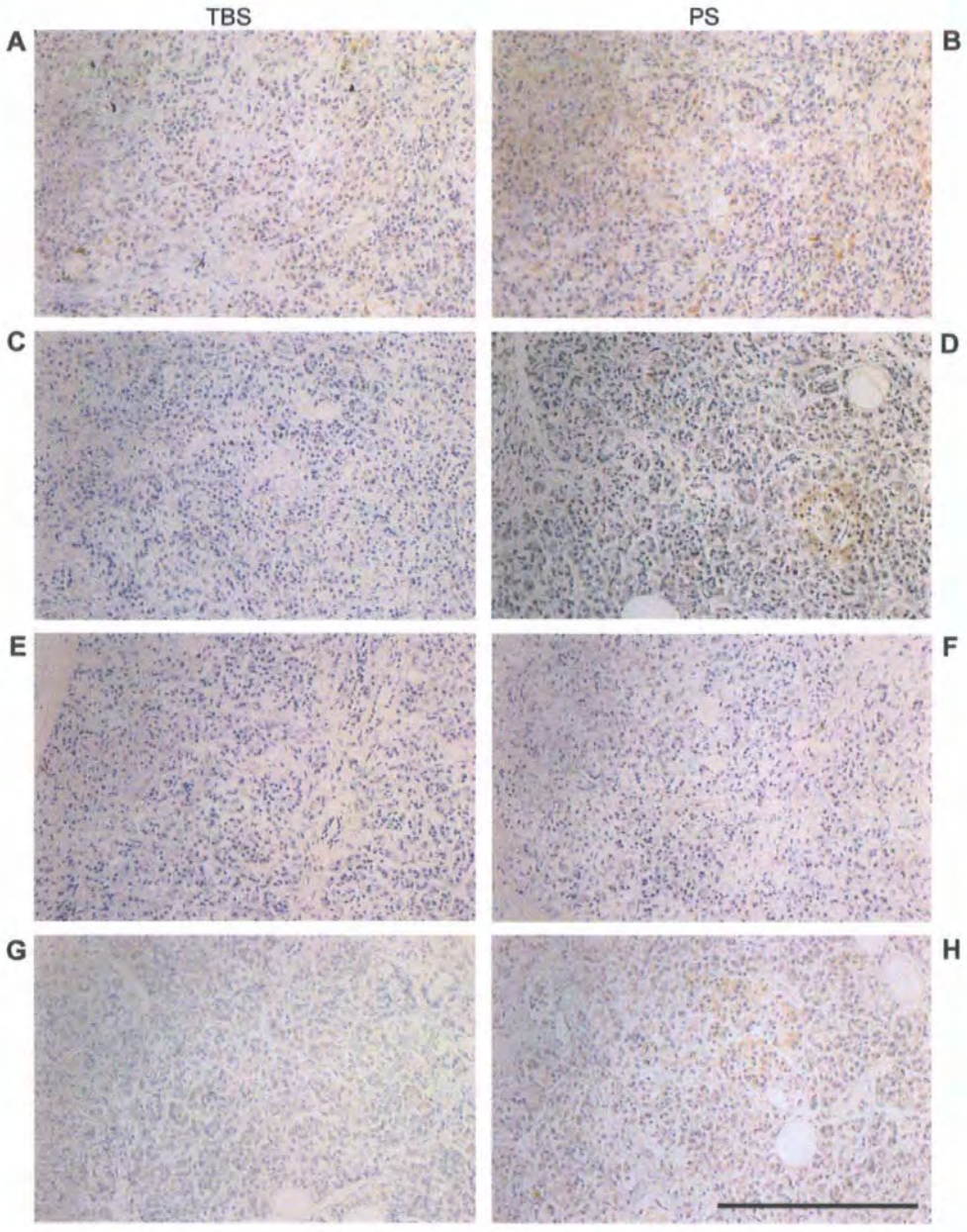

FIGURE 6.1: Optimisation of digestion techniques for human pancreatic tissue
Paraffin embedded human pancreas sections were cleared through xylene, taken through a 100 – 70% alcohol series and endogenous peroxidase activity blocked in H_2O_2 prior to performing four different antigen retrieval techniques; microwave with high pH citrate buffer (**A** and **B**), microwave with citrate buffer (**C** and **D**), trypsinisation (**E** and **F**) and pressure cooker with citrate buffer (**G** and **H**). Primary antibody was omitted (TBS; **A**, **C**, **E** and **G**) or sections exposed to pre-immune serum (PS; **B**, **D**, **F** and **H**) prior to detection with DAB; bar = 200 μm. Overall TBS and PS all showed non-specific staining with all four digestion techniques.

The insulin antibody, H-86, was used as a pancreatic islet marker with the same four digestion techniques as in Figure 6.1. This antibody specifically stained the pancreatic islets (arrows), but with different specificities after each of the antigen retrieval techniques (Figure 6.2). Microwave with citrate buffer was the least specific antigen retrieval step for the H-86 antibody which showed very faint staining of the islets (Figure 6.2, *A* and *B*). Trypsinisation allowed more access for the H-86 antibody and thus resulted in recognition of islets more effectively (Figure 6.2, *C* and *D*). However, microwave with high pH citrate buffer (Figure 6.2, *E* and *F*) and pressure cooker with citrate buffer (Figure 6.2, *G* and *H*) proved to be the most effective digestion techniques for H-86, showing strong staining of the islets. Pressure cooker with citrate buffer (Figure 6.2, *G* and *H*) however, did show the highest level of specificity, with almost exclusive staining of the islets when compared with the surrounding acinar cells, and so was chosen as the optimal digestion technique for H-86 antibody. Results from figures 6.1 and 6.2 are summarised in table 6.1.

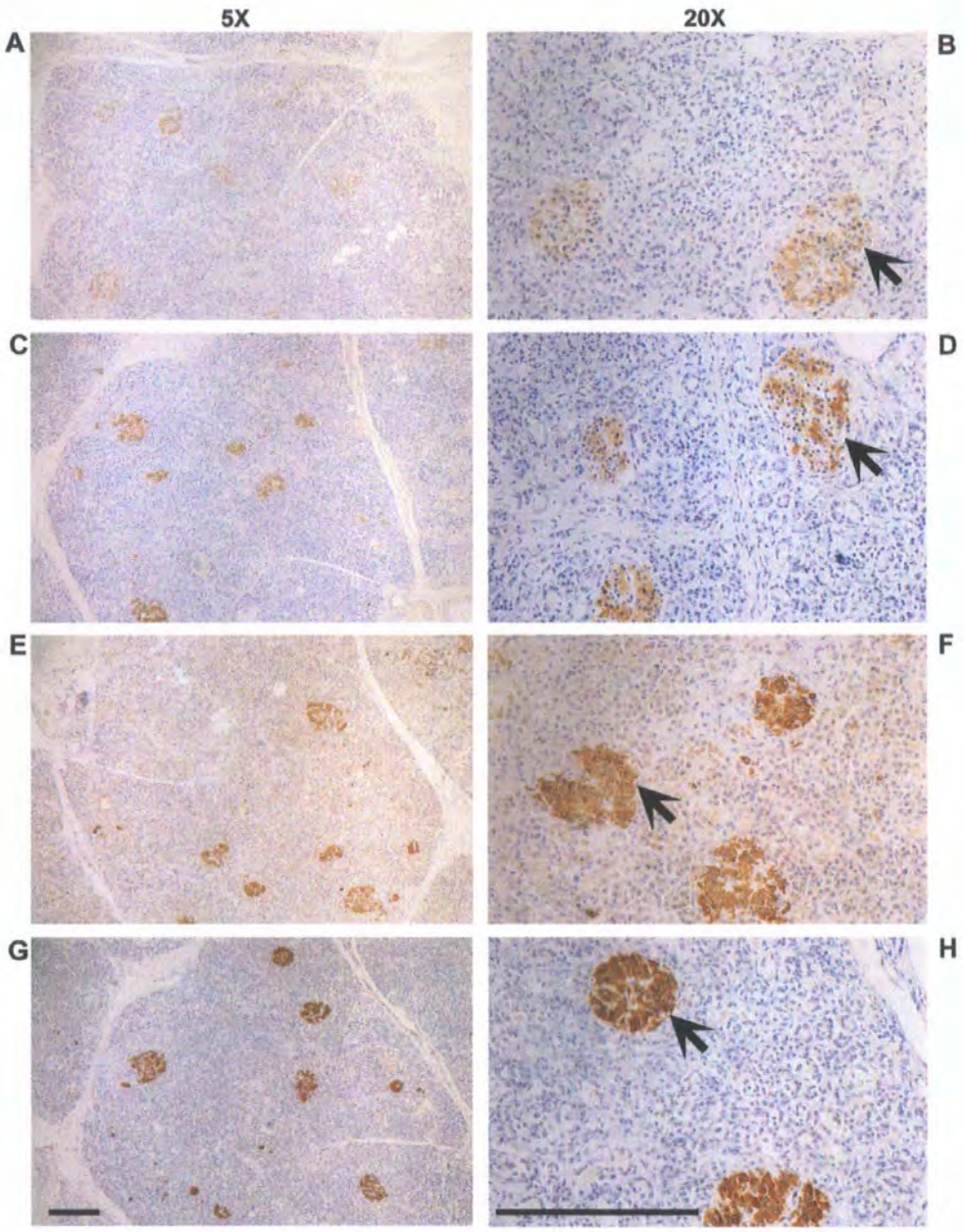

FIGURE 6.2: Optimisation of antigen retrieval technique for insulin antibody

Paraffin embedded human pancreas sections were cleared through xylene, taken through a 100 – 70% alcohol series and endogenous peroxidase activity blocked in H_2O_2 prior to performing four different antigen retrieval techniques; microwave with citrate buffer (**A** and **B**), trypsinisation (**C** and **D**), microwave with high pH citrate buffer (**E** and **F**) and pressure cooker with citrate buffer (**G** and **H**). All sections were probed with the H-86 (insulin) primary antibody prior to detection with DAB and photographed at 5X (**A**, **C**, **E** and **G**) and 20X (**B, D**, **F** and **H**) magnification. Bar = 200 μm, arrow = islets. The best digestion technique was pressure cooker with citrate buffer (**G** and **H**).

Table 6.1: Summary of results from optimisation of digestion techniques for wax embedded human pancreas sections

Antibody	Antigen retrieval technique			
	Microwave with citrate buffer	**Trypsinisation**	**Microwave with high pH buffer**	**Pressure cooker with citrate buffer**
TBS	Negative	Negative	Very weak non-specific staining	Negative
Pre-immune serum (PS)	Negative	Negative	Weak, non-specific staining	Weak, non-specific staining
H-86	Very weak staining of the islets	Weak staining of the islets	Strong but less specific staining of the islets	Strong and specific staining of the islets

6.2.1.2 Expression of hEROs and chaperone proteins

Ero1β was expressed in both islets (arrow) and the surrounding enzyme producing acinar cells, with a stronger expression in the islets (Figure 6.3, *A-C*). This expression pattern was also seen with different digestion techniques and primary antibody dilutions tested in this study (Figure 6.3, *A-C*). The expression of the second mammalian oxidoreductase Ero1α was studied using the D5 primary antibody. After digestion of the tissue, D5 showed no specific staining in the pancreas (Figure 6.3*D*).

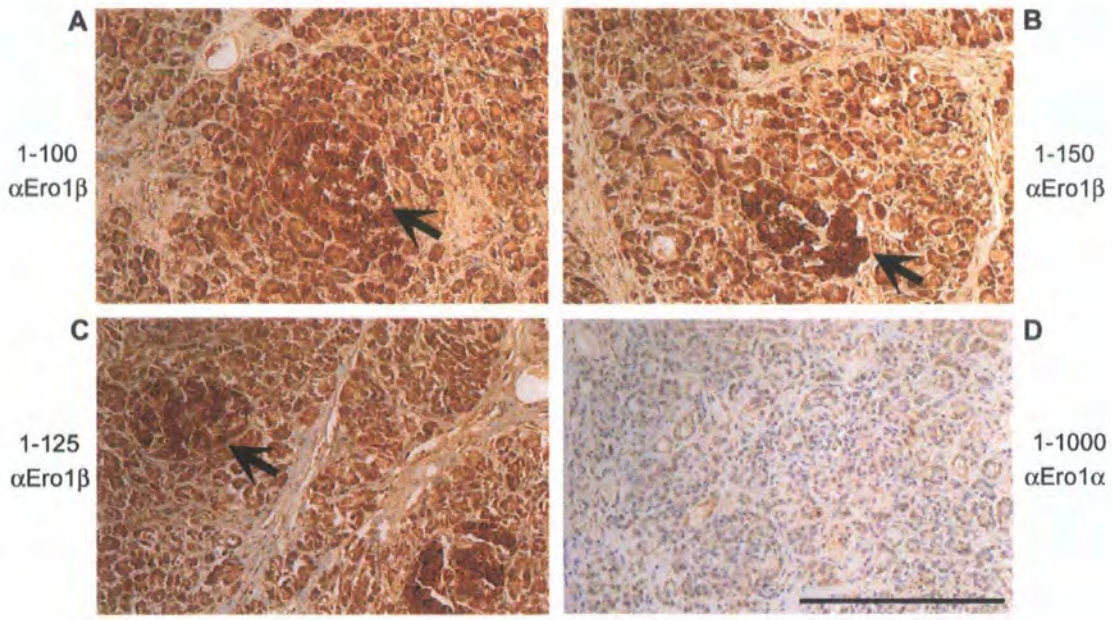

FIGURE 6.3: Ero1β is expressed strongly in the pancreatic islets

Paraffin embedded human pancreas sections were cleared through xylene, taken through a 100 – 70% alcohol series and blocked for endogenous peroxidase in H_2O_2. Prior to incubating with primary antibody, sections were digested in microwave with citrate buffer (**A**, **B** and **D**) and pressure cooker with citrate buffer (**C**). Sections were incubated with αEro1β primary antibody at 1-100 (**A**), 1-150 (**B**), 1-125 (**C**) and αEro1α (D5) primary antibody at 1-1000 (**D**) dilution prior to detection with DAB and photographed at 20X magnification (**A-D**). Ero1β is expressed in both exocrine and endocrine tissue with stronger expression in endocrine tissue. Bar = 200 μm, arrow = islets.

Next, the expression pattern of ER chaperones involved in protein oxidation and folding was investigated. The pancreas-specific PDI homolog, PDIp, showed expression in the acinar cells with very weak staining of the islets, as previously reported (Figure 6.4, *A* and *B*, (Desilva et al., 1997)). However in contrast to Ero1β, PDI expression was lower in the islets (arrow) compared with the surrounding acinar cells (Figure 6.4*C*). Having seen a difference in expression patterns between Ero1β and PDI, the expression of several other ER chaperones was also tested.

αERp57 antibody (after tissue digestion in pressure cooker with citrate buffer) gave a similar staining to Ero1β with the islets staining stronger than the acinar cells (Figure 6.4*D*), although the overall staining wasn't as strong as with the αEro1β serum. The αERp57 antibody gave less distinct staining patterns after trypsinisation and microwave digestion with citrate buffer (data not shown). αBiP (Figure 6.4*E*) and αERp72 (Figure 6.4*F*) showed strong expression throughout the pancreas, including the islets which were difficult to identify after αERp72 antibody staining and thus not labelled. Two antibodies against full length ERp44 from two different hybridomas (ERp44a and ERp44b) were also tested. Digestion with citrate buffer in microwave gave no staining with either antibody (data not shown) whereas digestion in pressure cooker did give some signal (Figure 6.4, *G* and *H*). However, these expression levels were quite similar to pre-immune sera staining (Figure 6.1*H*), demonstrating that under conditions used in this study ERp44 was not detectable in the pancreas. Taken together the data suggest that Ero1β is found in both exocrine and endocrine tissue, with stronger expression in endocrine tissue, whereas PDI is more prominently expressed in exocrine tissues. ERp57, ERp72 and BiP are however expressed in pancreatic endocrine tissue, indicating a possible involvement of these proteins with Ero1β. An

interaction between ERp72 and Ero1β was already shown under steady state conditions (Figure 5.3*A*), whereas no direct interaction could be detected between BiP and Ero1β (Figure 5.3*E*).

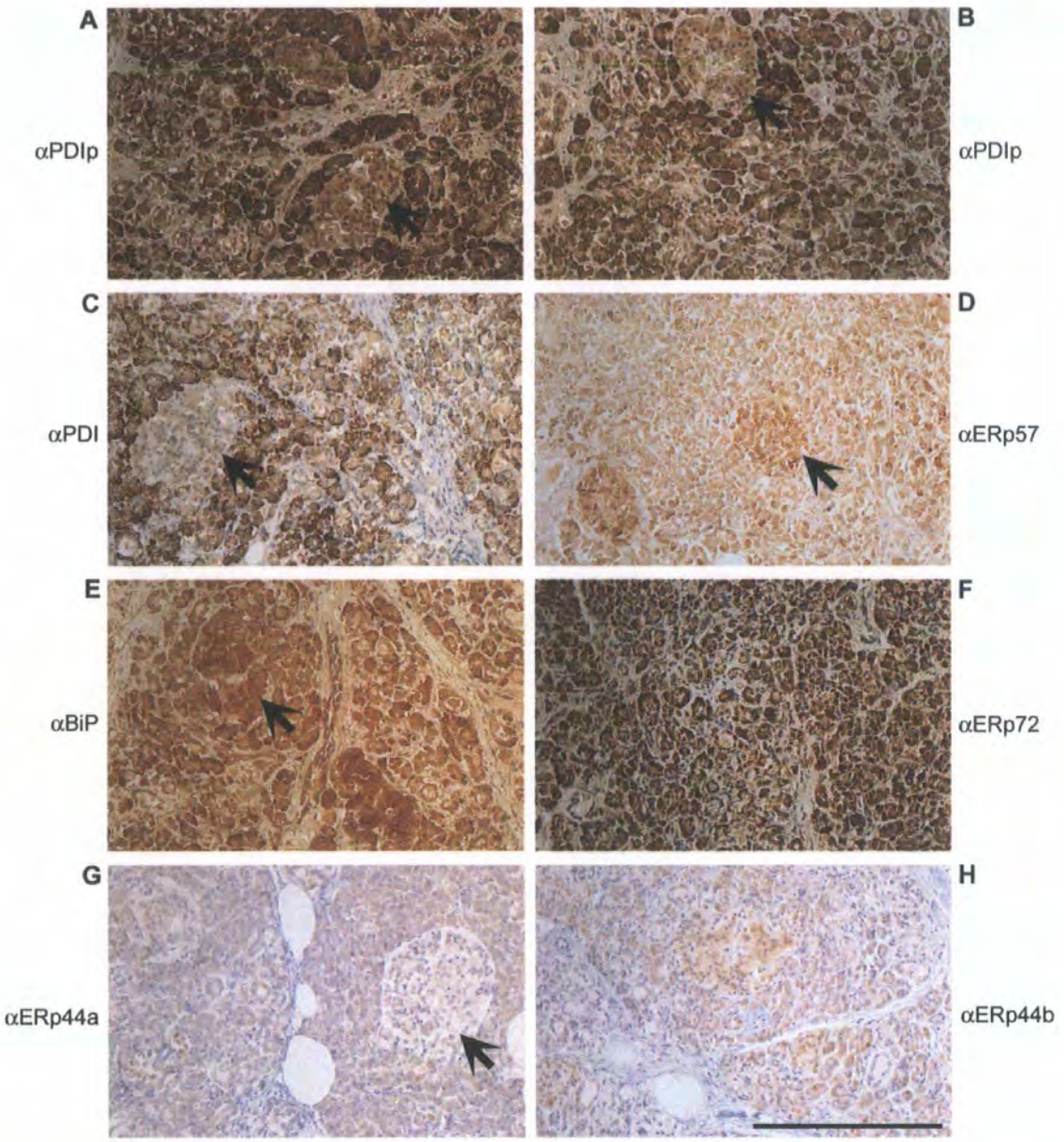

FIGURE 6.4: ER chaperone expression in human pancreatic tissue

Paraffin embedded human pancreas sections were cleared through xylene, taken through a 100 – 70% alcohol series and blocked for endogenous peroxidase in H_2O_2. Prior to incubating with primary antibody, sections were digested in microwave with citrate buffer (**A**, **C** and **E**), pressure cooker with citrate buffer (**B**, **D**, **G** and **H**) and water bath with citrate buffer (**F**). Sections were incubated with αPDIp at 1-1000 (**A** and **B**), αPDI at 1-800 (**C**), αERp57 at 1-200 (**D**), αBiP at 1-40 (**E**), αERp72 at 1-1000 (**F**), αERp44a at 1-200 (**G**) and αERp44b at 1-200 (**H**) prior to detection with DAB and photographed at 20X magnification (**A-H**). Bar = 200 μm, arrow = islets.

6.2.2 *Ero1β interacts with PDIp*

The pancreas specific PDI homolog, PDIp is expressed strongly in the exocrine tissue (Figure 6.4, *A* and *B*, (Desilva et al., 1997)). Since Ero1β was also expressed in exocrine tissue, the ability of Ero1β to interact with PDIp was investigated. Samples of mouse pancreas were lysed in the presence of NEM, clarified by centrifugation and either directly analysed by reducing SDS-PAGE or subjected to concanavalin A (con A) affinity chromatography prior to reducing SDS-PAGE analysis. Immunoblotting with αEro1β showed expression in mouse pancreatic tissue but not in kidney tissue lysates as expected (Figure 6.5*A*, compare *lanes 1* and *5* with *2* and *6*). Wild-type Ero1β-Myc transfected HeLa lysate was used as a positive control (Figure 6.5*A*, *lane 3*). The same tissue lysates were used in an immunoprecipitation with αPDIp antibody prior to reducing SDS-PAGE. Probing the western blotted membrane with αEro1β gave a signal from the pancreatic lysates (Figure 6.5*A*, *lane 8*) but not the kidney lysates (Figure 6.5*A*, *lane 9*), confirming that PDIp interacted with Ero1β *in vivo*. The same mouse tissue lysates as in figure 6.5*A* together with Ero1α-Myc transfected HeLa cell lysates were analysed by reducing SDS-PAGE and transferred proteins probed with D5 antibody to detect the expression of Ero1α. Ero1α expression was detected in transfected cell lysate (Figure 6.5*B*, *lane 3*) but was not detected in pancreas or kidney tissue lysates (Figure 6.5*B*, *lane 1-2*). Immunoprecipitation with αPDIp, showed no interaction between PDIp and Ero1α (Figure 6.5*B*, *lane 4-5*). PDIp expression in the pancreas was confirmed through western blotting before and after con A precipitation (Figure 6.5*B*, *compare lanes 6* and *9* with *7* and *10*). The data suggests that the pancreas specific PDI family member PDIp binds to one of the hEROs, Ero1β, in the pancreas.

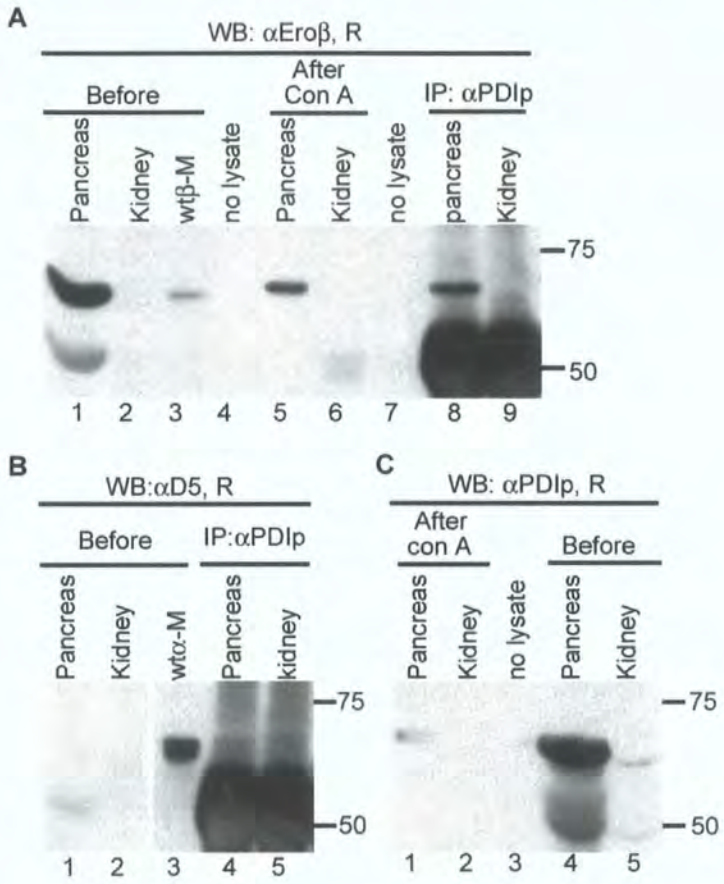

FIGURE 6.5: PDIp interacts with Ero1β *in vivo*

A. Mouse pancreas and kidney tissue samples or wtEro1β-myc transfected HeLa cells were lysed in the presence of NEM, and analysed directly (*lanes 1-3)* or subjected to con A affinity chromatography (*lanes 5-6*) or subjected to immunoprecipitation with αPDIp (*lanes 8-9*) prior to reducing SDS-PAGE. Western blotted membrane was probed with αEro1β. *Lanes 4* and *7* are loaded with sample buffer only. **B.** wtEro1α-myc cell lysate (*lane 3*), pancreas and kidney lysates (*lanes 1-2, 4-5*) were directly analysed by reducing SDS-PAGE (*lanes 1-2*) or first subjected to immunoprecipitation with αPDIp (*lanes 4-5*). Immunoblotting was with D5 (*lanes 1-5*). **C.** Pancreas and kidney lysates were directly analysed (*lanes 4-5*) or first subjected to con A affinity chromatography (*lanes 1-2*) prior to immunoblotting with αPDIp after reducing SDS-PAGE. *Lane 3* is loaded with sample buffer only.

6.2.3 Expression of hEROs and chaperone proteins in healthy human stomach

6.2.3.1 Optimisation of antigen retrieval techniques

Human stomach tissue sections were examined using immunohistochemistry to further investigate whether high levels of Ero1β expression correlated with high expression levels of ER chaperone proteins, similar to that observed in the pancreas. Paraffin embedded stomach sections were subjected to four different antigen retrieval techniques; microwave digestion in high pH buffer, microwave digestion in citrate buffer, trypsinisation and pressure cooker digestion. When primary antibody was omitted (TBS, Figure 6.6 left hand panel) stomach sections showed faint background staining after microwave with high pH buffer (Figure 6.6*A*), negative staining after microwave with citrate buffer, and trypsinisation (Figure 6.6, *C*, and *E* respectively) and non-specific but relatively high levels of staining after pressure cooker digestions (Figure 6.6*G*). Sections exposed to pre-immune rabbit sera (PS, Figure 6.6 right hand panel) showed a patchy staining pattern after microwave with high pH buffer (Figure 6.6*B*), non-specific faint staining after microwave with citrate buffer (Figure 6.6*D*), non-specific but relatively high levels of staining after pressure cooker digestions (Figure 6.6*F*), and negative staining after trypsinisation (Figure 6.6*H*). Due to the higher level of staining observed after microwave digestion with high pH buffer and pressure cooker digestion with citrate buffer, these two antigen retrieval techniques were not used with specific antibodies on human stomach sections. Results from figure 6.6 are summarised in table 6.2.

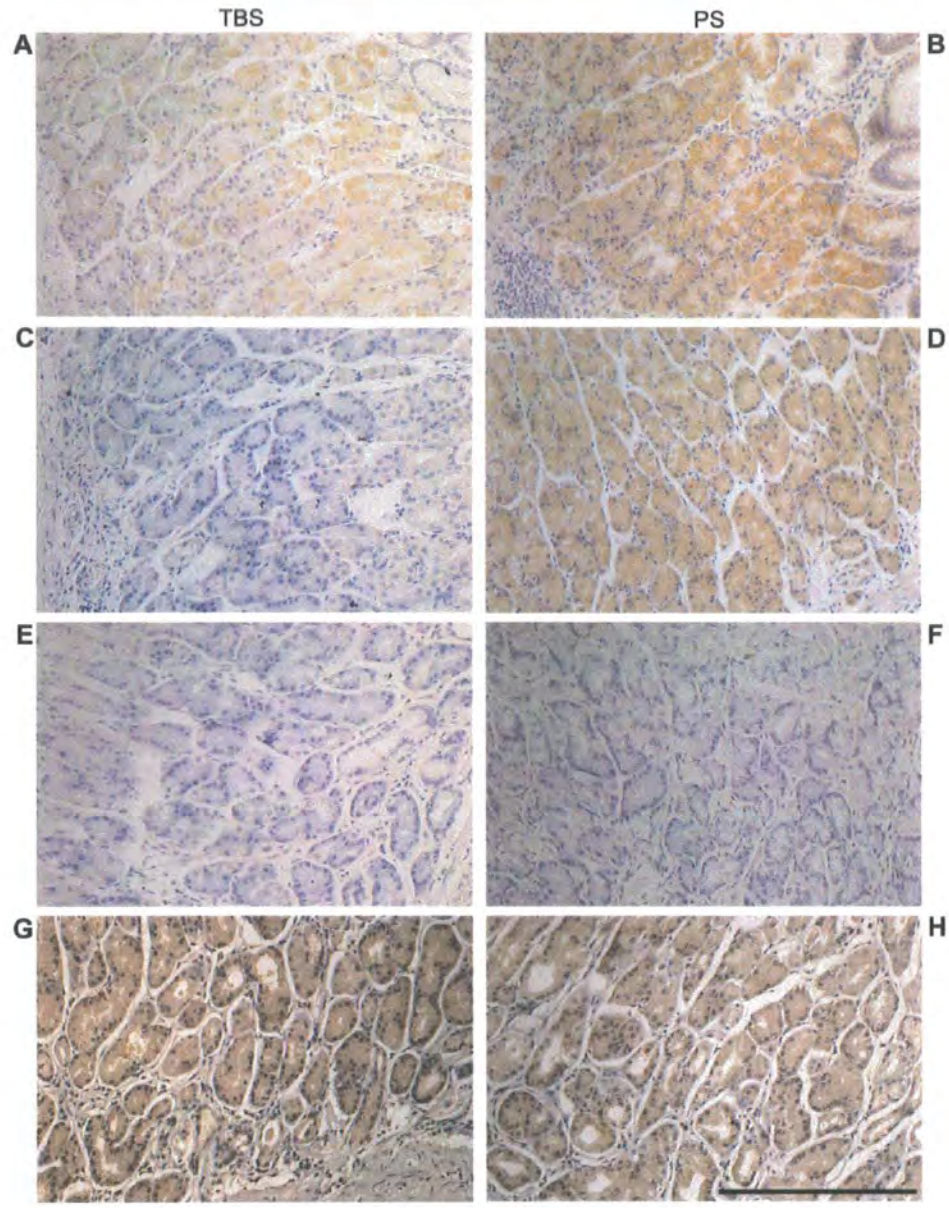

FIGURE 6.6: Optimisation of digestion techniques for human stomach tissue

Paraffin embedded human stomach sections were cleared through xylene, taken through a 100 – 70% alcohol series and endogenous peroxidase activity blocked in H_2O_2 prior to performing four different antigen retrieval techniques; microwave with high pH buffer (**A** and **B**), microwave with citrate buffer (**C** and **D**), trypsinisation (**E** and **F**) and pressure cooker with citrate buffer (**G** and **H**). Primary antibody was omitted (TBS; **A**, **C**, **E** and **G**) or sections exposed to pre-immune serum (PS; **B**, **D**, **F** and **H**) prior to detection with DAB and photography at 20X magnification (**A-H**); bar = 200 μm. Microwave with high pH buffer and pressure cooker with citrate buffer gave a fairly high level of non-specific staining after TBS and pre-immune serum and so was not used as a antigen retrieval technique with subsequent antibodies on stomach tissue sections.

Table 6.2: Summary of results from optimisation of digestion techniques for wax embedded human stomach sections

Antibody	Antigen retrieval technique			
	Microwave with citrate buffer	**Trypsinisation**	**Microwave with high pH buffer**	**Pressure cooker with citrate buffer**
TBS	Negative	Negative	Very weak non-specific staining	Non-specific but strong staining
Pre-immune serum (PS)	Weak, non-specific staining	Negative	Weak, patchy staining	Non-specific but strong staining

6.2.3.2 Ero1β and ER chaperone proteins are expressed in the chief cells of the stomach

Sections probed with the Ero1β antiserum showed very strong, specific staining in the basal area of the stomach (Figure 6.7*A*). At higher magnification, Ero1β showed a patchwork like distribution representing strong expression in the enzyme producing chief cells of the stomach (arrows) and weaker expression in the acid producing parietal cells (arrowhead) within the same glands (Figure 6.7, *B-D*). This staining pattern was evident after microwave with citrate buffer with three Ero1β antibody concentrations (Figure 6.7, *B-D*). Expression of the second oxidoreductase Ero1α was also analysed after microwave with citrate buffer conditions using two antibody concentrations (Figure 6.7, *E* and *F*), which gave a similar but a weaker expression pattern to Ero1β.

To look for any correlation between oxidoreductase expression and ER chaperone expression within the stomach, a selection of ER chaperone proteins were tested under the same optimal digestion conditions as for Ero1α and Ero1β. Unlike pancreatic tissue, in the stomach, PDI expression was identical to Ero1β expression, with staining observed in chief cells (arrows) but weaker in parietal cells (arrowheads, Figure 6.7*G*). BiP (Figure 6.7*H*), ERp57 (Figure 6.7*I*), ERp72 (Figure 6.7*J*), and ERp44 (Figure 6.7*K*) were all expressed at a high level in the same cell types. The ERp44b (Figure 6.7*L*) antiserum did not show any staining in the stomach. Data from this study suggest that ER chaperones as well as oxidoreductases are expressed at high levels in enzyme producing cells in the stomach.

Table 6.3 summarises the hERO and chaperone protein staining results from the human pancreas and stomach tissues.

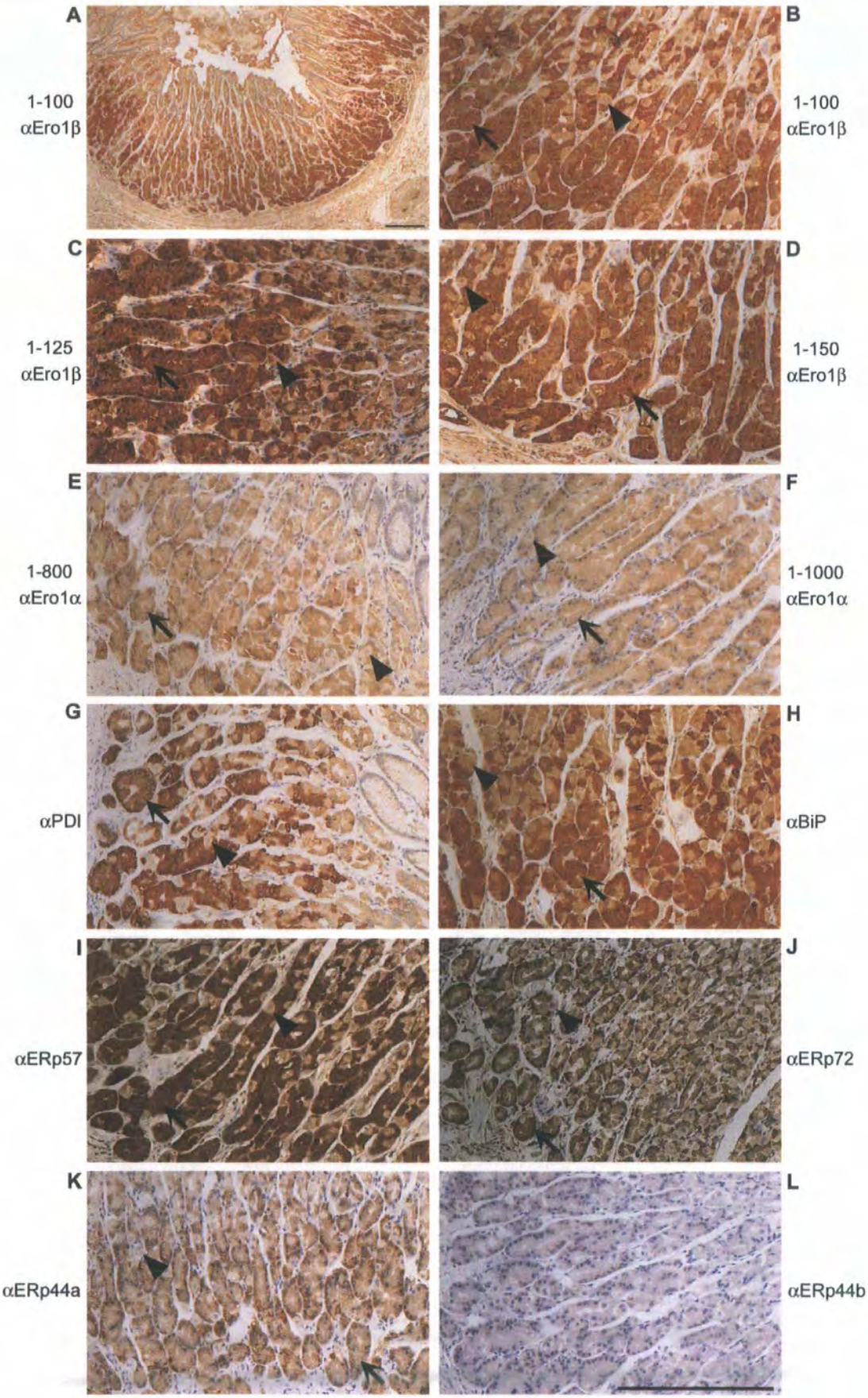

FIGURE 6.7: Ero1β and ER chaperones strongly expressed in chief cells of the stomach

FIGURE 6.7: Ero1β and ER chaperones strongly expressed in chief cells of the stomach

Paraffin embedded human stomach sections were cleared through xylene, taken through a 100 – 70% alcohol series and endogenous peroxidase activity blocked in H_2O_2. Prior to incubating with primary antibody sections were digested in a microwave with citrate buffer (**A-I** and **K-L**) or digested according to the protocol in section 2.2.2 (**J**) and were incubated with αEro1β at 1-100 (**A** and **B**), αEro1β at 1-125 (**C**), αEro1β at 1-150 (**D**), D5 at 1-800 (**E**), D5 at 1-1000 (**F**), αPDI at 1-800 (**G**), αBiP at 1-40 (**H**), αERp57 at 1-200 (**I**), αERp72 at 1-1000 (**J**), αERp44a at 1-200 (**K**), αERp44b at 1-200 (**L**) dilutions prior to detection with DAB and photographed at 5X (**A**) and 20X magnification (**B-L**); bar = 200 μm. Arrow = chief cells, arrowhead = parietal cells.

Table 6.3: hERO and ER chaperone protein expression in human pancreas and stomach tissue. Summary of results when using the optimum digestion technique for each antibody.

Antibody used	Expression levels	
	Pancreatic tissue	**Stomach tissue**
αEro1β	Expressed in acinar cells and stronger in islets	Strong expression in chief cells and weaker in parietal cells
αEro1α (D5)	Not detected	Similar to αEro1β, but weaker
αPDI	Expressed in acinar cells but weak in islets	Similar to αEro1β
αPDIp	Expressed in acinar cells but very weak in islets	Not detected
αERp57	Similar to αEro1β, but overall weaker	Similar to αEro1β
αERp72	Expressed in acinar cells and in islets	Similar to αEro1β
αERp44a	Not detected	Similar to αEro1β
αERp44b	Not detected	Not detected
αBiP	Similar to αERp72	Similar to αEro1β

6.2.4 Expression of hEROs and chaperone proteins in human oesophagus

6.2.4.1 Normal oesophagus

Ero1α transcripts were found to be up regulated in human oesophagus tissue compared to Ero1β levels (Pagani et al., 2000), and to investigate whether this pattern is repeated at the protein level, immunohistochemistry was used on healthy human oesophagus sections (3396-00 B1). Sections were digested by following protocol 2 (section 2.2.2) and incubated with pre-immune serum (PS, Figure 6.8*A* and *B*) or primary antibody was omitted (TBS, Figure 6.8*C* and *D*), both of which did not stain the stratified squamous epithelium (double headed arrow). Sections probed with the Ero1β antiserum showed weak staining throughout the epithelium (Figure 6.8*E* and *F*). Ero1α expression however was more prominent and was detected in more mature epithelial cells (arrows) compared to cells closer to the basal membrane (Figure 6.9, *C-H*). This expression pattern was also seen with several D5 antibody dilutions, although at the highest antibody concentration (1-50) this pattern was less prominent (Figure 6.9, compare *C-H* with *A-B*).

To investigate the expression of ER chaperone proteins in healthy oesophagus tissue, sections were probed with αPDI (Figure 6.10*A* and *B*), αBiP (Figure 6.10*C* and *D*), αERp72 (Figure 6.10*E* and *F*) and αERp57 (Figure 6.10*G* and *H*) which all showed different expression patterns. BiP showed only very weak expression, PDI was expressed throughout the epithelium whereas ERp72 showed the strongest expression. ERp57, however, showed no expression throughout the epithelium.

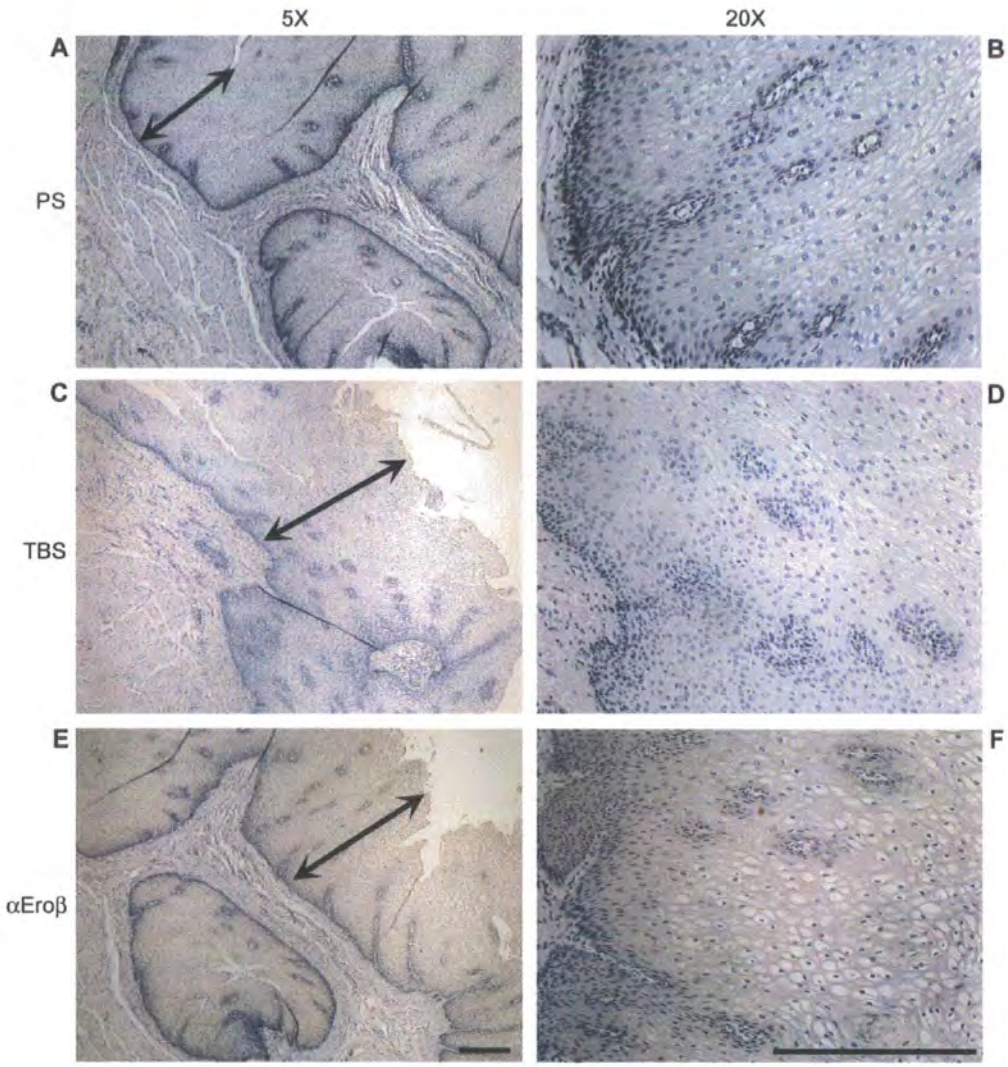

FIGURE 6.8: Weak expression of Ero1β in normal oesophagus (3396-00 B1)

Paraffin embedded human normal oesophagus sections were cleared through histoclear, taken through a 100 – 70% alcohol series and endogenous peroxidase activity blocked in H_2O_2. Prior to incubating with primary antibody sections were digested in a water bath with citrate buffer according to section 2.2.2 (**A-F**) and were incubated with pre-immune serum (PS, **A** and **B**), TBS (**C** and **D**) and αEro1β at 1-150 (**E** and **F**) dilutions prior to detection with DAB and photography at 5X (**A**, **C**, **E**) and 20X magnification (**B**, **D**, **F**). Double headed arrows indicate the stratified squamous epithelium; bar = 200 μm.

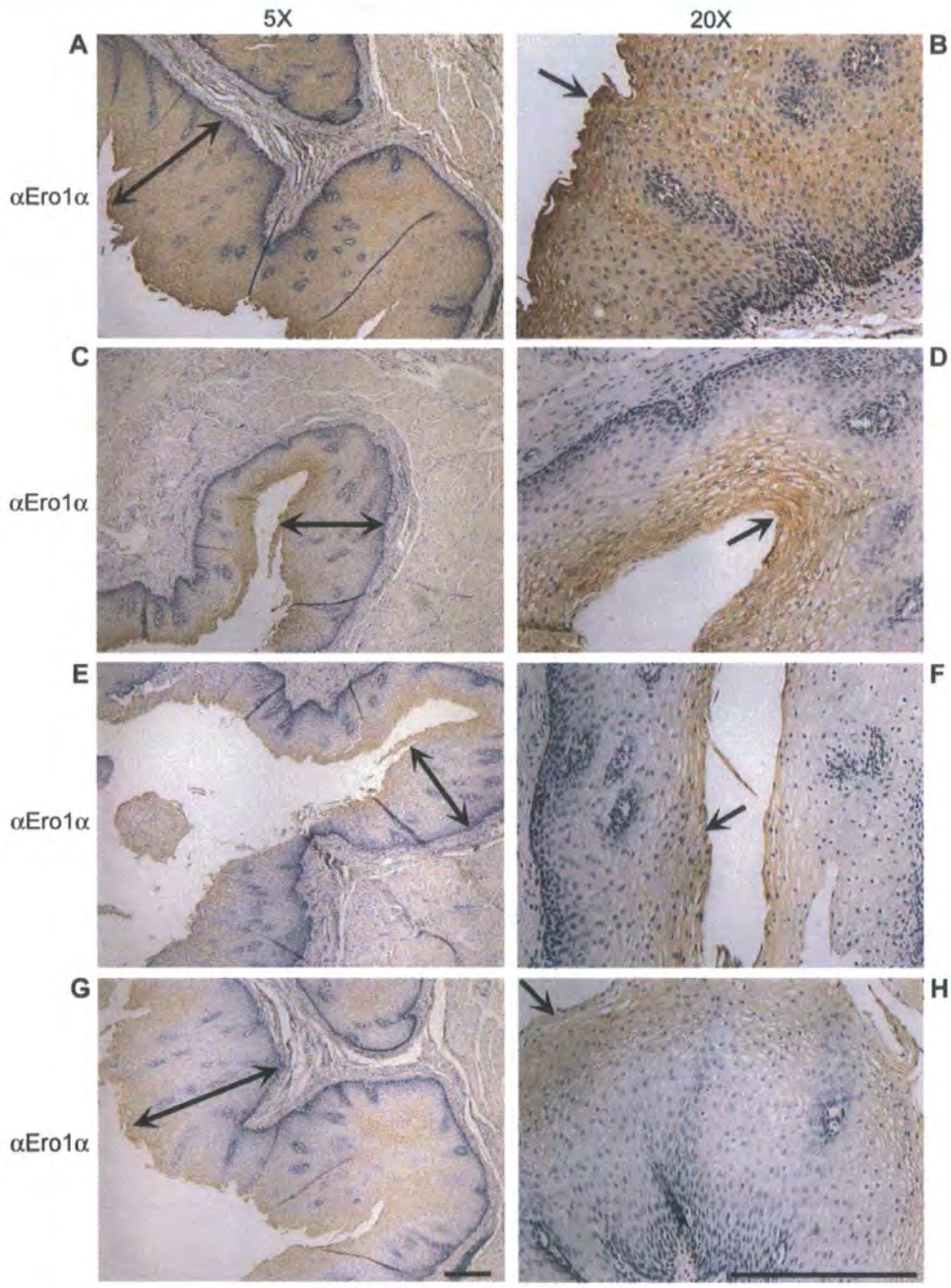

FIGURE 6.9: Specific expression of Ero1α in normal oesophagus (3396-00 B1)

Paraffin embedded human normal oesophagus sections were cleared through histoclear, taken through a 100 – 70% alcohol series and endogenous peroxidase activity blocked in H_2O_2. Prior to incubating with primary antibody, sections were digested in a water bath with citrate buffer according to section 2.2.2 (**A-H**) and were incubated with αEro1α (D5 antibody) at 1-50 (**A** and **B**), 1-200 (**C** and **D**), 1-500 (**E** and **F**) and at 1-800 (**G** and **H**) dilutions prior to detection with DAB and photographed at 5X (**A**, **C**, **E**, **G**) and 20X magnification (**B**, **D**, **F**, **H**). Double headed arrows indicate the stratified squamous epithelium and the single headed arrows indicate the mature epithelium cells with higher Ero1α expression. bar = 200 μm.

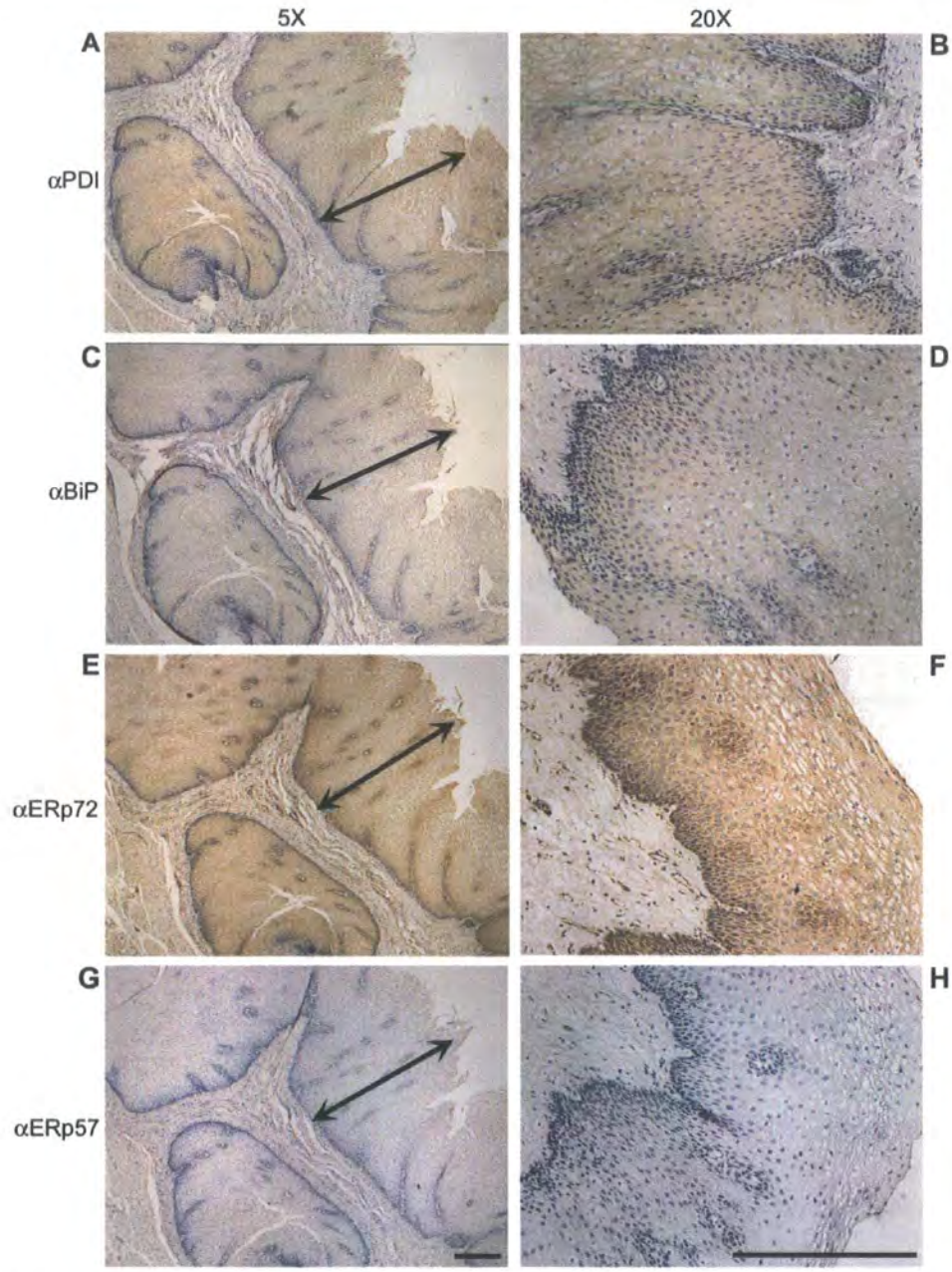

FIGURE 6.10: Expression of ER chaperones in normal oesophagus (3396-00 B1)
Paraffin embedded human normal oesophagus sections were cleared through histoclear, taken through a 100 – 70% alcohol series and endogenous peroxidase activity blocked in H_2O_2. Prior to incubating with primary antibody sections were digested in a water bath with citrate buffer according to section 2.2.2 (**A-H**) and were incubated with αPDI at 1-400 (**A** and **B**), αBiP at 1-40 (**C** and **D**), αERp72 at 1-1000 (**E** and **F**) and αERp57 at 1-800 (**G** and **H**) dilutions prior to detection with DAB and photography at 5X (**A**, **C**, **E**, **G**) and 20X magnification (**B**, **D**, **F**, **H**). Double headed arrow = stratified squamous epithelium. ERp72 expression is high throughout the epithelium compared to low expression of PDI and very weak expression of BiP. αERp57 shows negative staining. bar =200 μm.

6.2.4.2 Barrett's oesophagus

To study the expression pattern of hEROs and ER chaperone proteins in Barrett's oesophagus, sections were digested by following protocol 2 (section 2.2.2) and first tested with two negative controls; incubating with pre-immune serum (PS, Figure 6.11*A* and *B*) and omitting primary antibody (TBS, Figure 6.11*C* and *D*), both of which did not stain the columnar type epithelium (arrowhead) or the goblet cells (arrows). This Barrett's epithelium is non-dysplastic and due to the presence of goblet cells can be classified as intestinal type glandular epithelium. The stratified squamous epithelium in healthy oesophagus tissue (double headed arrow in Figures 6.8 - 6.10) is replaced by the columnar type epithelium in Barrett's. Sections probed with the Ero1β antiserum showed very faint staining throughout the epithelium (Figure 6.11*E* and *F*). However, Ero1α expression (using D5 antibody) was strong throughout the columnar epithelium (arrows, Figure 6.11, *G* - *J*)). This pattern was repeated with the use of two different D5 antibody dilutions (Figure 6.11, *G* - *J*).

To identify any changes in expression of ER chaperone proteins, sections were probed with αPDI (Figure 6.12*A* and *B*), αBiP (Figure 6.12*C* and *D*), αERp72 (Figure 6.12*E* and *F*) and αERp57 (Figure 6.12*G* and *H*). ERp72 showed the strongest expression compared with PDI and BiP, and was expressed in the columnar epithelium. αERp57 gave a similar result as in the healthy oesophagus (Figure 6.10*G* and *H*) with no staining observed throughout the epithelium.

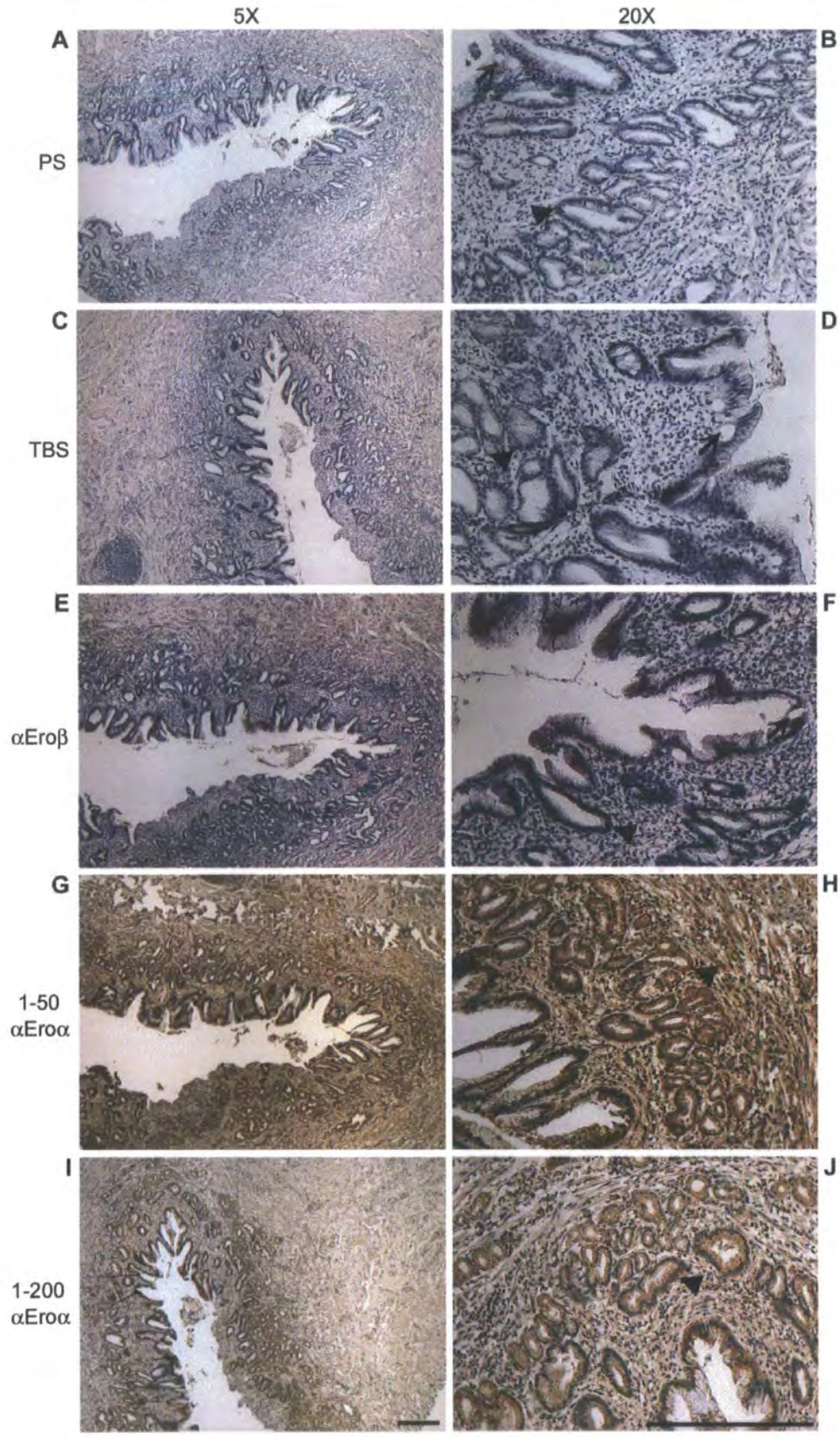

FIGURE 6.11: hERO expression in Barrett's oesophagus (6199-02 A2)

Paraffin embedded human Barretts oesophagus sections were cleared through histoclear, taken through a 100 – 70% alcohol series and endogenous peroxidase activity blocked

in H_2O_2. Prior to incubating with primary antibody sections were digested in a water bath with citrate buffer according to section 2.2.2 (**A-J**) and were incubated with pre-immune serum (PS, **A** and **B**), TBS (**C** and **D**) and αErol1β at 1-150 (**E** and **F**), αErol1α at 1-50 (**G** and **H**) and αErol1α at 1-200 (**I** and **J**) dilutions prior to detection with DAB and photographed at 5X (**A**, **C**, **E, G, I**) and 20X magnification (**B**, **D**, **F, H, J**). Goblet cells are indicated with arrows and the columnar epithelium is indicated with an arrowhead. Erol1α expression is strong in the columnar epithelium whereas Erol1β is not detected; bar = 200 μm.

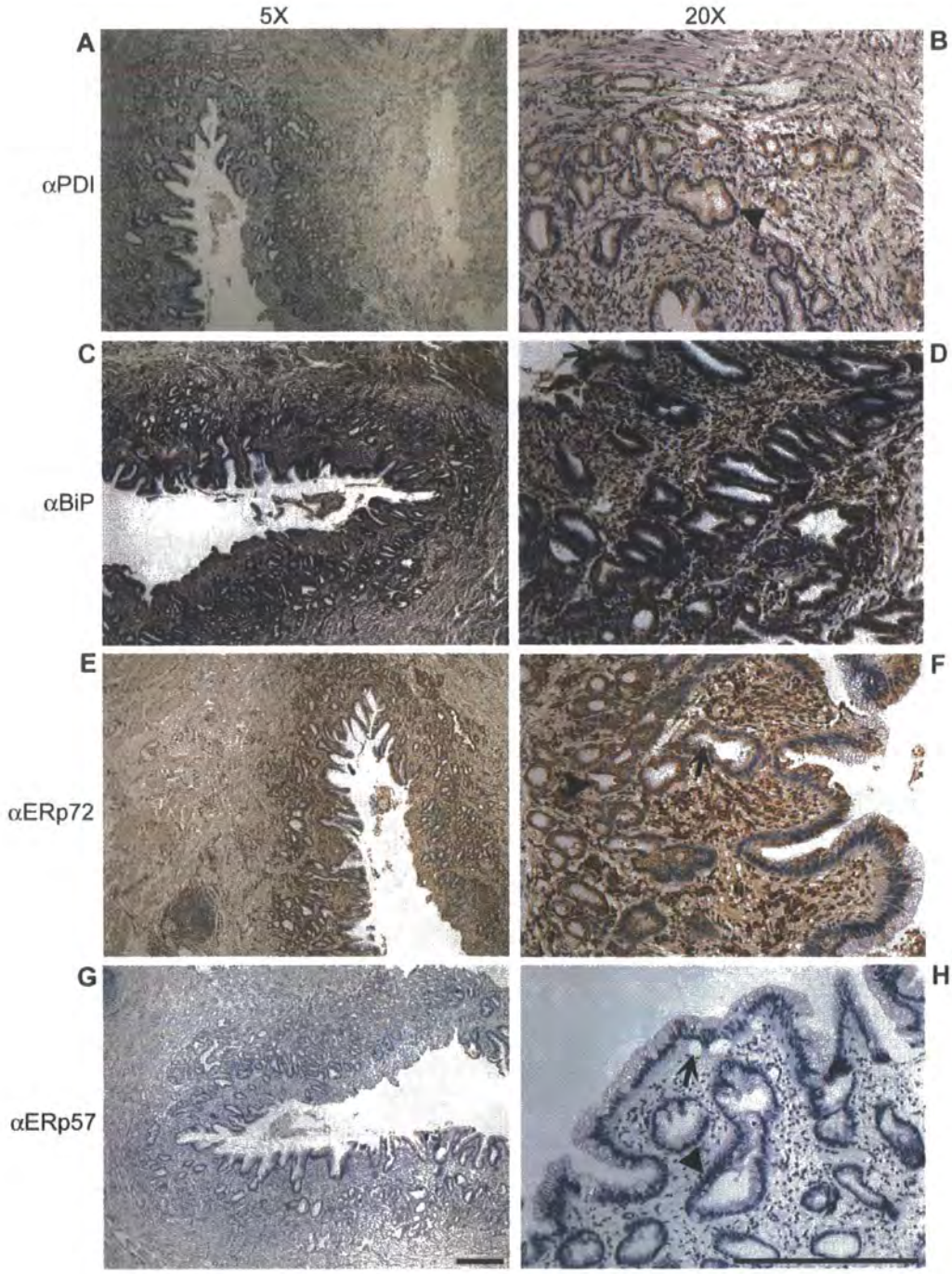

FIGURE 6.12: ER chaperone protein expression in Barretts oesophagus (6199-02 A2)

Paraffin embedded human Barretts oesophagus sections were cleared through histoclear, taken through a 100 – 70% alcohol series and endogenous peroxidase activity blocked in H_2O_2. Sections were digested in a water bath with citrate buffer according to section 2.2.2 (**A-H**) and were incubated with αPDI at 1-400 (**A** and **B**), αBiP at 1-40 (**C** and **D**), αERp72 at 1-1000 (**E** and **F**) and αERp57 at 1-800 (**G** and **H**) dilutions prior to detection with DAB and photographed at 5X (**A**, **C**, **E**, **G**) and 20X magnification (**B**, **D**,

F, **H**). Goblet cells are indicated with arrows and the glandular epithelium is indicated with an arrowhead. PDI, BiP and ERp72 are expressed in the glandular epithelium at varying levels whereas ERp57 is not detected; bar = 200 μm.

6.2.4.3 Oesophageal tumour

Next, the expression pattern of hERO and ER chaperone proteins was investigated in oesophageal tumour (1039-03 B2) sections. Figure 6.13 represents an area in this tissue block representing dysplasia (at low power magnification, area within the double headed arrow, Figure 6.13*A*), where some of the single layer columnar epithelium found in Barrett's oesophagus (Figure 6.11-6.12) is replaced by a multi-cellular glandular epithelium (arrows, Figure 6.13, *B-J*), with some of the cells having an increased nuclear/cytoplasm ratio. Sections were digested by following protocol 2 (section 2.2.2) and incubated with pre-immune serum (PS, Figure 6.13*A* and *B*) or omitting primary antibody (TBS, Figure 6.13*C*), both of which showed negative staining throughout the epithelium. Sections probed with αEro1β (Figure 6.13*D*) and αEro1α (using D5, Figure 6.13*E* and *F*) antisera showed strong staining throughout the dysplastic epithelium. The Ero1α expression pattern was repeated with the use of two different D5 antibody dilutions (Figure 6.13*E* and *F*). To identify any changes in expression of ER chaperone proteins, sections were probed with αPDI (Figure 6.13*G*), αBiP (Figure 6.13*H*), αERp72 (Figure 6.13*I*) and αERp57 (Figure 6.13*J*). PDI, ERp72 and ERp57 all showed strong expression compared to BiP, which showed very faint staining in the dysplastic tissue. The ERp57 result contrasts with the negative staining seen in normal (Figure 6.10) and Barrett's oesophagus (Figure 6.12).

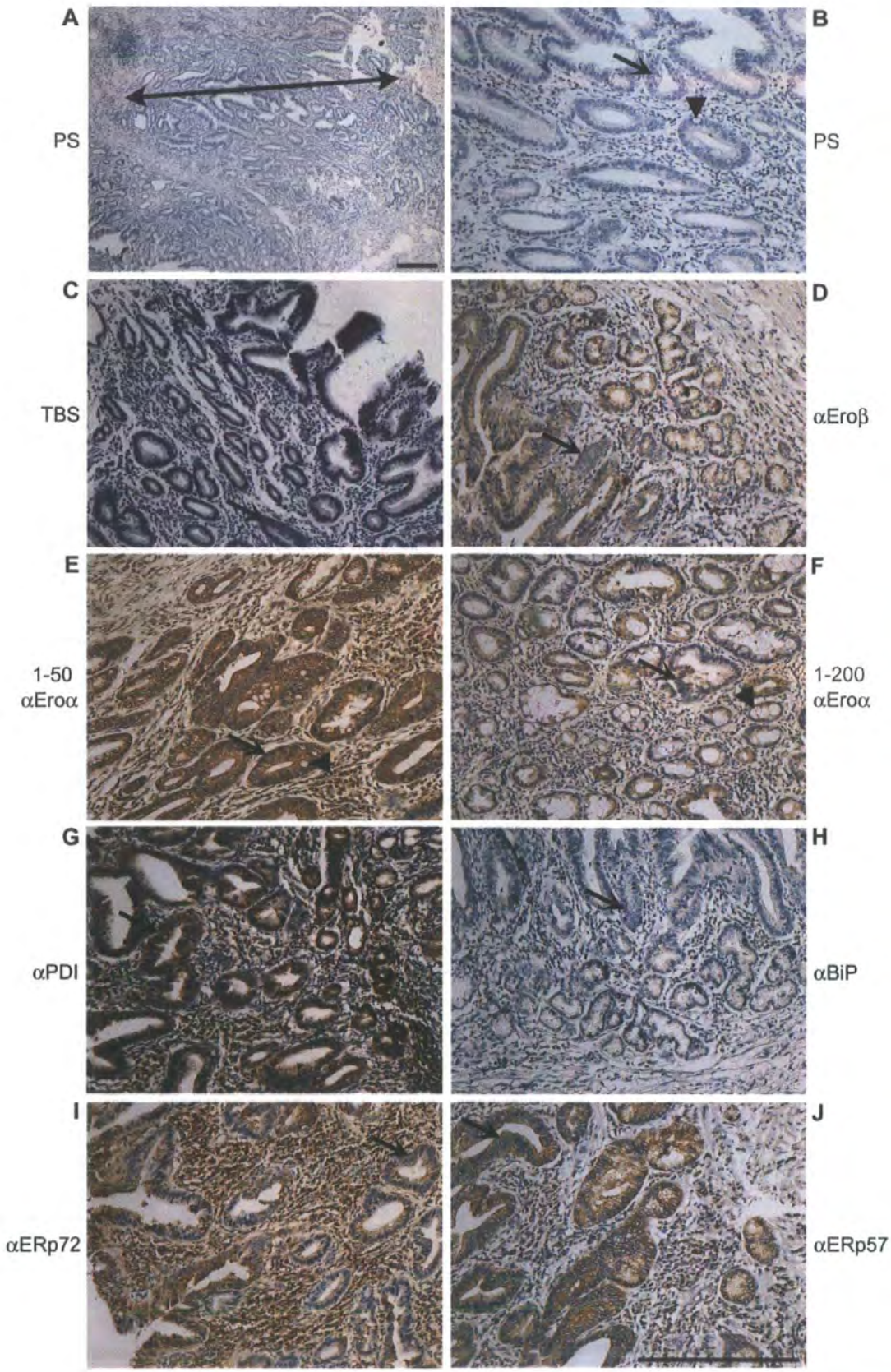

FIGURE 6.13: Expression in dysplastic tissue from oesophageal tumour (1039-03 B2)

FIGURE 6.13: Expression in dysplastic tissue from oesophageal tumour (1039-03 B2)

Paraffin embedded human oesophageal tumour sections were cleared through histoclear, taken through a 100 – 70% alcohol series and endogenous peroxidase activity blocked in H_2O_2. Prior to incubating with primary antibody sections were digested in a water bath with citrate buffer according to section 2.2.2 (**A-J**) and were incubated with pre-immune serum (PS, **A** and **B**), TBS (**C**), with αEroβ at 1-150 (**D**), αEro1α at 1-50 (**E**), αEro1α at 1-200 (**F**), αPDI at 1-400 (**G**), αBiP at 1-40 (**H**), αERp72 at 1-1000 (**I**) and αERp57 at 1-800 (**J**) dilutions prior to detection with DAB and photographed at 5X (**A**) and 20X magnification (**B-J**). Goblet cells are indicated with arrowheads and the dysplastic epithelium is indicated with a double headed arrow. The arrows show multi-nuclei cells in the glandular epithelium. Ero1β, Ero1α, and the ER chaperone proteins are all expressed in the glandular epithelium at varying levels. BiP shows the weakest expression; bar = 200 μm.

The same tissue block (1039-03 B2) was also used to study hERO and chaperone protein expression patterns in adenocarcinoma tissue. Sections were digested by following protocol 2 (section 2.2.2) and when primary antibody was omitted (TBS, Figure 6.14*A* and *B*), the dysplastic epithelium (*) and the infiltrating neoplastic cells (area within double headed arrow at low power magnification, Figure 6.14*A*) showed negative staining. Incubating with pre-immune serum (PS, Figure 6.14*C*) also showed negative staining. Sections probed with αEro1β (Figure 6.14*D*) and two concentrations of αEro1α antisera (using D5, Figure 6.14*E* and *F*) showed expression in the infiltrating cells. To identify any changes in expression of ER chaperone proteins, sections were probed with αPDI (Figure 6.14*G*), αBiP (Figure 6.14*H*), αERp72 (Figure 6.14*I*) and αERp57 (Figure 6.14*J*). PDI, ERp72 and ERp57 are all expressed in the infiltrating cells, whereas BiP is expressed at very low levels.

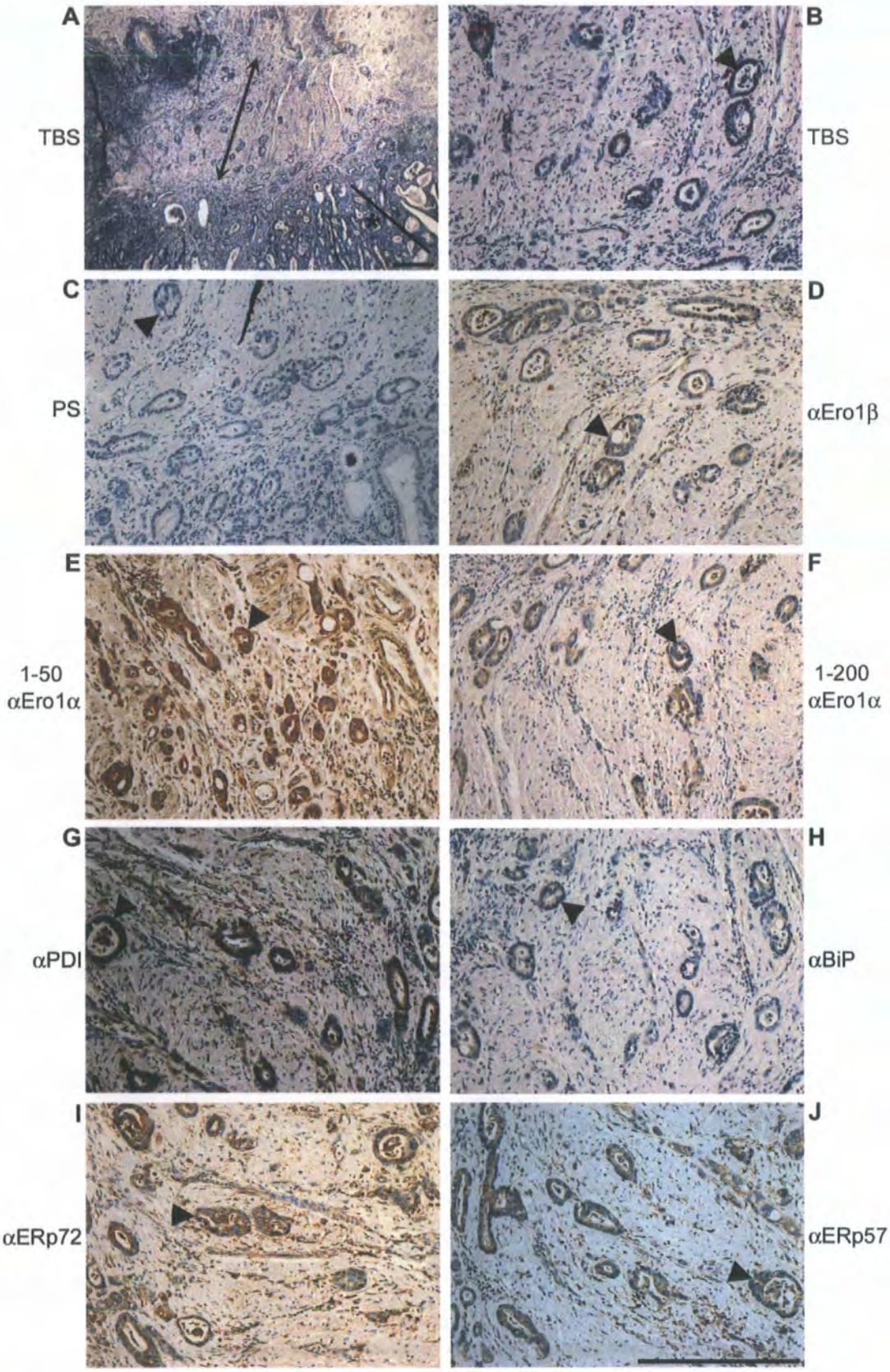

FIGURE 6.14: Expression in adenocarcinoma tissue from oesophageal tumour (1039-03 B2)

FIGURE 6.14: Expression in adenocarcinoma tissue from oesophageal tumour (1039-03 B2)

Paraffin embedded human oesophageal tumour sections were cleared through histoclear, taken through a 100 – 70% alcohol series and endogenous peroxidase activity blocked in H_2O_2. Prior to incubating with primary antibody sections were digested in a water bath with citrate buffer according to section 2.2.2 (**A-J**) and primary antibody was omitted (TBS, **A** and **B**) or incubated with pre-immune serum (PS, **C**), αEroβ at 1-150 (**D**), αEro1α at 1-50 (**E**), αEro1α at 1-200 (**F**), αPDI at 1-400 (**G**), αBiP at 1-40 (**H**), αERp72 at 1-1000 (**I**) and αERp57 at 1-800 (**J**) dilutions prior to detection with DAB and photographed at 5X (**A**) and 20X magnification (**B-J**). The dysplastic epithelium is indicated with a *, the adenocarcinoma with infiltrating cells is indicated with a double headed arrow and the infiltrating cells are indicated with arrowheads. Ero1β, Ero1α, and the ER chaperone proteins are all expressed in the adenocarcinoma at varying levels. BiP shows weak expression; bar = 200 μm.

6.2.5 Expression of hEROs and chaperone proteins in OG junction tumour and gastric tumour

To study the expression pattern of hEROs and ER chaperone proteins in gastroesophageal tumour, sections were digested by following protocol 2 (section 2.2.2) and first tested with two negative controls; incubating with pre-immune serum (PS, Figure 6.15*A* and *B*) and omitting primary antibody (TBS, Figure 6.15*C*), both of which did not stain the tumour tissue. At low magnification (Figure 6.15*A*) the carcinoma has several areas differentiated into glands (double headed arrow), where as some areas are poorly differentiated and glands are not visible (not shown). Multi-nuclear cells with decreasing cytoplasm are evident under higher magnification (arrows). Sections probed with the αErol1β (Figure 6.15*D*), and αErol1α (using two concentrations of D5 antibody, Figure 6.15*E* and *F*) showed strong expression in neoplastic cells. PDI (Figure 6.15*G*), ERp72 (Figure 6.15*I*) and ERp57 (Figure 6.15*J*) were all expressed comparable to Erol1α and Erol1β, whereas BiP (Figure 6.15*H*) expression was not detected.

Next the expression patterns were compared with gastric tumour sections after antigen retrieval according section 2.2.2. The two negative controls (Figure 6.16, *A-C*) showed no staining throughout the gastric tumour, whereas Erol1β (Figure 6.16*D*), Erol1α (Figure 6.16*E and F*), PDI (Figure 6.16*G*), BiP (Figure 6.16*H*), ERp72 (Figure 6.16*I*), and ERp57 (Figure 6.16*J*) were all strongly expressed in the neoplastic cells (arrows). The results from Figures 6.8 - 6.16 are summarised in table 6.4.

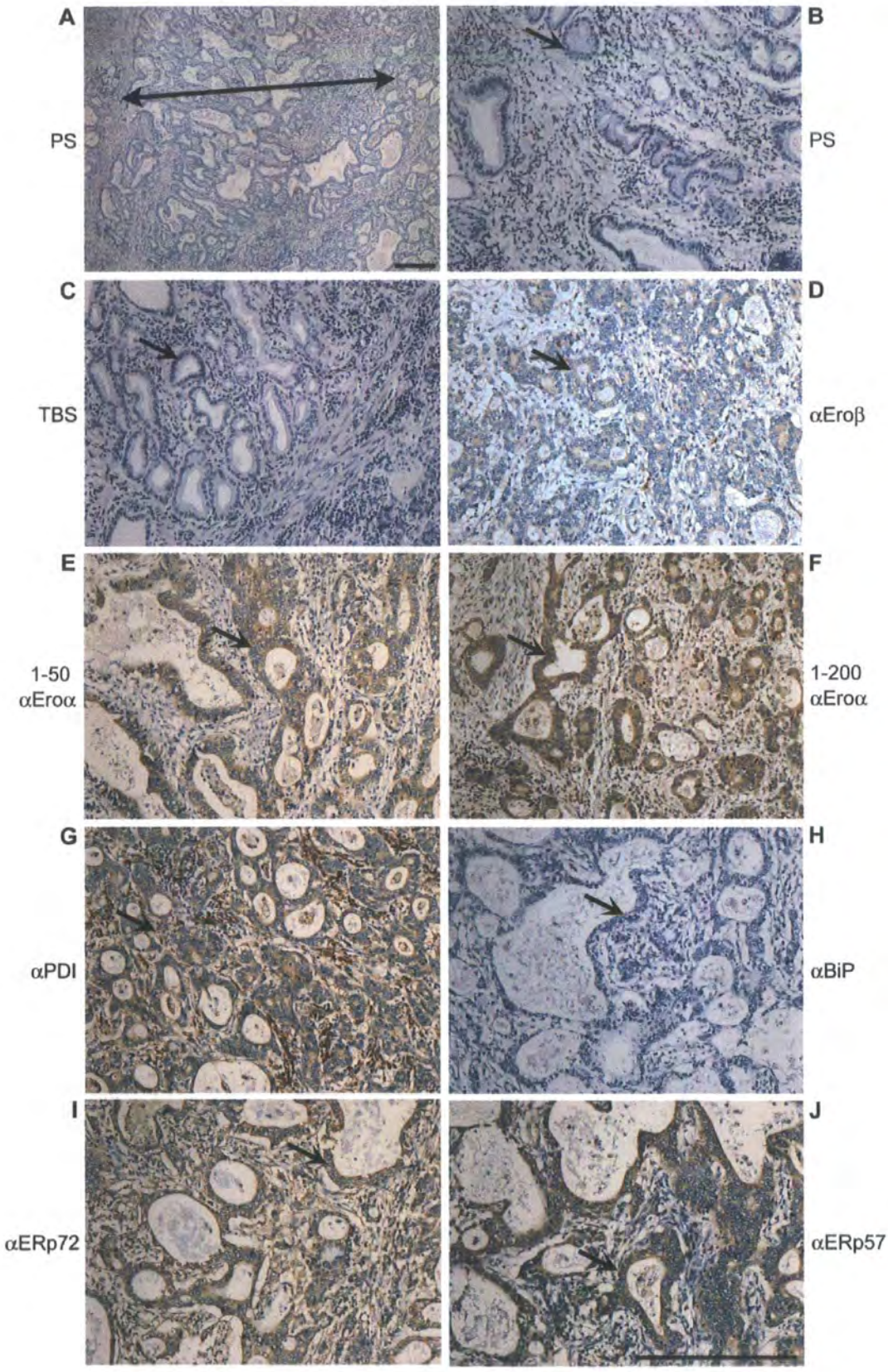

FIGURE 6.15: hERO and chaperone protein expression in OG junction tumour (6591-01 C4)

FIGURE 6.15: hERO and chaperone protein expression in OG junction tumour (6591-01 C4)

Paraffin embedded human oesophageal tumour sections were cleared through histoclear, taken through a 100 – 70% alcohol series and endogenous peroxidase activity blocked in H_2O_2. Prior to incubating with primary antibody sections were digested in a water bath with citrate buffer according to section 2.2.2 (**A-J**) and incubated with pre-immune serum (PS, **A** and **B**), TBS (**C**), αEroβ at 1-150 (**D**), αEro1α at 1-50 (**E**), αEro1α at 1-200 (**F**), αPDI at 1-400 (**G**), αBiP at 1-40 (**H**), αERp72 at 1-1000 (**I**) and αERp57 at 1-800 (**J**) dilutions prior to detection with DAB and photographed at 5X (**A**) and 20X magnification (**B-J**). Carcinoma tissue is indicated with a double headed arrow and neoplastic glands are indicated with an arrow. Ero1β, Ero1α, and the ER chaperone proteins are all expressed in the tumour tissue at varying levels, expect for BiP, which shows negative staining; bar = 200 μm.

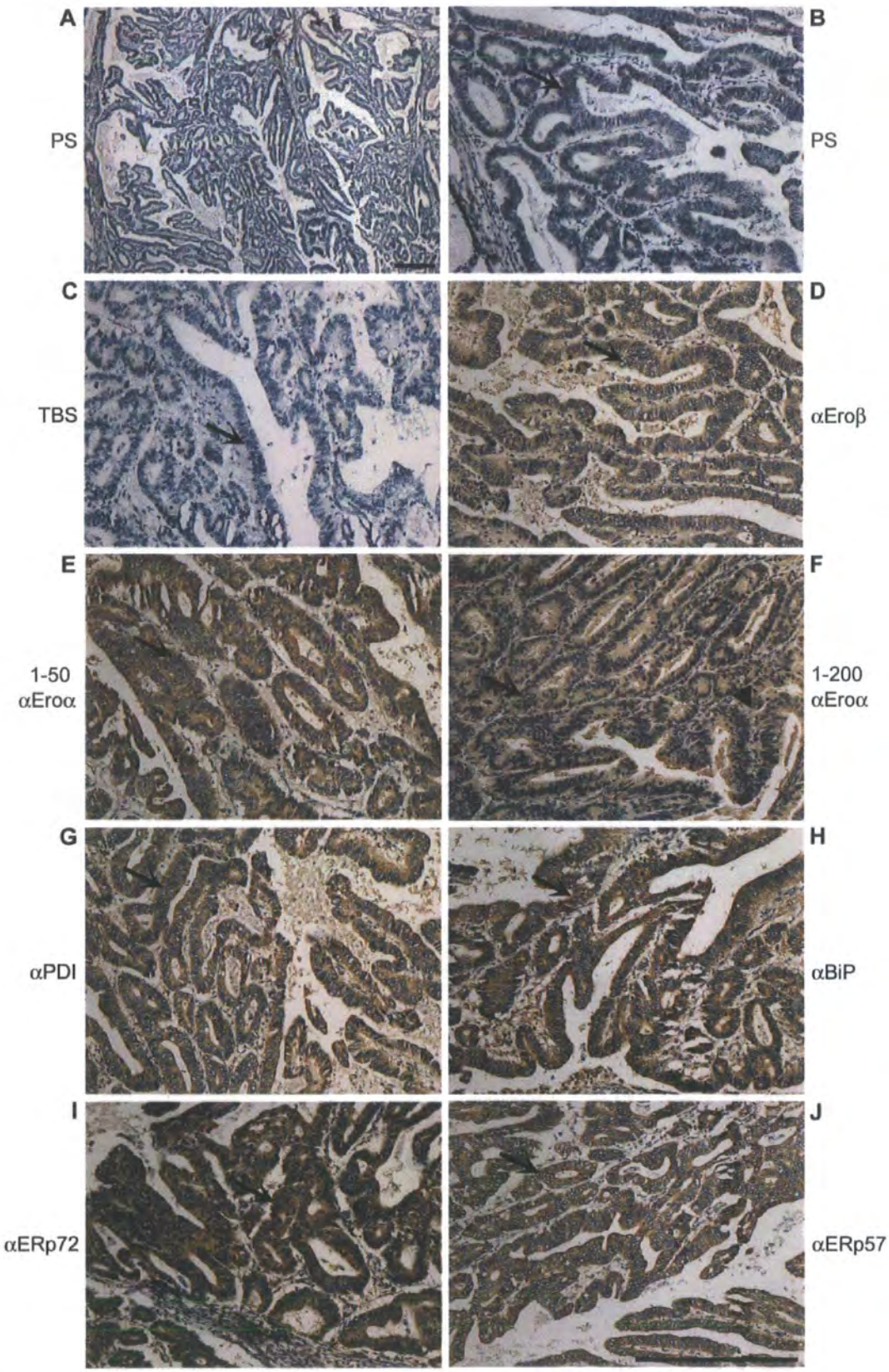

FIGURE 6.16: Strong expression of hEROs and chaperone proteins in Gastric tumour (6591-01 C4)

FIGURE 6.16: Strong expression of hEROs and chaperone proteins in Gastric tumour (6591-01 C4)

Paraffin embedded human oesophageal tumour sections were cleared through histoclear, taken through a 100 – 70% alcohol series and endogenous peroxidase activity blocked in H_2O_2. Prior to incubating with primary antibody sections were digested in a water bath with citrate buffer according to section 2.2.2 (**A-J**) and incubated with pre-immune serum (PS, **A** and **B**), TBS (**C**), αEroβ at 1-150 (**D**), αEro1α at 1-50 (**E**), αEro1α at 1-200 (**F**), αPDI at 1-400 (**G**), αBiP at 1-40 (**H**), αERp72 at 1-1000 (**I**) and αERp57 at 1-800 (**J**) dilutions prior to detection with DAB and photographed at 5X (**A**) and 20X magnification (**B-J**). Neoplastic glands are indicated with an arrow. Bar = 200 μm.

Table 6.4: Expression of hEROs and ER chaperone proteins in patient tissue sections

	Healthy oesophagus	**Barrett's oesophagus**	**Oesophageal tumour (dysplastic and adenocarcinoma)**	**OG junction tumour**	**Gastro Tumour**
Ero1β	very weak	Not detected	strong	strong	strong
Ero1α	strong in mature epithelium cells	strong	strong	strong	strong
PDI	stronger than Ero1β	strong	strong	strong	strong
BiP	very weak	weak	weak	Not detected	strong
ERp72	strong	strong	strong	strong	strong
ERp57	Not detected	Not detected	strong	strong	strong

6.3 Discussion

The expression patterns of Ero1β, Ero1α and several ER chaperone proteins were studied in this chapter. Prior to this study it was known that Ero1β can be induced by UPR and that at the mRNA level it is highly expressed in secretory tissues (Pagani et al., 2000). Nothing was known about the protein expression of Ero1β in these tissues. The Ero1β expression pattern was first studied in pancreatic tissue, which showed that it was present in both endocrine and exocrine cells, but with stronger expression in endocrine tissue. However, the low level of PDI expression in the islets suggests that perhaps PDI might not be the sole electron donor for Ero1β in the pancreas. The pancreas specific PDI homologue PDIp, can use hydroxyl groups as ligands (Klappa et al., 2001) and in theory could replace PDI function in the islets. However, PDIp is only expressed strongly in acinar cells (Desilva et al., 1997). ERp57 and ERp72 are both expressed strongly in the islet cells, and could be alternative electron donors. Specific interactions between Ero1β and ERp57 have not so far been detected in transfected HeLa cells under pulse-chase conditions but further analysis in pancreatic tissue could shed light on possible endogenous Ero1β interactions with ERp57. An interaction between Ero1β and ERp72 was shown in transfected HeLa cells in Chapter 5 (section 5.3.2), and therefore ERp72 could be a potential electron donor in the pancreas. Human Quiescin-sulphydryl oxidase 1 (QSOX1) has also been reported (using immunohistochemistry) to be highly expressed in the islets of Langerhans compared with weak expression in acinar cells (Thorpe et al., 2002). Quiescin-sulphydryl oxidases (QSOX) are flavin-dependent enzymes that catalyse the formation of disulfide bonds in proteins and peptides with the net production of hydrogen peroxide from oxygen. More recently using in situ hybridisation (ISH) and immunohistochemistry

(IHC), Tury and colleagues have shown that the rat quiescin-sulphydryl oxidase (rQSOX) is mostly expressed in α-cells of the islets compared to very weak expression in β-cells (Tury et al., 2006). Since the main secreted protein in α-cells is the non-disulfide containing hormone glucagon, a potential substrate for rQSOX still needs to be discovered from these cells (Tury et al., 2006). This contrast in expression of QSOX proteins from human and rat pancreatic tissue will no doubt need further investigation. Although Ero1β antibody shows similar staining to the insulin antibody (H-86) indicating expression in β-cells, a true functional relationship between Ero, PDI and QSOX proteins has yet to be determined *in vivo*. Ero1α and ERp44 expression could not be detected in the pancreatic tissue.

Having seen Ero1β and PDIp both expressed in pancreatic acinar cells, it was interesting to detect an interaction *in vivo* (Figure 6.5). What this interaction means in terms of functionality in the pancreas remains unclear. The finding that a tryptophan or tyrosine residue is sufficient to allow PDIp recognition of a peptide/protein (Ruddock et al., 2000), probably via the hydroxyl group, suggests that different members of the PDI family might be able to recognise the same unfolded protein but at different exposed amino acid residues (Klappa et al., 2001). Thus Ero1β might be involved in electron transfer with both PDI and PDIp. Reconstituting oxidative protein folding *in vitro* (Tu et al., 2000), using purified PDIp and Ero to monitor refolding of RNAse A could be used to see whether PDIp and Eros are involved in a disulfide bond formation pathway. Although the data suggests that PDIp preferentially binds to Ero1β, due the very low level of Ero1α detected from pancreatic tissue (by western blotting and immunohistochemistry), it wasn't surprising that an interaction couldn't be detected between PDIp and Ero1α. For more conclusive evidence of a specific interaction

between the hEROs and PDIp, one possible strategy would be the use of *in vitro* translation. Co-translating both PDIp and Ero1β or to PDIp and Ero1α would provide direct evidence of an interaction.

In the stomach, Ero1β and the ER chaperone proteins (PDI, ERp57, ERp72 and ERp44) showed cell specific expression, with strong expression detected in enzyme producing chief cells. Ero1α was also expressed very weakly in the chief cells. Although the Ero1α antibody (D5) concentrations used in pancreas and stomach tissue (1:1000) stainings were relatively low when compared to Ero1β antibody concentrations (1:150), these concentrations were based on previous work in the lab in which Ero1α protein could be detected in other tissues. In addition, using a series of Ero1α antibody (D5) concentrations to study the expression in normal oesophagus tissue (Figure 6.9) suggests that concentrations as low as 1:800 are still sufficient to detect a specific expression pattern. Ero1β shows tissue-specific (at the mRNA level and at the protein level; Figure 3.5) as well as cell-specific expression within stomach and pancreas tissue. The implication of having high levels of Ero1β expression will be discussed in Chapter 7.

In normal oesophagus, Ero1α protein expression was higher than for Ero1β, which complements the mRNA data (Pagani et al., 2000). Ero1α however, was expressed in the more mature epithelial cells, an expression pattern that was not detected with other chaperone proteins. Ero1α expression remained strong in Barrett's epithelium and oesophageal tumour, whereas Ero1β expression seemed to get switched on in dysplastic and adenocarcinoma tissue. Although PDI and ERp72 expression remained relatively high throughout these different stages, ERp57 shows dramatic up regulation

in the oesophageal tumour tissue. This up regulation in Ero1β and ERp57 protein levels could be necessary to cope with the increase in unfolded proteins in rapidly dividing neoplastic cells. Further implications of ERp57 up regulation are discussed in Chapter 7. Patients with Barrett's oesophagus have a 30 to 40 fold increased risk of developing adenocarcinoma (Kumar et al., 1997) but not all patients with Barrett's will develop cancer. Finding suitable markers that could be used to discriminate between Barrett's and dysplastic epithelium would be very useful to predict cancer onset and to prevent unnecessary surgery.

CHAPTER 7

DISCUSSION

The present study focused on characterising the expression and interactions of the human endoplasmic reticulum oxidoreductase Ero1β. The results presented in this work lead to the following main conclusions:

a) Ero1β is able to homodimerise and heterodimerise with Ero1α. The redox active 396 cysteine at the C-terminal C*XX*C*XX*C motif was identified as important for Ero1β homodimer formation.

b) When temperature and reducing stress (DTT) conditions were encountered, the FAD binding domain mutations (G252S and H254Y) resulted in misoxidation of Ero1β.

c) Ero1β was expressed in the endocrine and exocrine tissue of the pancreas as well as in the enzyme producing chief cells of the stomach.

d) In the oesophagus, ERp57 displayed differential expression in healthy, Barrett's and oesophageal tumour tissue.

7.1 Importance of Ero1β homodimer formation

Results from this study reveal that the mammalian homologues of Ero1p, Ero1α and Ero1β, are able to form homodimers when expressed in human cell lines (section 3.2.3), which suggests the possibility of intermolecular electron transfer. Intramolecular electron transfer between an Ero N-terminus and C-terminus active site cysteine pair was first suggested by Frand and Kaiser using a panel of yeast Ero1p cysteine mutants (Frand & Kaiser, 1999). This was later supported by evidence from the Ero1p crystal

structure which showed that the C100/C105 was on a flexible loop that could undergo conformational change to be positioned within disulfide bond formation distance from the C353/C355 (Gross et al., 2004). A recent study with Ero1p has provided evidence for intermolecular electron transfer (Sevier & Kaiser, 2006b). Sevier and Kaiser made use of two mutant forms of Ero1p (one with the amino-terminus of Ero1p containing the C100/C105 pair, second with full length Ero1p containing only the C353/C355 pair) which, when expressed independently, were unable to complement *ero1-1* cells at 37°C. However, when co-expressed these two mutant Ero proteins were able to complement *ero1-1*, restoring viability and partially restoring oxidative folding of carboxypeptidase (CPY). Inter-domain disulfide bonds were also detected *in vivo* when expressed in ero1Δ cells (Sevier & Kaiser, 2006b). Taken together their results show that electron transfer can occur between two Ero proteins.

Mutating cysteine 396 (C*XX*C*XX*A, equivalent to C355 in Ero1p) prevents homodimer formation. The disruption of dimers is probably due to loss of FAD at the dimer interface upon loss of the coordinating C396 residue. However, for the formation of a functional dimer the C393/C396 pair (which is buried within the Ero1β monomer, Figure 4.10) must undergo substantial conformational change. The recent mutational analysis of Ero1p by Sevier and Kaiser did show that the C353/C355 (equivalent to C393/C396 pair in Ero1β) pair is capable of undergoing structural changes to allow direct oxidation of substrates (Sevier & Kaiser, 2006b), indicating that this cysteine pair could be involved in electron transfer even within an Ero dimer.

Possible dimer complexes were also detected *in vivo* using gel filtration studies (section 3.2.4). Complexes other than Ero1β-PDI were detected from mouse stomach and

pancreas tissue some of which were likely to be dimers when compared with the molecular weights of the standards. However, to conclusively prove the existence of dimers *in vivo*, one method would be the use of mass spectrometry following gel filtration from mouse tissue. Availability of an immunoprecipitating Ero1β antibody could also allow identification of complexes by mass spectrometry. Depletion of PDI from mouse tissue lysates (similar to Figure 3.8) could also be used as an alternative method to identify non Ero-PDI complexes *in vivo*. This method would require an Ero1β antibody capable of recognising higher molecular weight complexes under non-reducing SDS-PAGE, conditions under which the Ero1β antibody used in this study failed to recognise these complexes (Figure 3.4).

The general view is for the existence of a linear Ero-PDI-substrate oxidation chain (Tu et al., 2000; Tu & Weissman, 2002) which makes the transfer of electrons between two Ero molecules seem unlikely at first. However, it has not been shown that the Ero-PDI heterodimer can exclusively and directly mediate oxidative protein folding. Although experiments by Sevier and Kaiser have not directly proven that Ero1p forms dimers which are enzymatically active (Sevier & Kaiser, 2006b), work from this study (Chapters 3 & 4) taken together with data from Sevier and Kaiser (Sevier & Kaiser, 2006b) and Pagani and colleagues (discussed in 4.3; (Pagani et al., 2001)), suggest that Ero-Ero molecules could exchange electrons and maybe form PDI-Ero-Ero-PDI tetramers to facilitate efficient oxidative folding in the ER. An alternative function of Ero dimers could be in the storage of oxidizing equivalents in tissues with a high demand for secretory proteins, thereby allowing the rapid mobilization of disulfide bond donors. However, this function seems unlikely for Ero1β (although possible for Ero1p) which is a UPR induced protein (Pagani et al., 2000), and a cell might not

switch on expression of a protein only to be stored in an inactive form. It will be of interest to find out the behavior of Ero dimers under UPR and hypoxic conditions.

The equilibrium between dimeric and PDI bound forms of Ero could be used to regulate oxidoreductase activity through occupation/protection of the active site. In this respect, over-expression of the C396A mutant unable to dimerise might be informative as it might lead to oxidative stress when compared with the C390A mutant which is able to dimerise but unable to bind PDI.

7.2 FAD binding domain mutants

The yeast *ero1-1* (with a G229S mutation in Ero1p) and *ero1-2* (with a H231Y mutation in Ero1p) mutants caused temperature sensitivity and DTT hyper-sensitivity phenotypes respectively. These FAD binding domain mutations were studied in Ero1β (G252S and H254Y, Chapter 5) which showed that the corrupted FAD binding domain destabilises the Ero1β protein when subjected to reducing and temperature stress (section 5.2.7 and 5.2.8). Although an increase in temperature is unlikely to occur within mammalian cells under normal physiological conditions, a more reducing environment might be mimicked during an UPR response and be more physiologically relevant. It would also be interesting to observe whether FAD mutants in Ero1α misoxidise during hypoxia.

It is possible that these two mutants no longer bind FAD. In the yeast Ero1p crystal structure, the H231 (equivalent to H254 in Ero1β) residue is in contact (within hydrogen bonding distance) with the AMP phosphate of FAD thus the mutation to tyrosine could lead to unstable binding of FAD. The G229 (equivalent to G252 in

Ero1β) residue is, however, not in contact with FAD, and so the mutation to serine might lead to local conformational changes leading to loss of FAD binding. To address how the FAD binding domain is able to stabilise this protein under stress conditions requires expression of the recombinant proteins and subsequent crystallisation to study the structure of these mutant proteins.

Purified wild type Ero1β as well as mutant Ero1β proteins will be useful in oxidative folding assays to determine the importance of active site cysteines and FAD binding domain residues in Ero1β function and also to identify potential target substrates. Attempts to purify wild-type Ero1β from transfected human cells using FAD affinity chromatography failed (data not shown), indicating that the co-factor was tightly bound and may-not exchange with external FAD (Gross et al., 2004). Wild-type Ero1β could be purified from mouse stomach or pancreas tissue, however purification from these organs will be difficult due to the presence of high concentrations of proteolytic enzymes. Alternatively insect expression systems could be used to express and purify glycosylated wild-type and mutant Ero1β protein.

In yeast, both Ero1p and Erv2p are membrane associated flavoproteins able to directly oxidise PDI and catalyse disulfide bond formation. However unlike Erv2p, Ero1p does not have a hydrophobic channel that can enable molecular oxygen access to the active site FAD (Gross et al., 2004; Gross et al., 2002). Therefore the final steps of electron transfer involving Ero proteins are yet to be determined.

7.3 *Ero1β and ERp57 in stomach and pancreas*

At the transcriptional level, Ero1β mRNA is induced during the course of an unfolded protein response (Pagani et al., 2000). Thus up-regulation of Ero1β protein levels would not be expected under normal protein folding conditions *in vivo*. However, healthy stomach and pancreas tissue had very high relative expression levels of Ero1β in chief cells and islets (section 6.2.1.2 and 6.2.3.2). This indicates that although Ero1β is physiologically required in cells with a high secretory demand it may-not solely function as an UPR responsive gene.

High constitutive expression of Ero1β in tissues is surprising because this could lead to production of high levels of reactive oxygen species (ROS) ultimately leading to oxidative stress. Maybe Ero1β dimers play a role in keeping reactive cysteines away from non-target proteins which would prevent an unregulated increase in ROS. Other disulfide oxidoreductases are also highly co-expressed with Ero1β. Perhaps, the reason for high level of ERp57 expression in the pancreatic islets (Figure 6.4) and in stomach chief cells (Figure 6.7) would be to help refold glycoproteins as part of its reductive/isomerase pathway (Jessop & Bulleid, 2004) together with the calnexin/calreticulin cycle (discussed in section 1.4.1).

Ero1β has not been detected in the pancreatic cell line PANC1, which is surprising if Ero1β levels are constitutively 'switched on' in the pancreatic tissue. However, this cell line is epithelial in nature, thus not actively producing enzymes. It might be that Ero1β expression *in vivo* is regulated by many factors including the nutritional status and the demand for protein secretion at a given time, which are unlikely to affect cells in culture. These cell lines could be treated with UPR-inducing agents (DTT,

tunicamycin) to determine whether Ero1β expression would get induced. However, it is becoming clear that the physiological UPR is different from UPR induced by chemical reagents. It should be noted that immunohistochemistry is not a quantitative technique and so to measure the levels of Ero1β more accurately, mouse pancreatic tissue samples from islet and acinar cells (isolated by laser-capture microdissection) could be used to compare Ero1β and ER chaperone protein expression levels using western blotting and RT-PCR. The pancreatic tissue used in this study was from a healthy individual, but the level of Ero1β expression might also be different between healthy and diseased individuals. A larger scale study to establish the relative levels of Ero1β expression in normal and type 2 diabetic individuals would be interesting, given the recent link between diabetes and UPR (Ozcan et al., 2004).

7.4 ERp57 expression in oesophagus

ERp57 is up-regulated in oesophageal tumour (Figures 6.13 and 6.14), OG junction tumour (Figure 6.15) and gastric tumour (Figure 6.16) compared with the healthy oesophagus and pre-cancerous stage (Figures 6.10, 6.12). Why would ERp57 show dramatic up-regulation in tumour tissue? Tumours require a constant supply of nutrients and oxygen to aid in cell division and rapid growth and would also benefit from secretion of growth factors. ERp57 might be required for the proper folding and secretion of growth factors to keep up with the demands of tumour cell proliferation. These initial studies indicate that ERp57 expression gets 'switched on' between the Barrett's and dysplastic tissue. To confirm the exact point of ERp57 up-regulation would require the use of different stages of dysplastic tissue, from low-grade to high-grade dysplasia.

Although similar results were observed from duplicate patient tissues, these results are initial observations and thus need further investigation. The different stages from normal oesophagus to oesophageal tumour tissue studied in Chapter 6 were obtained from different individuals, thus making a direct comparison of the protein expression within one individual more difficult. A biopsy taken from a patient with for example Barrett's or adenocarcinoma could have areas/patches of different stages of the tumour (similar to tissue block 1039-03 B2 which was used to look at dysplastic and adenocarcinoma tissue) as well as healthy tissue. These biopsies would provide a better platform for studying how protein expression alters (using immunohistochemistry and western blotting) in individuals and to study variations between different individuals. Studying the expression patterns of a range of oxidoreductase proteins (for example ERp57 and ERp72, which is strongly expressed throughout the stages studied) might provide a basis for defining a grading system for the progression to cancer; i.e. from healthy, Barrett's, low-grade dysplasia and high-grade dysplasia to invasive adenocarcinoma. Studying the mRNA expression patterns from biopsy samples of these different stages (using RT-PCR) would provide further quantitative evidence to support the immunohistochemistry data.

Expression profiling has been reported for normal oesophageal epithelium, premalignant Barrett's metaplasia, and oesophageal adenocarcinoma samples from eight patients (http://www.ncbi.nlm.nih.gov/projects/geo/). Here, the general mRNA expression pattern for ERp57 is found to be up-regulated in adenocarcinoma tissue. However, there is a noticeable variation in expression between the different patients. It would be very interesting to relate the gene expression profiles with the protein expression patterns to better understand how Erp57 is regulated and at what stage. The

possibility of using expression of ER chaperone proteins as a potential marker for oesophageal tumour looks promising.

In conclusion the present thesis has comprehensively detailed the biosynthesis, oxidation and expression of Ero1β and its C*XX*C*XX*C and FAD binding domain mutants. Several novel interactions namely Ero dimers and complexes with ERp72 and PDIp have been identified *in vivo* and in transfectants. The expression pattern of Ero1β and several ER chaperone proteins have also been thoroughly characterised in the digestive system for the first time.

REFERENCES

Aguzzi, A., Heikenwalder, M., and Miele, G. (2004). Progress and problems in the biology, diagnostics, and therapeutics of prion diseases. *J Clin Invest* **114**, 153-160.

Alanen, H. I., Williamson, R. A., Howard, M. J., Hatahet, F. S., Salo, K. E., Kauppila, A., Kellokumpu, S., and Ruddock, L. W. (2006). ERP27, a new non-catalytic endoplasmic reticulum located human pdi-family member, interacts with ERP57. *J Biol Chem*, M604314200.

Alanen, H. I., Williamson, R. A., Howard, M. J., Lappi, A.-K., Jantti, H. P., Rautio, S. M., Kellokumpu, S., and Ruddock, L. W. (2003). Functional Characterization of ERp18, a New Endoplasmic Reticulum-located Thioredoxin Superfamily Member. *J Biol Chem* **278**, 28912-28920.

Andersen, C. L., Matthey-Dupraz, A., Missiakas, D., and Raina, S. (1997). A new Escherichia coli gene, dsbG, encodes a periplasmic protein involved in disulphide bond formation, required for recycling DsbA/DsbB and DsbC redox proteins. *Mol Microbiol* **26**, 121-132.

Andersson, H., and Garoff, H. (2003). Lectin-mediated retention of p62 facilitates p62-E1 heterodimerization in endoplasmic reticulum of Semliki Forest virus-infected cells. *J Virol* **77**, 6676-6682.

Anelli, T., Alessio, M., Bachi, A., Bergamelli, L., Bertoli, G., Camerini, S., Mezghrani, A., Ruffato, E., Simmen, T., and Sitia, R. (2003). Thiol-mediated protein retention in the endoplasmic reticulum: the role of ERp44. *EMBO J* **22**, 5015-5022.

Anelli, T., Alessio, M., Mezghrani, A., Simmen, T., Talamo, F., Bachi, A., and Sitia, R. (2002). ERp44, a novel endoplasmic reticulum folding assistant of the thioredoxin family. *EMBO J* **21**, 835-844.

Anfinsen, C. B., Haber, E., Sela, M., and White, F. H., Jr. (1961). The kinetics of formation of native ribonuclease during oxidation of the reduced polypeptide chain. *Proc Natl Acad Sci U S A* **47**, 1309-1314.

Apweiler, R., Hermjakob, H., and Sharon, N. (1999). On the frequency of protein glycosylation, as deduced from analysis of the SWISS-PROT database. *Biochim Biophys Acta* **1473**, 4-8.

Ashby, M. C., and Tepikin, A. V. (2001). ER calcium and the functions of intracellular organelles. *Semin Cell Dev Biol* **12**, 11-17.

Aslund, F., Berndt, K. D., and Holmgren, A. (1997). Redox potentials of glutaredoxins and other thiol-disulfide oxidoreductases of the thioredoxin superfamily determined by direct protein-protein redox equilibria. *J Biol Chem* **272**, 30780-30786.

Bader, M. W., Hiniker, A., Regeimbal, J., Goldstone, D., Haebel, P. W., Riemer, J., Metcalf, P., and Bardwell, J. C. (2001). Turning a disulfide isomerase into an oxidase: DsbC mutants that imitate DsbA. *EMBO J* **20**, 1555-1562.

Bakke, O., and Dobberstein, B. (1990). MHC class II-associated invariant chain contains a sorting signal for endosomal compartments. *Cell* **63**, 707-716.

Bardwell, J. C., Lee, J. O., Jander, G., Martin, N., Belin, D., and Beckwith, J. (1993). A pathway for disulfide bond formation in vivo. *Proc Natl Acad Sci U S A* **90**, 1038-1042.

Bardwell, J. C., McGovern, K., and Beckwith, J. (1991). Identification of a protein required for disulfide bond formation in vivo. *Cell* **67**, 581-589.

Bass, R., Ruddock, L. W., Klappa, P., and Freedman, R. B. (2004). A major fraction of endoplasmic reticulum-located glutathione is present as mixed disulfides with protein. *J Biol Chem* **279**, 5257-5262.

Benham, A. M., Cabibbo, A., Fassio, A., Bulleid, N., Sitia, R., and Braakman, I. (2000). The CXXCXXC motif determines the folding, structure and stability of human Ero1-Lalpha. *EMBO J* **19**, 4493-4502.

Bergman, L. W., and Kuehl, W. M. (1979a). Formation of an intrachain disulfide bond on nascent immunoglobulin light chains. *J Biol Chem* **254**, 8869-8876.

Bergman, L. W., and Kuehl, W. M. (1979b). Formation of intermolecular disulfide bonds on nascent immunoglobulin polypeptides. *J Biol Chem.* **254**, 5690-5694.

Berridge, M., Lipp, P., and Bootman, M. (1999). Calcium signalling. *Curr Biol* **9**, R157-159.

Bertoli, G., Simmen, T., Anelli, T., Molteni, S. N., Fesce, R., and Sitia, R. (2004). Two conserved cysteine triads in human Ero1alpha cooperate for efficient disulfide bond formation in the endoplasmic reticulum. *J Biol Chem* **279**, 30047-30052.

Bessette, P. H., Cotto, J. J., Gilbert, H. F., and Georgiou, G. (1999). In vivo and in vitro function of the Escherichia coli periplasmic cysteine oxidoreductase DsbG. *J Biol Chem* **274**, 7784-7792.

Bohni, P. C., Deshaies, R. J., and Schekman, R. W. (1988). SEC11 is required for signal peptide processing and yeast cell growth. *J Cell Biol* **106**, 1035-1042.

Bottomley, M. J., Batten, M. R., Lumb, R. A., and Bulleid, N. J. (2001). Quality control in the endoplasmic reticulum: PDI mediates the ER retention of unassembled procollagen C-propeptides. *Curr Biol* **11**, 1114-1118.

Braakman, I., Helenius, J., and Helenius, A. (1992). Manipulating disulfide bond formation and protein folding in the endoplasmic reticulum. *EMBO J* **11**, 1717-1722.

Braakman, I., Hoover-Litty, H., Wagner, K., and Helenius, A. (1991). Folding of influenza hemagglutinin in the endoplasmic reticulum. *J Cell Biol* **114**, 401-411.

Brange, J., and Langkjoer, L. (1993). Insulin structure and stability. *Pharm Biotechnol* **5**, 315-350.

Braud, V. M., Allan, D. S., O'Callaghan, C. A., Soderstrom, K., D'Andrea, A., Ogg, G. S., Lazetic, S., Young, N. T., Bell, J. I., Phillips, J. H., Lanier, L. L., and McMichael, A. J. (1998). HLA-E binds to natural killer cell receptors CD94/NKG2A, B and C. *Nature* **391**, 795-799.

Breyton, C., Haase, W., Rapoport, T. A., Kuhlbrandt, W., and Collinson, I. (2002). Three-dimensional structure of the bacterial protein-translocation complex SecYEG. *Nature* **418**, 662-665.

Brooks, D. A. (1997). Protein processing: a role in the pathophysiology of genetic disease. *FEBS Lett* **409**, 115-120.

Brundage, L., Hendrick, J. P., Schiebel, E., Driessen, A. J., and Wickner, W. (1990). The purified E. coli integral membrane protein SecY/E is sufficient for reconstitution of SecA-dependent precursor protein translocation. *Cell* **62**, 649-657.

Cabibbo, A., Pagani, M., Fabbri, M., Rocchi, M., Farmery, M. R., Bulleid, N. J., and Sitia, R. (2000). ERO1-L, a human protein that favors disulfide bond formation in

the endoplasmic reticulum. *J Biol Chem* **275**, 4827-4833.

Camacho, P., and Lechleiter, J. D. (1993). Increased frequency of calcium waves in Xenopus laevis oocytes that express a calcium-ATPase. *Science* **260**, 226-229.

Cannon, K. S., and Cresswell, P. (2001). Quality control of transmembrane domain assembly in the tetraspanin CD82. *EMBO J* **20**, 2443-2453.

Caramelo, J. J., Castro, O. A., Alonso, L. G., de Prat-Gay, G., and Parodi, A. J. (2003). Inaugural Article: UDP-Glc:glycoprotein glucosyltransferase recognizes structured and solvent accessible hydrophobic patches in molten globule-like folding intermediates. *Proc Natl Acad Sci U S A* **100**, 86-91.

Chakravarthi, S., and Bulleid, N. J. (2004). Glutathione is required to regulate the formation of native disulfide bonds within proteins entering the secretory pathway. *J Biol Chem* **279**, 39872-39879.

Chakravarthi, S., Jessop, C. E., and Bulleid, N. J. (2006). The role of glutathione in disulphide bond formation and endoplasmic-reticulum-generated oxidative stress. *EMBO Rep* **7**, 271-275.

Chen, J., Song, J. L., Zhang, S., Wang, Y., Cui, D. F., and Wang, C. C. (1999). Chaperone activity of DsbC. *J Biol Chem* **274**, 19601-19605.

Coleman, S. T., Epping, E. A., Steggerda, S. M., and Moye-Rowley, W. S. (1999). Yap1p Activates Gene Transcription in an Oxidant-Specific Fashion. *Mol Cell Biol* **19**, 8302-8313.

Collet, J.-F., and Bardwell, J. C. A. (2002). Oxidative protein folding in bacteria. *Molecular Microbiology* **44**, 1-8.

Cotterill, S. L., Jackson, G. C., Leighton, M. P., Wagener, R., Makitie, O., Cole, W. G., and Briggs, M. D. (2005). Multiple epiphyseal dysplasia mutations in MATN3 cause misfolding of the A-domain and prevent secretion of mutant matrilin-3. *Hum Mutat* **26**, 557-565.

Cresswell, P., Bangia, N., Dick, T., and Diedrich, G. (1999). The nature of the MHC class I peptide loading complex. *Immunol Rev* **172**, 21-28.

Crowley, K. S., Liao, S., Worrell, V. E., Reinhart, G. D., and Johnson, A. E. (1994). Secretory proteins move through the endoplasmic reticulum membrane via an aqueous, gated pore. *Cell* **78**, 461-471.

Cumming, R. C., Andon, N. L., Haynes, P. A., Park, M., Fischer, W. H., and Schubert, D. (2004). Protein Disulfide Bond Formation in the Cytoplasm during Oxidative Stress. *J Biol Chem* **279**, 21749-21758.

Cunnea, P. M., Miranda-Vizuete, A., Bertoli, G., Simmen, T., Damdimopoulos, A. E., Hermann, S., Leinonen, S., Huikko, M. P., Gustafsson, J.-A., Sitia, R., and Spyrou, G. (2003). ERdj5, an Endoplasmic Reticulum (ER)-resident Protein Containing DnaJ and Thioredoxin Domains, Is Expressed in Secretory Cells or following ER Stress. *J Biol Chem* **278**, 1059-1066.

D'Andrea, P., and Vittur, F. (1995). Spatial and temporal Ca2+ signalling in articular chondrocytes. *Biochem Biophys Res Commun* **215**, 129-135.

Daniels, R., Kurowski, B., Johnson, A. E., and Hebert, D. N. (2003). N-linked glycans direct the cotranslational folding pathway of influenza hemagglutinin. *Mol Cell* **11**, 79-90.

Danilczyk, U. G., and Williams, D. B. (2001). The Lectin Chaperone Calnexin Utilizes Polypeptide-based Interactions to Associate with Many of Its Substrates in Vivo. *J Biol Chem* **276**, 25532-25540.

Darby, N. J., Kemmink, J., and Creighton, T. E. (1996). Identifying and characterizing a structural domain of protein disulfide isomerase. *Biochemistry* **35**, 10517-10528.

Darby, N. J., Penka, E., and Vincentelli, R. (1998). The multi-domain structure of protein disulfide isomerase is essential for high catalytic efficiency. *J Mol Biol* **276**, 239-247.

David, V., Hochstenbach, F., Rajagopalan, S., and Brenner, M. (1993). Interaction with newly synthesized and retained proteins in the endoplasmic reticulum suggests a chaperone function for human integral membrane protein IP90 (calnexin). *J Biol Chem* **268**, 9585-9592.

Deprez, P., Gautschi, M., and Helenius, A. (2005). More than one glycan is needed for ER glucosidase II to allow entry of glycoproteins into the calnexin/calreticulin cycle. *Mol Cell* **19**, 183-195.

Desilva, M. G., Notkins, A. L., and Lan, M. S. (1997). Molecular characterization of a pancreas-specific protein disulfide isomerase, PDIp. *DNA Cell Biol* **16**, 269-274.

Dias-Gunasekara, S., and Benham, A. M. (2005). Defining the protein-protein interactions of the mammalian endoplasmic reticulum oxidoreductases (EROs). *Biochem Soc Trans* **33**, 1382-1384.

Dick, T. P., Bangia, N., Peaper, D. R., and Cresswell, P. (2002). Disulfide bond isomerization and the assembly of MHC class I-peptide complexes. *Immunity* **16**, 87-98.

Dixon, D. P., Van Lith, M., Edwards, R., and Benham, A. (2003). Cloning and initial characterization of the Arabidopsis thaliana endoplasmic reticulum oxidoreductins. *Antioxid Redox Signal* **5**, 389-396.

Egea, P. F., Stroud, R. M., and Walter, P. (2005). Targeting proteins to membranes: structure of the signal recognition particle. *Curr Opin Struct Biol* **15**, 213-220.

Ellgaard, L., and Helenius, A. (2003). Quality control in the endoplasmic reticulum. *Nat Rev Mol Cell Biol* **4**, 181-191.

Ellgaard, L., and Ruddock, L. W. (2005). The human protein disulphide isomerase family: substrate interactions and functional properties. *EMBO Rep* **6**, 28-32.

Ellgaard, L., Molinari, M., and Helenius, A. (1999). Setting the standards: quality control in the secretory pathway. *Science* **286**, 1882-1888.

Ellgaard, L., Riek, R., Herrmann, T., Guntert, P., Braun, D., Helenius, A., and Wuthrich, K. (2001). NMR structure of the calreticulin P-domain. *Proc Natl Acad Sci U S A* **98**, 3133-3138.

Ellis, C. D., Macdiarmid, C. W., and Eide, D. J. (2005). Heteromeric protein complexes mediate zinc transport into the secretory pathway of eukaryotic cells. *J Biol Chem* **280**, 28811-28818.

Ellis, C. D., Wang, F., MacDiarmid, C. W., Clark, S., Lyons, T., and Eide, D. J. (2004). Zinc and the Msc2 zinc transporter protein are required for endoplasmic reticulum function. *J Cell Biol* **166**, 325-335.

Evans, E. A., Gilmore, R., and Blobel, G. (1986). Purification of microsomal signal peptidase as a complex. *Proc Natl Acad Sci U S A* **83**, 581-585.

Falcke, M., Li, Y., Lechleiter, J. D., and Camacho, P. (2003). Modeling the dependence of the period of intracellular Ca2+ waves on SERCA expression. *Biophys J* **85**, 1474-1481.

Farquhar, R., Honey, N., Murant, S. J., Bossier, P., Schultz, L., Montgomery, D., Ellis, R. W., Freedman, R. B., and Tuite, M. F. (1991). Protein disulfide

isomerase is essential for viability in Saccharomyces cerevisiae. *Gene* **108**, 81-89.

Fassio, A., and Sitia, R. (2002). Formation, isomerisation and reduction of disulphide bonds during protein quality control in the endoplasmic reticulum. *Histochem Cell Biol* **117**, 151-157.

Fliegel, L., Burns, K., MacLennan, D., Reithmeier, R., and Michalak, M. (1989). Molecular cloning of the high affinity calcium-binding protein (calreticulin) of skeletal muscle sarcoplasmic reticulum. *J Biol Chem* **264**, 21522-21528.

Forster, M. L., Sivick, K., Park, Y. N., Arvan, P., Lencer, W. I., and Tsai, B. (2006). Protein disulfide isomerase-like proteins play opposing roles during retrotranslocation. *J Cell Biol* **173**, 853-859.

Forsythe, J., Jiang, B., Iyer, N., Agani, F., Leung, S., Koos, R., and Semenza, G. (1996). Activation of vascular endothelial growth factor gene transcription by hypoxia-inducible factor 1. *Mol Cell Biol* **16**, 4604-4613.

Fra, A., and Sitia, R. (1993). The endoplasmic reticulum as a site of protein degradation. *Subcell Biochem* **21**, 143-168.

Fraaije, M. W., and Mattevi, A. (2000). Flavoenzymes: diverse catalysts with recurrent features. *Trends Biochem Sci* **25**, 126-132.

Frand, A. R., and Kaiser, C. A. (1998). The ERO1 gene of yeast is required for oxidation of protein dithiols in the endoplasmic reticulum. *Mol Cell* **1**, 161-170.

Frand, A. R., and Kaiser, C. A. (1999). Ero1p oxidizes protein disulfide isomerase in a pathway for disulfide bond formation in the endoplasmic reticulum. *Mol Cell* **4**, 469-477.

Frand, A. R., and Kaiser, C. A. (2000). Two pairs of conserved cysteines are required for the oxidative activity of Ero1p in protein disulfide bond formation in the endoplasmic reticulum. *Mol Biol Cell* **11**, 2833-2843.

Freedman, R. B., Hirst, T. R., and Tuite, M. F. (1994). Protein disulphide isomerase: building bridges in protein folding. *Trends Biochem Sci* **19**, 331-336.

Freedman, R. B., Gane, P. J., Hawkins, H. C., Hlodan, R., McLaughlin, S. H., and Parry, J. W. (1998). Experimental and theoretical analyses of the domain architecture of mammalian protein disulphide-isomerase. *Biol Chem* **379**, 321-328.

Freedman, R. B., Klappa, P., and Ruddock, L. W. (2002). Protein disulfide isomerases exploit synergy between catalytic and specific binding domains. *EMBO Rep* **3**, 136-140.

Frenkel, Z., Gregory, W., Kornfeld, S., and Lederkremer, G. Z. (2003). Endoplasmic reticulum-associated degradation of mammalian glycoproteins involves sugar chain trimming to Man6-5GlcNAc2. *J Biol Chem* **278**, 34119-34124.

Frickel, E. M., Frei, P., Bouvier, M., Stafford, W. F., Helenius, A., Glockshuber, R., and Ellgaard, L. (2004). ERp57 is a multifunctional thiol-disulfide oxidoreductase. *J Biol Chem* **279**, 18277-18287.

Gerber, J., Muhlenhoff, U., Hofhaus, G., Lill, R., and Lisowsky, T. (2001). Yeast ERV2p is the first microsomal FAD-linked sulfhydryl oxidase of the Erv1p/Alrp protein family. *J Biol Chem* **276**, 23486-23491.

Gess, B., Hofbauer, K. H., Wenger, R. H., Lohaus, C., Meyer, H. E., and Kurtz, A. (2003). The cellular oxygen tension regulates expression of the endoplasmic oxidoreductase ERO1-Lalpha. *Eur J Biochem* **270**, 2228-2235.

Gillece, P., Luz, J. M., Lennarz, W. J., de La Cruz, F. J., and Romisch, K. (1999). Export of a cysteine-free misfolded secretory protein from the endoplasmic

reticulum for degradation requires interaction with protein disulfide isomerase. *J Cell Biol* **147**, 1443-1456.

Gilmore, R. (1991). The protein translocation apparatus of the rough endoplasmic reticulum, its associated proteins, and the mechanism of translocation. *Curr Opin Cell Biol* **3**, 580-584.

Goldberger, R. F., Epstein, C. J., and Anfinsen, C. B. (1963). Acceleration of reactivation of reduced bovine pancreatic ribonuclease by a microsomal system from rat liver. *J Biol Chem* **238**, 628-635.

Gonz lez, R., Andrews, B. A., and Asenjo, J. A. (2002). Kinetic model of BiP- and PDI-mediated protein folding and assembly. *J Theor Biol* **214**, 529-537.

Gorlich, D., and Rapoport, T. A. (1993). Protein translocation into proteoliposomes reconstituted from purified components of the endoplasmic reticulum membrane. *Cell* **75**, 615-630.

Gow, A., and Lazzarini, R. A. (1996). A cellular mechanism governing the severity of Pelizaeus-Merzbacher disease. *Nat Genet* **13**, 422-428.

Griffith, O. W., and Meister, A. (1979). Potent and specific inhibition of glutathione synthesis by buthionine sulfoximine (S-n-butyl homocysteine sulfoximine). *J Biol Chem* **254**, 7558-7560.

Gross, E., Kastner, D. B., Kaiser, C. A., and Fass, D. (2004). Structure of Ero1p, source of disulfide bonds for oxidative protein folding in the cell. *Cell* **117**, 601-610.

Gross, E., Sevier, C. S., Heldman, N., Vitu, E., Bentzur, M., Kaiser, C. A., Thorpe, C., and Fass, D. (2006). Generating disulfides enzymatically: reaction products and electron acceptors of the endoplasmic reticulum thiol oxidase Ero1p. *Proc Natl Acad Sci U S A* **103**, 299-304.

Gross, E., Sevier, C. S., Vala, A., Kaiser, C. A., and Fass, D. (2002). A new FAD-binding fold and intersubunit disulfide shuttle in the thiol oxidase Erv2p. *Nat Struct Biol* **9**, 61-67.

Haas, I. G., and Wabl, M. (1983). Immunoglobulin heavy chain binding protein. *Nature* **306**, 387-389.

Halic, M., and Beckmann, R. (2005). The signal recognition particle and its interactions during protein targeting. *Curr Opin Struct Biol* **15**, 116-125.

Hamman, B. D., Hendershot, L. M., and Johnson, A. E. (1998). BiP maintains the permeability barrier of the ER membrane by sealing the lumenal end of the translocon pore before and early in translocation. *Cell* **92**, 747-758.

Hammond, C., and Helenius, A. (1994b). Folding of VSV G protein: sequential interaction with BiP and calnexin. *Science* **266**, 456-458.

Hammond, C., Braakman, I., and Helenius, A. (1994a). Role of N-Linked Oligosaccharide Recognition, Glucose Trimming, and Calnexin in Glycoprotein Folding and Quality Control. *Proc Natl Acad Sci U S A* **91**, 913-917.

Harding, H. P., Zhang, Y., Zeng, H., Novoa, I., Lu, P. D., Calfon, M., Sadri, N., Yun, C., Popko, B., Paules, R., Stojdl, D. F., Bell, J. C., Hettmann, T., Leiden, J. M., and Ron, D. (2003). An integrated stress response regulates amino acid metabolism and resistance to oxidative stress. *Mol Cell* **11**, 619-633.

Haugstetter, J., Blicher, T., and Ellgaard, L. (2005). Identification and Characterization of a Novel Thioredoxin-related Transmembrane Protein of the Endoplasmic Reticulum. *J Biol Chem* **280**, 8371-8380.

Haynes, C. M., Caldwell, S., and Cooper, A. A. (2002). An HRD/DER-independent ER

quality control mechanism involves Rsp5p-dependent ubiquitination and ER-Golgi transport. *J Cell Biol* **158**, 91-102.

Haynes, C. M., Titus, E. A., and Cooper, A. A. (2004). Degradation of misfolded proteins prevents ER-derived oxidative stress and cell death. *Mol Cell* **15**, 767-776.

Hebert, D. N., Garman, S. C., and Molinari, M. (2005). The glycan code of the endoplasmic reticulum: asparagine-linked carbohydrates as protein maturation and quality-control tags. *Trends Cell Biol* **15**, 364-370.

Helenius, A. (1994). How N-linked oligosaccharides affect glycoprotein folding in the endoplasmic reticulum. *Mol Biol Cell* **5**, 253-265.

Helenius, A., and Aebi, M. (2004). Roles of N-linked glycans in the endoplasmic reticulum. *Annu Rev Biochem* **73**, 1019-1049.

Hickman, S., and Kornfeld, S. (1978). Effect of tunicamycin on IgM, IgA, and IgG secretion by mouse plasmacytoma cells. *J Immunol* **121**, 990-996.

Higo, T., Hattori, M., Nakamura, T., Natsume, T., Michikawa, T., and Mikoshiba, K. (2005). Subtype-specific and ER lumenal environment-dependent regulation of inositol 1,4,5-trisphosphate receptor type 1 by ERp44. *Cell* **120**, 85-98.

Hirao, K., Natsuka, Y., Tamura, T., Wada, I., Morito, D., Natsuka, S., Romero, P., Sleno, B., Tremblay, L. O., Herscovics, A., Nagata, K., and Hosokawa, N. (2006). EDEM3, a soluble EDEM homolog, enhances glycoprotein endoplasmic reticulum-associated degradation and mannose trimming. *J Biol Chem* **281**, 9650-9658.

Hong, T., Summers, M. D., and Braunagel, S. C. (1997). N-terminal sequences from Autographa californica nuclear polyhedrosis virus envelope proteins ODV-E66 and ODV-E25 are sufficient to direct reporter proteins to the nuclear envelope, intranuclear microvesicles and the envelope of occlusion derived virus. *Proc Natl Acad Sci U S A* **94**, 4050-4055.

Hosokawa, N., Tremblay, L. O., You, Z., Herscovics, A., Wada, I., and Nagata, K. (2003). Enhancement of endoplasmic reticulum (ER) degradation of misfolded Null Hong Kong alpha1-antitrypsin by human ER mannosidase I. *J Biol Chem* **278**, 26287-26294.

Hosokawa, N., Wada, I., Hasegawa, K., Yorihuzi, T., Tremblay, L. O., Herscovics, A., and Nagata, K. (2001). A novel ER alpha-mannosidase-like protein accelerates ER-associated degradation. *EMBO Rep* **2**, 415-422.

Houry, W. A. (2001). Chaperone-assisted protein folding in the cell cytoplasm. *Curr Protein Pept Sci* **2**, 227-244.

Hwang, C., Sinskey, A. J., and Lodish, H. F. (1992). Oxidized redox state of glutathione in the endoplasmic reticulum. *Science* **257**, 1496-1502.

Ihara, Y., Cohen-Doyle, M. F., Saito, Y., and Williams, D. B. (1999). Calnexin discriminates between protein conformational states and functions as a molecular chaperone in vitro. *Mol Cell* **4**, 331-341.

Ihrke, G., Bruns, J. R., Luzio, J. P., and Weisz, O. A. (2001). Competing sorting signals guide endolyn along a novel route to lysosomes in MDCK cells. *EMBO J* **20**, 6256-6264.

Inoue, K. (2005). PLP1-related inherited dysmyelinating disorders: Pelizaeus-Merzbacher disease and spastic paraplegia type 2. *Neurogenetics* **6**, 1-16.

Isidoro, C., Maggioni, C., Demoz, M., Pizzagalli, A., Fra, A. M., and Sitia, R. (1996).

Exposed thiols confer localization in the endoplasmic reticulum by retention rather than retrieval. *J Biol Chem* **271**, 26138-26142.

Jahn, T. R., and Radford, S. E. (2005). The Yin and Yang of protein folding. *FEBS Journal* **272**, 5962-5970.

Jakob, C. A., Burda, P., Roth, J., and Aebi, M. (1998). Degradation of misfolded endoplasmic reticulum glycoproteins in Saccharomyces cerevisiae is determined by a specific oligosaccharide structure. *J Cell Biol* **142**, 1223-1233.

Jarosch, E., Taxis, C., Volkwein, C., Bordallo, J., Finley, D., Wolf, D. H., and Sommer, T. (2002). Protein dislocation from the ER requires polyubiquitination and the AAA-ATPase Cdc48. *Nat Cell Biol* **4**, 134-139.

Jessop, C. E., and Bulleid, N. J. (2004). Glutathione directly reduces an oxidoreductase in the endoplasmic reticulum of mammalian cells. *J Biol Chem* **279**, 55341-55347.

Johnson, A. E. (2004). Functional ramifications of FRET-detected nascent chain folding far inside the membrane-bound ribosome. *Biochem Soc Trans* **32**, 668-672.

Johnson, A. E., and van Waes, M. A. (1999). The translocon: a dynamic gateway at the ER membrane. *Annu Rev Cell Dev Biol* **15**, 799-842.

Jones, T. R., and Sun, L. (1997). Human cytomegalovirus US2 destabilizes major histocompatibility complex class I heavy chains. *J Virol* **71**, 2970-2979.

Kadokura, H., Katzen, F., and Beckwith, J. (2003). Protein disulfide bond formation in prokaryotes. *Annu Rev Biochem* **72**, 111-135.

Kadokura, H., Tian, H., Zander, T., Bardwell, J. C., and Beckwith, J. (2004). Snapshots of DsbA in action: detection of proteins in the process of oxidative folding. *Science* **303**, 534-537.

Kakiuchi, C., Iwamoto, K., Ishiwata, M., Bundo, M., Kasahara, T., Kusumi, I., Tsujita, T., Okazaki, Y., Nanko, S., Kunugi, H., Sasaki, T., and Kato, T. (2003). Impaired feedback regulation of XBP1 as a genetic risk factor for bipolar disorder. *Nature Genetics* **35**, 171-175.

Katiyar, S., Joshi, S., and Lennarz, W. J. (2005). The retrotranslocation protein Derlin-1 binds peptide:N-glycanase to the endoplasmic reticulum. *Mol Biol Cell* **16**, 4584-4594.

Kaufman, R. J., Scheuner, D., Schroder, M., Shen, X., Lee, K., Liu, C. Y., and Arnold, S. M. (2002). The unfolded protein response in nutrient sensing and differentiation. *Nat Rev Mol Cell Biol* **3**, 411-421.

Kemmink, J., Darby, N. J., Dijkstra, K., Nilges, M., and Creighton, T. E. (1997). The folding catalyst protein disulfide isomerase is constructed of active and inactive thioredoxin modules. *Curr Biol* **7**, 239-245.

Kierszenbaum, A. L. (2002). Histology and Cell Biology, An Introduction to Pathology.

Kitzmuller, C., Caprini, A., Moore, S. E., Frenoy, J. P., Schwaiger, E., Kellermann, O., Ivessa, N. E., and Ermonval, M. (2003). Processing of N-linked glycans during endoplasmic-reticulum-associated degradation of a short-lived variant of ribophorin I. *Biochem J* **376**, 687-696.

Klappa, P., Freedman, R. B., Langenbuch, M., Lan, M. S., Robinson, G. K., and Ruddock, L. W. (2001). The pancreas-specific protein disulphide-isomerase PDIp interacts with a hydroxyaryl group in ligands. *Biochem J* **354**, 553-559.

Klappa, P., Ruddock, L. W., Darby, N. J., and Freedman, R. B. (1998). The b' domain provides the principal peptide-binding site of protein disulfide isomerase but all domains contribute to binding of misfolded proteins. *EMBO J* **17**, 927-935.

Kleizen, B., van Vlijmen, T., de Jonge, H. R., and Braakman, I. (2005). Folding of CFTR is predominantly cotranslational. *Mol Cell* **20**, 277-287.

Knoblach, B., Keller, B. O., Groenendyk, J., Aldred, S., Zheng, J., Lemire, B. D., Li, L., and Michalak, M. (2003). ERp19 and ERp46, New Members of the Thioredoxin Family of Endoplasmic Reticulum Proteins. *Mol Cell Proteomics* **2**, 1104-1119.

Knop, M., Finger, A., Braun, T., Hellmuth, K., and Wolf, D. H. (1996). Der1, a novel protein specifically required for endoplasmic reticulum degradation in yeast. *EMBO J* **15**, 753-763.

Kobayashi, T., and Ito, K. (1999). Respiratory chain strongly oxidizes the CXXC motif of DsbB in the Escherichia coli disulfide bond formation pathway. *EMBO J* **18**, 1192-1198.

Koivu, J., Myllyla, R., Helaakoski, T., Pihlajaniemi, T., Tasanen, K., and Kivirikko, K. I. (1987). A single polypeptide acts both as the beta subunit of prolyl 4-hydroxylase and as a protein disulfide-isomerase. *J Biol Chem* **262**, 6447-6449.

Koivunen, P., Salo, K. E., Myllyharju, J., and Ruddock, L. W. (2005). Three binding sites in protein-disulfide isomerase cooperate in collagen prolyl 4-hydroxylase tetramer assembly. *J Biol Chem* **280**, 5227-5235.

Koizume, S., Takizawa, S., Fujita, K., Aida, N., Yamashita, S., Miyagi, Y., and Osaka, H. (2006). Aberrant trafficking of a proteolipid protein in a mild Pelizaeus-Merzbacher disease. *Neuroscience* **141**, 1861-1869.

Kopito, R. R. (1999). Biosynthesis and degradation of CFTR. *Physiol Rev* **79**, S167-173.

Kosower, N. S., and Kosower, E. M. (1995). Diamide: an oxidant probe for thiols. *Methods Enzymol* **251**, 123-133.

Kostova, Z., and Wolf, D. H. (2003). For whom the bell tolls: protein quality control of the endoplasmic reticulum and the ubiquitin-proteasome connection. *EMBO J* **22**, 2309-2317.

Kowarik, M., Kung, S., Martoglio, B., and Helenius, A. (2002). Protein folding during cotranslational translocation in the endoplasmic reticulum. *Mol Cell* **10**, 769-778.

Kozlov, G., Maattanen, P., Schrag, J. D., Pollock, S., Cygler, M., Nagar, B., Thomas, D. Y., and Gehring, K. (2006). Crystal structure of the bb' domains of the protein disulfide isomerase ERp57. *Structure* **14**, 1331-1339.

Kuge, S., Jones, N., and Nomoto, A. (1997). Regulation of yAP-1 nuclear localization in response to oxidative stress. *EMBO J* **16**, 1710-1720.

Kulp, M. S., Frickel, E. M., Ellgaard, L., and Weissman, J. S. (2006). Domain architecture of protein-disulfide isomerase facilitates its dual role as an oxidase and an isomerase in Ero1p-mediated disulfide formation. *J Biol Chem* **281**, 876-884.

Kumar, V., Cotran, R. S., and Robbins, S. L. (1997). Basic Pathology. *Sixth Ed.*

Laboissière, M. C. A., Sturley, S. L., and Raines, R. T. (1995). The Essential Function of Protein-disulfide Isomerase Is to Unscramble Non-native Disulfide Bonds. *J Biol Chem* **270**, 28006-28009.

Laemmli, U. K. (1970). Cleavage of structural proteins during the assembly of the head of bacteriophage T4. *Nature* **227**, 680-685.

Lanier, L. L. (1998). NK cell receptors. *Annu Rev Immunol* **16**, 359-393.

Lario, P. I., Sampson, N., and Vrielink, A. (2003). Sub-atomic resolution crystal structure of cholesterol oxidase: what atomic resolution crystallography reveals

about enzyme mechanism and the role of the FAD cofactor in redox activity. *J Mol Biol* **326**, 1635-1650.

Lawless, M. W., Greene, C. M., Mulgrew, A., Taggart, C. C., O'Neill, S. J., and McElvaney, N. G. (2004). Activation of endoplasmic reticulum-specific stress responses associated with the conformational disease Z alpha 1-antitrypsin deficiency. *J Immunol* **172**, 5722-5726.

Leach, M. R., and Williams, D. B. (2004). Lectin-deficient Calnexin Is Capable of Binding Class I Histocompatibility Molecules in Vivo and Preventing Their Degradation. *J Biol Chem* **279**, 9072-9079.

Lechleiter, J., Girard, S., Peralta, E., and Clapham, D. (1991). Spiral calcium wave propagation and annihilation in Xenopus laevis oocytes. *Science* **252**, 123-126.

Lee, N., Goodlett, D. R., Ishitani, A., Marquardt, H., and Geraghty, D. E. (1998). HLA-E surface expression depends on binding of TAP-dependent peptides derived from certain HLA class I signal sequences. *J Immunol* **160**, 4951-4960.

Lemberg, M. K., Bland, F. A., Weihofen, A., Braud, V. M., and Martoglio, B. (2001). Intramembrane Proteolysis of Signal Peptides: An Essential Step in the Generation of HLA-E Epitopes. *J Immunol* **167**, 6441-6446.

Li, Y., and Camacho, P. (2004). Ca2+-dependent redox modulation of SERCA 2b by ERp57. *J Cell Biol* **164**, 35-46.

Liao, S., Lin, J., Do, H., and Johnson, A. E. (1997). Both lumenal and cytosolic gating of the aqueous ER translocon pore are regulated from inside the ribosome during membrane protein integration. *Cell* **90**, 31-41.

Liepinsh, E., Baryshev, M., Sharipo, A., Ingelman-Sundberg, M., Otting, G., and Mkrtchian, S. (2001). Thioredoxin fold as homodimerization module in the putative chaperone ERp29: NMR structures of the domains and experimental model of the 51 kDa dimer. *Structure* **9**, 457-471.

Linke, K., and Jakob, U. (2003). Not every disulfide lasts forever: disulfide bond formation as a redox switch. *Antioxid Redox Signal* **5**, 425-434.

Linke, K., Wolfram, T., Bussemer, J., and Jakob, U. (2003). The roles of the two zinc binding sites in DnaJ. *J Biol Chem* **278**, 44457-44466.

Lisanti, M. P., Caras, I. W., Davitz, M. A., and Rodriguez-Boulan, E. (1989). A glycophospholipid membrane anchor acts as an apical targeting signal in polarized epithelial cells. *J Cell Biol* **109**, 2145-2156.

Ljunggren, H. G., and Karre, K. (1990). In search of the 'missing self': MHC molecules and NK cell recognition. *Immunol Today* **11**, 237-244.

Loureiro, J., Lilley, B. N., Spooner, E., Noriega, V., Tortorella, D., and Ploegh, H. L. (2006). Signal peptide peptidase is required for dislocation from the endoplasmic reticulum. *Nature* **441**, 894-897.

Lowry, O. H., Rosebrough, N. J., Farr, A. L., and Randall, R. J. (1951). Protein measurement with the Folin Phenol reagent. *J Biol Chem* **193**, 265-275.

Lowry, O. H., Rosebrough, N. J., Farr, A. L., and Randall, R. J. (1951). Protein measurement with the Folin Phenol reagent. *J Biol Chem.* **193**, 265-275.

Luirink, J., and Sinning, I. (2004). SRP-mediated protein targeting: structure and function revisited. *Biochim Biophys Acta* **1694**, 17-35.

Lundstrom, J., and Holmgren, A. (1993). Determination of the reduction-oxidation potential of the thioredoxin-like domains of protein disulfide-isomerase from the equilibrium with glutathione and thioredoxin. *Biochemistry* **32**, 6649-6655.

Maecker, H., Todd, S., and Levy, S. (1997). The tetraspanin superfamily: molecular facilitators. *FASEB J.* **11**, 428-442.

Magnuson, B., Rainey, E. K., Benjamin, T., Baryshev, M., Mkrtchian, S., and Tsai, B. (2005). ERp29 triggers a conformational change in polyomavirus to stimulate membrane binding. *Mol Cell* **20**, 289-300.

Margeta-Mitrovic, M., Jan, Y. N., and Jan, L. Y. (2000). A trafficking checkpoint controls GABA(B) receptor heterodimerization. *Neuron* **27**, 97-106.

Marquardt, T., Hebert, D. N., and Helenius, A. (1993). Post-translational folding of influenza hemagglutinin in isolated endoplasmic reticulum-derived microsomes. *J Biol Chem* **268**, 19618-19625.

Martin, V., Groenendyk, J., Steiner, S. S., Guo, L., Dabrowska, M., Parker, J. M. R., Muller-Esterl, W., Opas, M., and Michalak, M. (2006). Identification by Mutational Analysis of Amino Acid Residues Essential in the Chaperone Function of Calreticulin. *J Biol Chem* **281**, 2338-2346.

Mast, S. W., Diekman, K., Karaveg, K., Davis, A., Sifers, R. N., and Moremen, K. W. (2005). Human EDEM2, a novel homolog of family 47 glycosidases, is involved in ER-associated degradation of glycoproteins. *Glycobiology* **15**, 421-436.

Matlack, K. E., Misselwitz, B., Plath, K., and Rapoport, T. A. (1999). BiP acts as a molecular ratchet during posttranslational transport of prepro-alpha factor across the ER membrane. *Cell* **97**, 553-564.

Mattaj, I. W. (2004). Sorting out the nuclear envelope from the endoplasmic reticulum. *Nat Rev Mol Cell Biol* **5**, 65-69.

Matter, K., Yamamoto, E. M., and Mellman, I. (1994). Structural requirements and sequence motifs for polarized sorting and endocytosis of LDL and Fc receptors in MDCK cells. *J Cell Biol* **126**, 991-1004.

May, D., Itin, A., Gal, O., Kalinski, H., Feinstein, E., and Keshet, E. (2005). Ero1-L alpha plays a key role in a HIF-1-mediated pathway to improve disulfide bond formation and VEGF secretion under hypoxia: implication for cancer. *Oncogene* **24**, 1011-1020.

McCarthy, A. A., Haebel, P. W., Torronen, A., Rybin, V., Baker, E. N., and Metcalf, P. (2000). Crystal structure of the protein disulfide bond isomerase, DsbC, from Escherichia coli. *Nat Struct Biol* **7**, 196-199.

McKee, M. L., and FitzGerald, D. J. (1999). Reduction of furin-nicked Pseudomonas exotoxin A: an unfolding story. *Biochemistry* **38**, 16507-16513.

Meister, A., and Anderson, M. E. (1983). Glutathione. *Annu Rev Biochem* **52**, 711-760.

Melnick, J., Dul, J. L., and Argon, Y. (1994). Sequential interaction of the chaperones BiP and GRP94 with immunoglobulin chains in the endoplasmic reticulum. *Nature* **370**, 373-375.

Meng, X., Zhang, C., Chen, J., Peng, S., Cao, Y., Ying, K., Xie, Y., and Mao, Y. (2003). Cloning and identification of a novel cDNA coding thioredoxin-related transmembrane protein 2. *Biochem Genet* **41**, 99-106.

Meusser, B., Hirsch, C., Jarosch, E., and Sommer, T. (2005). ERAD: the long road to destruction. *Nat Cell Biol* **7**, 766-772.

Meyer, G. A., and Radsak, K. D. (2000). Identification of a novel signal sequence that targets transmembrane proteins to the nuclear envelope inner membrane. *J Biol Chem* **275**, 3857-3866.

Meyer, G., Gicklhorn, D., Strive, T., Radsak, K., and Eickmann, M. (2002). A three-

residue signal confers localization of a reporter protein in the inner nuclear membrane. *Biochem Biophys Res Commun* **291**, 966-971.

Mezghrani, A., Fassio, A., Benham, A., Simmen, T., Braakman, I., and Sitia, R. (2001). Manipulation of oxidative protein folding and PDI redox state in mammalian cells. *EMBO J* **20**, 6288-6296.

Michelsen, K., Yuan, H., and Schwappach, B. (2005). Hide and run. Arginine-based endoplasmic-reticulum-sorting motifs in the assembly of heteromultimeric membrane proteins. *EMBO Rep* **6**, 717-722.

Miyazaki, J., Appella, E., Zhao, H., Forman, J., and Ozato, K. (1986). Expression and function of a nonglycosylated major histocompatibility class I antigen. *J Exp Med* **163**, 856-871.

Molinari, M., and Helenius, A. (1999). Glycoproteins form mixed disulphides with oxidoreductases during folding in living cells. *Nature* **402**, 90-93.

Molinari, M., and Helenius, A. (2000). Chaperone selection during glycoprotein translocation into the endoplasmic reticulum. *Science* **288**, 331-333.

Molinari, M., Calanca, V., Galli, C., Lucca, P., and Paganetti, P. (2003). Role of EDEM in the release of misfolded glycoproteins from the calnexin cycle. *Science* **299**, 1397-1400.

Molteni, S. N., Fassio, A., Ciriolo, M. R., Filomeni, G., Pasqualetto, E., Fagioli, C., and Sitia, R. (2004). Glutathione limits Ero1-dependent oxidation in the endoplasmic reticulum. *J Biol Chem* **279**, 32667-32673.

Mori, H., and Ito, K. (2001). The Sec protein-translocation pathway. *Trends Microbiol* **9**, 494-500.

Mulvey, M., and Brown, D. (1995). Involvement of the molecular chaperone BiP in maturation of Sindbis virus envelope glycoproteins. *J Virol* **69**, 1621-1627.

Munro, S., and Pelham, H. R. B. (1987). A C-terminal signal prevents secretion of luminal ER proteins. *Cell* **48**, 899-907.

Myllyharju, J. (2003). Prolyl 4-hydroxylases, the key enzymes of collagen biosynthesis. *Matrix Biol* **22**, 15-24.

Nagai, K., Oubridge, C., Kuglstatter, A., Menichelli, E., Isel, C., and Jovine, L. (2003). Structure, function and evolution of the signal recognition particle. *EMBO J* **22**, 3479-3485.

Nathanson, M. H., Burgstahler, A. D., and Fallon, M. B. (1994). Multistep mechanism of polarized Ca2+ wave patterns in hepatocytes. *Am J Physiol* **267**, G338-349.

Nelson, W. J., and Yeaman, C. (2001). Protein trafficking in the exocytic pathway of polarized epithelial cells. *Trends Cell Biol* **11**, 483-486.

Ng, D. T., Brown, J. D., and Walter, P. (1996). Signal sequences specify the targeting route to the endoplasmic reticulum membrane. *J Cell Biol* **134**, 269-278.

Nilsson, I., and von Heijne, G. (1993). Determination of the distance between the oligosaccharyltransferase active site and the endoplasmic reticulum membrane. *J Biol Chem* **268**, 5798-5801.

Nilsson, T., Jackson, M., and Peterson, P. A. (1989). Short cytoplasmic sequences serve as retention signals for transmembrane proteins in the endoplasmic reticulum. *Cell* **58**, 707-718.

Norgaard, P., Westphal, V., Tachibana, C., Alsoe, L., Holst, B., and Winther, J. R. (2001). Functional differences in yeast protein disulfide isomerases. *J Cell Biol* **152**, 553-562.

Oda, Y., Hosokawa, N., Wada, I., and Nagata, K. (2003). EDEM as an acceptor of terminally misfolded glycoproteins released from calnexin. *Science* **299**, 1394-1397.

Oda, Y., Okada, T., Yoshida, H., Kaufman, R. J., Nagata, K., and Mori, K. (2006). Derlin-2 and Derlin-3 are regulated by the mammalian unfolded protein response and are required for ER-associated degradation. *J Cell Biol* **172**, 383-393.

Olden, K., Parent, J. B., and White, S. L. (1982). Carbohydrate moieties of glycoproteins. A re-evaluation of their function. *Biochim Biophys Acta* **650**, 209-232.

Olden, K., Pratt, R. M., and Yamada, K. M. (1978). Role of carbohydrates in protein secretion and turnover: effects of tunicamycin on the major cell surface glycoprotein of chick embryo fibroblasts. *Cell* **13**, 461-473.

Olivari, S., Galli, C., Alanen, H., Ruddock, L., and Molinari, M. (2005). A novel stress-induced EDEM variant regulating endoplasmic reticulum-associated glycoprotein degradation. *J Biol Chem* **280**, 2424-2428.

Oliver, J. D., van der Wal, F. J., Bulleid, N. J., and High, S. (1997). Interaction of the thiol-dependent reductase ERp57 with nascent glycoproteins. *Science* **275**, 86-88.

Ortega, S., Schaeffer, M. T., Soderman, D., DiSalvo, J., Linemeyer, D. L., Gimenez-Gallego, G., and Thomas, K. A. (1991). Conversion of cysteine to serine residues alters the activity, stability, and heparin dependence of acidic fibroblast growth factor. *J Biol Chem* **266**, 5842-5846.

Osborne, A. R., Rapoport, T. A., and van den Berg, B. (2005). Protein translocation by the sec61/secY channel. *Annual Review of Cell and Developmental Biology* **21**, 529-550.

Otsu, M., Bertoli, G., Fagioli, C., Guerini-Rocco, E., Nerini-Molteni, S., Ruffato, E., and Sitia, R. (2006). Dynamic Retention of Ero1alpha and Ero1beta in the Endoplasmic Reticulum by Interactions with PDI and ERp44. *Antioxid Redox Signal* **8**, 274-282.

Ozcan, U., Cao, Q., Yilmaz, E., Lee, A. H., Iwakoshi, N. N., Ozdelen, E., Tuncman, G., Gorgun, C., Glimcher, L. H., and Hotamisligil, G. S. (2004). Endoplasmic reticulum stress links obesity, insulin action, and type 2 diabetes. *Science* **306**, 457-461.

Pagani, M., Fabbri, M., Benedetti, C., Fassio, A., Pilati, S., Bulleid, N. J., Cabibbo, A., and Sitia, R. (2000). Endoplasmic reticulum oxidoreductin 1-lbeta (ERO1-Lbeta), a human gene induced in the course of the unfolded protein response. *J Biol Chem* **275**, 23685-23692.

Pagani, M., Pilati, S., Bertoli, G., Valsasina, B., and Sitia, R. (2001). The C-terminal domain of yeast Ero1p mediates membrane localization and is essential for function. *FEBS Lett* **508**, 117-120.

Paget, M. S., and Buttner, M. J. (2003). Thiol-based regulatory switches. *Annu Rev Genet* **37**, 91-121.

Pastore, A., Federici, G., Bertini, E., and Piemonte, F. (2003). Analysis of glutathione: implication in redox and detoxification. *Clin Chim Acta* **333**, 19-39.

Patterson, R. L., Boehning, D., and Snyder, S. H. (2004). Inositol 1,4,5-trisphosphate receptors as signal integrators. *Annu Rev Biochem* **73**, 437-465.

Pelham, H. R. (1989). Control of protein exit from the endoplasmic reticulum. *Annu Rev Cell Biol* **5**, 1-23.

Pelham, H. R., and Munro, S. (1993). Sorting of membrane proteins in the secretory pathway. *Cell* **75**, 603-605.

Peters, T., Jr, and Davidson, L. (1982). The biosynthesis of rat serum albumin. In vivo studies on the formation of the disulfide bonds. *J Biol Chem* **257**, 8847-8853.

Pilon, M., Schekman, R., and Romisch, K. (1997). Sec61p mediates export of a misfolded secretory protein from the endoplasmic reticulum to the cytosol for degradation. *EMBO J* **16**, 4540-4548.

Pirneskoski, A., Klappa, P., Lobell, M., Williamson, R. A., Byrne, L., Alanen, H. I., Salo, K. E., Kivirikko, K. I., Freedman, R. B., and Ruddock, L. W. (2004). Molecular characterization of the principal substrate binding site of the ubiquitous folding catalyst protein disulfide isomerase. *J Biol Chem* **279**, 10374-10381.

Plemper, R. K., Bohmler, S., Bordallo, J., Sommer, T., and Wolf, D. H. (1997). Mutant analysis links the translocon and BiP to retrograde protein transport for ER degradation. *Nature* **388**, 891-895.

Pollard, M. G., Travers, K. J., and Weissman, J. S. (1998). Ero1p: a novel and ubiquitous protein with an essential role in oxidative protein folding in the endoplasmic reticulum. *Mol Cell* **1**, 171-182.

Pollock, S., Kozlov, G., Pelletier, M. F., Trempe, J. F., Jansen, G., Sitnikov, D., Bergeron, J. J., Gehring, K., Ekiel, I., and Thomas, D. Y. (2004). Specific interaction of ERp57 and calnexin determined by NMR spectroscopy and an ER two-hybrid system. *EMBO J* **23**, 1020-1029.

Potter, B. A., Hughey, R. P., and Weisz, O. A. (2006). Role of N- and O-glycans in polarized biosynthetic sorting. *Am J Physiol Cell Physiol* **290**, C1-C10.

Potter, B. A., Ihrke, G., Bruns, J. R., Weixel, K. M., and Weisz, O. A. (2004). Specific N-glycans direct apical delivery of transmembrane, but not soluble or glycosylphosphatidylinositol-anchored forms of endolyn in Madin-Darby canine kidney cells. *Mol Biol Cell* **15**, 1407-1416.

Qin, Z. H., and Gu, Z. L. (2004). Huntingtin processing in pathogenesis of Huntington disease. *Acta Pharmacol Sin* **25**, 1243-1249.

Ramos, M., and Lopez de Castro, J. A. (2002). HLA-B27 and the pathogenesis of spondyloarthritis. *Tissue Antigens* **60**, 191-205.

Ridgway, E. B., Gilkey, J. C., and Jaffe, L. F. (1977). Free Calcium Increases Explosively in Activating Medaka Eggs. *Proc Natl Acad Sci U S A* **74**, 623-627.

Rietsch, A., Bessette, P., Georgiou, G., and Beckwith, J. (1997). Reduction of the periplasmic disulfide bond isomerase, DsbC, occurs by passage of electrons from cytoplasmic thioredoxin. *J Bacteriol* **179**, 6602-6608.

Ritter, C., and Helenius, A. (2000). Recognition of local glycoprotein misfolding by the ER folding sensor UDP-glucose:glycoprotein glucosyltransferase. *Nat Struct Biol* **7**, 278-280.

Roderick, H. L., Lechleiter, J. D., and Camacho, P. (2000). Cytosolic phosphorylation of calnexin controls intracellular Ca(2+) oscillations via an interaction with SERCA2b. *J Cell Biol* **149**, 1235-1248.

Rossi, A. E., and Dirksen, R. T. (2006). Sarcoplasmic reticulum: the dynamic calcium governor of muscle. *Muscle Nerve* **33**, 715-731.

Ruddock, L., Freedman, R., and Klappa, P. (2000). Specificity in substrate binding by protein folding catalysts: tyrosine and tryptophan residues are the recognition motifs for the binding of peptides to the pancreas-specific protein disulfide

isomerase PDIp. *Protein Sci* **9**, 758-764.

Sadlish, H., Pitonzo, D., Johnson, A. E., and Skach, W. R. (2005). Sequential triage of transmembrane segments by Sec61alpha during biogenesis of a native multispanning membrane protein. *Nat Struct Mol Biol* **12**, 870-878.

Saito, Y., Ihara, Y., Leach, M. R., Cohen-Doyle, M. F., and Williams, D. B. (1999). Calreticulin functions in vitro as a molecular chaperone for both glycosylated and non-glycosylated proteins. *EMBO J* **18**, 6718-6729.

Saksena, S., Shao, Y., Braunagel, S. C., Summers, M. D., and Johnson, A. E. (2004). Cotranslational integration and initial sorting at the endoplasmic reticulum translocon of proteins destined for the inner nuclear membrane. *Proc Natl Acad Sci U S A* **101**, 12537-12542.

Saksena, S., Summers, M. D., Burks, J. K., Johnson, A. E., and Braunagel, S. C. (2006). Importin-alpha-16 is a translocon-associated protein involved in sorting membrane proteins to the nuclear envelope. *Nat Struct Mol Biol* **13**, 500-508.

Sargsyan, E., Baryshev, M., Szekely, L., Sharipo, A., and Mkrtchian, S. (2002). Identification of ERp29, an endoplasmic reticulum lumenal protein, as a new member of the thyroglobulin folding complex. *J Biol Chem* **277**, 17009-17015.

Scheibel, T., and Buchner, J. (2006). Protein aggregation as a cause for disease. *Handb Exp Pharmacol*, 199-219.

Scheiffele, P., Peranen, J., and Simons, K. (1995). N-glycans as apical sorting signals in epithelial cells. *Nature* **378**, 96-98.

Schrag, J. D., Bergeron, J. J., Li, Y., Borisova, S., Hahn, M., Thomas, D. Y., and Cygler, M. (2001). The Structure of calnexin, an ER chaperone involved in quality control of protein folding. *Mol Cell* **8**, 633-644.

Schroder, M., and Kaufman, R. J. (2005). The mammalian unfolded protein response. *Annu Rev Biochem* **74**, 739-789.

Seckler, R., and Jaenicke, R. (1992). Protein folding and protein refolding. *FASEB J* **6**, 2545-2552.

Sevier, C. S., and Kaiser, C. A. (2006a). Conservation and diversity of the cellular disulfide bond formation pathways. *Antioxid Redox Signal* **8**, 797-811.

Sevier, C. S., and Kaiser, C. A. (2006b). Disulfide transfer between two conserved cysteine pairs imparts selectivity to protein oxidation by Ero1. *Mol Biol Cell* **17**, 2256-2266.

Sevier, C. S., Cuozzo, J. W., Vala, A., Aslund, F., and Kaiser, C. A. (2001). A flavoprotein oxidase defines a new endoplasmic reticulum pathway for biosynthetic disulphide bond formation. *Nat Cell Biol* **3**, 874-882.

Sharma, M., Pampinella, F., Nemes, C., Benharouga, M., So, J., Du, K., Bache, K. G., Papsin, B., Zerangue, N., Stenmark, H., and Lukacs, G. L. (2004). Misfolding diverts CFTR from recycling to degradation: quality control at early endosomes. *J Cell Biol* **164**, 923-933.

Shelness, G. S., Lin, L., and Nicchitta, C. V. (1993). Membrane topology and biogenesis of eukaryotic signal peptidase. *J Biol Chem* **268**, 5201-5208.

Shikano, S., and Li, M. (2003). Membrane receptor trafficking: evidence of proximal and distal zones conferred by two independent endoplasmic reticulum localization signals. *Proc Natl Acad Sci U S A* **100**, 5783-5788.

Silberstein, S., Schlenstedt, G., Silver, P. A., and Gilmore, R. (1998). A Role for the DnaJ Homologue Scj1p in Protein Folding in the Yeast Endoplasmic Reticulum. *J*

Cell Biol **143**, 921-933.

Simons, J. F., Ferro-Novick, S., Rose, M. D., and Helenius, A. (1995). BiP/Kar2p serves as a molecular chaperone during carboxypeptidase Y folding in yeast. *J Cell Biol* **130**, 41-49.

Smith, M. J., and Koch, G. L. (1989). Multiple zones in the sequence of calreticulin (CRP55, calregulin, HACBP), a major calcium binding ER/SR protein. *EMBO J* **8**, 3581-3586.

Solda, T., Garbi, N., Hammerling, G. J., and Molinari, M. (2006). Consequences of ERp57 deletion on oxidative folding of obligate and facultative clients of the calnexin cycle. *J Biol Chem* **281**, 6219-6226.

Solovyov, A., Xiao, R., and Gilbert, H. F. (2004). Sulfhydryl Oxidation, Not Disulfide Isomerization, Is the Principal Function of Protein Disulfide Isomerase in Yeast Saccharomyces cerevisiae. *J Biol Chem* **279**, 34095-34100.

Sonnichsen, B., Fullekrug, J., Nguyen Van, P., Diekmann, W., Robinson, D., and Mieskes, G. (1994). Retention and retrieval: both mechanisms cooperate to maintain calreticulin in the endoplasmic reticulum. *J Cell Sci* **107**, 2705-2717.

Sorensen, S., Ranheim, T., Bakken, K. S., Leren, T. P., and Kulseth, M. A. (2006). Retention of Mutant Low Density Lipoprotein Receptor in Endoplasmic Reticulum (ER) Leads to ER Stress. *J Biol Chem* **281**, 468-476.

Spooner, R. A., Watson, P. D., Marsden, C. J., Smith, D. C., Moore, K. A., Cook, J. P., Lord, J. M., and Roberts, L. M. (2004). Protein disulphide-isomerase reduces ricin to its A and B chains in the endoplasmic reticulum. *Biochem J* **383**, 285-293.

Stevens, A., and Lowe, J. (1993). Histology.

Swanton, E., High, S., and Woodman, P. (2003). Role of calnexin in the glycan-independent quality control of proteolipid protein. *EMBO J* **22**, 2948-2958.

Szabo, A., Korszun, R., Hartl, F. U., and Flanagan, J. (1996). A zinc finger-like domain of the molecular chaperone DnaJ is involved in binding to denatured protein substrates. *EMBO J* **15**, 408-417.

Thorpe, C., Hoober, K. L., Raje, S., Glynn, N. M., Burnside, J., Turi, G. K., and Coppock, D. L. (2002). Sulfhydryl oxidases: emerging catalysts of protein disulfide bond formation in eukaryotes. *Arch Biochem Biophys* **405**, 1-12.

Tian, G., Xiang, S., Noiva, R., Lennarz, W. J., and Schindelin, H. (2006). The crystal structure of yeast protein disulfide isomerase suggests cooperativity between its active sites. *Cell* **124**, 61-73.

Townsley, F. M., and Pelham, H. R. (1994). The KKXX signal mediates retrieval of membrane proteins from the Golgi to the ER in yeast. *Eur J Cell Biol* **64**, 211-216.

Tsai, B., Rodighiero, C., Lencer, W. I., and Rapoport, T. A. (2001). Protein disulfide isomerase acts as a redox-dependent chaperone to unfold cholera toxin. *Cell* **104**, 937-948.

Tu, B. P., and Weissman, J. S. (2004). Oxidative protein folding in eukaryotes: mechanisms and consequences. *J Cell Biol* **164**, 341

Tu, B. P., and Weissman, J. S. (2002). The FAD- and O(2)-dependent reaction cycle of Ero1-mediated oxidative protein folding in the endoplasmic reticulum. *Mol Cell* **10**, 983-994.

Tu, B. P., Ho-Schleyer, S. C., Travers, K. J., and Weissman, J. S. (2000). Biochemical basis of oxidative protein folding in the endoplasmic reticulum. *Science* **290**, 1571-1574.

Tury, A., Mairet-Coello, G., Esnard-Feve, A., Benayoun, B., Risold, P. Y., Griffond, B., and Fellmann, D. (2006). Cell-specific localization of the sulphydryl oxidase QSOX in rat peripheral tissues. *Cell Tissue Res* **323**, 91-103.

Uehara, T., Nakamura, T., Yao, D., Shi, Z. Q., Gu, Z., Ma, Y., Masliah, E., Nomura, Y., and Lipton, S. A. (2006). S-nitrosylated protein-disulphide isomerase links protein misfolding to neurodegeneration. *Nature* **441**, 513-517.

van Lith, M., Hartigan, N., Hatch, J., and Benham, A. M. (2005). PDILT, a divergent testis-specific protein disulfide isomerase with a non-classical SXXC motif that engages in disulfide-dependent interactions in the endoplasmic reticulum. *J Biol Chem* **280**, 1376-1383.

Vashist, S., and Ng, D. T. (2004). Misfolded proteins are sorted by a sequential checkpoint mechanism of ER quality control. *J Cell Biol* **165**, 41-52.

Vauloup-Fellous, C., Pene, V., Garaud-Aunis, J., Harper, F., Bardin, S., Suire, Y., Pichard, E., Schmitt, A., Sogni, P., Pierron, G., Briand, P., and Rosenberg, A. R. (2006). Signal peptide peptidase-catalyzed cleavage of hepatitis C virus core protein is dispensable for virus budding, but destabilizes the viral capsid. *J Biol Chem*.

Voisset, C., and Dubuisson, J. (2004). Functional hepatitis C virus envelope glycoproteins. *Biol Cell* **96**, 413-420.

Vuori, K., Pihlajaniemi, T., Marttila, M., and Kivirikko, K. I. (1992a). Characterization of the human prolyl 4-hydroxylase tetramer and its multifunctional protein disulfide-isomerase subunit synthesized in a baculovirus expression system. *Proc Natl Acad Sci U S A* **89**, 7467-7470.

Vuori, K., Pihlajaniemi, T., Myllyla, R., and Kivirikko, K. I. (1992b). Site-directed mutagenesis of human protein disulphide isomerase: effect on the assembly, activity and endoplasmic reticulum retention of human prolyl 4-hydroxylase in Spodoptera frugiperda insect cells. *EMBO J* **11**, 4213-4217.

Wada, I., Rindress, D., Cameron, P., Ou, W., Doherty, J., 2d, Louvard, D., Bell, A., Dignard, D., Thomas, D., and Bergeron, J. (1991). SSR alpha and associated calnexin are major calcium binding proteins of the endoplasmic reticulum membrane. *J Biol Chem* **266**, 19599-19610.

Wang, C. C., and Tsou, C. L. (1993). Protein disulfide isomerase is both an enzyme and a chaperone. *Faseb J* **7**, 1515-1517.

Wang, Q., and Chang, A. (1999). Eps1, a novel PDI-related protein involved in ER quality control in yeast. *EMBO J* **18**, 5972-5982.

Wang, Q., and Chang, A. (2003). Substrate recognition in ER-associated degradation mediated by Eps1, a member of the protein disulfide isomerase family. *EMBO J* **22**, 3792-3802.

Watanabe, R., and Riezman, H. (2004). Differential ER exit in yeast and mammalian cells. *Curr Opin Cell Biol* **16**, 350-355.

Wearsch, P. A., Jakob, C. A., Vallin, A., Dwek, R. A., Rudd, P. M., and Cresswell, P. (2004). Major Histocompatibility Complex Class I Molecules Expressed with Monoglucosylated N-Linked Glycans Bind Calreticulin Independently of Their Assembly Status. *J Biol Chem* **279**, 25112-25121.

Weihofen, A., and Martoglio, B. (2003). Intramembrane-cleaving proteases: controlled liberation of proteins and bioactive peptides. *Trends Cell Biol* **13**, 71-78.

Weihofen, A., Binns, K., Lemberg, M. K., Ashman, K., and Martoglio, B. (2002).

Identification of signal peptide peptidase, a presenilin-type aspartic protease. *Science* **296**, 2215-2218.

Weihofen, A., Lemberg, M. K., Ploegh, H. L., Bogyo, M., and Martoglio, B. (2000). Release of signal peptide fragments into the cytosol requires cleavage in the transmembrane region by a protease activity that is specifically blocked by a novel cysteine protease inhibitor. *J Biol Chem* **275**, 30951-30956.

Wetterau, J. R., Combs, K. A., Spinner, S. N., and Joiner, B. J. (1990). Protein disulfide isomerase is a component of the microsomal triglyceride transfer protein complex. *J Biol Chem* **265**, 9801-9807.

Wiertz, E. J., Jones, T. R., Sun, L., Bogyo, M., Geuze, H. J., and Ploegh, H. L. (1996). The human cytomegalovirus US11 gene product dislocates MHC class I heavy chains from the endoplasmic reticulum to the cytosol. *Cell* **84**, 769-779.

Wiertz, E. J., Tortorella, D., Bogyo, M., Yu, J., Mothes, W., Jones, T. R., Rapoport, T. A., and Ploegh, H. L. (1996). Sec61-mediated transfer of a membrane protein from the endoplasmic reticulum to the proteasome for destruction. *Nature* **384**, 432-438.

Wild, K., Rosendal, K. R., and Sinning, I. (2004). A structural step into the SRP cycle. *Mol Microbiol* **53**, 357-363.

Williams, D. B. (2006). Beyond lectins: the calnexin/calreticulin chaperone system of the endoplasmic reticulum. *J Cell Sci* **119**, 615-623.

Wilson, I. A., Skehel, J. J., and Wiley, D. C. (1981). Structure of the haemagglutinin membrane glycoprotein of influenza virus at 3 A resolution. *Nature* **289**, 366-373.

Wilson, R., Lees, J. F., and Bulleid, N. J. (1998). Protein disulfide isomerase acts as a molecular chaperone during the assembly of procollagen. *J Biol Chem* **273**, 9637-9643.

Wirth, A., Jung, M., Bies, C., Frien, M., Tyedmers, J., Zimmermann, R., and Wagner, R. (2003). The Sec61p complex is a dynamic precursor activated channel. *Mol Cell* **12**, 261-268.

Wolynes, P. G. (2005). Energy landscapes and solved protein-folding problems. *Philos Transact A Math Phys Eng Sci* **363**, 453-464.

Woolhead, C. A., McCormick, P. J., and Johnson, A. E. (2004). Nascent membrane and secretory proteins differ in FRET-detected folding far inside the ribosome and in their exposure to ribosomal proteins. *Cell* **116**, 725-736.

Worman, H. J., and Courvalin, J. C. (2000). The inner nuclear membrane. *J Membr Biol* **177**, 1-11.

Xia, W., and Wolfe, M. S. (2003). Intramembrane proteolysis by presenilin and presenilin-like proteases. *J Cell Sci* **116**, 2839-2844.

Ye, Y., Shibata, Y., Yun, C., Ron, D., and Rapoport, T. A. (2004). A membrane protein complex mediates retro-translocation from the ER lumen into the cytosol. *Nature* **429**, 841-847.

Yoshida, H., Matsui, T., Yamamoto, A., Okada, T., and Mori, K. (2001). XBP1 mRNA is induced by ATF6 and spliced by IRE1 in response to ER stress to produce a highly active transcription factor. *Cell* **107**, 881-891.

Zapun, A., Bardwell, J. C., and Creighton, T. E. (1993). The reactive and destabilizing disulfide bond of DsbA, a protein required for protein disulfide bond formation in vivo. *Biochemistry* **32**, 5083-5092.

Zapun, A., Missiakas, D., Raina, S., and Creighton, T. E. (1995). Structural and

functional characterization of DsbC, a protein involved in disulfide bond formation in Escherichia coli. *Biochemistry* **34**, 5075-5089.

Zerangue, N., Schwappach, B., Jan, Y. N., and Jan, L. Y. (1999). A new ER trafficking signal regulates the subunit stoichiometry of plasma membrane K(ATP) channels. *Neuron* **22**, 537-548.

Zhang, F., Kartner, N., and Lukacs, G. L. (1998). Limited proteolysis as a probe for arrested conformational maturation of delta F508 CFTR. *Nat Struct Biol* **5**, 180-183.

Zhang, Y., Baig, E., and Williams, D. B. (2006). Functions of ERp57 in the folding and assembly of major histocompatibility complex class I molecules. *J Biol Chem* **281**, 14622-14631.

Zhao, Z., Peng, Y., Hao, S. F., Zeng, Z. H., and Wang, C. C. (2003). Dimerization by domain hybridization bestows chaperone and isomerase activities. *J Biol Chem* **278**, 43292-43298.

Ziegler, D. M. (1985). Role of reversible oxidation-reduction of enzyme thiols-disulfides in metabolic regulation. *Annu Rev Biochem* **54**, 305-329.

PUBLICATIONS ARISING FROM THIS THESIS

1. **Dias-Gunasekara, S., van Lith, M., Williams, J. A., Kataky, R., and Benham, A. M.** (2006). Mutations in the FAD binding domain cause stress-induced misoxidation of the endoplasmic reticulum oxidoreductase Ero1beta. *J Biol Chem* **281**, 25018-25025

2. **Dias-Gunasekara, S., Gubbens, J., van Lith, M., Dunne, C., Williams, J. A. G., Kataky, R., Scoones, D., Lapthorn, A., Bulleid, N. J., and Benham, A. M.** (2005). Tissue-specific Expression and Dimerization of the Endoplasmic Reticulum Oxidoreductase Ero1{beta}. *J Biol Chem* **280**, 33066-33075.

3. **Dias-Gunasekara, S., and Benham, A. M.** (2005). Defining the protein-protein interactions of the mammalian endoplasmic reticulum oxidoreductases (EROs). *Biochem Soc Trans* **33**, 1382-1384.